Winter 2018

Wet and Dry Atmospheric Deposition of Nutrients and Bioactive Trace Metals to Coastal Waters of the Mid-Atlantic Bight

Christine Sookhdeo
Old Dominion University

WET AND DRY ATMOSPHERIC DEPOSITION OF NUTRIENTS AND BIOACTIVE TRACE METALS TO COASTAL WATERS OF THE MID-ATLANTIC BIGHT

by

Christine Sookhdeo
B.S. May 2012, Rider University

A Thesis Submitted to the Faculty of
Old Dominion University in Partial Fulfilment of the
Requirements for the Degree of

MASTER OF SCIENCE

OCEAN AND EARTH SCIENCES

OLD DOMINION UNIVERSITY
December 2018

Approved by:

Peter N. Sedwick (Co-Director)

Margaret R. Mulholland (Co-Director)

Dreux P. Chappell (Member)

ABSTRACT

WET AND DRY ATMOSPHERIC DEPOSITION OF NUTRIENTS AND BIOACTIVE TRACE METALS TO COASTAL WATERS OF THE MID-ATLANTIC BIGHT

Christine Sookhdeo
Old Dominion University, 2018
Co-Directors: Dr. Peter N. Sedwick
Dr. Margaret R. Mulholland

Atmospheric deposition provides a significant source of nutrients and bioactive trace metals to the surface ocean, including the seasonally oligotrophic waters of the Mid-Atlantic Bight. These atmospherically derived nutrients and trace metals enter the surface ocean via dry deposition of aerosols and wet deposition in rain. To estimate the aeolian input of nutrients and trace metals to coastal waters east of the Delmarva Peninsula, wet and dry atmospheric deposition samples were collected over a one-year time series at the Anheuser-Busch Coastal Research Center, Oyster, Virginia. Weekly composite samples were collected from May 2014 through June 2015. Nutrient species examined were nitrate, ammonium and phosphate, and trace metals included aluminum, titanium, vanadium, chromium, manganese, iron, cobalt, nickel, copper, zinc, cadmium, antimony, and lead. Aerosol samples were leached with deionized water to estimate the fluxes of soluble nutrients and trace metals, and acid digestions of aerosol samples were performed to estimate the total fluxes of trace metals and their fractional solubility. Wet deposition was the dominant deposition mode for nutrients accounting for 47 %, 78 %, and 80 % of the total (wet+dry) deposition of soluble nitrate, ammonium and phosphate, respectively. The average fractional solubility of the aerosol iron fine fraction ranged from 5.5-7.3 %, whereas that of the coarse fraction ranged from 1.5-2.5 %. These values were higher than typically reported for mineral dust and suggest anthropogenic aerosol inputs. Wet deposition was the dominant deposition mode for chromium, nickel, and cadmium, whereas dry deposition was the dominant deposition mode for all other trace metals.

Wet and dry deposition samples were also collected during a cruise in the Mid-Atlantic Bight during summer 2014. Results obtained from shipboard aerosol and rain samples suggest that atmospheric

deposition of trace metals at the land-based station is generally comparable to that of adjacent coastal waters. However, nutrient data for shipboard aerosol samples reveal major differences from the land-based station, as the mean dry deposition of nitrate was three times greater than that for ammonium, whereas the dry deposition of nitrate and ammonium were roughly equal at the land-based station.

This thesis is dedicated to my family and friends.

ACKNOWLEDGEMENTS

I am grateful for the guidance offered by my committee throughout the completion of this research project. I would specifically like to thank my advisors, Dr. Peter Sedwick and Dr. Margaret Mulholland, for their patience and untiring efforts to improve this thesis. I would like to thank Bettina Sohst for teaching me trace metal clean laboratory techniques, providing assistance and guidance with experiments, and for analyzing all ICP-MS samples. I thank Peter Bernhardt who ran nutrient samples and would like to acknowledge Brittany Widner who conducted ammonium analysis for cruise samples and who taught me the method for ammonium analysis. I extend thanks to Dr. John Klinck for running the empirical orthogonal function analysis for the trace metal data and for guidance with data interpretation. I would like to thank Dr. Gregory Cutter and Dr. Richard Zimmerman for allowing me to use instruments in their laboratories, as well as Lisa Oswald and Zoe Wambaugh for their assistance with instrument troubleshooting. I thank personnel at the Anheuser-Busch Coastal Research Center for assisting with the installation and monitoring of instruments at the land-based field station, the captain and crew of the R/V *Hugh R. Sharp*, and all DANCE cruise participants. Finally, this research would not have been possible without the financial support of the National Science Foundation.

TABLE OF CONTENTS

Page

Page

LIST OF TABLES

Table Page

LIST OF FIGURES

Figure Page

Figure Page

Figure Page

Figure Page

Figure Page

Figure Page

CHAPTER 1
INTRODUCTION

The major nutrients nitrogen (N) and phosphorous (P), as well as the micronutrient iron (Fe), are necessary for primary production [Paerl et al, 2002; Jickells et al., 2005; Paytan et al., 2009; Okin et al. 2011], and the concentrations of bioavailable forms of these nutrients may limit marine productivity, particularly in regions that do not receive nutrient additions from continental runoff, groundwater discharge or upwelling [Duce and Tindale, 1991; Mackey et al., 2015]. Atmospheric deposition has been recognized as an important source of N, P, and Fe to the remote ocean [Jickells et al., 2005; Baker et al, 2006a, 2006b; Duce et al., 2008, Krishnamurthy et al., 2010; Martino et al., 2014], where it can contribute significantly to primary production [Jickells et al., 2005; Duce et al., 2008, Krishnamurthy et al., 2010; Martino et al., 2014]. Therefore N, P, and Fe must all be considered when examining the potential influence of atmospheric deposition on marine primary productivity [Baker et al., 2003; Okin et al., 2011], and ocean carbon storage [Boyd et al., 2000; Okin et al., 2011; Wang et al., 2015a; Jickells et al., 2017]

The high nutrient low chlorophyll (HNLC) regions of the Southern Ocean, the equatorial Pacific Ocean, and subarctic Pacific Ocean account for more than 20% of the world's oceans [Martin et al., 1994], and primary production within these regions is thought to be limited by the availability of dissolved Fe [Martin and Fitzwater, 1988; Martin et al., 1994; Coale et al., 1996; Boyd et al., 2000, 2004; Coale et al., 2004; Mahowald et al., 2005; Baker et al., 2013]. This Fe limitation results in low algal abundance and a surplus of the macronutrients nitrate (NO_3^-), phosphate (PO_4^{3-}), and silicic acid (H_4SiO_4) in surface waters [Martin and Fitzwater, 1988; Jickells et al., 2005; Winton et al., 2015]. Most of the HNLC regions are rich in macronutrients, which are supplied through upwelling (e.g., the Southern Ocean) [Martin 1990; Falkowski et al., 1998; Boyd et al., 2000; Franck et al., 2003; Eldridge et al., 2004; Moore et al., 2013]. A major source of Fe to the open ocean, including these HNLC regions, is aeolian dust transported from the arid regions of North Africa, central Asia, Australia, the Arabian Peninsula,

China, and North America [Duce and Tindale, 1991; Gao et al., 2001; Mahowald et al., 2005; Li et al., 2008; Mahowald et al., 2008]. Iron-rich dust deposition is thought to stimulate primary production, macronutrient uptake, and carbon dioxide (CO_2) drawdown in HNLC regions [Coale et al., 1996, Boyd et al., 2000; Coale et al., 2004; Mahowald et al., 2005].

Due to its proximity to the arid Saharan and Sahel regions of North Africa, the North Atlantic Ocean receives ~43% (193.5 Tg yr^{-1}) of the total dust deposition to the world's oceans, which exceeds that received by any other individual ocean basin [Prospero at al., 1996; Jickells et al., 2005]. Dust deposition to the North Pacific and South Atlantic oceans is significantly lower at 15% and 4% of the total global atmospheric dust deposition, respectively [Jickells et al., 2005]. The North Atlantic Ocean receives inputs of Fe-rich Saharan dust, which enhances rates of dinitrogen (N_2) fixation by diazotrophic organisms [Capone et al., 1997; Galloway et al., 2003; Duce et al., 2008; Okin et al., 2011; Ratten et al., 2015] within the subtropical gyre, thereby reducing N-limitation and causing bioavailable inorganic P to become depleted before N [Wu et al., 2000; Moore et al., 2009; Martino et al., 2014; Schlosser et al., 2014]. Although dissolved organic P accounts for a significant fraction of the total dissolved P [Kolowith et al., 2001; Björkman et al., 2003; Mather et al., 2008], the bioavailability of this nutrient pool remains uncertain [Zamora et al., 2013; Karl and Björkman, 2014]. In contrast to the North Atlantic, the North Pacific subtropical gyre receives lower aeolian Fe inputs, which support lower rates of N_2 fixation and restricts removal of available inorganic P [Wu et al., 2000; Moore et al., 2009; Martino et al., 2014; Schlosser et al., 2014]. In summary, primary production in the North Atlantic subtropical gyre is thought to be subjected to greater P-limitation than the North Pacific subtropical gyre, which is presumed to be mainly N-limited.

The atmosphere is a major pathway by which nutrients and trace metals are transferred from the continents to surface waters in coastal and open ocean regions [Prospero et al., 1996; Paerl et al., 1999; Ridame and Guieu, 2002; Galloway et al., 2004; Doney et al., 2007; Galloway et al., 2008; Kim et al., 2014]. In addition, atmospheric deposition is thought to be an important source of nutrients and trace metals to coastal waters that become oligotrophic during the summer months. One such region is the Mid-

Atlantic Bight (MAB), which stretches from Nantucket, Massachusetts to Cape Hatteras, North Carolina. In the MAB, primary production is at a maximum during the spring bloom [Fennel et al., 2006]. The MAB region is characteristically N-limited and, during the summer, the water column is thermally stratified and surface waters are nutrient deplete [Houghton et al., 1982; Lentz et al., 2003; Fennel et al., 2006; Castelao et al., 2010]. This N-limitation results in lowered chlorophyll levels compared to spring [Fennel et al., 2006].

Atmospherically transported macronutrients and micronutrients enter the water column either through dry (direct) deposition of aerosols or by wet (rain out) deposition during which precipitation scavenges substances present in the atmosphere [Chester et al., 1999; Paerl et al., 2002; Jickells et al., 2005; Baker et al., 2007; Aneja et al., 2008; Rojas and Venegas, 2010; Jickells and Moore, 2015]. Dry deposition can be separated further by the size of the aerosol particles. Generally, coarse aerosol particles (>1 μm) are mechanically generated (e.g., mineral dust, sea spray), while fine particles (<1 μm) are produced in the atmosphere by gas to particle conversion processes [Spokes et al., 2001; Baker et al., 2007; Baker and Croot, 2010]. Atmospherically transported macronutrients and micronutrients can be deposited great distances from their source regions [Mahowald et al., 2005; Jickells & Moore, 2015], with the size of the particle determining the distance from the source it is transported. Smaller particles have lower deposition velocities and can experience long range transport, whereas coarser particles have higher deposition velocities and are more likely to be deposited closer to the source [Mahowald et al., 2005].

Nitrogen compounds may be grouped as reactive or unreactive [Galloway et al., 2003]. Although ~78% of the atmosphere is dinitrogen (N_2), this form of N is unreactive and only available to organisms that can "fix" N_2 [Capone et al., 1997; Galloway et al., 2003; Duce et al., 2008; Okin et al., 2011; Ratten et al., 2015]. Most marine organisms can only use reactive N (fixed N, N_r), and therefore photosynthetic organisms unable to "fix" N_2 rely on new N_r supplied to the surface ocean through upwelling, groundwater discharge, riverine input, atmospheric deposition, and N_2 fixation [Capone et al., 1997, Pearl 1997; Capone et al., 2005; Jickells et al., 2017], or on regenerated N produced by organic matter remineralization [Paerl, 1997; Jickells et al., 2017]. Lightning and marine biological nitrogen fixation

(BNF) are the two natural processes by which N_r is produced [Galloway et al., 1995; Prospero et al., 1996; Falkowski et al., 1997; Russell et al., 1998], and account for 5 Tg N_r yr^{-1} and 125 Tg N_r yr^{-1}, respectively [Fowler et al., 2013]. Biological nitrogen fixation can alleviate N_r limitation, but requires both Fe and P [Okin et al., 2011; Martino et al., 2015], therefore atmospheric Fe may stimulate N_2 fixation and increase rates of primary production in oligotrophic waters if P is available [Baker et al., 2003; Mills et al., 2004; Baker and Croot, 2010; Fernandez et al., 2010; Martino et al., 2015].

Increased anthropogenic activities over the last 150 years have led to major changes in the global N cycle [Baker et al., 2010], as humans currently convert unreactive N_2 to N_r at roughly the same rate as BNF [Spokes and Jickells, 2005; Jickells et al., 2017]. The most recent estimate for the global marine N_2-fixation rate, based on direct measurements, is 177 Tg N yr^{-1} [Grosskopf et al., 2012]. Anthropogenic production of N_r increased from 15 Tg N yr^{-1} in 1860 to 156 Tg N yr^{-1} in 1995, then to 187 Tg N yr^{-1} in 2005 [Galloway et al., 2008], and now currently stands at more than 210 Tg N yr^{-1} [Fowler et al., 2013; Galloway et al., 2013; Fowler et al., 2015]. Atmospheric input of N_r to the oceans (67 Tg yr^{-1}) is approximately equal to riverine input, which is estimated to be 50 to 80 Tg yr^{-1} [Duce et al., 2008], and is derived mainly from emissions produced during agricultural activities and combustion processes [Pearl et al., 1997; Cornell et al., 2003; Martino et al., 2014].

The atmospheric N_r includes inorganic oxidized N (nitric acid, HNO_3; nitrogen dioxide, NO_2; nitrate, NO_3^-; and nitrogen oxides, $NO_x = NO + NO_2$) [Paerl et al., 1997, 2002; Galloway et al., 2003; Whitall et al., 2003; Galloway et al., 2004; Krishnamurthy et al., 2007; Galloway et al., 2013], inorganic reduced N (ammonia, NH_3, and ammonium, NH_4^+) [Prospero et al., 1996; Galloway et al., 2003, 2004; Li et al., 2016], and organic N compounds (urea, amines, proteins, and nucleic acids) [Cowling et al., 2003; Galloway et al., 2003; Whitall et al., 2003; Galloway et al., 2004]. Nitrate supplied to coastal waters through riverine input is estimated to be 40 to 70 Tg N yr^{-1}, whereas input from atmospheric deposition is almost equal at 30 Tg N yr^{-1} [van Vuuren et al., 2011; Fowler et al., 2013]. Inorganic species of N are known to be water-soluble, and therefore all forms are efficiently removed from the atmosphere by wet deposition [Paerl et al., 2002].

The three most important N_r species released into the atmosphere from anthropogenic activities are nitrous oxide (N_2O), NO_x, and NH_3 [Cornell et al., 2003; Duce et al., 2008; van Vuuren et al., 2011; Fowler et al., 2013]. Nitric oxide emissions are released into the atmosphere from soils, plants, animal waste, and lightning, and are produced during combustion processes, including fossil fuel combustion from vehicles and industry, and biomass burning [Ayars and Gao, 2007], along with N_2O [Jickells et al., 2005; Rojas and Venegas, 2010; van Vuuren et al., 2011; Li et al., 2016]. These N_r species are primarily of anthropogenic origin and have atmospheric residence times of ~1 week [Cornell et al., 2003; Hagens et al., 2014]. Nitrogen oxides (NO and NO_2) undergo long-range transport and are deposited mainly in coastal regions downwind of the terrestrial source regions [Cornell et al., 2003; Spokes et al., 2005; Hagens et al., 2014] or in regions of intensive shipping [Corbett et al., 1999; Eyring et al., 2005, 2007]. Once in the atmosphere, NO_x is oxidized to HNO_3 within ~1 day or less [Li et al., 2016], and gaseous HNO_3 may either be directly (wet or dry) deposited [de Leeuw et al., 2003; Galloway et al., 2003] or react with alkaline aerosols, such as NH_3 or calcium carbonate, to form aerosols which later are wet or dry deposited [Spokes et al., 2000; Galloway et al., 2003; Jickells et al., 2005; Li et al., 2014, 2016]. The dry deposition velocity of gaseous HNO_3 is larger than that for particulate NO_3^-, therefore the formation of aerosol NO_3^- increases the atmospheric residence time of NO_3^- [de Leeuw et al., 2003; Li et al., 2014]. Nitrate in precipitation can result from the dissolution of gaseous HNO_3, which originates mainly from NO_x emissions [Russell et al., 1998]. Nitric acid (gaseous) may react with soil dust or coarse sea salt (equation 1) [Raes et al., 2000; Spokes et al., 2000; de Leeuw et al., 2001, Baker et al., 2006b; Baker and Croot, 2010] when marine and continental air masses mix, which causes aerosol NO_3^- to shift from the fine aerosol size fraction to the coarse fraction in the marine environment [Pearl et al., 2002; Spokes et al., 2000, 2005; Baker et al., 2006b; Li et al., 2016]. The particles formed by this reaction are larger and therefore are more efficiently removed from the atmosphere by wet and dry deposition processes [Spokes et al., 2000; Spokes and Jickells, 2005].

$$NaCl\ (s) + HNO_3\ (g) \rightarrow HCl\ (g) + NaNO_3\ (s) \quad (1)$$

Aerosol NH_3 originates mainly from animal husbandry and fertilizer application [Bouwman et al., 1997; Aneja et al., 2001; Paerl et al., 2002; Hagens et al., 2014], but can also be released from biomass burning, terrestrial soils, emissions from waste, industrial processes, and as losses from oceans [Russell et al., 1998; van Vuuren et al., 2011]. Ammonia gas that is not deposited or scavenged is converted to particulate NH_4^+ [Walker et al., 2000; Baek and Aneja, 2004]. Atmospheric gaseous NH_3 can react with gaseous HNO_3, sulfuric acid (H_2SO_4), and hydrochloric acid (HCl) to form NH_4^+ aerosols including ammonium nitrate (NH_4NO_3), ammonium sulfate ($(NH_4)_2SO_4$), ammonium bisulfate (NH_4HSO_4) (equations 2, 3, and 4) [Baek and Aneja, 2004; Rojas and Venegas, 2009], and ammonium chloride (NH_4Cl) [Cornell et al., 2003; Baek and Aneja, 2004; Aneja et al., 2008; Rojas and Venegas, 2010; Li et al., 2016].

$$NH_3\,(g) + HNO_3\,(g) \rightarrow NH_4NO_3\,(s) \text{ or } (l) \quad (2)$$

$$NH_3\,(g) + H_2SO_4\,(l) \rightarrow NH_4HSO_4\,(l) \quad (3)$$

$$NH_3\,(g) + NH_4HSO_4\,(aq) \rightarrow (NH_4)_2SO_4\,(s) \text{ or } (l) \quad (4)$$

These NH_4^+ aerosols are fine particles [de Leeuw et al., 2001; Paerl et al., 2002; Li et al., 2014, 2016] with aerodynamic diameters < 2.5 μM [Aneja et al., 2008], have relatively longer atmospheric residence times (5-10 days) than NH_3 (0.5 hours to 5 days), and, unlike NH_3, are capable of long-range transport [Walker et al., 2000; Aneja et al., 2001; Baek and Aneja, 2004]. The formation of NH_4NO_3 and NH_4Cl aerosols is reversible as these aerosols can dissociate as HNO_3, HCl, and NH_3 [Spokes et al., 2005]. Ammonia reacts with H_2SO_4, in preference to HNO_3 [Spokes et al., 2005], to form $NH_4SO_4^-$ and $(NH_4)_2SO_4$ [Baek and Aneja, 2004]. The formation of NH_4^+ aerosols is dependent on the concentration of strong acids (HNO_3, H_2SO_4 or HCl) and the water vapor content of the atmosphere [Walker et al., 2000; Baek and Aneja, 2004; Aneja et al., 2008]. An increase in relative humidity increases the liquid water content of atmospheric particulate matter and, consequently, enhances the ability of aerosols to absorb gaseous H_2SO_4 and HNO_3 [Baek and Aneja, 2004]. Atmospheric NO_3^- and NH_4^+ are reactive and bioavailable (soluble) [Jickells and Moore, 2015], and the scavenging of gaseous HNO_3 and NH_3, and particulate NO_3^- and NH_4^+, produces wet deposition containing soluble NH_4^+ and NO_3^- [Russell et al.,

1998; Li et al., 2016]. All forms of inorganic N are water-soluble [Paerl et al., 2002], and atmospheric N_r species can be present as aerosols (or liquid droplets) and gaseous compounds [Li et al., 2016]. Anthropogenic emissions of oxidized N, from high combustion processes, and reduced N emissions, mainly from agriculture, control the atmospheric N_r inventory [Jickells and Moore, 2015].

Globally, agricultural activities have played a significant role in the release of NH_3 emissions with approximately 54 Tg N emitted annually [Bouwman et al., 1997] of which ~40% [32 Tg N] is attributed to domestic animals [Stephen and Aneja, 2008]. The atmospheric residence time of NH_3 released from animal waste treatment lagoons, livestock housing, and agricultural fields is relatively short (~1-5 days) [Aneja et al., 2001], therefore NH_3 is likely to be wet or dry deposited near the source [Stephen and Aneja, 2008]. Agricultural activity in the United States (U.S.) southeast is thought to have a considerable influence on the atmospheric deposition of nutrients, particularly NH_3, to coastal waters of the western North Atlantic Ocean [Paerl et al., 1997]. The southeastern states, including Alabama, Arkansas, Delaware, Florida, Georgia, Louisiana, Maryland, Mississippi, North Carolina, South Carolina, and Virginia, account for only 12% of the total U.S. land area, however, crop and livestock sales for this region amount to 18% of the total sales for the U.S. [U.S. Department of Agriculture, 1999; Franzluebbers et al., 2005]. Broiler poultry production is highly concentrated in the southeast and southcentral U.S., which account for >85% of the broiler meat supplied nationwide [Paudel and McIntosh, 2005]. Swine production in North Carolina has remained among the highest in the nation in recent years and a recent census ranks this state as the second largest swine producer in the U.S. [U.S. Department of Agriculture, 2014]. Agricultural activity in the U.S. southeast and surrounding states, including broiler and swine production, and crop related management (soil tillage and fertilizer application), is thought to influence nutrient input in coastal waters within the MAB region [Paerl et al., 1997, 1998].

The agricultural soils of the southeastern U.S. are eroded, compacted, and have low pH and organic matter, as a result from continuous row crop agriculture involving soil tillage and inorganic fertilizer application [Adeli et al., 2017]. Due to its abundance, poultry litter is applied to crop fields of

this region to increase soil organic matter, replenish nutrients, and improve soil fertility [Edwards and Daniel, 1992; Adeli et al., 2017]. This is the most common use of this waste product [Paudel and McIntosh, 2005], and in the U.S. accounts for 35-45% of NH_3 emissions due to livestock production [Gay and Knowlton, 2005]. Urea and uric acid in animal waste may be converted to either NH_4^+ under acidic or neutral pH conditions or NH_3 under higher pH conditions [Bouwman et al., 1997; Gay and Knowlton, 2005]. The later pathway represents the more important source of atmospheric NH_3 emissions [Bouwman et al., 1997]. Several factors, including the concentration of manure NH_3 and urea, temperature, air velocity, surface area, and moisture, influence the rate of NH_3 volatilization [Gay and Knowlton, 2005; El Kader et al., 2007].

The majority of atmospheric N_r is inorganic, as organic N (ON) accounts for only ~25% of the total global N deposition [Cornell et al., 2003; Duce et al., 2008; Cornell et al., 2011; Jickells et al., 2013; Kanakidou et al., 2016], and not all of this ON is bioavailable [Peierls and Paerl, 1997; Seitzinger et al., 1999; Cornell et al., 2003; Spokes and Jickells, 2005; Cornell et al., 2011]. Atmospheric ON is not always measured in studies and sources are not well understood [Russell et al., 1998; Keene et al., 2002; Whitall et al., 2003; Jickells et al., 2013, 2016]. Organic N in wet and dry deposition is produced from reactions of gas phase species and mechanical processes [Prospero et al., 1996] with coarse mode particles (> 1 μm) being associated with soil dust and sea spray, whereas fine particles (<1 μm) tend to have gas-phase precursors [Jickells et al., 2013]. Organic N was not measured in this thesis and is not discussed further, although it merits future study.

Primary production in marine environments may be limited or co-limited by P availability [Wu et al., 2000; Mills et al., 2004; Nenes et al., 2011]. Phosphorus is a component of natural waters, soil, sediments, and the atmosphere, exists in both dissolved and particulate forms, and can be organic or inorganic [Violaki et al., 2017]. Atmospheric P originates from mineral dust, biomass and fossil fuel combustion, sea spray, and volcanic ash, and is present predominantly in the particulate phase [Mahowald et al., 2008; Baker et al., 2010; Vet et al., 2014; Wang et al., 2015b]. The dominant source of new P to the open ocean is atmospherically transported soil-derived dust [Jickells, 2005; Krishnamurthy et al., 2010;

Nenes et al., 2011; Zamora et al., 2013]. These dust particles occur mainly as apatite minerals and P-containing iron hydroxide minerals, and are very insoluble under alkaline and oxygenated conditions [Atlas and Pytkowicz, 1997; Anderson et al., 2010; Nenes et al., 2011]. Aeolian P can further be divided into inorganic and organic particles. Inorganic P in seawater exists mainly as orthophosphate (PO_4^{3-} and HPO_4^{2-}), pyrophosphate ($P_2O_7^{4-}$), and other condensed cyclic (metaphosphate) and linear (polyphosphate) polymers [Karl and Björkman, 2014]. Organic P includes monomeric and polymeric esters, phosphonate, and organic condensed phosphates [Karl and Björkman, 2014], and is likely partly biologically available [Mahowald et al., 2008; Mahaffey et al., 2014].

Past studies have found atmospheric deposition in the Atlantic to be strongly deficient in P, versus N, relative to phytoplankton nutrient requirements [Baker et al., 2003, 2010; Zamora et al., 2013]. Using measurements of P concentrations in various fuels and estimates of partitioning during combustion, Wang et al. [2015b] calculated the global combustion-related emissions of P to be 1.8 Tg yr^{-1}, which accounts for more than 50% of the global atmospheric sources of P. Model predictions for their study indicated that the total global emissions of P to the atmosphere is 3.5 Tg yr^{-1} of which 2.7 Tg yr^{-1} is deposited over the land and 0.8 Tg yr^{-1} is deposited over the oceans [Wang et al., 2015b]. For both wet and dry atmospheric deposition, the molar ratio of inorganic N to P has been found to exceed the Redfield ratio (16:1) [Baker et al., 2003, 2010], resulting in a system that is P deficient relative to phytoplankton nutrient requirements [Baker et al., 2003].

Iron is required by marine organisms for cellular processes such as photosynthesis, respiration, and N_2-fixation [Jickells et al., 2005; Baker and Croot, 2010], but its concentration in the surface open ocean is often low (<1 nM), due to its low solubility in oxic seawater [Mendez et al., 2010]. Present reported water solubilities for Fe in aerosols fall within the range of 0.001 to 90% [Boyd et al., 2010], and the true effective solubility remains unknown, but is likely influenced by aerosol chemical composition and nature of the source (e.g., Saharan vs anthropogenic) [Sedwick et al., 2007; Sholkovitz et al., 2009, 2012; Wozniak et al., 2015]. Desert dust is the dominant source of Fe atmospherically transported to the open ocean [Fung et al., 2000]. However, mineral aerosols are very insoluble [Fung et al., 2000]

compared to those produced anthropogenically, thus research has been focused on determining the proportion of atmospheric Fe emissions that is bioavailable. Past studies have found that the fractional solubility of anthropogenic aerosols produced by combustion processes is 1-2 orders of magnitude greater than that for Saharan dust [Sedwick et al., 2007; Sholkovitz et al., 2009; Buck et al., 2010]. Although anthropogenic emissions of Fe account for only ~5% of the total global aerosol emissions over the open ocean, they may comprise 20-100% of the total soluble Fe [Luo et al., 2008; Buck et al., 2010], and therefore provide an important source of bioavailable Fe and thus play a significant role in stimulating primary production in open ocean regions [Wozniak et al., 2015]. In contrast, the water solubility of Fe in desert dust averages ~1% [Sholkovitz et al., 2012].

In addition to N, P, and Fe, marine phytoplankton also require several trace metals for growth including manganese (Mn), cobalt (Co), nickel (Ni), copper (Cu), and zinc (Zn) [Bruland et al., 1991, Morel and Price, 2003; Ho et al., 2013]. These elements are key components of enzymes present in marine phytoplankton and bacteria [Mackey et al., 2014; Jickells and Moore, 2015], and can influence oceanic primary production and community structure [Paytan et al., 2009], as a deficiency in these metals may limit primary production, although an excess may be toxic to plankton [Bruland et al., 1991]. For example, Cu is required by phytoplankton at low concentrations, but at high concentrations becomes toxic [Paytan et al., 2009; Jordi et al., 2012]. Anthropogenically derived trace metals tend to be elevated in the fine aerosol size fraction, as a result of high-temperature combustion processes [Spokes et al., 2001]. As seen with Fe, the solubility of other trace metals depends on the nature of the source (e.g., crustal versus anthropogenic), as trace metals in mineral particles have been found to be less water-soluble than those produced from anthropogenic sources [Jickells et al., 1999; Paytan et al., 2009; Mackey et al., 2015]. Sholkovitz et al. [2010] reported fractional solubilities of 1-7% for Cu present in Saharan dust over the Sargasso Sea and Bermuda, whereas Paytan et al. [2009] report a Cu solubility of 40% for anthropogenic aerosols. Manganese is found in metalloproteins such as superoxide dismutase, arginase, and phosphotransferases [Buck et al., 2013]. Atmospheric deposition has been identified as a major source of

this element to the surface ocean, where concentrations of Mn are relatively high (compared to Fe) due to slow oxidation kinetics and photoreduction [Mendez et al., 2010].

Past studies conducted at land-based field stations on the U.S. east coast have provided background information on the atmospheric deposition of nutrients and trace metals to the adjacent North Atlantic Ocean. Shipboard bioassay experiments conducted using rainwater and synthetic nutrient additions (N, P, Fe) were found to stimulate net increases in chlorophyll concentrations, illustrating the potential influence of atmospheric deposition on primary productivity in coastal and offshore waters [e.g., Paerl et al., 1999; Sedwick et al., 2018]. Kim et al. [2000] examined trace metals in wet deposition samples collected at Lewes, Delaware and Still Pond, Maryland, and found Al and Fe to be of crustal origin, while Cr, Mn, Pb, Cu, and Ni were primarily enriched in anthropogenic emissions at both sites. Conko et al. [2004] examined wet deposition of trace elements in the developed and densely populated suburban area in Reston, Virginia, while other studies examined wet deposition to the North Atlantic Ocean using field stations in remote locations away from urban contamination, allowing them to provide a regional assessment of trace metal deposition [Scudlark et al., 1994; Kim et al., 2000]. Gao et al. [2016] compared wet and dry deposition of trace metals from northern coastal New Jersey, a heavily polluted environment, and southern coastal New Jersey, a rural environment, and found wet deposition to be dominant deposition mode for most trace metals, including Zn, V, Sb, Pb, Ni, Cu, Co, and Cd, while dry deposition was the dominant deposition mode for Al and Fe, which occurred predominantly as coarse particles.

Although studies have been conducted on the U.S. east coast to estimate the atmospheric deposition of nutrients and trace metals to the North Atlantic, these studies were typically conducted over select seasons or months. There is need to provide a more comprehensive data set for the wet and dry atmospheric deposition of nutrients and trace metals to the ocean waters in the southern MAB, during a continuous sampling year, to understand seasonal trends and variability. In this thesis, data from a one-year time series study (May 2014 - June 2015) of wet and dry atmospheric deposition of nutrients and trace metals obtained from a rural, land-based field station on the Eastern Shore of Virginia are presented.

The wet and dry deposition data collected at this field station were compared to those for offshore ocean samples collected during a 2-week cruise to the coastal North Atlantic during summer 2014, to assess any offshore attenuation of nutrients and trace metals deposition. The macronutrient species examined were NO_3^-, NH_4^+, and PO_4^{3-}. Trace metal analyses included aluminum (Al), titanium (Ti), vanadium (V), chromium (Cr), Mn, Fe, Co, Ni, Cu, Zn, Cd, antimony (Sb), and lead (Pb). Data obtained were used to answer the following questions:

1. How does the atmospheric deposition (wet and dry) of nutrients and trace metals to coastal waters in the MAB vary seasonally?
2. What is the dominant deposition mode (wet versus dry) of nutrients and trace metals to the coastal MAB over the annual cycle?
3. How do the dry fluxes of trace metals to the coastal MAB change relative to one another over time, that is, are there trace metals that exhibit the same temporal pattern suggesting a common aerosol source?
4. How representative are wet and dry fluxes of nutrients and trace metals from the coastal field station for deposition in offshore waters (beyond the continental shelf)?

Specifically, the data from this thesis will be used to test the following hypotheses:

Hypothesis 1: Atmospheric deposition of inorganic N species, particularly NO_3^-, will be greatest during the winter months due to increased fossil fuel combustion on the U.S. east coast.

Nitrate aerosol is derived mainly from NO_x species, which are produced by high-temperature combustion processes [Jickells et al., 2006; Li et al., 2016], and the production of NO_x on the U.S. east coast is expected to be greatest during the winter months due to increased fossil fuel consumption for residential space heating [Roberts-Semple et al., 2012]. Although summer cooling and winter heating are both responsible for observed peaks in annual energy consumption, residential space heating is responsible for a much greater proportion of the total annual residential energy than does air condition cooling [U.S. Energy Information Administration, 2012].

Hypothesis 2: The deposition of water-soluble Fe will be greatest for samples collected during the winter months, due the dominant presence of polluted North American air masses passing over Virginia's Eastern Shore.

Aerosols formed from the combustion of oil and other fossil fuels are typically associated with North American air masses, and anthropogenically produced aerosol Fe has been found to be more water-soluble than that in Saharan mineral dust [Fung et al., 2000; Sedwick et al., 2007; Luo et al., 2008; Sholkovitz et al., 2009, 2012; Buck et al., 2010; Sholkovitz et al., 2012]. Saharan mineral dust is transported westward across the North Atlantic by prevailing easterly winds [Jickells et al., 2005; Ussher et al., 2013], and sometimes north by the anticyclone over the Azores [Kaufman et al., 2005]. The seasonal migration of the Intertropical Convergence Zone (ITCZ) influences the latitudinal region of maximum dust transport [Shelley et al., 2017], as this zone shifts northwards from between 0° and 10°N during the Northern Hemisphere winter to between 10° and 20°N during the Northern Hemisphere summer [Moulin et al., 1997; Jickells, 1999; Barrett et al., 2012]. The northward migration of the ITCZ coupled with the occurrence of Bermuda-Azores high pressure systems causes the pulses of Saharan dust deposition observed in the western North Atlantic during the warmer months [Chen and Duce, 1983; Jickells, 1999; Tian et al., 2008]. In the winter months, North American (anthropogenically influenced) air masses are thought to dominate over the U.S. east coast [Duce and Hoffman, 1976; Chen and Duce, 1983; Sholkovitz et al., 2010], therefore it is expected that aerosol samples collected during these winter months will display higher solubilities of aerosol Fe.

Hypothesis 3: Aerosol Fe aqueous solubility (fractional solubility) will be significantly greater for fine mode (< 1 μm) aerosol particles than that for coarse mode (>1 μm) aerosol particles.

High-temperature combustion processes release trace metal emissions predominantly in the fine mode and reported fractional solubilities for Fe in anthropogenic aerosols are greater than those for mineral dust aerosols [Chuang et al., 2005; Sedwick et al., 2007; Sholkovitz et al., 2009, 2012; Buck et al., 2010].

Hypothesis 4: Groups of certain trace metals will show similar changes in deposition over the annual cycle, indicating a common source.

Atmospheric fluxes of trace metals which are produced by similar processes (natural or anthropogenic) should increase or decrease during the same periods of the time series. For example, Ti, Fe, Co, Mn, and Al are trace metals typically associated with crustal material [Scudlark et al., 1994; Wu et al., 1994; Chester et al., 1999; Spokes et al., 2001; Morel and Price, 2003; Jickells et al., 2016], and therefore an increase in these five elements, during the same time periods, would indicate that the air mass sampled was likely influenced by terrigenous dust. Trace metals are associated with several different aerosol sources [Chester et al., 1999; Jickells et al., 2016, 2017], with different elemental signatures [Jickells et al., 2017], and it is not likely that an aerosol source can be simply classified as completely "anthropogenic" or "crustal".

Hypothesis 5: Wet and dry fluxes of nutrients and trace metals estimated for the land-based field station on the Eastern Shore of Virginia are representative of deposition in offshore MAB waters (beyond the continental shelf).

Land-based measurements have shown that the magnitude of wet and dry deposition of nutrients and trace metals varies spatially and temporally [Scudlark et al., 1994; Kim et al., 2000; Spokes and Jickells, 2005; Gao et al., 2016]. Scientists have depended on land-based sampling sites to provide estimates of atmospheric deposition of nutrients and trace metals to adjacent near shore coastal and open ocean waters, because land-based measurements are more conducive to long-term sampling than shipboard campaigns. It has been shown that coastal land-based measurements for nutrients and trace metals are comparable to shipboard measurements in adjacent waters [e.g., Chester et al., 1993; Kane et al., 1994], therefore it is expected that the relative location and proximity of the Eastern Shore site, to shipboard sampling locations in the adjacent southern MAB, will yield representative atmospheric deposition estimates for offshore ocean waters.

CHAPTER 2
METHODS

2.1 AEROSOL AND RAIN SAMPLE COLLECTION

Aerosol and rainwater collectors were installed on a platform on a dock at The Anheuser-Busch Coastal Research Center (ABCRC) located in a rural, coastal area at Oyster on the Eastern Shore of Virginia (37.288°N, 75.925°W) (Figure 1). The ABCRC is owned and managed by the University of Virginia. Weekly composite samples were collected from 22 May 2014 through 17 June 2015. Aerosol and rainwater samples were also collected during a research cruise conducted aboard the R/V *Hugh R. Sharp* from 30 July to 15 August 2014, to compare the atmospheric deposition of nutrients and trace metals offshore to values estimated at ABCRC (Figure 1). During the time of the cruise, samples were not collected at the land-based station, and thus there is a discontinuity in the time series data set from 23 July through 20 August 2014. Aboard the R/V *Hugh R. Sharp*, samplers were mounted on a platform above the ship's wheelhouse as far away as possible from overhanging structures, masts or cables, and samples were only collected when the ship was steaming into the prevailing wind to avoid contamination from the ship's exhaust. The ship's speed was maintained at ~3 knots during atmospheric sample collection. To avoid contamination from the ship's exhaust, samples were collected only when the wind direction ranged from -90° to 90° relative to the ship's bow [Shi et al., 2013]. The relative wind speed during atmospheric deposition sample collection varied from ~2.8 to 42 knots, which was appropriate as previous cruises along the U.S. east coast suggest that relative winds with speeds greater than 1 m s^{-1} (~1.95 knots) ahead of the ship's beam provide samples that are representative of ambient aerosol concentrations [Keene et al., 2004]. The instruments were switched off if there was risk of contamination due to exhaust or sea spray.

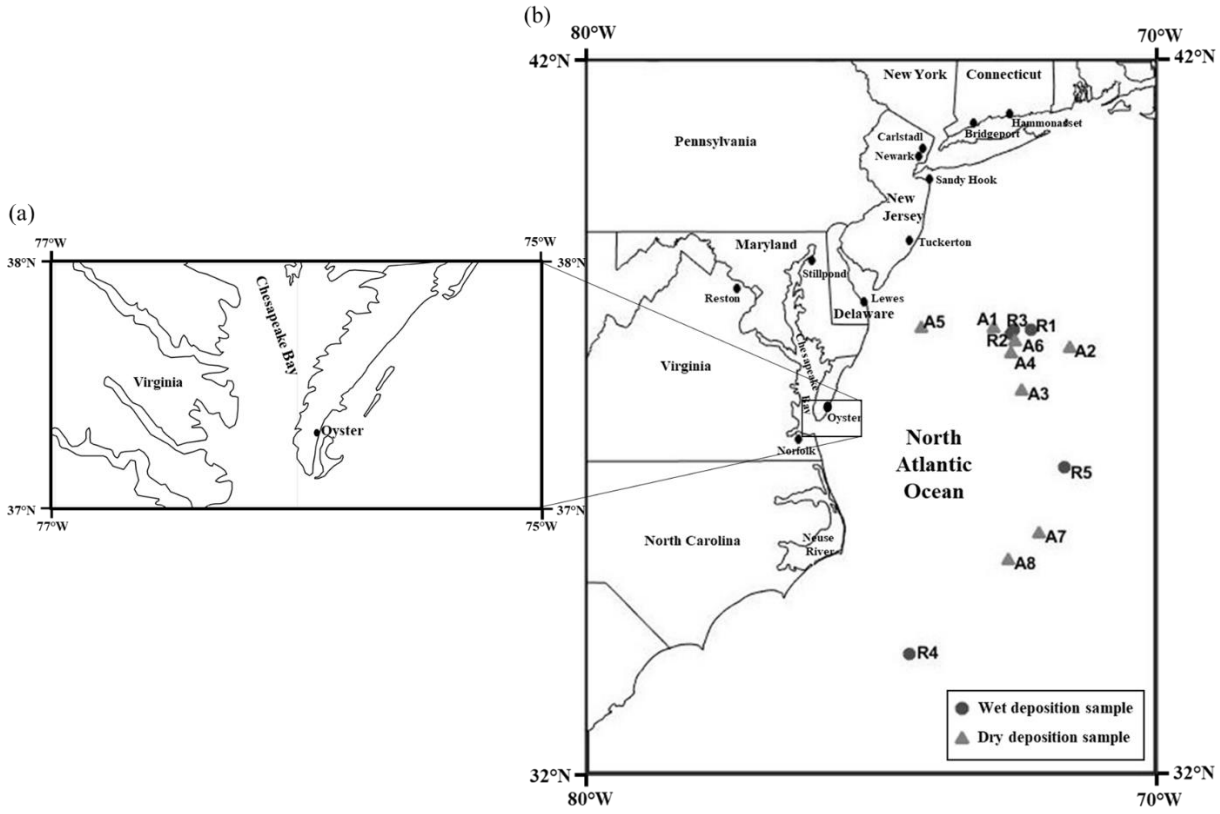

Figure 1 (a) Location of the Eastern Shore land-based field station at Oyster, Virginia (37.288°N, 75.925°W) and (b) offshore wet deposition (black circles) and aerosol (grey triangles) sampling sites (~200 km offshore). The locations of other land-based nutrient and trace metal atmospheric deposition study sites to which data from this study were compared are shown in (b).

2.2 AEROSOL SAMPLE COLLECTION AND PROCESSING

A high volume (air flow 1 m^3 min^{-1}) aerosol collector equipped with a 6-stage cascade impactor (Tisch Series 235) and configured for separation of fine (<1 µm) and coarse (>1 µm) aerosol fractions was used to collect aerosol samples. The cascade impactor was loaded with Whatman 41 cellulose filters which were cleaned using 0.1 N and 0.5 N hydrochloric acid (Fisher, trace metal grade) in a clean lab using a procedure adapted from Baker et al. [2006c]. Filters were pre-cleaned with acid to reduce trace metal blanks [Baker et al., 2006d; Morton et al., 2013]. Whatman 41 filters were used for this study as they are highly efficient at collecting aerosol particles [Morton et al., 2013] and can be easily divided into subsamples. Six cellulose filters (five 25 cm x 25 cm slotted filters; Tisch Environmental TE-230-WH

and one 8” x 10” backing filter; Tisch Environmental TE-241) were used for the collection of each aerosol sample. Aerosol samples were used to estimate the water-soluble and total (acid-soluble) dry deposition flux for each weekly composite sample, which were calculated using the water-soluble and total (acid-soluble) aerosol trace metal concentrations. For nutrients, only the water-soluble concentration and estimated water-soluble deposition flux was examined. Detailed descriptions of the methods for measuring water-soluble and acid-soluble trace metal concentrations are presented in Sections 2.2.1 and 2.2.2

All filter manipulations were conducted under a Class-100 laminar flow clean air bench using trace metal clean techniques. Each slotted filter came pre-cut with ten open slots, and the filters were staggered so that the strips of each filter were positioned directly beneath the slots of the overlying stage. After filters were loaded onto the cascade impactor, the entire filter assembly was placed in a clean polyethylene bag until installed in the aerosol sampler to avoid contamination of filter substrates. The uppermost four filters (stages 1 through 4) of the cascade impactor corresponded to the coarse (>1 μm) aerosol size fraction, and the fifth slotted filter (stage 5), along with the backing filter (stage 6), corresponded to the fine (<1 μm) aerosol size fraction. Air is pulled through the slots in each stage of the cascade impactor [Morton et al., 2013]. There is no loss of volume as the air is pulled through the impactor and the same volume of air is received by each stage [Morton et al., 2013]. The aerosol particles sort by size as particles with the largest aerodynamic diameter settle out first and are deposited on the slotted filter positioned beneath the uppermost stage, and the finest particles deposit on the backing filter as they can weave through the slots of all overlying stages of the cascade impactor. After the cascade impactor was installed in the aerosol sampler, the instrument was switched on and the pressure drop across the filters measured using a handheld digital manometer (Dwyer Series). The filter pressure drop was also recorded immediately prior to sample retrieval. Sample installation and retrieval times, as well as ambient temperature and barometric pressure, at the start and end of each sampling period were noted. Conversion tables provided with each Tisch Environmental aerosol sampler were used for calculating the air flow rate for each aerosol sample using the pressure drop ratio and temperature at the start and end of

each sampling period. The total air volume sampled and analyte concentrations (water-soluble and/or total) were used to calculate the dry deposition flux (water-soluble and/or total) for each sampling period. The average flow rate for each weekly sample was used for flux calculation purposes. A detailed description of the calculation of wet and dry deposition fluxes is provided in Section 2.6. Aerosol field blanks were collected by installing precleaned filters in the cascade impactor without turning the pump on. These filters were left in the sampler for a period representative of the sample collection time for the site (1 week for the land-based samples, 5 hours for shipboard samples). Separate aerosol filter field blanks were obtained for the land-based and shipboard samples. Baker et al. [2006a] have identified that this "exposure blank" may overestimate the field blanks, because the filters are susceptible to passive dry deposition that does not occur during sample collection.

2.2.1 PROCESSING FOR SOLUBLE AEROSOL SPECIES

Aerosol samples were processed under a small Class-100 laminar flow hood within hours of sample retrieval. Filter sub-samples for each aerosol size fraction (<1 μm and >1 μm) were each leached using 750 mL of 18.2 MΩ-cm resistivity deionized (Barnstead, Nanopure) water to obtain the operationally defined soluble fraction of aerosol constituents [Buck et al., 2006]. Poretics polycarbonate filter membranes (pore size 0.4 μm) were used for obtaining water-soluble leachate solutions of each aerosol size fraction. This operationally defined soluble fraction includes both dissolved Fe (truly soluble, < 0.02 μm) as well as colloidal Fe species (0.02 - 0.4 μm) that can pass through the 0.4 μm pore polycarbonate filter membrane. The use of ultrapure 18.2 MΩ-cm resistivity deionized (Barnstead, Nanopure) water in a flow-through leaching procedure provided a consistent leaching solution, unlike filtered seawater which may contain varying concentrations of dissolved Fe and Fe binding ligands, and therefore present inconsistencies in the procedure [Buck et al., 2006; Sedwick et al., 2007]. The use of this flow-through (rather than batch) procedure also reduced the possibility of saturation of the leaching solution with precipitated Fe hydroxides prior to leachate filtration [Buck et al., 2006]. The leaching procedure was performed separately for the fine and coarse aerosol size fractions, so that one 750 mL

leachate solution was obtained for each aerosol size fraction (<1 μm and >1 μm) for each sampling period.

One quarter of each filter was used for aerosol leaching, and the remaining three-quarters was stored in a vacuum desiccator for later acid digestions. Individual filters were folded inwards to protect aerosol deposits prior to being placed in a clean polyethylene bag for storage in the desiccator. The "active" area of each slotted filter (the portion of the filter containing aerosol deposits) consisted of ten bands of impacted aerosols. Nine of these bands were located between adjacent slots of the filter, while the tenth deposit band was located between the last slot on one end of the filter and the filter border. Morton et al. [2013] found this tenth band to contain approximately 75% of aerosols deposited on each of the other nine bands. Slotted filters were folded along the fifth deposit band at which they were cut, and the quarter of each slotted filter selected for aerosol leaching was obtained by dividing the half of the slotted filter that did not have the tenth band in two sections. The total mass of the water-soluble fraction of each nutrient and trace metal for each aerosol sample was obtained by multiplying the concentration of aerosol leachate solution by the volume of the leachate solution (750 mL), and by a factor of 4.158 for the fine (<1 μm) size fraction and 4.333 for the coarse (>1 μm) size fraction. The flux of the water-soluble fraction for each element was then calculated using the total mass, volume of air sampled, and estimated deposition velocity. These calculations are later described in Section 2.6.

A 47 mm diameter Savillex perfluoroalkoxy alkane (PFA) filter funnel assembly was used for leaching filters for each aerosol size fraction sample. The two filter assemblies were loaded with pre-cleaned 0.4 μm polycarbonate filters (Poretics) after which one quarter of each filter (slotted and/or backing) corresponding to the aerosol filter size fraction (<1 μm or >1 μm) was cut and placed in the designated Savillex filter funnel assembly. The 750 mL of 18.2 MΩ-cm resistivity deionized (Barnstead, Nanopure) water was then gradually added to the contents of the filter funnel assembly and the leachate for each aerosol filter size fraction was immediately transferred to an acid-cleaned 125 mL low-density polyethylene (LDPE) bottle (Nalgene). The aerosol leachate solutions were then acidified with 6N quartz distilled hydrochloric acid (Fisher, Optima) to 0.4% v/v, to decrease the likelihood of Fe and other trace

metals being lost from solution. Concentrations of dissolved trace metals (Al, Ti, V, Cr, Mn, Fe, Co, Ni, Cu, Zn, Cd, Sb, and Pb) were determined in aerosol leachate solutions for both aerosol size fractions using high resolution inductively coupled plasma-mass spectrometry (HR-ICP-MS, ThermoFisher Element-2). The procedure for HR-ICP-MS analysis is described further in Section 2.4. Unacidified aerosol leachate solution aliquots of approximately 45 mL were placed in 50 mL polypropylene Falcon tubes for nutrient analysis, and these tubes were kept frozen until analysis.

2.2.2 PROCESSING FOR TOTAL (ACID-SOLUBLE) AEROSOL SPECIES

The method applied for aerosol filter digestions was adapted from Morton et al. [2013]. Sections cut from aerosol filter samples were placed in PFA microwave digestion vessels (CEM HP-500), which were previously cleaned using Nalgene L-900 detergent (10% v/v), 1 N HCl (Fisher, trace metal grade), and 6 N HCl (Fisher, trace metal grade). All aerosol filter manipulation was conducted under a Class-100 laminar flow hood, and digestions were performed separately for the coarse and fine size fractions, so that one 20 mL digest solution was obtained for each aerosol size fraction for each sampling period. A 1 cm^2 strip was cut from the center of each slotted filter and a 3.21 cm^2 strip was cut from each backing filter. The "active" area (area covered with aerosol deposits) of filter types (slotted and backing) differed and these filter dimensions were selected so that the same multiplicative factor could be applied to calculations for aerosol digest solutions of both size fractions. Aerosol filter samples used for digestions were divided into the two size fractions using the same definitions followed for aerosol leaching in Section 2.2. For all microwave digestions, the control vessel contained a 3.21 cm^2 section of the backing filter and a 1 cm^2 section of a slotted filter collected on 22 May 2015, which was prepared new for each sample run. The sample collected on 22 May 2015 had a high aerosol loading and was assumed to be representative of all samples digested. It served as a means of monitoring temperature and pressure of the vessels during the microwave digestion but was not used for analyses.

A Microwave Accelerated Reaction System (MARS, CEM Corporation) was used for digesting samples. On the day prior to the microwave treatment, 3 mL concentrated nitric acid (Fisher, Optima) and

0.2 mL hydrogen peroxide (Fisher, Optima) were added to the contents of each microwave vessel. Vessels were loosely capped and allowed to vent under a clean lab fume hood overnight. On the day of the microwave treatment, an additional 3 mL concentrated nitric acid (Fisher, Optima), 3 mL concentrated hydrochloric acid (Fisher, Optima) and 0.8 mL concentrated hydrofluoric acid (Fisher, Optima) were added to each microwave vessel. Lids were placed loosely on the vessels, which were allowed to vent under a clean lab fume hood for approximately 30 minutes. Samples were then digested in the microwave for 30 minutes at a constant temperature of 180 ºC. The instrument ramp to temperature time was set to 10 minutes and the maximum pressure set at 350 psi. After the microwave treatment, samples were allowed to cool in the instrument overnight.

The day following the microwave treatment, vessels were returned to the clean-lab fume hood where digest solutions were transferred to 22 mL Savillex PFA vials. Microwave vessels and lids were rinsed 3 times with 18.2 MΩ-cm resistivity deionized water (Barnstead, Nanopure) to ensure efficient transfer of sample digest solutions. The PFA vials were then placed uncapped on a hotplate set at 140-150 ºC, and samples were dried down until only a single concentrated droplet remained. Following dry down, 5 mL of 1% nitric acid (Fisher, Optima) was added to each vial, which was then tightly capped and placed on a hotplate set at 130-140 ºC for 30 minutes. Vials were then removed from the heat and samples transferred to pre-weighed acid-cleaned 30 mL LDPE sample bottles. Each PFA vial was rinsed 3 times with 5 mL 1% nitric acid (Fisher, Optima) to obtain a total digest sample volume of 20 mL. The LDPE sample bottles were then re-weighed to estimate exact volumes. These digest solutions were analyzed using HR-ICP-MS (ThermoFisher Element-2) to determine total aerosol trace element loadings for Al, Ti, V, Cr, Mn, Fe, Co, Ni, Cu, Zn, Cd, Sb, and Pb in fine and coarse aerosol size fractions. Detailed descriptions of the calculation of the total aerosol mass and flux of each trace metal are presented in Section 2.6.

2.3 WET DEPOSITION SAMPLE COLLECTION AND PROCESSING

An N-Con Systems National Atmospheric Deposition Program (NADP) precipitation sampler (ADS 00-120) was used for weekly composite rainwater collection at the ABCRC. Two 2 L high-density polyethylene (HDPE) bottles were used for each sample collection with one bottle designated for collection of the trace metal sample and the other for the nutrient sample. Bottles used for trace-metal samples were rigorously cleaned with Nalgene L-900 detergent, 1 N hydrochloric acid (Fisher, trace-metal grade), and 6 N hydrochloric acid (Fisher, trace-metal grade) using trace-metal clean techniques, while those used for nutrient samples were cleaned using only Nalgene L-900 detergent (10% v/v) and 1 N hydrochloric acid (Fisher, trace metal grade). Approximately 0.4 g thymol (Sigma-Aldrich, grade: >99.5%) was placed in nutrient bottles prior to installation in the field to slow bacterial degradation of nutrient species [Gillet and Ayers, 1991]. Rainwater collection bottles were weighed prior to installation in the field and upon return to the laboratory to determine the mass of rainwater collected. Trace element rainwater samples were acidified to 0.4% (v/v) with quartz distilled 6 N hydrochloric acid (Fisher, Optima) [Tramontano et al., 1987] and were transferred to 125 mL acid washed LDPE sample bottles one week following acidification. The unfiltered rainwater samples were acidified to promote trace metal desorption [Tramontano et al., 1987] and dissolution of acid-labile particulate trace metals. Measured concentrations represent total-dissolvable (TD) trace metals (e.g., see Sedwick et al., 2007). Nutrient rainwater samples were stored in sterile 50 mL polypropylene Falcon tubes, which were kept frozen until analysis. Rainwater samples were then thawed and filtered using a 0.2 μm nylon filter (Fisherbrand) loaded onto a 50 mL polypropylene (BD, Luer-Lok) syringe to remove thymol and other particles prior to nutrient analysis. Aerosol total-dissolvable trace metal and water-soluble nutrient concentrations were determined using the methods described in Sections 2.4 and 2.5.

During the cruise, two different methods were employed for the collection of five rainwater samples. In the first method, two rain samples were collected using an automated N-Con Systems (NADP) rain sampler, and in the second method three samples were obtained using a trace metal clean large polyethylene funnel attached to a 2 L fluorinated HDPE bottle by a Teflon collar [Sarthou et al.,

2003; Croot et al., 2004; Sedwick et al., 2007; Baker et al., 2007, 2010]. The bottles used for rainwater sample collection during the cruise did not contain thymol, due to the relatively short period before freezing of samples. The rain collection funnel with attached sample bottle was mounted on top of the ship's wheelhouse, away from overhanging structures, during the onset of rain and removed immediately after rainfall ceased. The funnel and sample bottles used for rainwater collection were rinsed with 18.2 MΩ-cm resistivity deionized water (Barnstead, Nanopure) and stored in double sealed plastic bags between rain events. Trace metal clean 125 mL LDPE bottles were used to store rainwater samples for total-dissolvable (TD) metals. These samples were acidified to 0.4% (v/v) quartz distilled 6 N hydrochloric acid (Fisher, Optima) and were unfiltered. Five water-soluble nutrient and 3 total-dissolvable (TD) trace metal rainwater samples were collected. Rainwater nutrient samples were placed in 50 mL polypropylene Falcon tubes which were kept frozen until analysis. During the cruise, the field blanks for the N-Con systems sampler were obtained by installing a 2 L fluorinated HDPE rainwater sample bottle containing 1 L ultrapure 18.2 MΩ-cm resistivity deionized (Barnstead, Nanopure) water in the sampler where it remained for 1 hour. The lid of this sample bottle was removed, and the sampler switched off after the instrument cover returned to the closed position. The field blanks for the land-based samples collected with the N-Con systems sampler were obtained similarly, except two 2 L fluorinated HDPE bottles were deployed instead to provide a field blank for nutrient rainwater samples, which contained thymol (Sigma-Aldrich, grade: >99.5%). Thymol (0.4 g) (Sigma-Aldrich, grade: >99.5%) was added to the contents of the nutrient rainwater blank bottle prior to deployment in the sampler.

2.4 TRACE METAL ANALYSIS BY HR-ICP-MS

Concentrations of Al, Ti, V, Cr, Mn, Fe, Co, Ni, Cu, Zn, Cd, Sb, and Pb in rainwater, aerosol leachate, aerosol digest solutions, and field and method blanks, were determined using HR-ICP-MS (ThermoFisher Element-2). All sample and field blank processing was conducted under a Class-100 laminar flow hood using trace metal clean techniques. An external calibration curve was obtained to determine the likely range of sample concentrations. Separate calibration curves were obtained for land-

based and offshore samples, since these offshore samples were expected to have lower atmospheric trace metal loadings. For each external calibration curve, a sub-sample of 5 mL of 4-5 samples with expected high atmospheric trace metal loadings was used, and the results of these samples used to estimate appropriate standard concentrations for calibration curves.

A 5 mL aliquot of each sample was transferred to an acid-cleaned 15 mL polypropylene Falcon tube using a 5 mL Finnpipette with an attached acid-cleaned polyethylene tip. A 2 ppb indium (In) internal standard was added to each sample and standard vial used for rainwater, aerosol leachate, and aerosol digest solution analysis. The In added was used to monitor signal drift during ICP-MS analysis. Standard solutions were prepared using SPEX CertiPrep Claritas PPT standards with concentrations listed in Tables 1 and 2. The matrix used for standards for aerosol leachate and rainwater analysis was 0.4% (v/v) hydrochloric acid (Fisher, Optima), while that of aerosol digest solutions was 1% (v/v) nitric acid (Fisher, Optima).

Samples were run in order of expected elemental concentrations, with samples with the lowest anticipated concentrations being analyzed first. The instrument sample probe was rinsed with 18.2 MΩ-cm resistivity deionized water (Barnstead, Nanopure) before and after each sample, and analyte signal intensities were recorded in units of counts per second. The HR-ICP-MS first analyzed the matrix rinse (0.4% v/v) hydrochloric acid for aerosol leachate and rainwater samples, and 1% (v/v) nitric acid for aerosol digest solutions), then standards and samples. Elements analyzed at low resolution were Cd, Sb, and Pb, while those analyzed at medium resolution were Al, Ti, V, Cr, Mn, Fe, Co, Ni, Cu, and Zn.

To maintain accuracy, calibration checks were performed every 10 samples, and accepted if within ± 10 % agreement with previous values for each element (Tables 1 and 2). Detection limits for aerosol leachate solutions, rainwater, and aerosol digest solutions are listed in Table 3. All HR-ICP-MS detection limits were determined by averaging the standard deviation of the concentrations of zero standard (blanks) for a given element and then multiplying that average by three. This calculated value was then added to the overall average blank signal for that element to calculate the detection limit for that element, using an appropriate standard curve. The detection limits for trace metals in aerosol digest

solutions are much higher than those for rainwater and aerosol leachate samples because of the differences in the matrix used for standards and samples.

Table 1. Standard Concentrations for HR-ICP-MS analysis of rain and aerosol leachate samples (µg L^{-1}).

	Al	Ti	V	Cr	Mn	Fe	Co
Standard 0	0	0	0	0	0	0	0
Standard 1	1	0.1	0.1	0.025	0.4	0.1	0.01
Standard 2	5	0.2	0.5	0.05	1	1	0.02
Standard 3	20	0.5	2	0.1	3	10	0.05
Standard 4	40	1.5	2.5	0.2	5	30	0.1

	Ni	Cu	Zn	Cd	Sb	Pb
Standard 0	0	0	0	0	0	0
Standard 1	0.05	0.5	0.5	0.01	0.05	0.1
Standard 2	0.2	1	2	0.05	0.1	0.2
Standard 3	1	2	8	0.1	0.3	0.8
Standard 4	1.2	2.5	12	0.15	0.5	1.2

Table 2. Standard Concentrations for HR-ICP-MS analysis of aerosol digest samples (µg L^{-1}).

	Al	Ti	V	Cr	Mn	Fe	Co
Standard 0	0	0	0	0	0	0	0
Standard 1	100	10	1	1	3	100	0.1
Standard 2	300	30	3	3	6	200	0.3
Standard 3	500	50	5	5	10	400	0.5

	Ni	Cu	Zn	Cd	Sb	Pb
Standard 0	0	0	0	0	0	0
Standard 1	0.5	1	5	0.05	1	2
Standard 2	1	3	10	0.1	2	4
Standard 3	2	5	15	0.2	4	6

Table 3. Detection limits for HR-ICP-MS analysis of rain, aerosol leachate, and aerosol digest samples ($\mu g\ L^{-1}$).

Element	Detection limit (rain and aerosol leachate)	Detection limit (aerosol digests)
Al	0.12	4.3
Ti	0.051	0.28
V	0.008	0.029
Cr	0.013	0.035
Mn	0.011	0.12
Fe	0.032	2.9
Co	0.003	0.004
Ni	0.081	0.015
Cu	0.018	0.098
Zn	0.087	0.27
Cd	0.003	0.002
Sb	0.007	0.040
Pb	0.006	0.12

2.5 NUTRIENT ANALYSIS

Rain and aerosol leachate samples were analyzed for NO_3^-, NH_4^+, and PO_4^{3-}. Nitrate and PO_4^{3-} concentrations were determined using an Astoria Pacific nutrient auto-analyzer according to the manufacturer's specifications and using standard colorimetric methods [Parsons et al., 1984]. Ammonium was analyzed fluorometrically using the orthophthaldialdehyde (OPA) method [Holmes et al., 1999] applying the modifications in Taylor et al. [2007]. For this method, 15 mL polypropylene tubes, preconditioned with OPA, were used for both standards and samples.

Prior to any analyses, rainwater samples collected at the ABCRC field station were thawed and allowed to reach room temperature. Samples were then filtered using a 0.2 µm nylon filter (Fisherbrand) loaded onto a 50 mL polypropylene syringe (BD, Luer-Lok), to remove the thymol and other particles. The matrix for standards used for NH_4^+ analysis of rainwater samples was prepared using a filtered, saturated thymol solution. This saturated thymol solution was made by dissolving 1.6 g of thymol in

200 mL of 18.2 MΩ-cm resistivity deionized water (Barnstead, Nanopure) on a stir plate overnight and then filtering the solution using a 0.2 µm nylon filter (Fisherbrand) loaded onto a 50 mL polypropylene syringe (BD, Luer-Lok). The filtrate was then diluted 50 times with 18.2 MΩ-cm resistivity deionized water (Barnstead, Nanopure) prior to being used for making standards. Both rainwater and aerosol leachate samples were diluted 50 times for NH_4^+ analysis. Detection limits were 140 nM, 10 nM, and 30 nM for NO_3^-, NH_4^+, and PO_4^{3-}, respectively. The detection limits were determined by first calculating the standard deviation on the average concentrations of all blanks. The standard deviation of the blanks was then multiplied by 3, and this value added to the overall average concentration for those blanks. Calculations for detection limits followed the guidelines outlined by the Wisconsin Department of Natural Resources [1996].

2.6 WET AND DRY ATMOSPHERIC DEPOSITION FLUX CALCULATIONS

Seasons were defined based on the National Oceanic and Atmospheric Administration (NOAA) 2014 and 2015 annual climate reports [NOAA, 2014, 2015] (Summer: June - August, Fall: September - November, Winter: December - March, and Spring: March - May). Summer 2014 samples were collected 29 May through 27 August 2014; fall 2014 samples were collected 3 September through 25 November 2014; winter 2014-2015 samples were collected 3 December 2014 through 22 February 2015, and spring 2015 samples were collected 3 March through 10 June 2015.

The fluxes of water-soluble nutrients and total-dissolvable trace metals for rainwater samples were calculated using equation 5 [Baker et al., 2010], where $[X_S]$ is the concentration of element X in µmol/m^3, p is the amount of precipitation (m) for that sample period, and t (in days) is the length of the sample period.

$$\text{wet deposition flux } X_S\ (\mu\text{mol/m}^2\text{/d}) = \frac{[X_S]\ (\mu\text{mol/m}^3) \times p\ (\text{m})}{t\ (\text{days})} \quad (5)$$

The total mass of water-soluble nutrients and trace metals (total mass X_S) present in each aerosol leachate sample was calculated using equation 6, which was derived from Baker et al. [2007], where $[X_S]$

is the water-soluble concentration of element X (in μmol L^{-1}), 0.75 L is the volume of leachate collected, and mf is a multiplication factor for that size fraction. Approximately one quarter of the active area of each filter was used for aerosol leaching and the mf value accounts for this so that the total mass of water-soluble nutrients and trace metals associated with each aerosol size fraction can be estimated. The mf values calculated for the two aerosol size fractions differed, as different filter types (slotted or backing) were used for the aerosol leaching procedure for each size fraction. The fine (< 1 μm) size fraction aerosol leachate was obtained using one quarter of the last slotted filter and one quarter of the backing filter, and the mf was calculated to be 4.158. The use of this multiplication factor introduces an error of ~4%, since slotted filters have 9.75 deposit bands, but the section of the slotted filter used for analysis did not contain the additional 0.75 deposit bands. The leachate for the coarse (> 1 μm) size fraction was obtained from one quarter of each of 4 slotted filters and the multiplication factor was calculated to be 4.333, as the section of each slotted filter used did not contain the extra 0.75 aerosol deposit band.

$$\text{total mass } X_S \text{ (μmol)} = [X_S] \text{ (μmol/L)} \times 0.75 \text{ L} \times \text{mf} \quad (6)$$

The dry flux of water-soluble nutrients and trace metals was estimated using equation 7 [Baker et al., 2007; Jung et al., 2013]. The deposition velocity used for the > 1 μm aerosol size fraction was 0.02 m s^{-1}, and that used for the < 1 μm size fraction was 0.001 m s^{-1} [Baker et al., 2003; Sarthou et al., 2003; Baker et al., 2007]. These deposition velocities were selected for this study because samples in the cited studies were similarly delineated using an aerodynamic diameter of 1 μm. Deposition velocities are poorly constrained and are influenced by particle size and other factors leading to uncertainties of up to a factor of 2-3 in flux calculations [Duce et al., 1991], and these values may vary between elements due to particle composition and size [Wu et al., 1994]. Previous studies have attempted to estimate deposition velocities both experimentally and using models. Dedeurwaerder et al. [1983] determined the atmospheric dry fall out rate using vaseline-coated plexiglass surfaces over a 12-day period in the North Sea. Slinn and Slinn [1980] modeled the dry deposition velocity of particles for a smooth water surface, and Gao et al. [2013] combined the equation of Williams [1982] for small particles, including those produced by white

caps and breaking waves, with that of Quinn and Ondov [1998], which examined the effect of relative humidity on the dry deposition of trace metal particles, to estimate deposition velocities.

$$\text{flux } X_S \text{ (µmol/m}^2\text{/d)} = \frac{X_S \text{ (µmol)}}{\text{volume of air (m}^3\text{)}} \text{ x deposition velocity (m/s) x 86400 (s/d)} \quad (7)$$

The total mass of aerosol trace metals was determined using equation 8 [Baker et al., 2007], where X_T is the total mass of element X in the digest solution, 0.02 L is the volume of the digest, and mf is the multiplication factor calculated by dividing the total active filter area by the fraction used for each digestion. The total aerosol trace metal flux was calculated by applying equation 9, using the same deposition velocities as equation 7 [Baker et al., 2007]. Digestions and respective calculations were performed separately for both aerosol size fractions.

$$\text{total mass } X_T \text{ (µg)} = [X_T] \text{ (µg/L) x 0.02 L x mf} \quad (8)$$

$$\text{flux } X_T \text{ (µmol/m}^2\text{/d)} = \frac{X_T \text{ (µmol)}}{\text{volume of air (m}^3\text{)}} \text{ x deposition velocity (m/s)} \quad (9)$$

The percent fractional (water) solubility (% X_S) was calculated using equation 10, where X is the element of interest [Baker et al., 2006a, 2006c; Gao et al., 2013].

$$\%X_S = \frac{\text{total mass } X_S}{\text{total mass } X_T} \text{ x 100} \quad (10)$$

Atmospheric deposition (total-dissolvable, water-soluble, and total) fluxes and fractional solubility were calculated for each sample collected during the time series. Data were smoothed using a running average of five weeks, and the residuals calculated as the difference between the overall mean flux or fractional solubility for the entire sampling period and the flux or fractional solubility for each specific sample. Additional plots were made of the smoothed data and the residuals to identify any seasonal trends in the flux data for each nutrient and trace metal. Statistical tests (discussed in Section 2.7) were performed to determine whether such seasonal trends and differences were statistically significant. MATLAB 2016b software was used to generate all figures and perform all statistical analyses.

The wet deposition fluxes calculated for soluble nutrients and total-dissolvable trace metals in offshore rain water samples were higher than those for the ABCRC station, since they are the fluxes

during rainfall, and do not account for periods when there was no rainfall during the cruise. The mean wet deposition flux for each soluble nutrient and total-dissolvable trace metal over the entire cruise period, was estimated using data for each nutrient or trace metal in offshore rainwater samples (equation 11), to compare the cruise wet deposition data to that for the ABCRC site. These estimated wet deposition fluxes assumed that the total number of rain events sampled, during the entire cruise period, were representative of the frequency of rainfall within the study region during summer.

$$\text{flux } X_S\ (\mu\text{mol/m}^2\text{/d}) = \frac{(f1\ (\mu\text{mol/m}^2\text{/s}) \times t1\ (s)) + (f2\ (\mu\text{mol/m}^2\text{/s}) \times t2) + (f3\ (\mu\text{mol/m}^2\text{/s}) \times t3(s)) \ldots}{\text{total cruise observation period (d)}} \quad (11)$$

The flux of each soluble nutrient or total-dissolvable trace metal (X_S) in equation 11 was calculated using the sum of the products of the wet deposition flux for each event (f1, f2, f3, etc.) and the duration of the corresponding rain event (t1, t2, t3, etc.). Dry deposition fluxes (water-soluble and total) and fractional solubility of offshore aerosol samples were calculated using the same procedure as for the ABCRC site.

2.7 STATISTICAL ANALYSIS OF NUTRIENT AND TRACE METAL FLUXES

The Shapiro Wilk test for normality was applied to determine if data were normally distributed [Hoff et al., 2014]. Non-normally distributed data were normalized using a log transformation and tested for equal variance to determine whether parametric or non-parametric tests should be applied to the data [Hoff et al., 2014]. To determine whether there were significant differences in the mean or median fluxes of nutrients or trace metals for the four seasons (groups), a one-way analysis of variance (ANOVA) or Kruskal-Wallis non-parametric test was applied to the data [Hoff et al., 2014]. A multiple comparison test was then used to identify groups that were significantly different [Hoff et al. 2014]. A one-way analysis of variance and multiple comparison test were applied to normally distributed data of equal variance, and used to determine whether the mean fluxes for the four seasons were significantly different [Hoff et al., 2014]. A Kruskal-Wallis non-parametric test and multiple comparison test were applied to non-normal data, which did not meet the requirements of a one-way ANOVA, to determine whether the median fluxes for the four seasons were significantly different. The values reported for the one-way ANOVA included

the p-value (p), degrees of freedom (df), and the F statistic (F), whereas those reported for the Kruskal-Wallis test included p, df, and the chi squared statistic (chi-sq).

A two-sample t-test was applied to normally distributed data to determine whether the annual mean nutrient and trace metal fluxes, for both aerosol size fractions, were significantly different. The t-test selected for analysis depended on whether the variances of groups, with normally distributed data, were equal or unequal. Log transformed data were used for all variables for which a one-way ANOVA or t-test was applied. A Wilcoxon rank sum test was applied to pairs of data where data for at least one size fraction were not normally distributed [Hoff et al., 2014]. The original flux or fractional solubility data were used for all non-parametric tests (Kruskal-Wallis and Wilcoxon rank sum). Results of these tests were used to determine whether the mean or median fluxes of nutrients and trace metals present in both aerosol size fractions were significantly different, and how these means or medians differed. The values reported for the two-sample t-test included p, df, and the t-statistic (t-stat). For the Wilcoxon rank sum test, the p, and z-value (z-val) were reported. All statistical analyses were performed using MATLAB 2016b software. A summary of one-way ANOVA and Kruskal-Wallis tests applied to wet and dry fluxes of soluble nutrient fluxes is provided in Appendices A and B. Statistical tests applied to the wet and dry fluxes of total-dissolvable and total trace metals, and aerosol fractional solubilities, are summarized in Appendices C, D, and E, respectively.

2.8 EMPIRICAL ORTHOGONAL FUNCTION ANALYSIS OF TOTAL TRACE METAL FLUXES

An empirical orthogonal function (EOF) analysis was performed using MATLAB 2016b software to determine if there were any temporal patterns in the total fluxes of trace metals from the ABCRC aerosol samples using the method described in Preisendorfer [1988]. The total flux data for both size fractions for each of the 13 trace metals examined were placed in a table where each column corresponded to the flux for one of the 26 variables (each of the 13 trace metals has two size fractions). Due to the large range in the magnitude of fluxes, the data in each column were scaled to a mean of zero and a variance of one. Each flux variable was assigned an arbitrary reference number from 1 to 26 prior to

analysis (Table 4). The total variance of the scaled flux data was equal to 26, as each variable has a variance equal to one. A total of 26 possible patterns (referred to as “EOF modes”) may be observed in the data, although not all modes explained a significant fraction of the total variance observed.

A p x p correlation matrix of the scaled flux data was created (where p = 26, the total number of variables). The sum of the diagonal elements (eigenvalues) of this matrix equaled the total variance of the 26 EOF modes. Each eigenvalue corresponded to the fraction of the total variance explained by an individual EOF mode. The eigenfunctions were calculated from the matrix and eigenvalues and determined the patterns (shapes) of the data. There are different approaches for determining how many of the 26 EOF modes are significant, with the simplest approach being the use of the average eigenvalue, which was 0.0385 (1/26). Eigenvalues greater than 0.0385 were considered significant.

The EOF analysis separated the flux data based on the patterns exhibited by the different trace metals, and how these patterns changed over time. In the flux mode plots produced, the “trace-metal” on the x-axis was the number assigned to each variable (Table 4), and the y-axis was the eigenfunction. The sign before the eigenfunction value was arbitrary. Trace metals with an eigenfunction of absolute value greater than 0.2 in the flux mode plots were represented by that EOF mode. The time flux mode plot (for each EOF mode) indicated how the fluxes of the trace metals grouped by the flux mode plot changed over time. The x-axis of the time flux mode plot was the sample collection date and the y-axis was the amplitude of the change in scaled flux above or below the mean for the trace metals identified in the flux mode plot.

Table 4. Variables used for empirical orthogonal function analysis of total trace metal flux data from ABCRC samples.

Trace metal variable	Description (flux)
1	Coarse Cd
2	Fine Cd
3	Coarse Sb
4	Fine Sb
5	Coarse Pb
6	Fine Pb
7	Coarse Al
8	Fine Al
9	Coarse Ti
10	Fine Ti
11	Coarse V
12	Fine V
13	Coarse Cr
14	Fine Cr
15	Coarse Mn
16	Fine Mn
17	Coarse Fe
18	Fine Fe
19	Coarse Co
20	Fine Co
21	Coarse Ni
22	Fine Ni
23	Coarse Cu
24	Fine Cu
25	Coarse Zn
26	Fine Zn

2.9 NOAA HYSPLIT MODEL AIR MASS BACKWARD TRAJECTORIES

Air mass backward trajectories (AMBTs) were obtained for both land-based and offshore aerosol samples using the NOAA Air Resources Laboratory Hybrid Single-Particle Lagrangian Integrated Trajectory (HYSPLIT) model (http://www.ready.noaa.gov/index.php) [Draxler and Rolph, 2003; Stein et al., 2015; Rolph et al., 2017]. These AMBTs were obtained to assess aerosol sources, that is, the region of origin for air masses sampled at the ABCRC field station and offshore sites. The AMBTs obtained were combined with the EOF model results for the ABCRC samples to examine the influence of air mass source on the total dry deposition of trace metals, and to infer activities or processes responsible for changes in these fluxes during a given sampling period.

Five-day air mass backward trajectories were obtained for both the start and end time of weekly composite aerosol samples for the ABCRC station. Due to the shorter timescale of shipboard aerosol sample collection (typically 6-7 hours), AMBTs for the end sampling time were used. The purpose of obtaining two AMBTs for ABCRC aerosol samples was to account for possible changes in the air mass sources during each sampling period. The location of the ABCRC field station (37.288°N, 75.925°W), along with the sampling period start or end time, was used for ABCRC AMBTs. For shipboard aerosol samples, the origin ($t = 0$) of each AMBT was defined as the end point of the sampling period and the ship's corresponding position. Arrival heights of 10 m, 500 m and 1000 m [Sarthou et al., 2003; Croot et al., 2004; Baker et al., 2006a] were applied to the HYSPLIT reanalysis data set [Sedwick et al., 2007; Shelley et al., 2015] to assess the source of aerosols. Aerosol samples were obtained from within the marine boundary layer, which is ~400-1200 m thick [Buck et al., 2006; Wozniak et al., 2013, 2015; Shelley et al., 2015].

2.10 CALCULATION OF ELEMENTAL ENRICHMENT FACTORS

Elemental enrichment factors (EFs), relative to crustal abundance, were calculated to determine if trace metals in aerosol samples were derived mainly from crustal, anthropogenic or other sources [Lantzy and Mackenzie, 1978; Song and Gao 2011; Shelley et al., 2015]. These calculations were performed separately for the fine and coarse aerosol size fractions of all trace metals using the total trace metal concentration data from the ABCRC aerosol samples. These values obtained were used, in conjunction with the AMBTs, to assess air mass and aerosol sources that contributed to the observed changes in the total trace metal fluxes during the study period.

The EFs were calculated using equation 12 [Duce and Hoffman, 1976, Wu et al., 1994; Chester et al., 1999; Jickells et al., 2016], where $([X]/[Al])_{Aerosol}$ is the ratio of the sample concentration of the element of interest (X) to that of Al in the same sample, and $([X]/[Al])_{Crust}$ is the ratio of the average concentration of element X in the upper continental crust (UCC) to that of Al in the UCC.

$$EF_x = \frac{([X]/[Al])_{Aerosol}}{([X]/[Al])_{Crust}} \quad (12)$$

Elements which are abundant in the earth's crust and do not have a significant non-crustal source may be used as lithogenic tracers [Shelley at al., 2015]. Although Ti may also be used for calculating enrichment factors, Al is most commonly used due to its high crustal abundance [Shelley et al., 2015]. The use of Al for normalizing the aerosol data assumes that Al in the sample was derived from the alumino-silicate matrix and therefore of crustal origin, and that the relative abundance of Al in crustal material remains constant [Shelley et al., 2015]. The relative abundance of elements in the UCC were thought to be representative of lithogenic aerosols sampled at the ABCRC station and at offshore sites, therefore the use of these average concentrations introduces some uncertainty in the calculated enrichment factors, given that lithogenic material may vary from UCC composition [Jickells et al., 2016]. All EFs were calculated using the average UCC concentrations provided by Taylor and McLennan [1985] and Li [2000].

The seasonal mean and overall mean EFs were calculated for each aerosol trace metal using the total concentration data for the ABCRC samples. Enrichment factors were calculated for the 3 shipboard aerosol samples that had total Al concentrations above the analytical detection limit (the fine fraction aerosol samples of 3 August and 9 August 2014, and the coarse aerosol fraction of 5 August 2014). If the source of a trace metal was primarily lithogenic then it should have an EF near unity, whereas if the EF is high the source is likely anthropogenic [Lantzy et al., 1978]. Biomass burning, including both human-induced and natural lightning-induced burning, can also produce aerosols with EFs that differ from unity [Echalar et al., 1995; Gaudichet et al., 1995; Vasconcellos et al., 2007; Calvo et al., 2013]. In this study, if the EF < 10, the element is considered of lithogenic origin, and if EF > 10 the aerosol is considered enriched and from a non-crustal source (anthropogenic source) [Lantzy and Mackenzie, 1978; Chester et al., 1999, 2000; Bacardit et al., 2010; Shelley et al., 2015; Jickells et al., 2016].

CHAPTER 3

RESULTS

3.1 WET DEPOSITION OF SOLUBLE NUTRIENTS - EASTERN SHORE

The estimated wet estimated flux of soluble NO_3^- at the ABCRC ranged from 7.60 to 40.3 µmol/m^2/d in summer, 2.70 to 22.9 µmol/m^2/d in fall, 4.45 to 23.8 µmol/m^2/d in winter, and 1.57 to 52.9 µmol/m^2/d in spring (Table 5 and Figure 2a). Wet deposition of soluble NO_3^- during each season was typically lower than that for NH_4^+ (Figures 2a and 2b), which ranged from 7.79 to 110 µmol/m^2/d in summer, 15.4 to 210 µmol/m^2/d in fall, 3.81 to 171 µmol/m^2/d in winter, and 50.3 to 284 µmol/m^2/d in spring (Table 5 and Figure 2b). Additionally, the overall mean wet flux of soluble NH_4^+ for the sampling period (71.2 ± 58.1 µmol/m^2/d) was more than 3 times greater than that for soluble NO_3^- (16.2 ± 11.2 µmol/m^2/d), and therefore NH_4^+ was the dominant source of wet soluble inorganic N at the Eastern Shore site (Table 5).

The overall mean wet flux of soluble PO_4^{3-} at ABCRC was more than 70 times and 300 times lower than those for soluble NO_3^- and NH_4^+, respectively (Table 5). The wet flux of soluble PO_4^{3-} remained consistently below 1 µmol/m^2/d throughout the sampling period, except on 18 June 2014, when the flux peaked at almost 5 µmol/m^2/d (Figure 3c). The seasonal wet flux of soluble PO_4^{3-} ranged from 0.030 to 4.91 µmol/m^2/d in summer, 0.021 to 0.471 µmol/m^2/d in fall, 0.018 to 0.160 µmol/m^2/d in winter, and 0.017 to 0.953 µmol/m^2/d in spring (Table 5 and Figure 2c).

The mean wet fluxes of soluble NO_3^- and PO_4^{3-} were greatest in summer, while the mean wet flux of soluble NH_4^+ was greatest in fall (Table 5). Ammonium was the dominant source of inorganic N in Eastern Shore wet deposition. Wet atmospheric deposition at the Eastern Shore was P deficient relative to phytoplankton requirements, as the soluble inorganic N:P ratio of ~387 far exceeded the Redfield ratio (16:1), where soluble N includes NO_3^- and NH_4^+, and soluble P includes PO_4^{3-}. This ratio does not account for wet soluble organic N and P, which were not determined in this study.

Table 5. Mean (± standard deviation) seasonal wet deposition flux (μmol/m^2/d) of soluble nutrients in Eastern Shore rain samples.

Season	NO_3^-		NH_4^+		PO_4^{3-}	
	Mean ± standard deviation (μmol/m^2/d)	Range (μmol/m^2/d)	Mean ± standard deviation (μmol/m^2/d)	Range (μmol/m^2/d)	Mean ± standard deviation (μmol/m^2/d)	Range (μmol/m^2/d)
Summer 2014	20.5 ± 14.1	7.60-40.3	35.9 ± 33.8	7.79-110	0.718 ± 1.41	0.0302-4.91
Fall 2014	12.5 ± 6.62	2.70-22.9	95.5 ± 59.7	15.4-210	0.109 ± 0.159	0.0210-0.471
Winter 2014-2015	14.4 ± 7.91	4.45-23.8	53.8 ± 5 4.1	3.81-171	0.0595 ± 0.0524	0.0182-0.160
Spring 2015	19.1 ± 13.7	1.57-52.9	86.9 ± 61.4	50.3-284	0.119 ± 0.245	0.0170-0.953
Overall annual	16.2 ± 11.2	1.57-52.9	71.2 ± 58.1	3.81-284	0.226 ± 0.705	0.0170-4.91

(a) Rain soluble nitrate from Eastern Shore samples

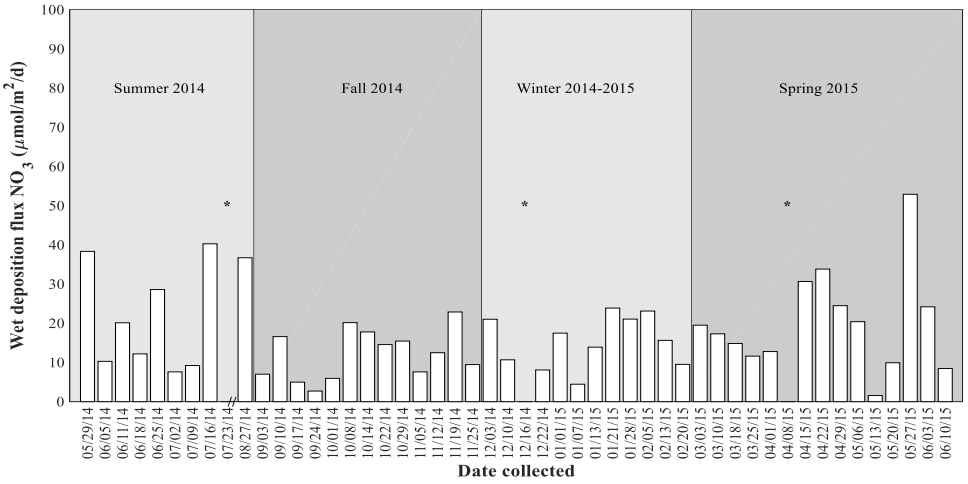

(b) Rain soluble ammonium from Eastern Shore samples

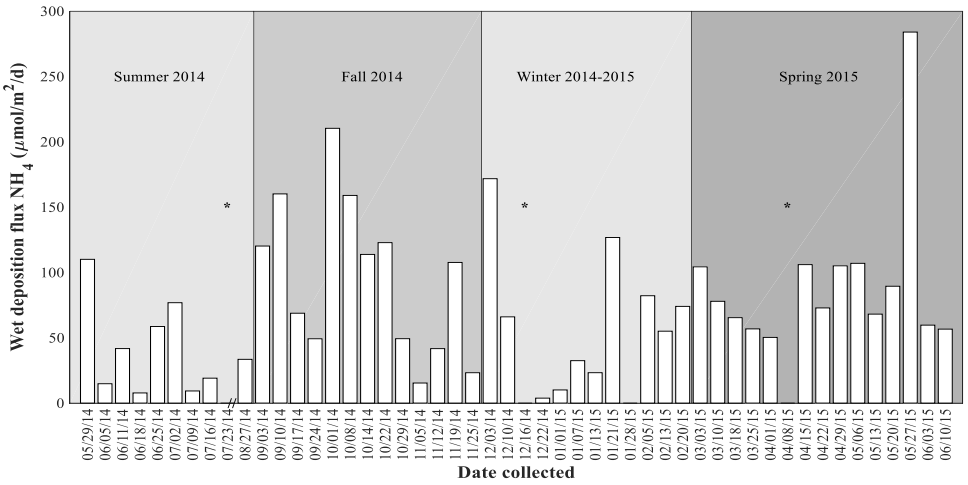

(c) Rain soluble phosphate from Eastern Shore samples

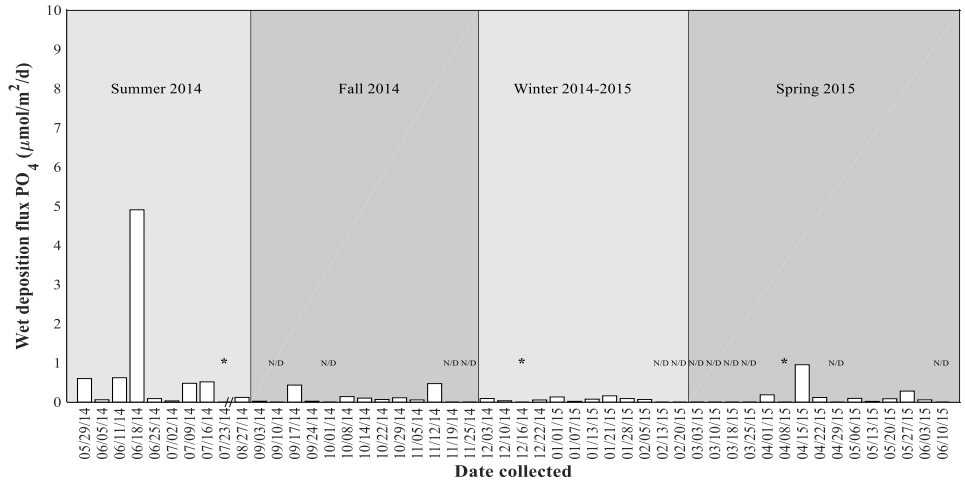

Figure 2. Seasonal wet deposition flux (µmol/m^2/d) of (a) NO_3^-, (b) NH_4^+, and (c) PO_4^{3-} at the Eastern Shore field station. "//" indicates a gap in data, "*****" denotes dates for which there was no rain and "N/D" indicates samples for which nutrients were not detectable.

The time series of smoothed data and residuals show that the wet flux of soluble NO_3^- remained near the overall mean throughout the sampling period (Figures 3a and 4a). The smoothed data and residuals for soluble NH_4^+ show that the wet flux varied seasonally, as the flux was elevated above the overall mean during fall and spring, and below the overall mean during summer and winter (Figures 3b and 4b). The smoothed data and residuals show that the wet flux of soluble PO_4^{3-} was elevated above the overall mean in summer (Figures 3c and 4c), largely due to the relatively high flux of 4.91 μmol/m^2/d on 18 June 2014 (Figure 2c), but remained near the overall mean throughout the fall, winter, and spring seasons (Figures 3c and 4c).

(a) Rain soluble nitrate from Eastern Shore samples - smoothed

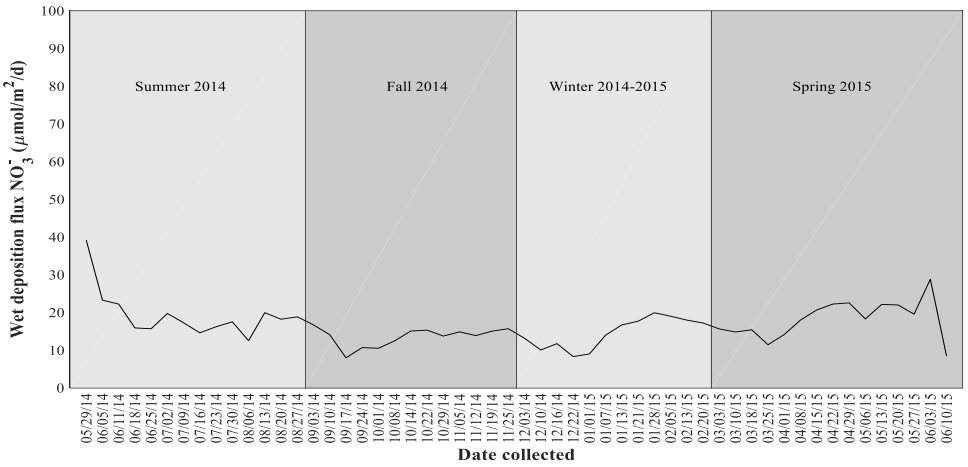

(b) Rain soluble ammonium from Eastern Shore samples - smoothed

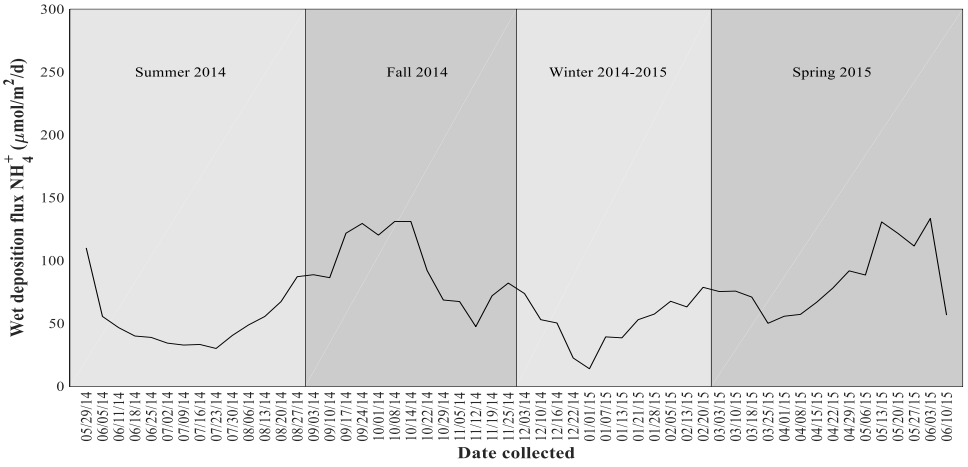

(c) Rain soluble phosphate from Eastern Shore samples - smoothed

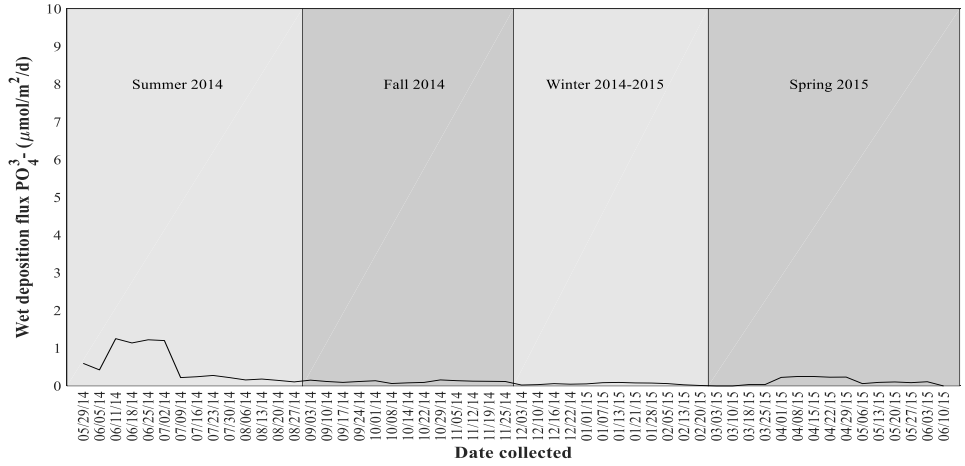

Figure 3. Smoothed seasonal wet deposition flux (µmol/m^2/d) of soluble (a) NO_3^-, (b) NH_4^+, and (c) PO_4^{3-} at the Eastern Shore field station. Note that data were interpolated for missing sampling dates 30 July 2014, 6 August 2014, 13 August 2014, and 20 August 2014 using the method described in Section 2.6.

(a) Rain soluble nitrate from Eastern Shore samples - residuals

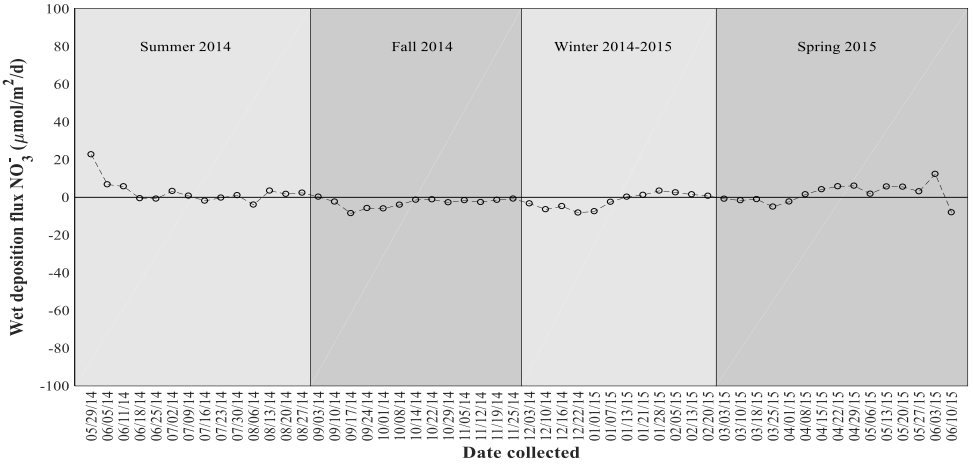

(b) Rain soluble ammonium from Eastern Shore samples - residuals

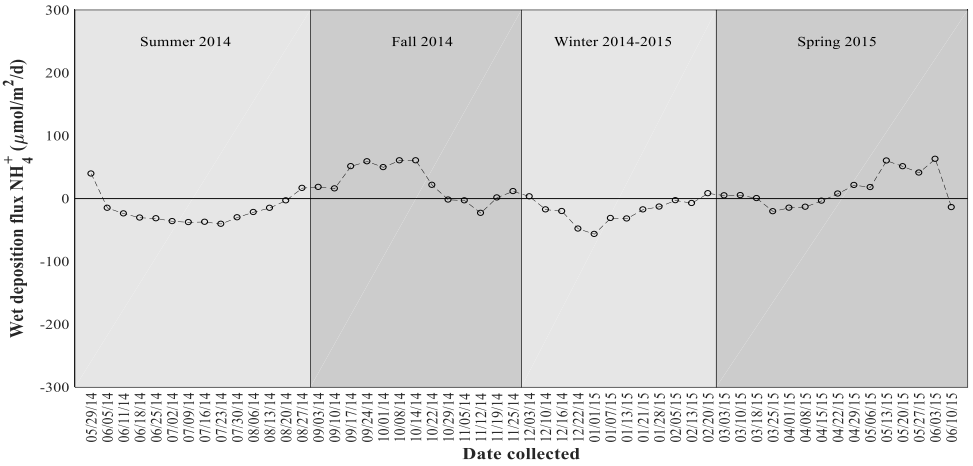

(c) Rain soluble phosphate from Eastern Shore samples - residuals

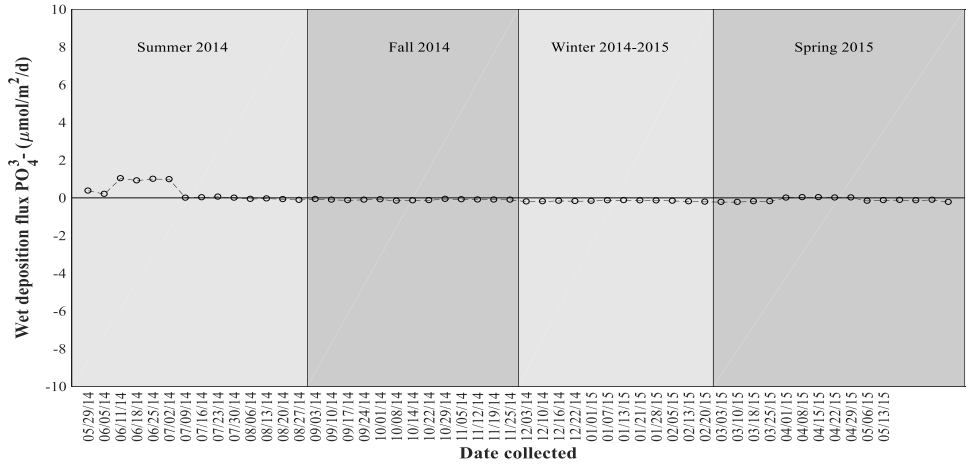

Figure 4. Residuals of wet deposition flux (µmol/m^2/d) of soluble (a) NO_3^-, (b) NH_4^+, and (c) PO_4^{3-} at the Eastern Shore field station. The black horizontal line is the annual mean flux calculated using data for the entire sampling period. Note that data were interpolated for dates 30 July 2014, 6 August 2014, 13 August 2014, and 20 August 2014 using the method described in Section 2.6.

Although the mean wet fluxes of soluble NO_3^- for summer (20.5 ± 14.1 µmol/m^2/d), fall (12.5 ± 6.62 µmol/m^2/d), and spring (19.1 ± 13.7 µmol/m^2/d) were greater than that for winter (14.4 ± 7.91 µmol/m^2/d) (Table 5), the means of wet soluble NO_3^- fluxes for the four seasons were not significantly different (p = 0.0908, df = 46, F = 1.55). The median wet fluxes of soluble NH_4^+ for fall (108 µmol/m^2/d), spring (72.9 µmol/m^2/d), summer (26.3 µmol/m^2/d), and winter (43.8 µmol/m^2/d) (Table 5) were not significantly different (p = 0.0532, df = 45, chi-sq = 767), as indicated by a Kruskal-Wallis test. Although the mean wet flux of soluble PO_4^{3-} was greater in summer (0.718 ± 1.41 µmol/m^2/d) than in fall (0.109 ± 0.159 µmol/m^2/d), winter (0.0595 ± 0.0524 µmol/m^2/d), and spring (0.119 ± 0.245 µmol/m^2/d) (Table 5), a one-way ANOVA confirmed that the means for the four seasons were not significantly different (p = 0.0908, df = 34, F= 2.36). Thus, there were no statistically significant differences in the seasonal wet fluxes of soluble NO_3^-, NH_4^+, and PO_4^{3-} at the Eastern Shore.

3.2 DRY DEPOSITION OF SOLUBLE NUTRIENTS - EASTERN SHORE

The estimated dry deposition flux of fine soluble NO_3^- ranged from to 0.234 to 0.689 µmol/m^2/d in summer, 0.331 to 0.812 µmol/m^2/d in fall, 0.487 to 1.99 µmol/m^2/d in winter, and 0.118 to 2.20 µmol/m^2/d in spring (Table 6 and Figure 5a). The dry flux of coarse soluble NO_3^- ranged from 8.84 to 23.1 µmol/m^2/d in summer, 9.95 to 23.9 µmol/m^2/d in fall, 7.54 to 26 µmol/m^2/d in winter, and 13.6 to 33.2 µmol/m^2/d in spring (Table 6 and Figure 5a).

The estimated dry fluxes of fine soluble NH_4^+ were also consistently lower than those for coarse soluble NH_4^+, and ranged from 2.48 to 4.47 µmol/m^2/d in summer, 1.88 to 3.77 µmol/m^2/d in fall, 1.61 to 6.40 µmol/m^2/d in winter, and 1.47 to 4.83 µmol/m^2/d in spring (Table 6 and Figure 5b). The dry flux of coarse soluble NH_4^+ ranged from 9.70 to 28.1 µmol/m^2/d in summer, 8.30 to 18.3 µmol/m^2/d in fall, 8.25 to 28.2 µmol/m^2/d in winter, and 12.9 to 26.3 µmol/m^2/d in spring (Table 6 and Figure 5b). The overall mean dry flux of coarse soluble NO_3^- (17.6 ± 7.52 µmol/m^2/d) was roughly equal to that for coarse soluble NH_4^+ (17.1 ± 5.74 µmol/m^2/d) (Table 6). In contrast, the overall mean dry flux of soluble fine NH_4^+ (3.30 ± 0.905 µmol/m^2/d) was more than 3 times greater than the overall mean dry flux of soluble fine NO_3^- (0.721 ± 0.503 µmol/m^2/d) (Table 6).

The dry flux of fine soluble PO_4^{3-} remained relatively constantly throughout the sampling period ranging from 1.49 x 10^{-3} to 7.56 x 10^{-3} µmol/m^2/d in summer, 0.575 x 10^{-3} to 7.18 x 10^{-3} µmol/m^2/d in fall, 1.08 x 10^{-3} to 3.19 x 10^{-3} µmol/m^2/d in winter, and 1.36 x 10^{-3} to 8.28 x 10^{-3} µmol/m^2/d in spring (Table 6 and Figure 5c). The dry flux of coarse soluble PO_4^{3-} declined from summer through winter then increased from 8 April 2015 through 10 June 2015 (Figure 5c). The dry flux of coarse soluble PO_4^{3-} ranged from 0.033 to 0.161 µmol/m^2/d in summer, 0.012 to 0.096 µmol/m^2/d in fall, 0.005 to 0.047 µmol/m^2/d in winter, and 0.005 to 0.092 in spring (Table 6).

For all three nutrients, the overall mean dry flux of the soluble coarse fraction was greater than that for the fine fraction (Table 6). The dry flux of coarse soluble NO_3^-, NH_4^+, and PO_4^{3-} was more than 20 times, 5 times, and 10 times greater, respectively, than those for the fine fraction (Table 6). On 27 May 2015, both the wet soluble flux and dry coarse soluble flux of NO_3^- peaked (Figures 2a and 5a). The

greatest wet flux of soluble NH_4^+ also occurred on 27 May 2015, however, the greatest dry flux of coarse soluble NH_4^+ occurred on 18 June 2014 (Figures 2b and 5b). The wet soluble flux and dry coarse soluble flux of PO_4^{3-} both peaked on 18 June 2014 as well (Figures 2c and 5c). Both wet and dry deposition samples collected on 18 June 2014 and 27 May 2015 at the Eastern Shore had relatively high atmospheric loadings of soluble nutrients.

Table 6. Mean (± standard deviation) and range (in parentheses) seasonal dry deposition flux (μmol/m^2/d) of soluble nutrients to the Eastern Shore.

Season	NO_3^- (μmol/m^2/d)		NH_4^+ (μmol/m^2/d)		PO_4^{3-} (μmol/m^2/d)	
	<1 μm	>1 μm	<1 μm	>1 μm	<1 μm	>1 μm
Summer 2014	0.377 ± 0.147 (0.234-0.689)	17.7 ± 4.53 (8.84-23.1)	3.19 ± 0.600 (2.48-4.47)	15.2 ± 7.35 (9.70-28.1)	$4.45 \times 10^{-3} \pm 1.85 \times 10^{-3}$ (1.49×10^{-3}-7.56×10^{-3})	$86.8 \times 10^{-3} \pm 36.3 \times 10^{-3}$ (33.0×10^{-3}-161×10^{-3})
Fall 2014	0.485 ± 0.250 (0.331-0.812)	13.8 ± 7.48 (9.95-23.9)	2.82 ± 0.496 (1.88-3.77)	14.0 ± 2.97 (8.30-18.3)	$3.95 \times 10^{-3} \pm 2.05 \times 10^{-3}$ (0.575×10^{-3}-7.18×10^{-3})	$61.1 \times 10^{-3} \pm 34.3 \times 10^{-3}$ (12.2×10^{-3}-96.3×10^{-3})
Winter 2014 - 2015	1.24 ± 0.471 (0.487-1.99)	15.9 ± 5.88 (7.54-26.0)	3.74 ± 1.26 (1.61-6.40)	19.0 ± 6.57 (8.25-28.2)	$1.99 \times 10^{-3} \pm 0.680 \times 10^{-3}$ (1.08×10^{-3}-3.19×10^{-3})	$34.7 \times 10^{-3} \pm 13.8 \times 10^{-3}$ (5.42×10^{-3}-47.0×10^{-3})
Spring 2015	0.738 ± 0.522 (0.118-2.20)	22.4 ± 8.35 (13.6-33.2)	4.29 ± 0.871 (1.47-4.83)	19.6 ± 3.44 (12.9-26.3)	$3.94 \times 10^{-3} \pm 2.20 \times 10^{-3}$ (1.36×10^{-3}-8.28×10^{-3})	$33.6 \times 10^{-3} \pm 32.1 \times 10^{-3}$ (5.08×10^{-3}-92.1×10^{-3})
Overall mean	0.721 ± 0.503 (0.118-0.812)	17.6 ± 7.52 (7.54-33.2)	3.30 ± 0.905 (1.47-6.40)	17.1 ± 5.74 (8.25-28.2)	$3.60 \times 10^{-3} \pm 1.90 \times 10^{-3}$ (0.575×10^{-3}-8.28×10^{-3})	$51.7 \times 10^{-3} \pm 36.2 \times 10^{-3}$ (5.08×10^{-3}-161×10^{-3})

(a) Aerosol leachate soluble nitrate from Eastern Shore samples

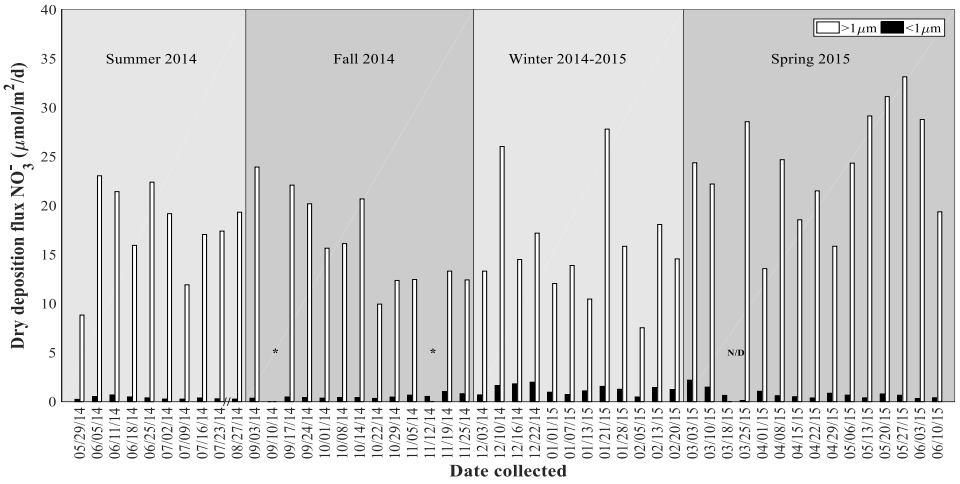

(b) Aerosol leachate soluble ammonium from Eastern Shore samples

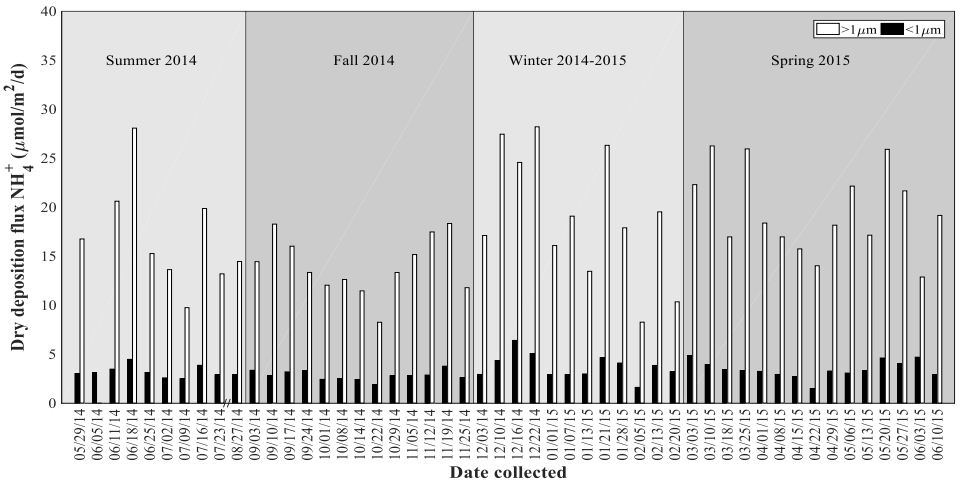

(c) Aerosol leachate soluble phosphate from Eastern Shore samples

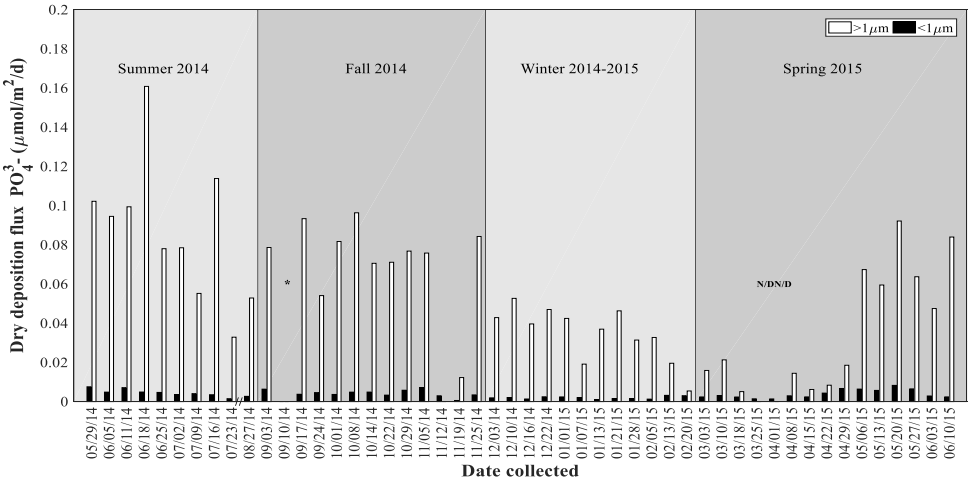

Figure 5. Seasonal dry deposition flux (μmol/m^2/d) of soluble (a) NO_3^-, (b) NH_4^+, and (c) PO_4^{3-} for weekly collected Eastern Shore samples. "//" indicates a gap in data, "*" denotes sample for which data is unavailable and "N/D" indicates samples for which nutrients were not detectable.

The time series of smoothed data and residuals show that the dry flux of fine soluble NO_3^- remained near the overall mean throughout the sampling period (Figures 6a and 7a). The smoothed data and residuals also show that the dry flux of coarse soluble NO_3^- changed little during summer and winter (Figures 6a and 7a). The flux of coarse soluble NO_3^- was above the overall mean during spring, near the mean during summer, and below this mean during fall and winter (Figure 7a).

The smoothed data and residuals also show that the dry flux of fine soluble NH_4^+ remained near the overall mean throughout the sampling period (Figures 6b and 7b). The dry flux of coarse soluble NH_4^+ was mostly above the overall mean during winter and spring, but below this mean during summer and fall (Figures 6b and 7b).

The dry flux of fine soluble PO_4^{3-} was fairly consistent and remained near the overall mean throughout the sampling period (Figures 6c and 7c). The smoothed data and residuals show that the dry flux of coarse soluble PO_4^{3-} declined from the start of summer sampling through 1 April 2015, after which it began to increase (Figures 6c and 7c). During summer and fall, the dry flux of coarse soluble PO_4^{3-} was above the overall mean, but during winter and most of spring this flux was below the overall mean (Figure 7c).

(a) Aerosol leachate soluble nitrate from Eastern Shore samples - smoothed

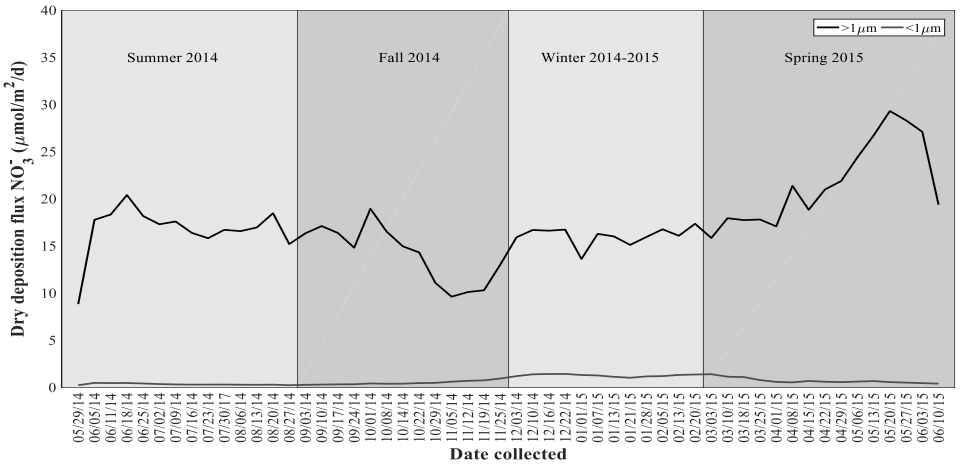

(b) Aerosol leachate soluble ammonium from Eastern Shore samples - smoothed

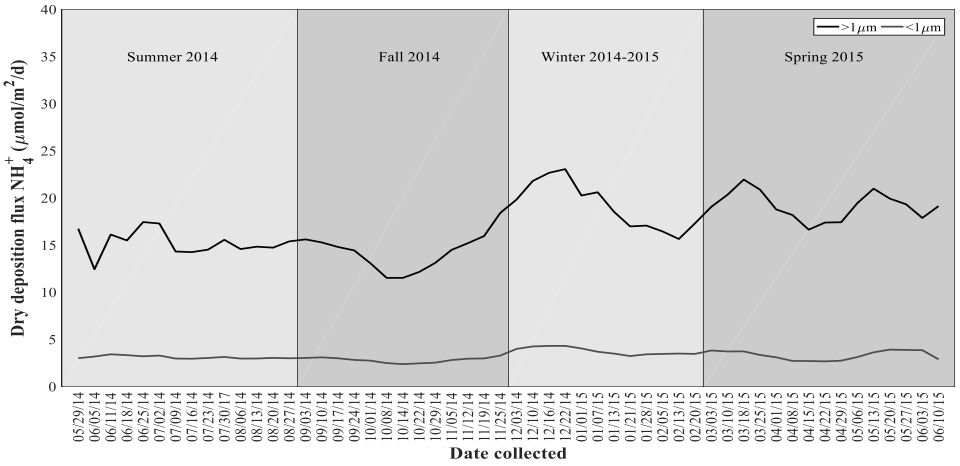

(c) Aerosol leachate soluble phosphate from Eastern Shore samples - smoothed

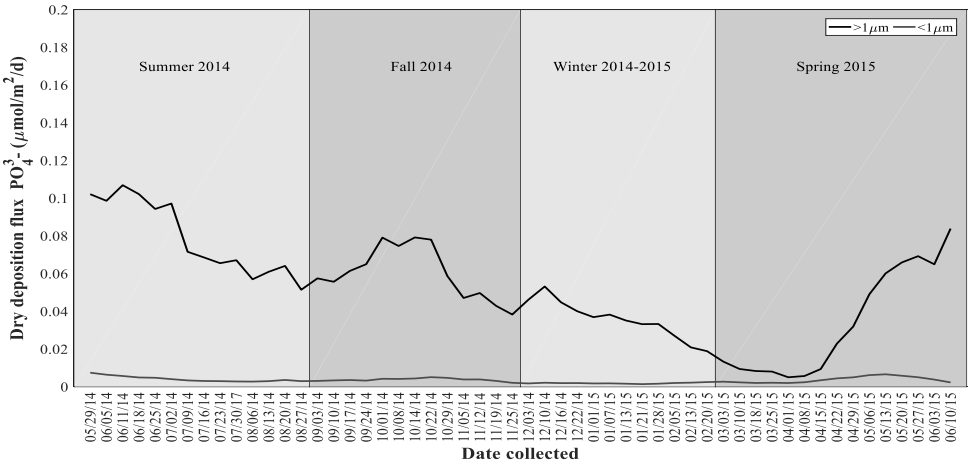

Figure 6. Smoothed seasonal dry deposition flux (μmol/m^2/d) of soluble (a) NO_3^-, (b) NH_4^+, and (c) PO_4^{3-} for weekly collected Eastern Shore samples. Note that data were interpolated for dates 30 July 2014, 6 August 2014, 13 August 2014, and 20 August 2014 using the method in Section 2.6.

(a) Aerosol leachate soluble nitrate from Eastern Shore samples - residuals

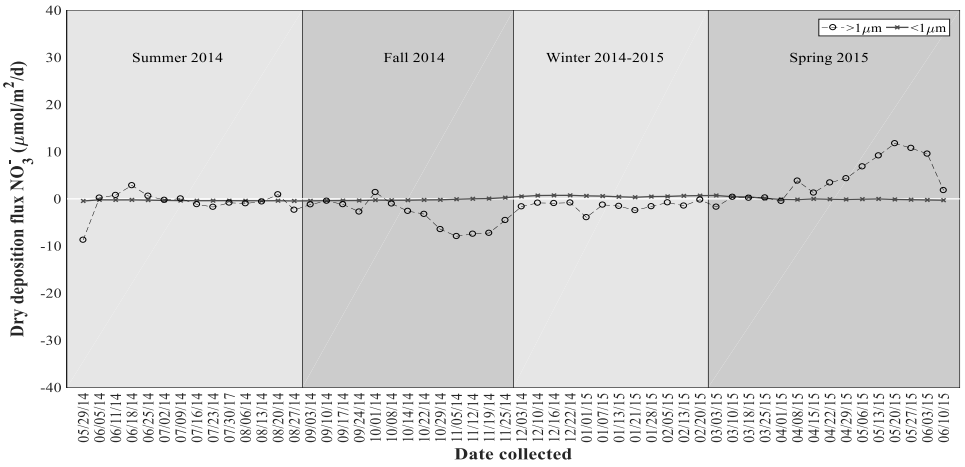

(b) Aerosol leachate soluble ammonium from Eastern Shore samples - residuals

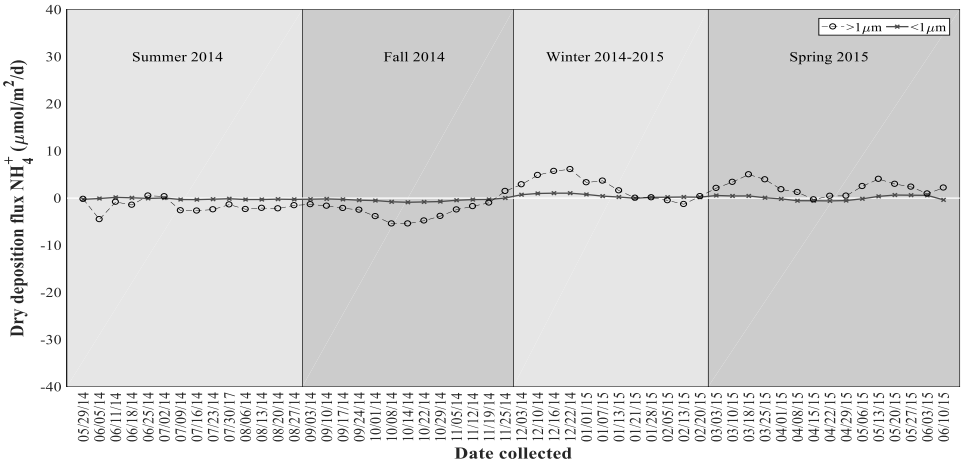

(c) Aerosol leachate soluble phosphate from Eastern Shore samples - residuals

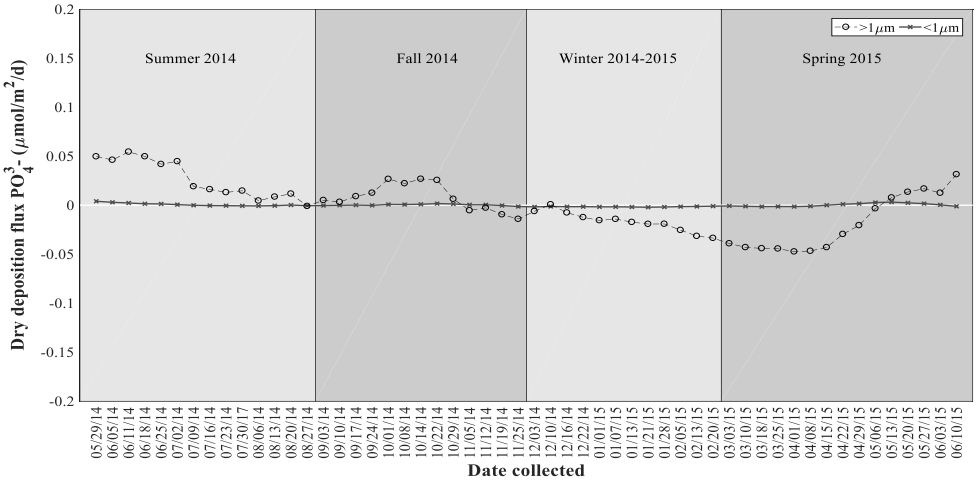

Figure 7. Residuals of total dry deposition flux (μmol/m^2/d) of soluble (a) NO_3^-, (b) NH_4^+, and (c) PO_4^{3-} for weekly collected Eastern Shore samples. Note that data were interpolated for dates 30 July 2014, 6 August 2014, 13 August 2014, and 20 August 2014 using the method in Section 2.6. The white horizontal line indicates the annual mean flux.

The seasonal mean dry fluxes of fine soluble NO_3^- were significantly different, as the mean dry fine soluble NO_3^- flux during winter (1.24 ± 0.471 μmol/m^2/d) was found to be significantly different ($p < 0.0001$, df = 48, F = 11.1) than means for summer (0.377 ± 0.147 μmol/m^2/d), fall (0.485 ± 0.250 μmol/m^2/d), and spring (0.738 ± 0.522 μmol/m^2/d) (Table 7), using a one-way ANOVA and a multiple comparison test. The mean dry flux of coarse soluble NO_3^- for spring (22. 4 ± 8.35 μmol/m^2/d) was significantly greater ($p = 0.0026$, df = 47, F = 5.57) than means for fall (13.8 ± 7.48 μmol/m^2/d) and winter (15.9 ± 5.88 μmol/m^2/d) (Table 7), as determined by a one-way ANOVA and multiple comparison test. A two-sample t-test confirmed that the overall mean flux of dry coarse soluble NO_3^- (17.6 ± 7.52 μmol/m^2/d) was significantly greater ($p < 0.0001$, df = 74.5, tstat = 32.5) than the overall mean flux of dry fine soluble NO_3^- (0.721 ± 0.503 μmol/m^2/d) (Table 6), as is apparent from Figure 5a.

The mean dry fluxes of fine soluble NH_4^+ for the four seasons were not significantly different ($p = 0.1148$, df = 48, F = 3.43). However, the mean dry flux of coarse soluble NH_4^+ for spring (19.6 ± 3.44 μmol/m^2/d) was found to be significantly greater ($p = 0.0248$, df = 48, F = 3.43) than that for fall (14.0 ± 2.97 μmol/m^2/d) (Table 7), using a one-way ANOVA and a multiple comparison test. A two-sample t-test confirmed that the overall mean dry flux of coarse soluble NH_4^+ (17.1 ± 5.74 μmol/m^2/d) was significantly greater ($p < 0.0001$, df = 97, tstat = 22.4) than the overall mean fine soluble NH_4^+ flux (3.30 ± 0.905 μmol/m^2/d) (Figures 6b and 7b), as is clear from Figure 5b.

The seasonal mean dry fluxes of fine soluble PO_4^{3-} were significantly different ($p = 0.0041$, df = 48, F = 5.08), with the mean fluxes for summer (4.45×10^{-3} μmol/m^2/d), fall (3.95×10^{-3} μmol/m^2/d), and spring (3.94×10^{-3} μmol/m^2/d) significantly greater ($p = 0.0041$, df = 48, F = 5.08) than the mean flux for winter (1.99×10^{-3} μmol/m^2/d) (Table 6). The median dry coarse soluble PO_4^{3-} flux for summer was significantly different ($p = 0.0002$, df = 45, chi-sq = 19.37) from those of winter and spring, and the median dry coarse PO_4^{3-} flux for fall was significantly different from those in winter and spring ($p = 0.0002$, df = 45, chi-sq = 19.37), using a Kruskal-Wallis test and a multiple comparison test. A Wilcoxon rank sum test confirmed that the median dry flux of coarse soluble PO_4^{3-} was significantly greater ($p <$

0.0001, zval = 8.18) than the median dry flux of fine soluble PO_4^{3-} throughout the sampling period (Figures 6c and 7c).

The mean total (fine+coarse) dry fluxes of soluble NO_3^- and NH_4^+ were greatest during spring, the mean total (fine+coarse) dry flux of soluble PO_4^{3-} was greatest during summer (Table 7). The overall mean total (fine+coarse) dry deposition fluxes of soluble NO_3^- (~18 µmol/m^2/d or 6.7 mmol/m^2/yr) and NH_4^+ (~20 µmol/m^2/d or 7.4 mmol/m^2/yr) were roughly equal for the Eastern Shore site (Table 7). The mean total (fine+coarse) dry deposition flux of soluble PO_4^{3-} (0.055 µmol/m^2/d or 0.020 mmol/m^2/yr) was more than 300 times lower than those for dry soluble NO_3^- (18 µmol/m^2/d or 6.7 mmol/m^2/yr) and NH_4^+ (20 µmol/m^2/d or 7.4 mmol/m^2/yr) (Table 7), resulting in a soluble inorganic N:P flux ratio of ~700, which far exceeded Redfield (16:1), where soluble N includes NO_3^- and NH_4^+,and soluble P includes PO_4^{3-}. This soluble inorganic N:P ratio does not account for the dry deposition flux of soluble organic N or P at the Eastern Shore, which was not determined in this study.

Table 7. Total (fine+coarse) dry flux of soluble NO_3^-, NH_4^+, and PO_4^{3-} from Eastern Shore samples.

Season	NO_3^-		NH_4^+		PO_4^{3-}	
	Estimated total dry flux (fine+coarse) (µmol/m^2/d)	Estimated total dry flux (fine+coarse) (mmol/m^2/yr)	Estimated total dry flux (fine+coarse) (µmol/m^2/d)	Estimated total dry flux (fine+coarse) (mmol/m^2/yr)	Estimated total dry flux (fine+coarse) (µmol/m^2/d)	Estimated total dry flux (fine+coarse) (mmol/m^2/yr)
Summer 2014	18	6.6	18	6.7	0.091	0.033
Fall 2014	14	5.2	17	6.1	0.065	0.024
Winter 2014 -2015	17	6.3	23	8.3	0.037	0.013
Spring 2015	23	8.4	24	8.7	0.038	0.014
Overall mean	18	6.7	20	7.4	0.055	0.020

In summary, there were no significant seasonal differences in the wet flux of soluble nutrients at the Eastern Shore site, however, there were significant seasonal differences in the dry flux of these soluble nutrients. The dry fine soluble NO_3^- flux during winter was significantly greater than those for fall and spring, and the mean dry flux of coarse soluble NO_3^- for spring was significantly greater than those for fall and winter. There were no significantly seasonal differences in the flux of fine soluble NH_4^+, however, the dry flux of coarse soluble NH_4^+ in spring was significantly greater than that in fall. The mean dry fluxes of fine soluble PO_4^{3-} in summer, fall, and spring were significantly greater than that for winter. The median dry fluxes of coarse PO_4^{3-} flux for summer and fall were significantly greater than those for winter and spring.

The total (fine+coarse) dry soluble NO_3^- flux was greatest during spring (23 µmol/m^2/d) and lowest in fall (14 µmol/m^2/d), while total (fine+coarse) fluxes for the summer and winter were roughly equal at 18 µmol/m^2/d and 17 µmol/m^2/d, respectively (Table 7). The total (fine+coarse) dry soluble NH_4^+ fluxes for spring (24 µmol/m^2/d) and winter (23 µmol/m^2/d) were also roughly equal, whereas total (fine+coarse) fluxes for summer and fall were lower at 18 µmol/m^2/d and 17 µmol/m^2/d, respectively (Table 7). The total (fine+coarse) dry soluble PO_4^{3-} flux was greatest in summer (0.091 µmol/m^2/d), during which it was more than twice those for winter (0.037 µmol/m^2/d) and spring (0.038 µmol/m^2/d) (Table 7). The fall total (fine+coarse) dry soluble PO_4^{3-} flux (0.065 µmol/m^2/d) was greater than those for winter (0.037 µmol/m^2/d) and spring (0.038 µmol/m^2/d), but lower than that for summer (0.091 µmol/m^2/d) (Table 7). The total (fine+coarse) dry soluble flux of inorganic N (NO_3^-+ NH_4^+) was greatest during spring (47 µmol/m^2/d) and lowest during fall (31 µmol/m^2/d). For the summer and winter seasons, the total (fine+coarse) dry soluble fluxes of NO_3^- + NH_4^+ were 36 µmol/m^2/d and 40 µmol/m^2/d, respectively.

In terms of the relative importance of wet and dry deposition to the supply of atmospherically derived nutrients at the Eastern Shore field station, wet deposition was the dominant deposition mode for soluble nutrients to this region (Tables 8, 9, and 10). At the Eastern Shore, wet deposition accounted for 47%, 78%, and 80% of the total (wet+dry) flux of soluble NO_3^-, NH_4^+, and PO_4^{3-}, respectively (Tables 8,

9, and 10). Although the total (fine+coarse) dry fluxes of soluble NO_3^- and NH_4^+ were similar, the wet flux of soluble NH_4^+ was much greater than that for soluble NO_3^-, thus the total (wet+dry) flux of soluble NH_4^+ was greater than that for soluble NO_3^- (Tables 8, 9, and 10). The overall mean total (wet+dry) flux of soluble NH_4^+ was 91.6 µmol/m^2/d or 33.4 mmol/m^2/yr (Table 9), more than twice that for soluble NO_3^- (34.5 µmol/m^2/d or 12.6 mmol/m^2/yr) (Table 8), therefore NH_4^+ was the dominant aeolian source of inorganic N to the Eastern Shore. The total (wet+dry) overall mean flux of soluble PO_4^{3-} (0.281 5µmol/m^2/d or 0.1 mmol/m^2/yr) was 125 times and 335 times lower than the total (wet+dry) overall mean flux of soluble NO_3^- and NH_4^+, respectively (Tables 8, 9, and 10). The overall mean total (wet+dry) deposition yielded an inorganic N:P deposition ratio of ~450, which far exceeds the Redfield ratio (16:1). Thus, atmospheric deposition to the coastal regions adjacent to the Eastern Shore was deficient in P relative to phytoplankton requirements.

Table 8. Mean (± standard deviation) total (wet+dry) flux of soluble NO_3^- from Eastern Shore samples.

Season	Dry deposition flux (µmol/m^2/d)		Total (fine+coarse) dry deposition flux	Wet deposition flux	Estimated total (wet+dry) flux	Estimated total (wet+dry) flux	Estimated wet deposition percentage of total
	<1µm	>1µm	(µmol/m^2/d)	(µmol/m^2/d)	(µmol/m^2/d)	(mmol/m^2/yr)	(%)
Summer 2014	0.377 ± 0.147	17.7 ± 4.53	18.1	20.5 ± 14.1	38.6	N/A	53.1
Fall 2014	0.485 ± 0.250	13.8 ± 7.48	14.3	12.5 ± 6.62	26.8	N/A	46.6
Winter 2014 -2015	1.24 ± 0.471	15.9 ± 5.88	17.1	14.4 ± 7.91	31.5	N/A	45.7
Spring 2015	0.738 ± 0.522	22. 4 ± 8.35	23.1	19.1 ± 13.7	42.2	N/A	45.3
Overall mean	0.721 ± 0.503	17.6 ± 7.52	18.3	16.2 ± 11.2	34.5	12.6	47.0

Table 9. Mean (± standard deviation) total (wet+dry) flux of soluble NH_4^+ from Eastern Shore samples.

Season	Dry deposition flux (µmol/m²/d)		Total (fine+coarse) dry deposition flux	Wet deposition flux	Estimated total (wet+dry) flux	Estimated total (wet+dry) flux	Estimated wet deposition percentage of total
	<1µm	>1µm	(µmol/m²/d)	(µmol/m²/d)	(µmol/m²/d)	(mmol/m²/yr)	(%)
Summer 2014	3.19 ± 0.600	15.2 ± 7.35	18.4	35.9 ± 33.8	54.3	N/A	66.1
Fall 2014	2.82 ± 0.496	14.0 ± 2.97	16.8	95.5 ± 59.7	112	N/A	85.0
Winter 2014 -2015	3.74 ± 1.26	19.0 ± 6.57	22.7	53.8 ± 54.1	76.5	N/A	70.3
Spring 2015	4.29 ± 0.871	19.6 ± 3.44	23.9	86.9 ± 61.4	111	N/A	78.4
Overall mean	3.30 ± 0.905	17.1 ± 5.74	20.4	71.2 ± 58.1	91.6	33.4	77.7

Table 10. Mean (± standard deviation) total (wet+dry) flux of soluble PO_4^{3-} from Eastern Shore samples.

Season	Dry deposition flux (µmol/m²/d)		Total (fine+coarse) dry deposition flux	Wet deposition flux	Estimated total (wet+dry) flux	Estimated (wet+dry) total flux	Estimated wet deposition percentage of total
	<1µm	>1µm	(µmol/m²/d)	(µmol/m²/d)	(µmol/m²/d)	(mmol/m²/yr)	(%)
Summer 2014	$4.45 \times 10^{-3} \pm 1.85 \times 10^{-3}$	$86.8 \times 10^{-3} \pm 36.3 \times 10^{-3}$	0.0913	0.718 ± 1.41	0.809	N/A	88.8
Fall 2014	$3.95 \times 10^{-3} \pm 2.05 \times 10^{-3}$	$61.1 \times 10^{-3} \pm 34.3 \times 10^{-3}$	0.0651	0.109 ± 0.159	0.174	N/A	62.6
Winter 2014 -2015	$1.99 \times 10^{-3} \pm 0.680 \times 10^{-3}$	$34.7 \times 10^{-3} \pm 13.8 \times 10^{-3}$	0.0367	0.0595 ± 0.0524	0.096	N/A	61.9
Spring 2015	$3.94 \times 10^{-3} \pm 2.20 \times 10^{-3}$	$33.6 \times 10^{-3} \pm 32.1 \times 10^{-3}$	0.0375	0.119 ± 0.245	0.157	N/A	75.8
Overall mean	$3.60 \times 10^{-3} \pm 1.90 \times 10^{-3}$	$51.7 \times 10^{-3} \pm 36.2 \times 10^{-3}$	0.0553	0.226 ± 0.705	0.281	0.1	80.4

3.3 WET DEPOSITION OF TOTAL-DISSOLVABLE TRACE METALS - EASTERN SHORE

The wet deposition flux of total-dissolvable aluminum (TDAl) ranged from 0.285 to 20.7 μmol/m^2/d in summer, 0.141 to 2.59 μmol/m^2/d in fall, 0.165 to 1.85 μmol/m^2/d in winter, and 1.36 to 3.48 μmol/m^2/d in spring (Table 11 and Figure 8a). The wet flux of TDAl was consistently below 5 μmol/m^2/d throughout the time series, except on 16 July 2014 when it peaked at over 20 μmol/m^2/d (Figure 8a). This elevated flux followed a sampling week during which no rain was collected (Figure 8a). The smoothed data and residuals (Figures 8b and 8c) show that the wet flux of TDAl remained was similar throughout fall, winter, and spring. The summer wet flux of TDAl was above the overall mean, largely due to the high flux associated with the sample of 16 July 2014 (Figure 8a). Although the mean summer wet flux of TDAl (2.70 ± 6.35 μmol/m^2/d) was greater than those for fall (0.718 ± 0.698 μmol/m^2/d), winter (0.507 ± 0.527 μmol/m^2/d), and spring (1.02 ± 0.958 μmol/m^2/d) (Table 11), there were no statistically significant differences in the means of the wet TDAl fluxes for the four seasons ($p = 109$, $df = 45$, $F = 2.14$).

Table 11. Mean (± standard deviation) and range (in parentheses) wet deposition flux (μmol/m^2/d) of total-dissolvable trace metals from Eastern Shore samples.

Trace metal	Summer 2014	Fall 2014	Winter 2014-2015	Spring 2015	Overall mean (μmol/m^2/d)	Overall mean (μmol/m^2/yr)
	Mean ± standard deviation	Mean ± standard deviation	Mean ± standard deviation	Mean ± standard deviation	Mean ± standard deviation	
Al	2.70 ± 6.35 (0.285-20.7)	0.718 ± 0.698 (0.141-2.59)	0.507 ± 0.527 (0.165-1.85)	1.02 ± 0.958 (1.36-3.48)	1.16 ± 2.92	423
Ti	$21.7 \times 10^{-3} \pm 38.3 \times 10^{-3}$ (4.01×10^{-3}-127×10^{-3})	$10.6 \times 10^{-3} \pm 9.38 \times 10^{-3}$ (1.91×10^{-3}-3.20×10^{-3})	$7.00 \times 10^{-3} \pm 7.39 \times 10^{-3}$ (0-22.3×10^{-3})	$13.3 \times 10^{-3} \pm 12.3 \times 10^{-3}$ (1.73×10^{-3}- 47.2×10^{-3})	$12.8 \times 10^{-3} \pm 19.3 \times 10^{-3}$	4.67
V	$4.89 \times 10^{-3} \pm 6.17 \times 10^{-3}$ (0.651×10^{-3}-16.9×10^{-3})	$24.2 \times 10^{-3} \pm 2.06 \times 10^{-3}$ (0.358×10^{-3}-8.07×10^{-3})	$1.51 \times 10^{-3} \pm 0.899 \times 10^{-3}$ (0.987×10^{-3}-3.34×10^{-3})	$2.18 \times 10^{-3} \pm 1.51 \times 10^{-3}$ (0.349×10^{-3}-4.68×10^{-3})	$2.60 \times 10^{-3} \pm 3.20 \times 10^{-3}$	0.949
Cr	$2.20 \times 10^{-3} \pm 3.48 \times 10^{-3}$ (0.401×10^{-3}-11.6×10^{-3})	$1.58 \times 10^{-3} \pm 1.51 \times 10^{-3}$ (0-4.86×10^{-3})	$1.30 \times 10^{-3} \pm 1.06 \times 10^{-3}$ (0.161×10^{-3}-3.75×10^{-3})	$1.54 \times 10^{-3} \pm 1.18 \times 10^{-3}$ (0.191×10^{-3}-3.96×10^{-3})	$1.60 \times 10^{-3} \pm 1.90 \times 10^{-3}$	0.584
Mn	$41.0 \times 10^{-3} \pm 62.7 \times 10^{-3}$ (5.68×10^{-3}-169×10^{-3})	$13.7 \times 10^{-3} \pm 7.61 \times 10^{-3}$ (2.12×10^{-3}-25.2×10^{-3})	$7.83 \times 10^{-3} \pm 7.64 \times 10^{-3}$ (1.81×10^{-3}-26.5×10^{-3})	$21.4 \times 10^{-3} \pm 19.8 \times 10^{-3}$ (1.50×10^{-3}-58.4×10^{-3})	$20.1 \times 10^{-3} \pm 31.6 \times 10^{-3}$	7.34
Fe	0.721 ± 1.41 (0.0883-4.63)	0.232 ± 0.178 (0.0424-0.670)	0.184 ± 0.173 (0.0417-0.558)	0.409 ± 0.385 (0.0510-1.34)	0.371 ± 0.680	136
Co	$5.28 \times 10^{-4} \pm 8.86 \times 10^{-4}$ (0.775×10^{-4}-28.8×10^{-4})	$1.30 \times 10^{-4} \pm 0.861 \times 10^{-4}$ (0-2.62×10^{-4})	$0.694 \times 10^{-4} \pm 0.917 \times 10^{-4}$ (0-2.75×10^{-4})	$2.06 \times 10^{-4} \pm 2.25 \times 10^{-4}$ (0-8.14×10^{-4})	$2.18 \times 10^{-4} \pm 4.35 \times 10^{-4}$	0.0769

Table 11. Continued.

Trace metal	Summer 2014 Mean ± standard deviation	Fall 2014 Mean ± standard deviation	Winter 2014-2015 Mean ± standard deviation	Spring 2015 Mean ± standard deviation	Overall mean ($\mu mol/m^2/d$) Mean ± standard deviation	Overall mean ($\mu mol/m^2/yr$)
Ni	0.939 ± 2.02 (0-5.58)	0.204 ± 0.735 (0-2.65)	– –	0.364 ± 1.02 (0-3.62)	0.350 ± 1.13	128
Cu	$5.73 \times 10^{-3} \pm 6.32 \times 10^{-3}$ (1.65×10^{-3}-17.2×10^{-3})	$4.53 \times 10^{-3} \pm 4.11 \times 10^{-3}$ (0.487×10^{-3}-16.2×10^{-3})	$2.54 \times 10^{-3} \pm 1.53 \times 10^{-3}$ (0.528×10^{-3}-5.16×10^{-3})	$4.23 \times 10^{-3} \pm 3.38 \times 10^{-3}$ (0.156×10^{-3}-10.1×10^{-3})	$4.20 \times 10^{-3} \pm 4.10 \times 10^{-3}$	1.53
Zn	$27.4 \times 10^{-3} \pm 31.8 \times 10^{-3}$ (6.79×10^{-3}-85.6×10^{-3})	$23.0 \times 10^{-3} \pm 25.5 \times 10^{-3}$ (10.1×10^{-3}-104×10^{-3})	$13.4 \times 10^{-3} \pm 8.97 \times 10^{-3}$ (3.71×10^{-3}-33.8×10^{-3})	$18.9 \times 10^{-3} \pm 14.8 \times 10^{-3}$ (4.54×10^{-3}-51.8×10^{-3})	$20.4 \times 10^{-3} \pm 21.2 \times 10^{-3}$	7.45
Cd	$0.982 \times 10^{-4} \pm 1.21 \times 10^{-4}$ (0-3.37×10^{-4})	$3.53 \times 10^{-4} \pm 2.83 \times 10^{-4}$ (0.915×10^{-4}-9.44×10^{-4})	$1.94 \times 10^{-4} \pm 1.57 \times 10^{-4}$ (0.646×10^{-4}-5.31×10^{-4})	$2.26 \times 10^{-4} \pm 1.38 \times 10^{-4}$ (0.522×10^{-4}-4.68×10^{-4})	$2.26 \times 10^{-4} \pm 2.03 \times 10^{-4}$	0.0825
Sb	$7.67 \times 10^{-4} \pm 8.43 \times 10^{-4}$ (1.21×10^{-4}-24.6×10^{-4})	$4.22 \times 10^{-4} \pm 3.16 \times 10^{-4}$ (0.477×10^{-4}-8.58×10^{-4})	$3.92 \times 10^{-4} \pm 2.24 \times 10^{-4}$ (1.49×10^{-4}-7.09×10^{-4})	$4.53 \times 10^{-4} \pm 3.90 \times 10^{-4}$ (0.325×10^{-4}-15.7×10^{-4})	$4.93 \times 10^{-4} \pm 4.79 \times 10^{-4}$	0.180
Pb	$4.98 \times 10^{-4} \pm 7.44 \times 10^{-4}$ (0.740×10^{-4}-25.1×10^{-4})	$4.37 \times 10^{-4} \pm 3.94 \times 10^{-4}$ (0-13.0×10^{-4})	$3.17 \times 10^{-4} \pm 1.87 \times 10^{-4}$ (0.719×10^{-4}-6.48×10^{-4})	$4.48 \times 10^{-4} \pm 3.39 \times 10^{-4}$ (0.0695×10^{-4}-10.1×10^{-4})	$4.24 \times 10^{-4} \pm 4.30 \times 10^{-4}$	0.155

(a) Rain total-dissolvable aluminum from Eastern Shore samples

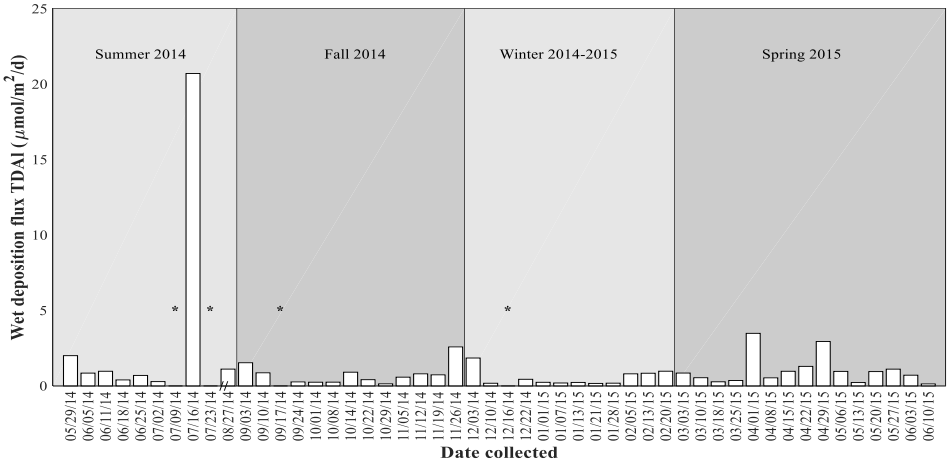

(b) Rain total-dissolvable aluminum from Eastern Shore samples - smoothed

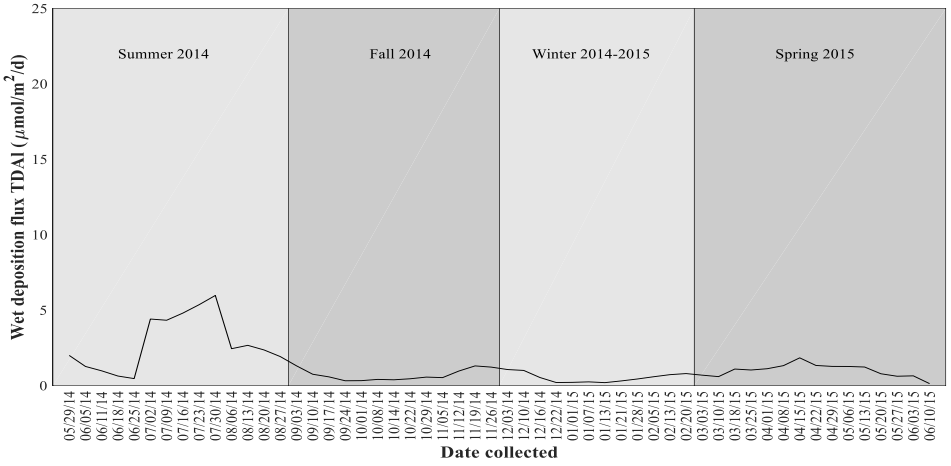

(c) Rain total-dissolvable aluminum from Eastern Shore samples - residuals

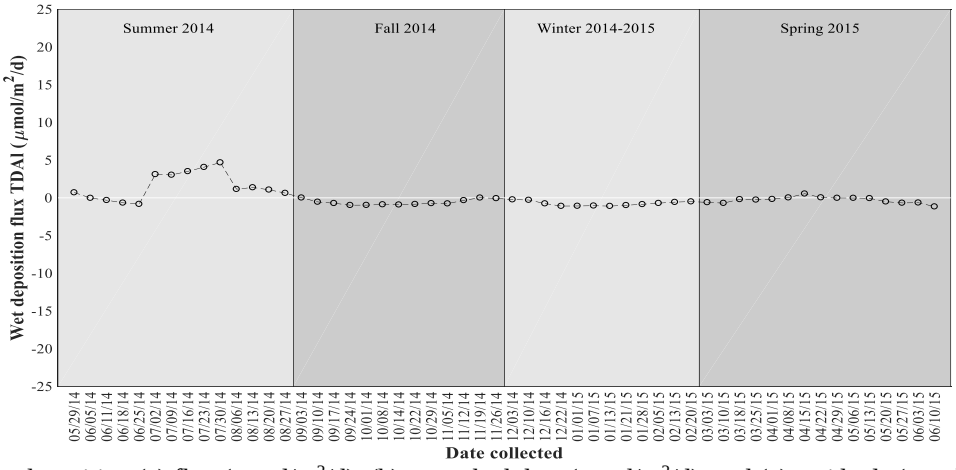

Figure 8. Wet deposition (a) flux (μmol/m^2/d), (b) smoothed data (μmol/m^2/d), and (c) residuals (μmol/m^2/d) for total-dissolvable aluminum (TDAl) from Eastern Shore samples. "//" indicates a break in the x-axis between 07/23/14 and 08/27/14 in (a) and "*" denotes dates for which no rain was collected. Note (b) and (c) included interpolated values for 30 July 2014, 6 August 2014, 13 August 2014, and 20 August 2014 using the method in Section 2.6. The white horizontal line in (c) indicates the annual mean flux.

The wet deposition flux of total-dissolvable titanium (TDTi) ranged from 4.01 x 10^{-3} to 127 x 10^{-3} µmol/m^2/d in summer, 1.91 x 10^{-3} to 3.20 x 10^{-3} (µmol/m^2/d) in fall, below the level of quantification to 22.3 x 10^{-3} µmol/m^2/d winter, and 1.73 x 10^{-3} to 47.2 x 10^{-3} µmol/m^2/d spring (Table 11 and Figure 9a). This flux was consistently below 0.05 µmol/m^2/d throughout the time series, except on 16 July 2014 when the flux was more than 3 times greater than those for all other samples (Figure 9a). The smoothed data and residuals show that the wet TDTi flux showed little variation throughout fall, winter, and spring (Figures 9b and 9c). The summer wet TDTi flux was above the overall mean, largely due to the high flux associated with the sample of 16 July 2014. The mean fluxes of wet TDTi for the four seasons were not significantly different ($p = 0.9039$, $df = 44$, $F = 1.25$).

(a) Rain total-dissolvable titanium from Eastern Shore samples

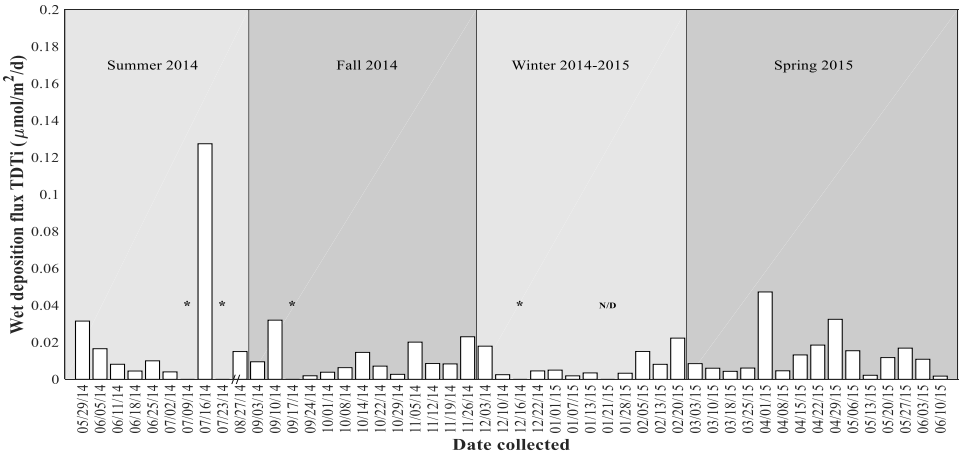

(b) Rain total-dissolvable titanium from Eastern Shore samples - smoothed

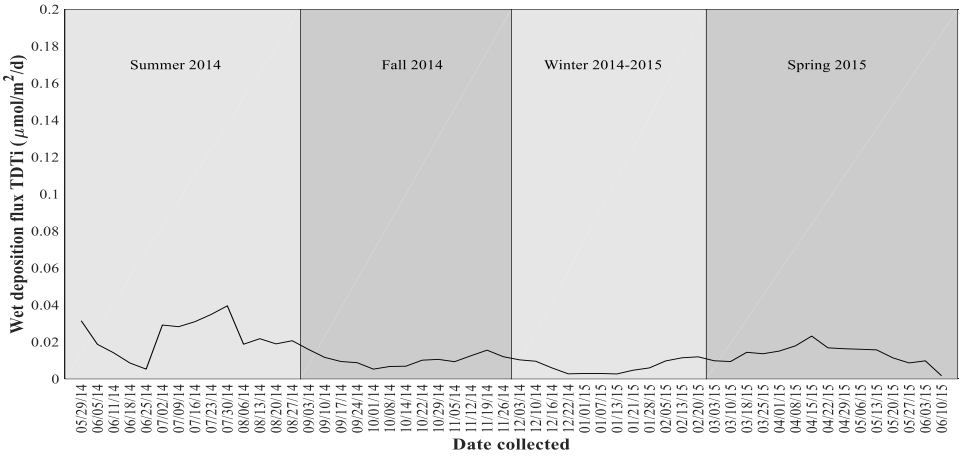

(c) Rain total-dissolvable titanium from Eastern Shore samples - residuals

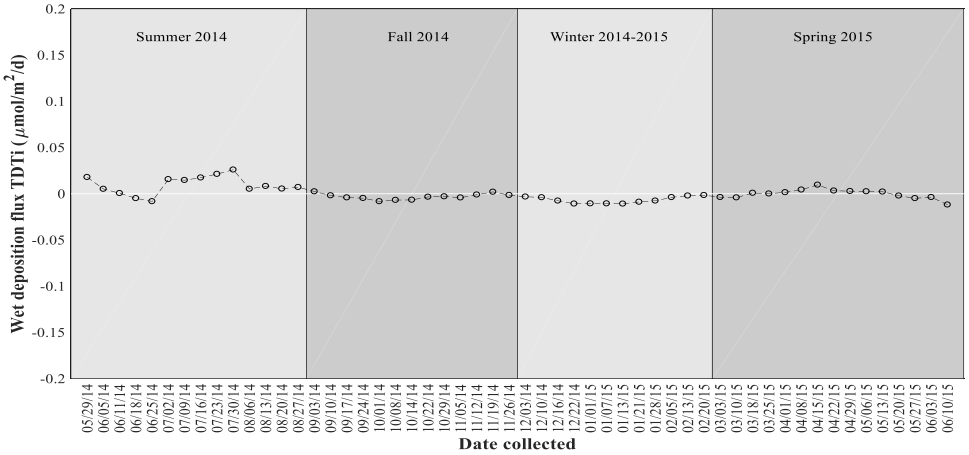

Figure 9. Wet deposition (a) flux (µmol/m^2/d), (b) smoothed data (µmol/m^2/d), and (c) residuals (µmol/m^2/d) for total-dissolvable titanium (TDTi) from Eastern Shore samples. "//" indicates a break in the x-axis between 07/23/14 and 08/27/14 in (a), "*" denotes dates for which no rain was collected, and "N/D" indicates samples for which titanium was not detectable. Note (b) and (c) included interpolated values for 30 July 2014, 6 August 2014, 13 August 2014, and 20 August 2014 using the method in Section 2.6. The white horizontal line in (c) indicates the annual mean flux.

The wet deposition flux of total-dissolvable vanadium (TDV), ranged from 0.651 x 10^{-3} to 16.9 x 10^{-3} µmol/m^2/d in summer, 0.358 x 10^{-3} to 8.07 x 10^{-3} in fall, 0.987 x 10^{-3} to 3.34 x 10^{-3} in winter, and 0.349 x 10^{-3} to 4.68 x 10^{-3} in spring (Table 11 and Figure 10a). The wet flux of TDV remained consistently below 5.00 x 10^{-3} µmol/m^2/d, except on 29 May 2014, 16 July 2014, 28 August 2014, and 19 November 2014 (Figure 10a). The smoothed data and residuals show that the wet flux of TDV was typically above the overall mean in summer, and below this mean during winter and spring (Figures 10b and 10c). The mean wet TDV flux for summer (4.89 x 10^{-3} ± 6.17 x 10^{-3} µmol/m^2/d) was found to be significantly greater ($p = 0.0115$, $df = 45$, $F = 4.15$) than those for both winter (1.51 x 10^{-3} ± 0.899 x 10^{-3} µmol/m^2/d) and spring (2.18 x 10^{-3} ± 1.51 x 10^{-3} µmol/m^2/d) (Table 11), using a one-way ANOVA and a multiple comparison test.

(a) Rain total-dissolvable vanadium from Eastern Shore samples

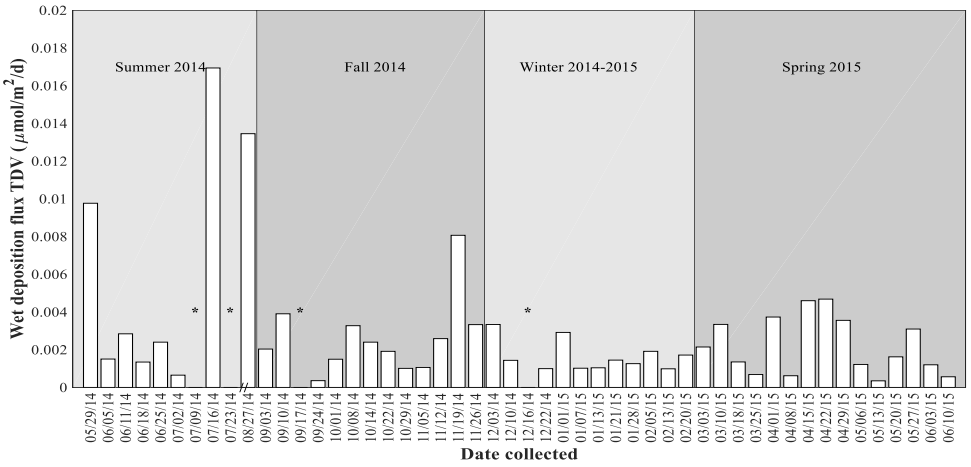

(b) Rain total-dissolvable vanadium from Eastern Shore samples - smoothed

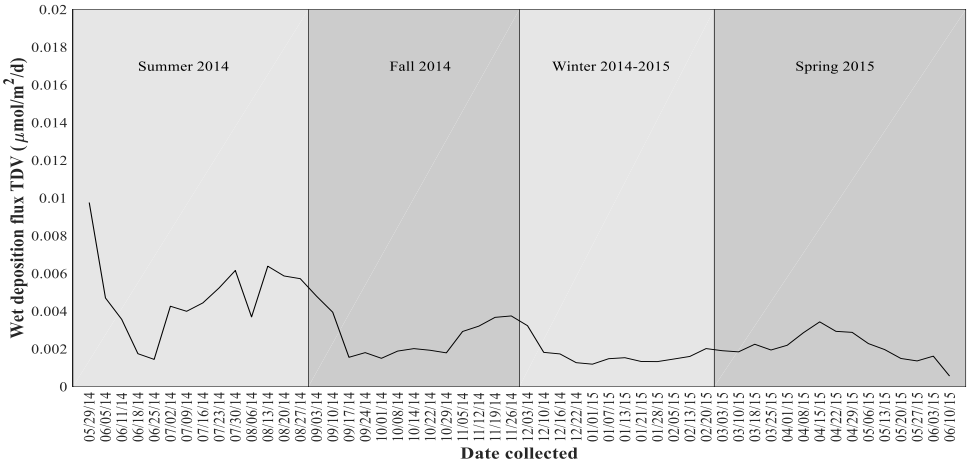

(c) Rain total-dissolvable vanadium from Eastern Shore samples - residuals

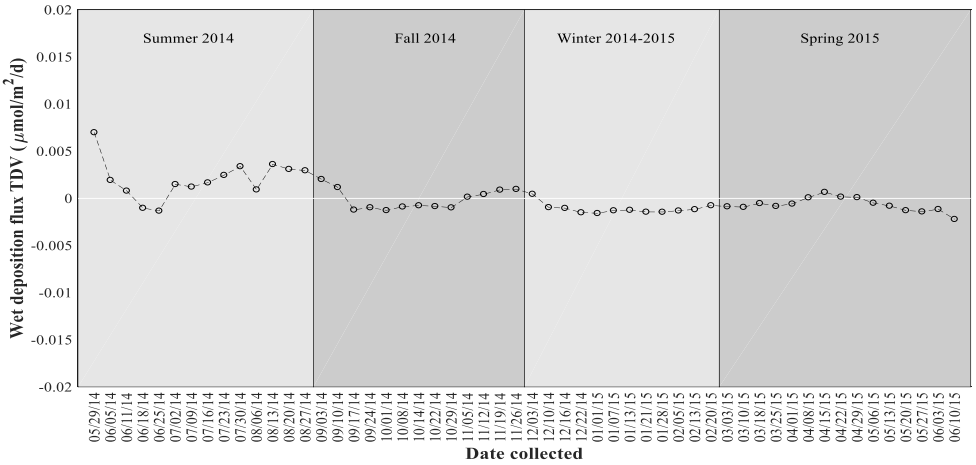

Figure 10. Wet deposition (a) flux (µmol/m^2/d), (b) smoothed data (µmol/m^2/d), and (c) residuals (µmol/m^2/d) for total-dissolvable vanadium (TDV) from Eastern Shore samples. "//" indicates a break in the x-axis between 07/23/14 and 08/27/14 in (a) and "*****" denotes dates for which no rain was collected. Note (b) and (c) included interpolated values for dates 30 July 2014, 6 August 2014, 13 August 2014, and 20 August 2014 using the method in Section 2.6. The white horizontal line in (c) indicates the annual mean flux.

The wet flux of total-dissolvable chromium (TDCr) ranged from 0.401 x 10^{-3} to 11.6 x 10^{-3} µmol/m^2/d in summer, below the level of quantification to 4.86 x 10^{-3} µmol/m^2/d in fall, 0.161 x 10^{-3} to 3.75 x 10^{-3} µmol/m^2/d in winter, and 0.191 x 10^{-3} to 3.96 x 10^{-3} µmol/m^2/d in spring (Table 11 and Figure 11a). The wet TDCr flux remained relatively constant throughout the time series, except on 16 July 2014 when the flux was more than twice those for all other samples (Figure 11a). The smoothed data and residuals (Figures 11b and 11c) show that the wet TDCr flux showed little variation throughout the fall, winter, and spring. The summer wet TDCr flux was above the overall mean due to the large flux on 16 July 2014, although the mean wet TDCr fluxes for the four seasons were not significantly different ($p = 0.7791$, $df = 44$, $F = 0.34$).

(a) Rain total-dissolvable chromium from Eastern Shore samples

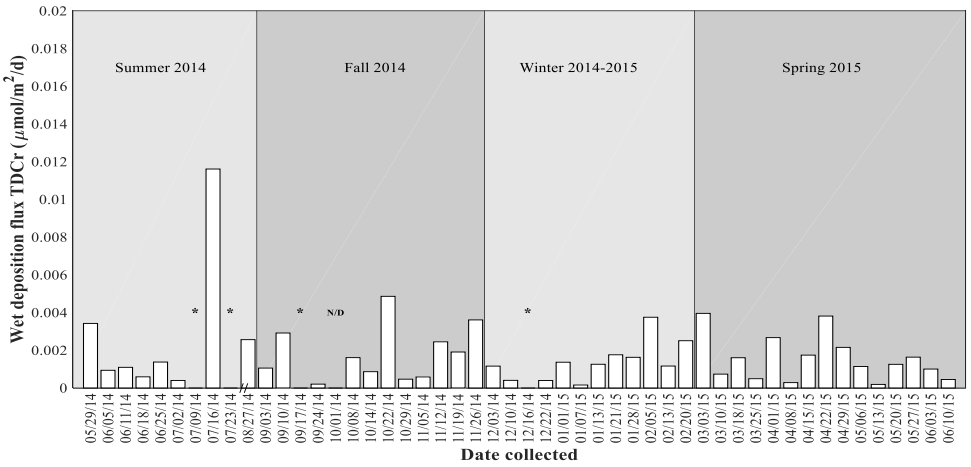

(b) Rain total-dissolvable chromium from Eastern Shore samples - smoothed

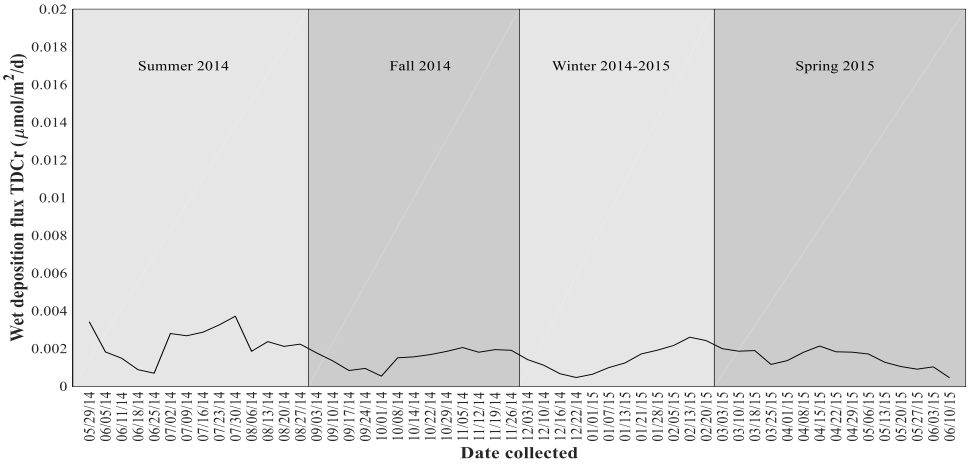

(c) Rain total-dissolvable chromium from Eastern Shore samples - residuals

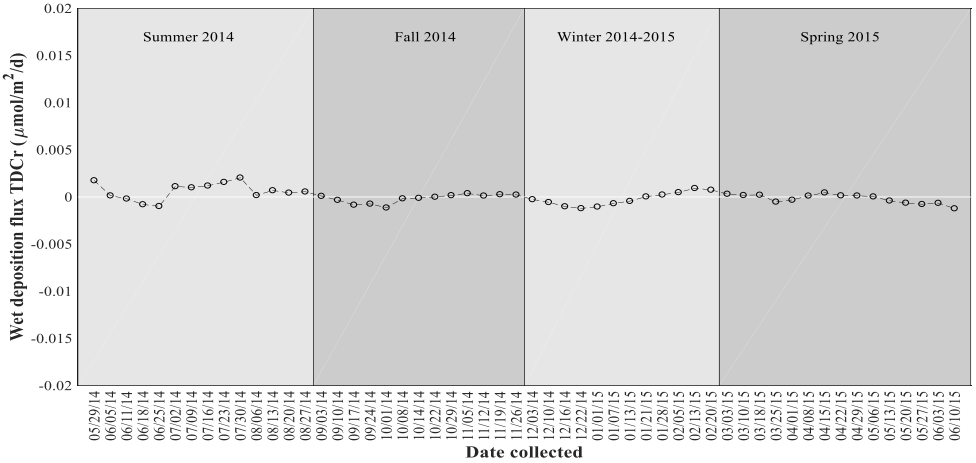

Figure 11. Wet deposition (a) flux (μmol/m^2/d), (b) smoothed data (μmol/m^2/d), and (c) residuals (μmol/m^2/d) for total-dissolvable chromium (TDCr) from Eastern Shore samples. "//" indicates a break in the x-axis between 07/23/14 and 08/27/14 in (a), "*" denotes dates for which no rain was collected, and "N/D" indicates non-detect samples. Note (b) and (c) included interpolated values for dates 30 July 2014, 6 August 2014, 13 August 2014, and 20 August 2014 using the method in Section 2.6. The white horizontal line in (c) indicates the annual mean flux.

The wet deposition flux of total-dissolvable manganese (TDMn) ranged from 5.68 x 10^{-3} to 169 x 10^{-3} µmol/m^2/d in summer, 2.12 x 10^{-3} to 25.2 x 10^{-3} µmol/m^2/d in fall, 1.81 x 10^{-3} to 26.5 x 10^{-3} µmol/m^2/d in winter, and 1.50 x 10^{-3} to 58.4 x 10^{-3} µmol/m^2/d in spring (Table 11). The wet TDMn flux peaked on 29 May 2014 and 16 July 2014, when the flux was more than twice that for all other samples (Figure 11a). The smoothed data and residuals (Figures 12b and 12c) show that the wet TDMn flux was typically above the overall mean during summer and spring, and below this mean during the fall and winter. The mean wet flux of TDMn in summer (41.0 x 10^{-3} ± 62.7 x 10^{-3} µmol/m^2/d) was significantly greater ($p = 0.0446$, $df = 45$, $F = 2.93$) than that for winter (21.4 x 10^{-3} ± 19.8 x 10^{-3} µmol/m^2/d) (Table 11), but not significantly different from those for fall and spring, as determined by a one-way ANOVA and a multiple comparison test.

(a) Rain total-dissolvable manganese from Eastern Shore samples

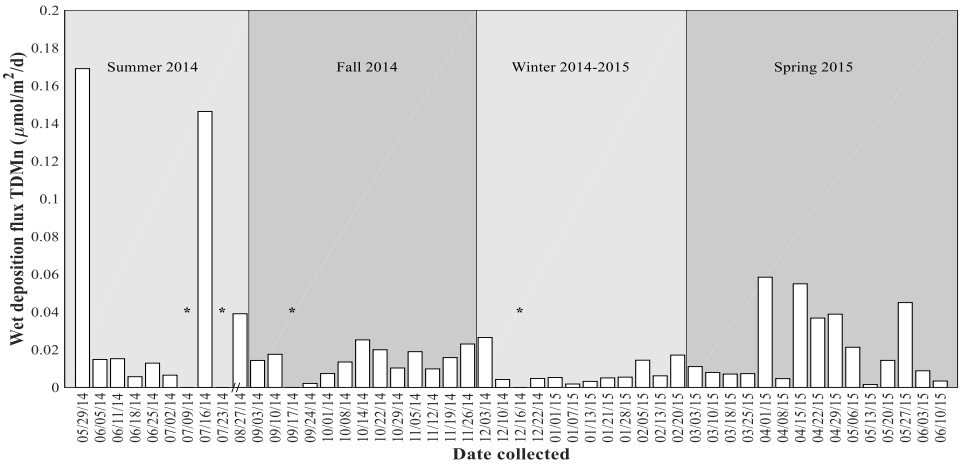

(b) Rain total-dissolvable manganese from Eastern Shore samples - smoothed

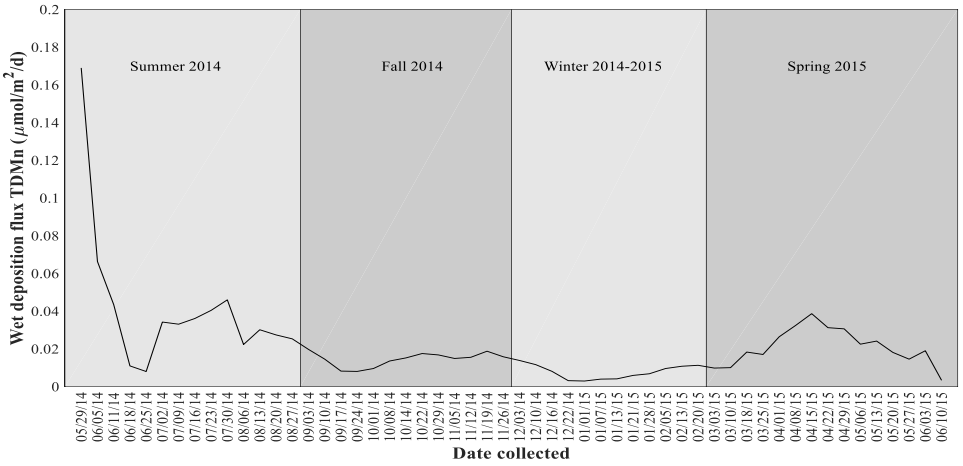

(c) Rain total-dissolvable manganese from Eastern Shore samples - residuals

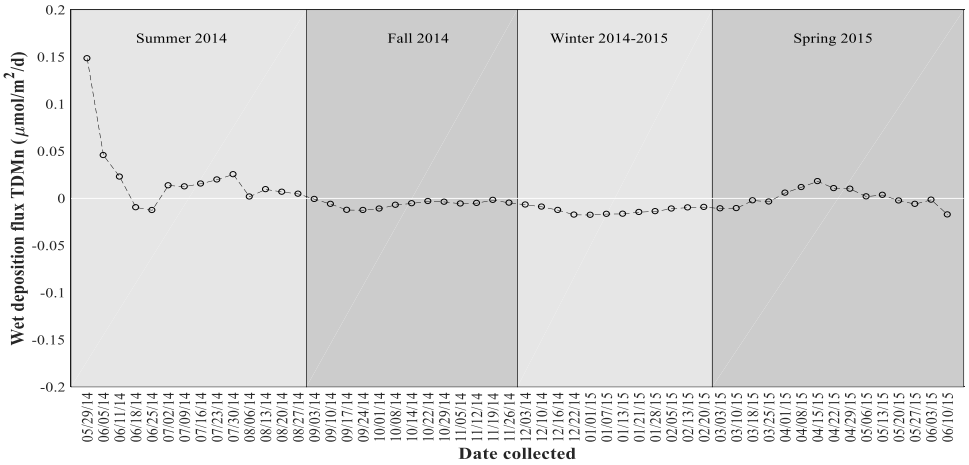

Figure 12. Wet deposition (a) flux (µmol/m^2/d), (b) smoothed data (µmol/m^2/d), and (c) residuals (µmol/m^2/d) for total-dissolvable manganese (TDMn) from Eastern Shore samples. "//" indicates a break in the x-axis between 07/23/14 and 08/27/14 in (a) and "*" denotes dates for which no rain was collected. Note (b) and (c) included interpolated values for dates 30 July 2014, 6 August 2014,13 August 2014, and 20 August 2014 using the method in Section 2.6. The white horizontal line in (c) indicates the annual mean flux.

The wet deposition flux of total-dissolvable iron (TDFe) ranged from 0.088 to 4.63 μmol/m^2/d in summer, 0.0424 to 0.670 μmol/m^2/d in fall, 0.0417 to 0.558 in winter, and 0.0510 to 1.34 μmol/m^2/d in spring (Table 11 and Figure 13a). The flux of TDFe peaked on 16 July 2014, when the flux was more than 3 times greater than that for other samples (Figure 12a). The smoothed data and residuals (Figure 12b and 12c) show that the wet TDFe flux was mostly above the overall mean during the summer, but remained relatively constant during the fall, winter, and spring. Although the mean wet fluxes of TDFe for summer and spring were greater than those for fall and winter (Table 11), the mean wet TDFe fluxes for the four seasons were not significantly different ($p = 0.1706$, $df = 45$, $F = 1.75$).

(a) Rain total-dissolvable iron from Eastern Shore samples

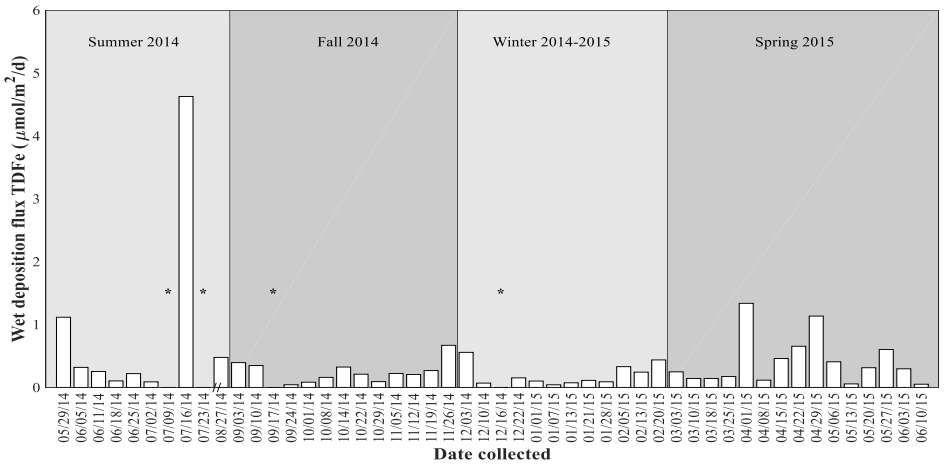

(a) Rain total-dissolvable iron from Eastern Shore samples - smoothed

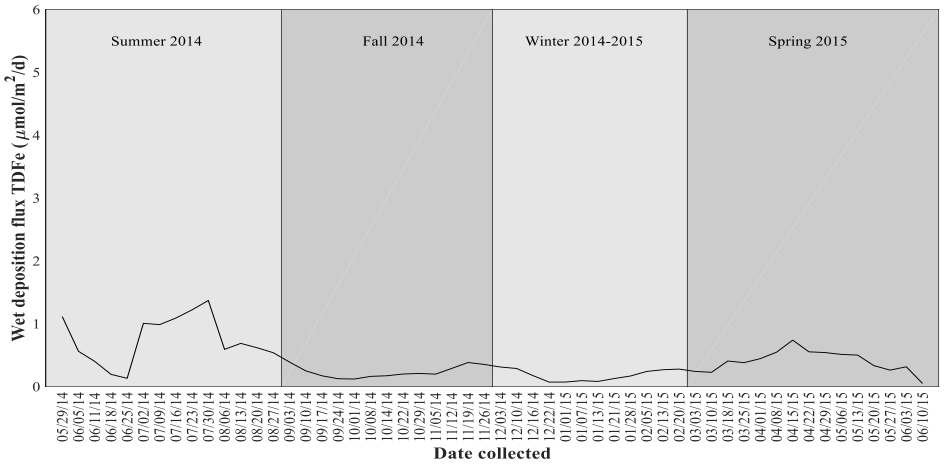

(b) Rain total-dissolvable iron from Eastern Shore samples - residuals

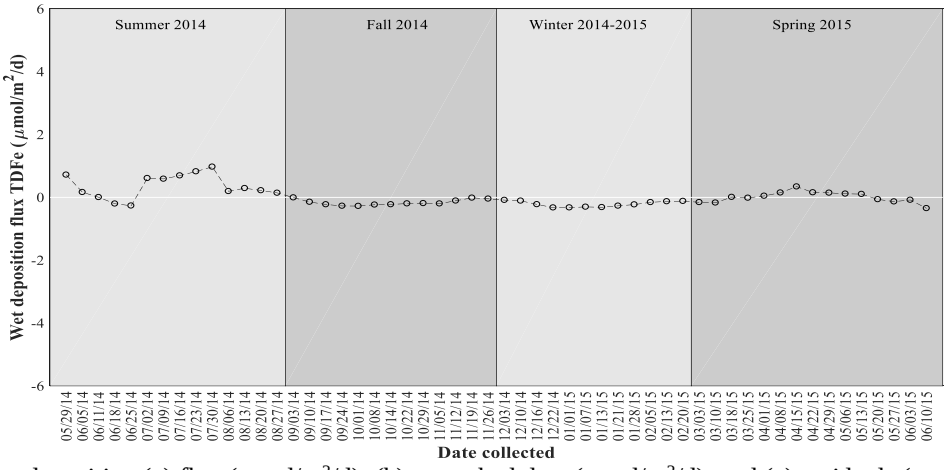

Figure 13. Wet deposition (a) flux (µmol/m^2/d), (b) smoothed data (µmol/m^2/d), and (c) residuals (µmol/m^2/d) for total-dissolvable iron (TDFe) from Eastern Shore samples. "//" indicates a break in the x-axis between 07/23/14 and 08/27/14 in (a) and "*" denotes dates for which no rain was collected. Note (b) and (c) included interpolated values for dates 30 July 2014, 6 August 2014, 13 August 2014, and 20 August 2014 using the method in Section 2.6. The white horizontal line in (c) indicates the annual mean flux.

The wet deposition flux of total-dissolvable cobalt (TDCo) ranged from 0.775 x 10^{-4} to 28.8 x 10^{-4} µmol/m^2/d in summer, below the level of quantification to 2.62 x 10^{-4} µmol/m^2/d in fall, below the level of quantification to 2.75 x 10^{-4} µmol/m^2/d in winter, and below the level of quantification to 8.14 x 10^{-4} µmol/m^2/d in spring (Table 11 and Figure 14a). The flux of TDCo peaked on 29 May 2014, 16 July 2014, 27 August 2014, and 1 April 2015 (Figure 14a). The smoothed data and residuals (Figures 14b and 14c) show that the TDCo flux was mostly above the overall mean during the summer, but remained relatively constant during fall, winter, and spring. Although the mean wet fluxes of TDCo were greater for summer (5.28 x 10^{-4} ± 8.86 x 10^{-4} µmol/m^2/d) and spring (2.06 x 10^{-4} ± 2.25 x 10^{-4} µmol/m^2/d), than those for fall (1.30 x 10^{-4} ± 0.861 x 10^{-4} µmol/m^2/d) and winter (0.694 x 10^{-4} ± 0.917 x 10^{-4} µmol/m^2/d), there were no statistically significant differences ($p = 0.0917$, $df = 38$, $F = 2.33$) in the mean wet fluxes of TDCo for the four seasons.

(a) Rain total-dissolvable cobalt from Eastern Shore samples

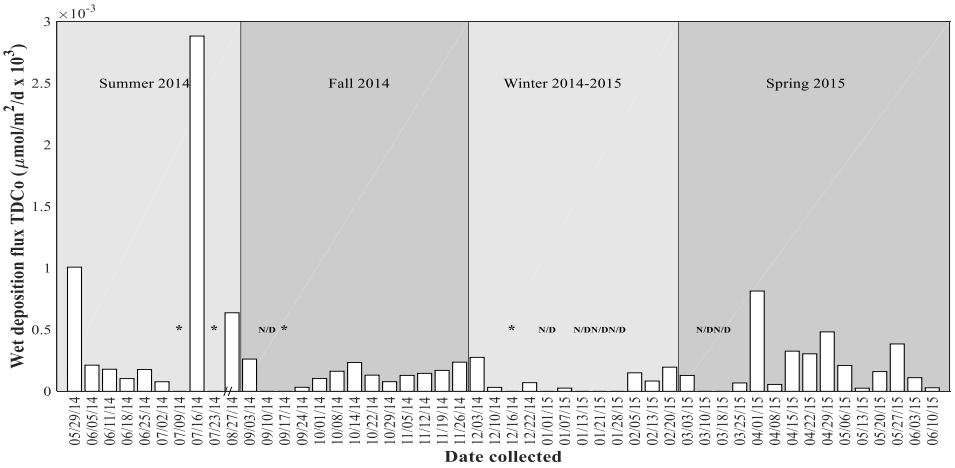

(b) Rain total-dissolvable cobalt from Eastern Shore samples - smoothed

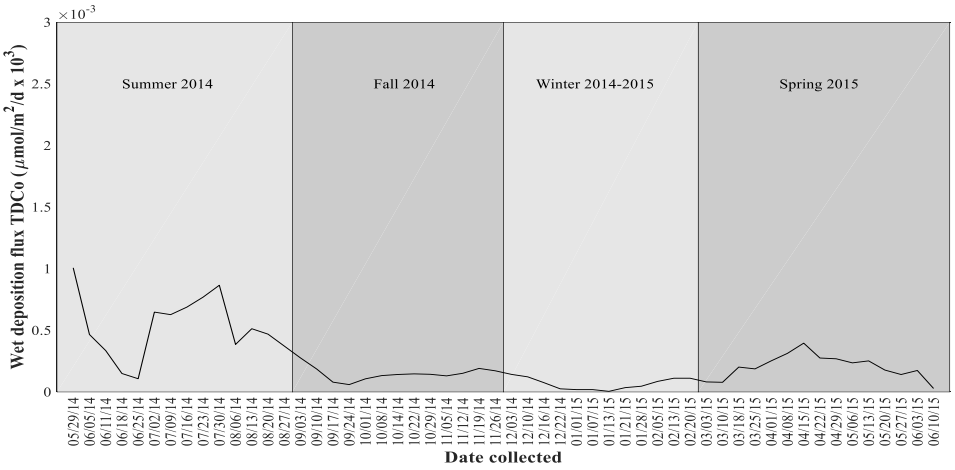

(c) Rain total-dissolvable cobalt from Eastern Shore samples - residuals

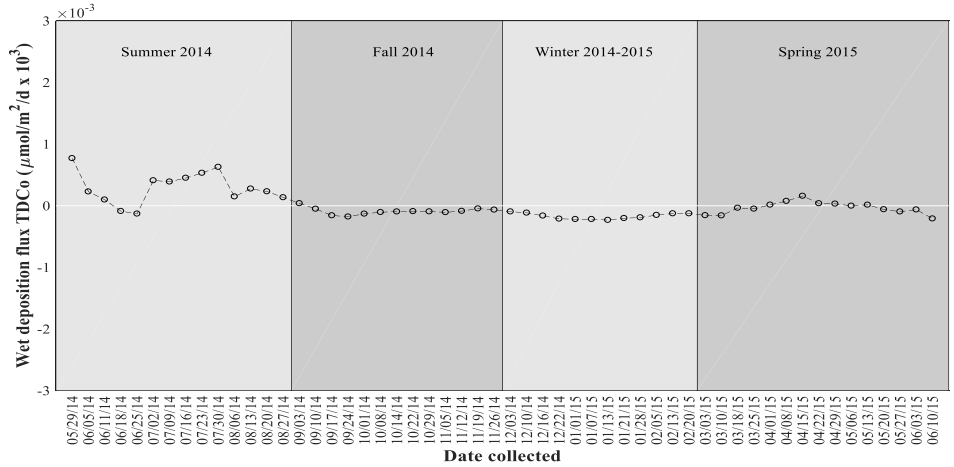

Figure 14. Wet deposition (a) flux (µmol/m^2/d x 10^3), (b) smoothed data (µmol/m^2/d x 10^3), and (c) residuals (µmol/m^2/d x 10^3) for total-dissolvable cobalt (TDCo) from Eastern Shore samples. "//" indicates a break in the x-axis between 07/23/14 and 08/27/14 in (a), "*" denotes dates for which no rain was collected, and "N/D" indicates non-detect samples. Note (b) and (c) included interpolated values for dates 30 July 2014, 6 August 2014, 13 August 2014, and 20 August 2014 using the method in Section 2.6. The white horizontal line in (c) indicates the annual mean flux.

The wet deposition flux of total-dissolvable nickel (TDNi) ranged below the level of quantification to 5.58 µmol/m^2/d in summer, below the level of quantification to 2.65 µmol/m^2/d in fall, and below the level of quantification to 3.62 µmol/m^2/d in spring (Table 11 and Figure 15a). Wet TDNi flux data was unavailable for winter, as the concentrations of TDNi in those samples were below the detection limit of 0.081 µg L^{-1} (Table 11 and Figure 15a). Most of the wet deposition samples collected had TDNi concentrations below the analytical detection limit (Figure 15a). The wet deposition samples with concentrations above the detection limit were collected mainly during summer and spring on 16 July 2014, 27 August 2014, 3 September 2014, 1 April 2015, and 8 April 2015 (Figure 15b and 15c). The small sample size (n = 5) of wet TDNi flux data was insufficient for use in statistical analysis (Figures 15b and 15c).

(a) Rain total-dissolvable nickel from Eastern Shore samples

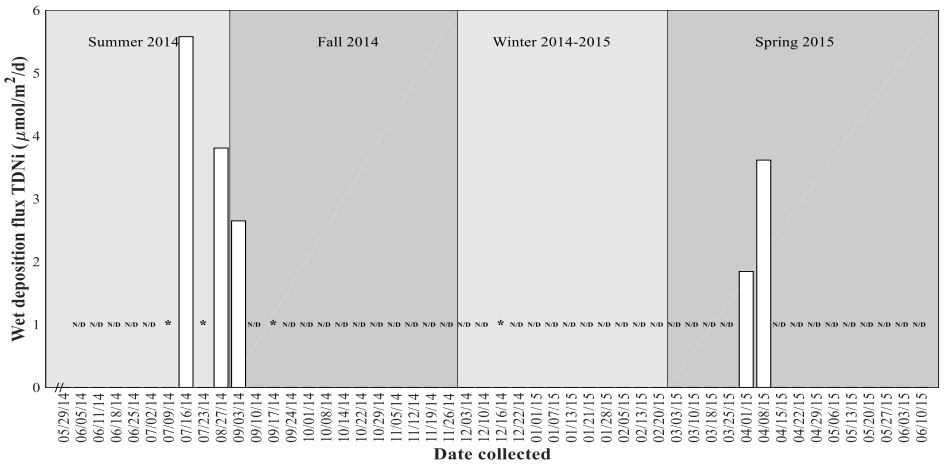

(b) Rain total-dissolvable nickel from Eastern Shore samples - smoothed

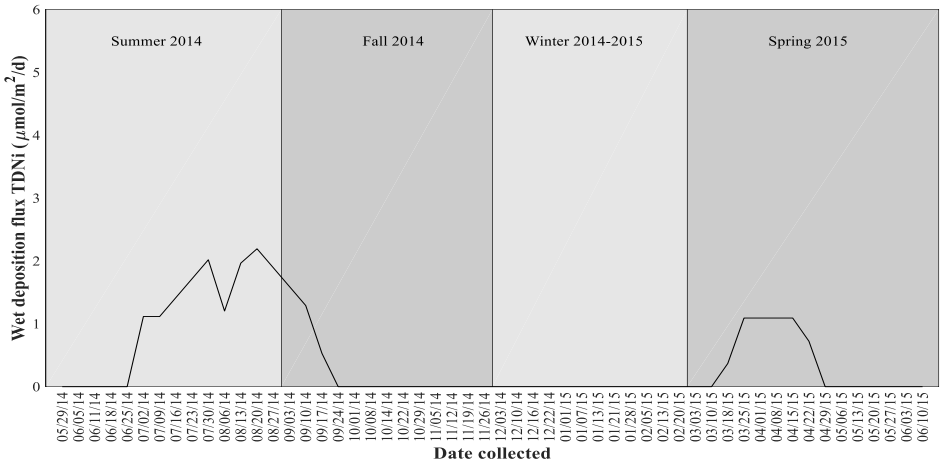

(c) Rain total-dissolvable nickel from Eastern Shore samples - residuals

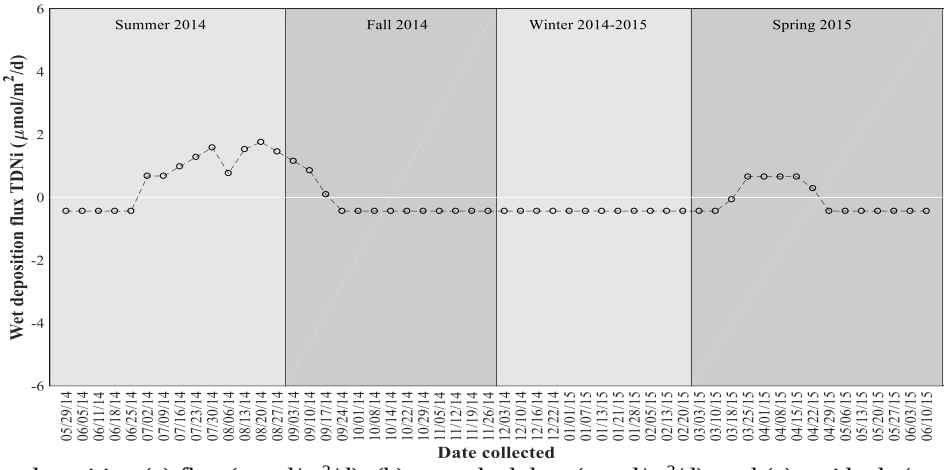

Figure 15. Wet deposition (a) flux (µmol/m^2/d), (b) smoothed data (µmol/m^2/d), and (c) residuals (µmol/m^2/d x 10^3) for total-dissolvable nickel (TDNi) from Eastern Shore samples. "//" indicates a break in the x-axis between 07/23/14 and 08/27/14 in (a), "*" denotes dates for which no rain was collected, and "N/D" indicates non-detect samples. Note (b) and (c) included interpolated values for dates 30 July 2014, 6 August 2014, 13 August 2014, and 20 August 2014 using the method in Section 2.6. The white horizontal line in (c) indicates the annual mean flux.

The wet deposition flux of total-dissolvable copper (TDCu) ranged from 1.65 x 10^{-3} to 17.2 x 10^{-3} µmol/m^2/d in summer, 0.487 x 10^{-3} to 16.2 x 10^{-3} µmol/m^2/d in fall, 0.528 x 10^{-3} to 5.16 x 10^{-3} µmol/m^2/d in winter, and 0.156 x 10^{-3} to 10.1 x 10^{-3} µmol/m^2/d in spring (Table 11 and Figure 16a). The smoothed data and residuals show that the wet flux of TDCu was often above the overall mean during summer and spring, and below this mean during winter (Figure 15c). However, there were no statistically significant differences in the median fluxes of TDCu for the four seasons ($p = 0.3577$, $df = 45$, chi-sq = 3.23), as determined by a Kruskal-Wallis test.

(a) Rain total-dissolvable copper from Eastern Shore samples

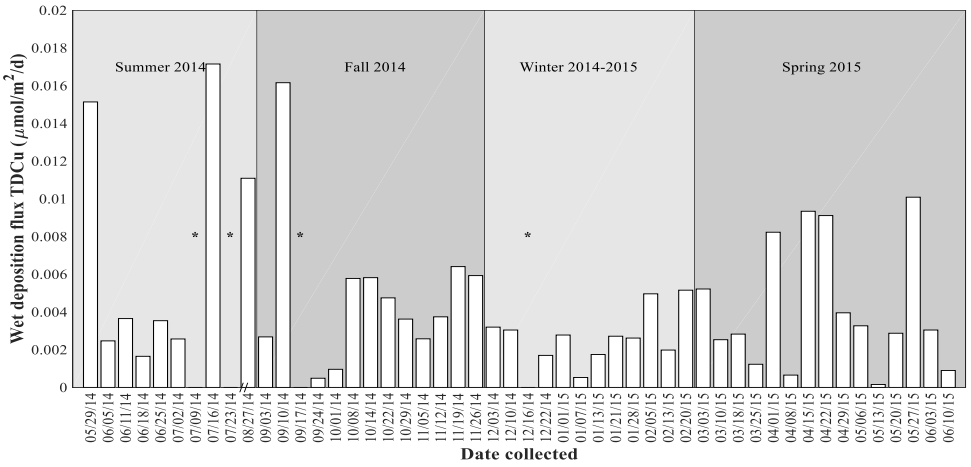

(b) Rain total-dissolvable copper from Eastern Shore samples - smoothed

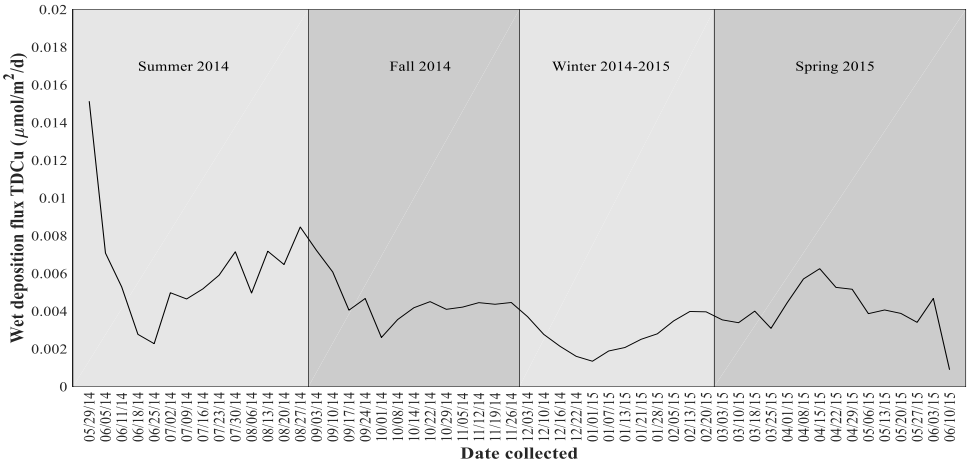

(c) Rain total-dissolvable copper from Eastern Shore samples - residuals

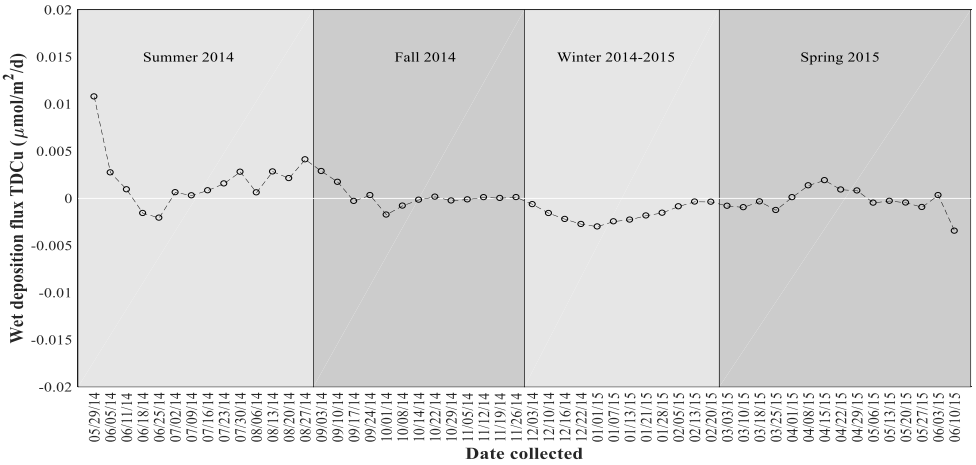

Figure 16. Wet deposition (a) flux (µmol/m^2/d), (b) smoothed data (µmol/m^2/d), and (c) residuals (µmol/m^2/d x 10^3) for total-dissolvable copper (TDCu) from Eastern Shore samples. "//" indicates a break in the x-axis between 07/23/14 and 08/27/14 in (a) and "*" denotes dates for which no rain was collected. Note (b) and (c) included interpolated values for dates 30 July 2014, 6 August 2014, 13 August 2014, and 20 August 2014 using the method in Section 2.6. The white horizontal line in (c) indicates the annual mean flux.

The wet deposition flux of total-dissolvable zinc (TDZn) ranged from 6.79 x 10^{-3} to 85.6 x 10^{-3} µmol/m^2/d in summer, 10.1 x 10^{-3} to 104 x 10^{-3} µmol/m^2/d in fall, 3.71 x 10^{-3} to 33.8 x 10^{-3} µmol/m^2/d in winter, and 4.54 x 10^{-3} to 51.8 x 10^{-3} µmol/m^2/d in spring (Table 11 and Figure 17a). The smoothed data and residuals show that the wet flux of TDZn was mostly above the overall mean during summer, and mostly below this mean during winter (Figures 17b and 17c). Although the mean wet flux of TDZn in the summer (27.4 x 10^{-3} ± 31.8 x 10^{-3} µmol/m^2/d) was greater than those for fall (23.0 x 10^{-3} ± 25.5 x 10^{-3} µmol/m^2/d), winter (13.4 x 10^{-3} ± 8.97 x 10^{-3} µmol/m^2/d), and spring (18.9 x 10^{-3} ± 14.8 x 10^{-3} µmol/m^2/d) (Table 11), the mean fluxes of TDZn for the seasons were not significantly different ($p = 0.2621$, $df = 45$, $F = 1.38$).

(a) Rain total-dissolvable zinc from Eastern Shore samples

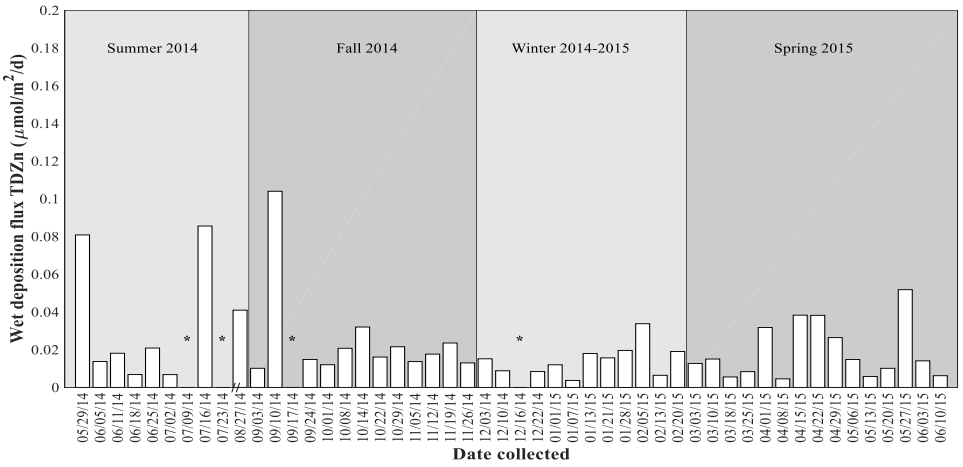

(b) Rain total-dissolvable zinc from Eastern Shore samples - smoothed

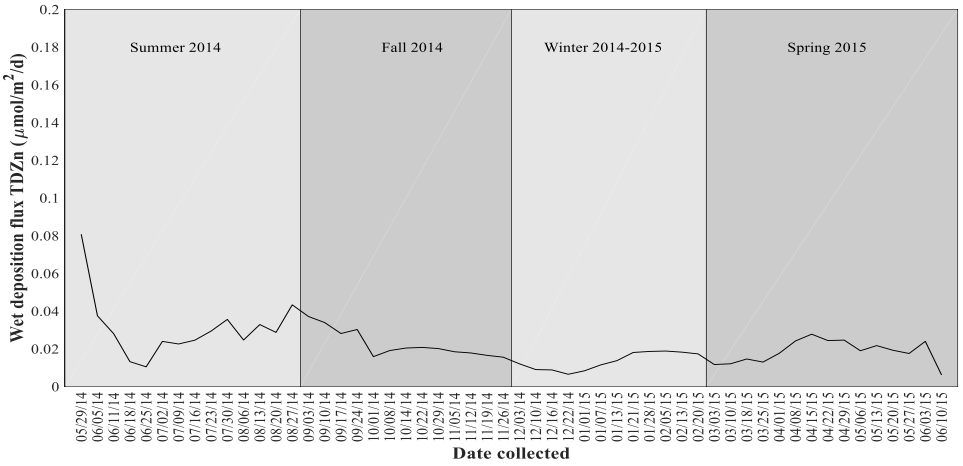

(c) Rain total-dissolvable zinc from Eastern Shore samples - residuals

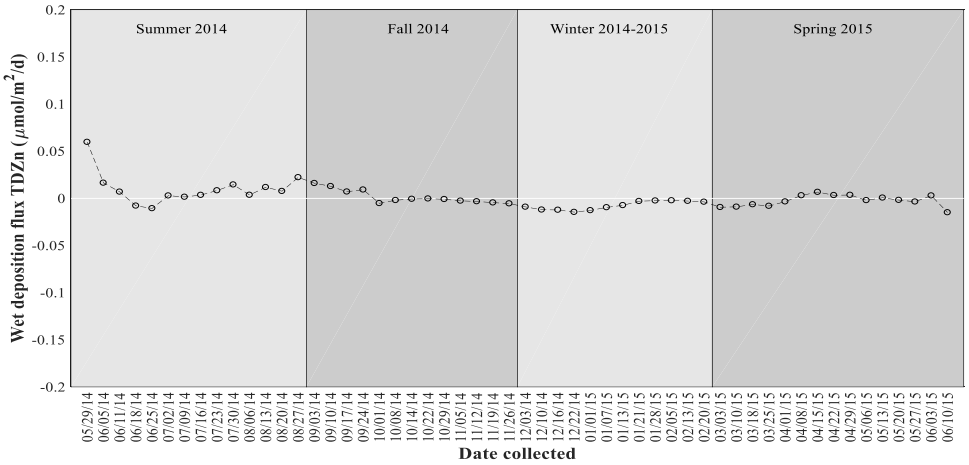

Figure 17. Wet deposition (a) flux (μmol/m^2/d), (b) smoothed data (μmol/m^2/d), and (c) residuals (μmol/m^2/d) for total-dissolvable zinc (TDZn) from Eastern Shore samples. "//" indicates a break in the x-axis between 07/23/14 and 08/27/14 in (a) and "*" denotes dates for which no rain was collected. Note (b) and (c) included interpolated values for dates 30 July 2014, 6 August 2014, 13 August 2014, and 20 August 2014 using the method in Section 2.6. The white horizontal line in (c) indicates the annual mean flux.

The wet flux of total-dissolvable cadmium (TDCd) ranged from below the level of quantification to 3.37 x 10^{-4} µmol/m^2/d in summer, 0.915 x 10^{-4} to 9.44 x 10^{-4} µmol/m^2/d in fall, 0.646 x 10^{-4} to 5.31 x 10^{-4} µmol/m^2/d in winter, and 0.522 x 10^{-4} to 4.68 x 10^{-4} µmol/m^2/d in spring (Table 11 and Figure 18a). The smoothed data and residuals show that the flux of TDCd was mostly above the overall mean during fall and mostly below this mean during summer (Figures 18b and 18c). During winter and spring, the flux of TDCd varied above and below the overall mean. The mean wet TDCd flux for fall (3.53 x 10^{-4} ± 2.83 x 10^{-4} µmol/m^2/d) was found to be significantly greater ($p = 0.0233$, $df = 44$, $F = 3.52$) than that for summer (0.982 x 10^{-4} ± 1.21 x 10^{-4} µmol/m^2/d) (Table 11), but was not significantly different from those for winter (1.94 x 10^{-4} ± 1.57 x 10^{-4} µmol/m^2/d) and spring (2.26 x 10^{-4} ± 1.38 x 10^{-4} µmol/m^2/d), as determined by a one-way ANOVA and a multiple comparison test.

(a) Rain total-dissolvable cadmium from Eastern Shore samples

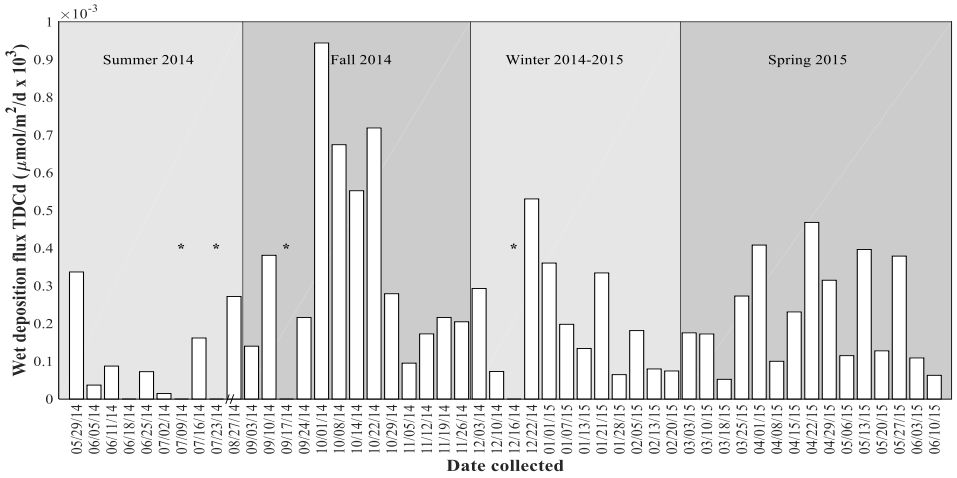

(b) Rain total-dissolvable cadmium from Eastern Shore samples - smoothed

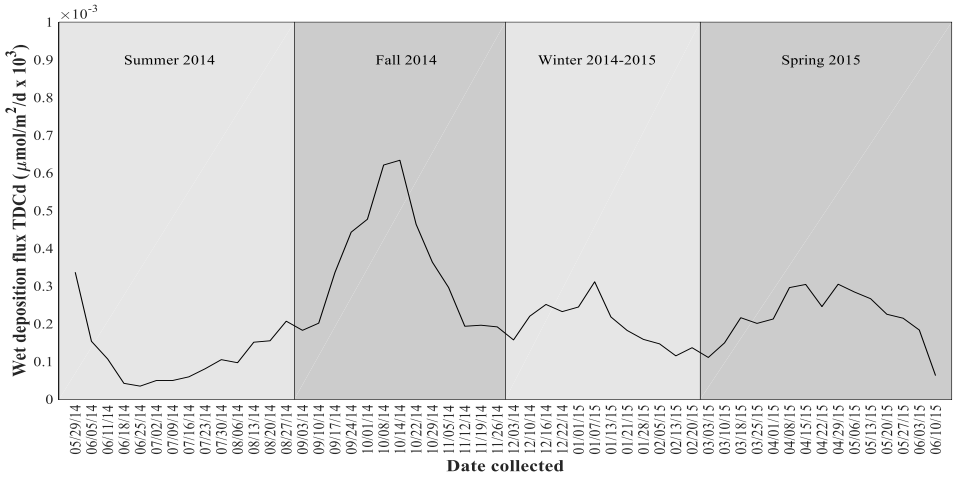

(c) Rain total-dissolvable cadmium from Eastern Shore samples - residuals

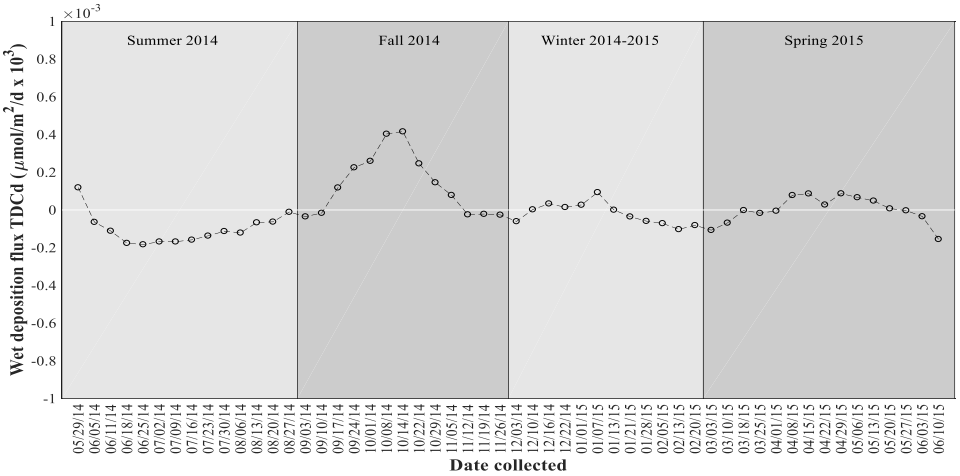

Figure 18. Wet deposition (a) flux (µmol/m^2/d x 10^3), (b) smoothed data (µmol/m^2/d x 10^3), and (c) residuals (µmol/m^2/d x 10^3) for total-dissolvable cadmium (TDCd) from Eastern Shore samples. "//" indicates a break in the x-axis between 07/23/14 and 08/27/14 in (a) and "*" denotes dates for which no rain was collected. Note (b) and (c) included interpolated values for dates 30 July 2014, 6 August 2014, 13 August 2014, and 20 August 2014 using the method in Section 2.6. The white horizontal line in (c) indicates the annual mean flux.

The wet flux of total-dissolvable antimony (TDSb) ranged from 0.121 x 10^{-4} to 2.46 x 10^{-4} µmol/m^2/d in summer, 0.477 x 10^{-4} to 8.58 x 10^{-4} µmol/m^2/d in fall, 1.49 x 10^{-4} to 7.09 x 10^{-4} µmol/m^2/d in winter, and 0.325 x 10^{-4} to 15.7 x 10^{-4} µmol/m^2/d in spring (Table 11 and Figure 19a). The wet flux of TDSb was elevated on 29 May 2014, 16 July 2014, 27 August 2014, and 27 May 2015 (Figure 19a). The smoothed data and residuals show that the wet flux of TDSb was mostly above the overall mean during summer, and remained near this mean for the duration of the sampling period (Figures 19b and 19c). The mean TDSb fluxes for the four seasons were not significantly different ($p = 0.2903$, $df = 45$, $F = 1.29$).

(a) Rain total-dissolvable antimony from Eastern Shore samples

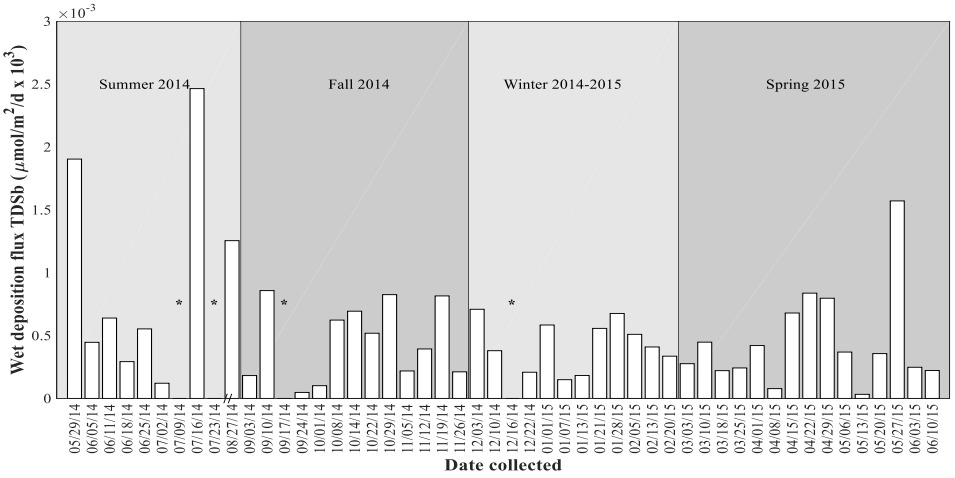

(b) Rain total-dissolvable antimony from Eastern Shore samples - smoothed

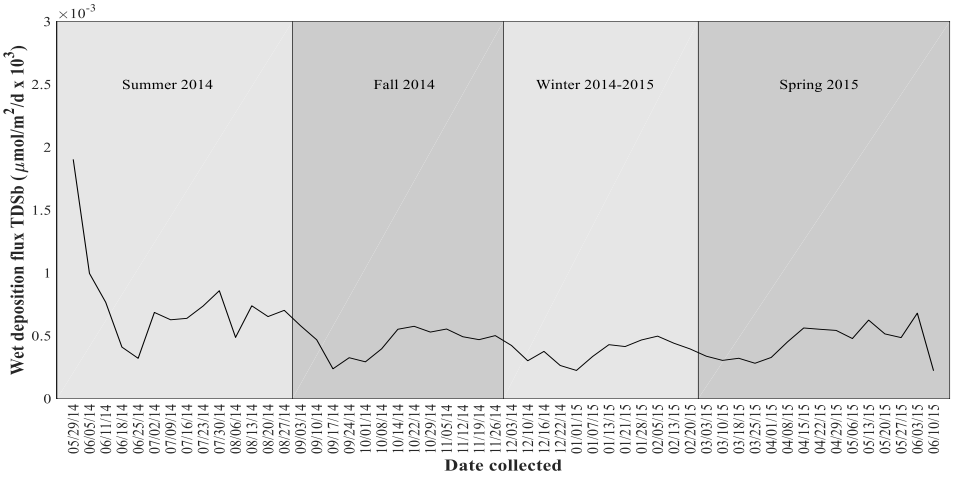

(c) Rain total-dissolvable antimony from Eastern Shore samples - residuals

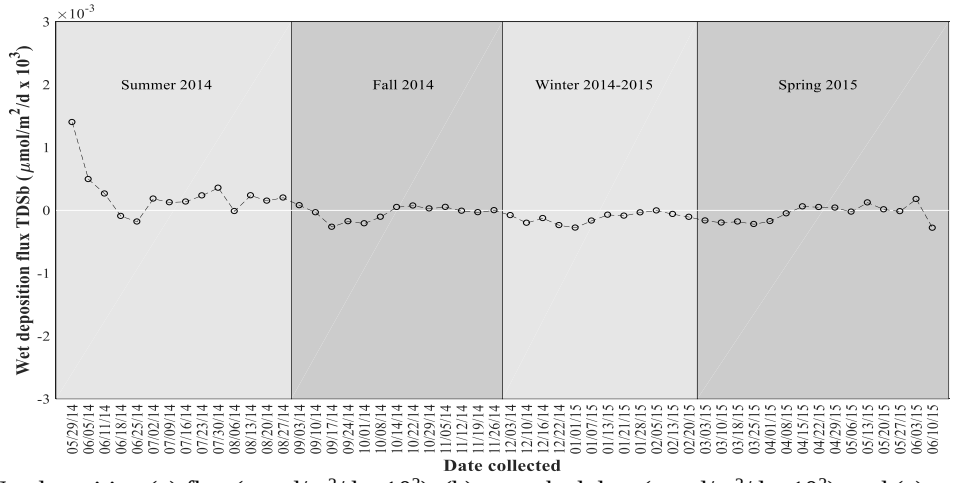

Figure 19. Wet deposition (a) flux (μmol/m^2/d x 10^3), (b) smoothed data (μmol/m^2/d x 10^3), and (c) residuals (μmol/m^2/d x 10^3) for total-dissolvable antimony (TDSb) from Eastern Shore samples. "//" indicates a break in the x-axis between 07/23/14 and 08/27/14 in (a) and "*" denotes dates for which no rain was collected. Note (b) and (c) included interpolated values for dates 30 July 2014, 6 August 2014, 13 August 2014, and 20 August 2014 using the method in Section 2.6. The white horizontal line in (c) indicates the annual mean flux.

The wet deposition flux of total-dissolvable lead (TDPb) ranged from 0.740 x 10^{-4} to 25.1 x 10^{-4} µmol/m^2/d in summer, below the level of quantification to 13.0 x 10^{-4} µmol/m^2/d in fall, 0.719 x 10^{-4} to 6.48 x 10^{-4} µmol/m^2/d in winter, and 0.070 x 10^{-4} to 10.1 x 10^{-4} in spring (Table 11 and Figure 20a). The wet flux of TDPb showed little variation throughout the time series (Figures 19 a-c), except for elevated fluxes on 29 May 2014 and 10 September 2014 (Figure 19a). The mean fluxes of TDPb for the four seasons were not significantly different ($p = 0.8287$, $df = 44$, chi-sq = 0.89).

(a) Rain total-dissolvable lead from Eastern Shore samples

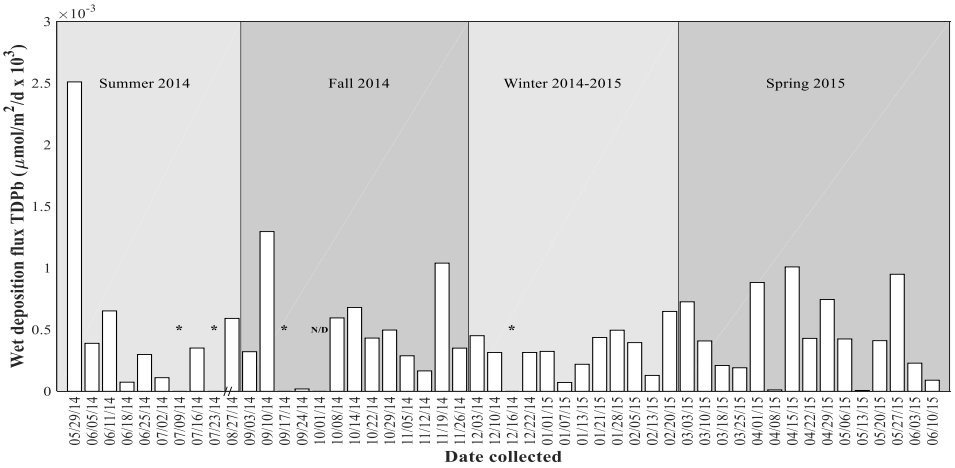

(b) Rain total-dissolvable lead from Eastern Shore samples - smoothed

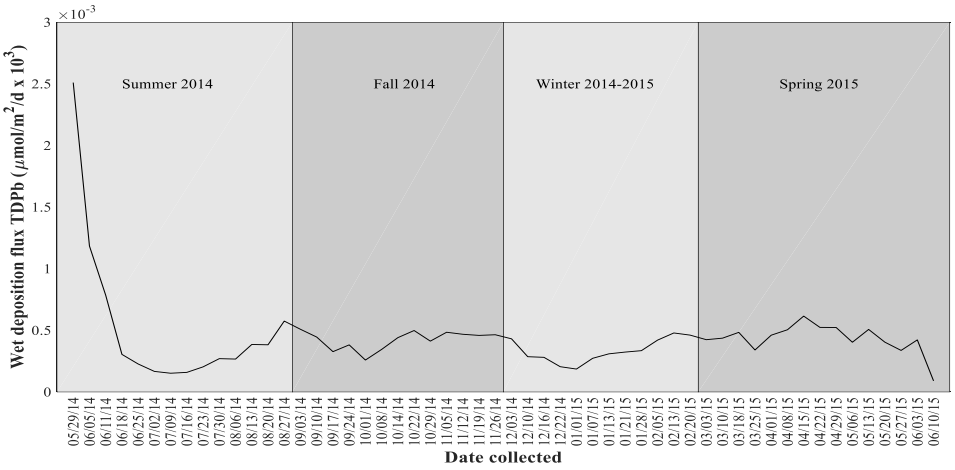

(c) Rain total-dissolvable lead from Eastern Shore samples - residuals

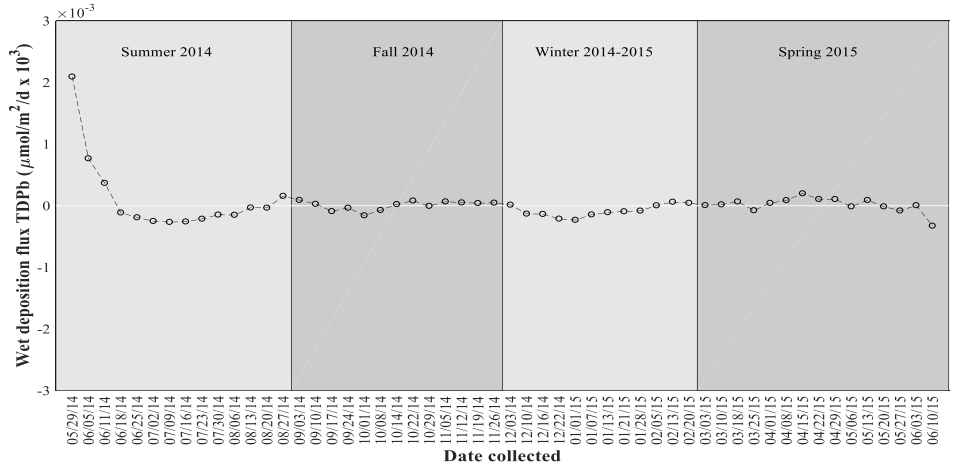

Figure 20. Wet deposition (a) flux (μmol/m^2/d x 10^3), (b) smoothed data (μmol/m^2/d x 10^3), and (c) residuals (μmol/m^2/d x 10^3) for total-dissolvable lead (TDPb) from Eastern Shore samples. "//" indicates a break in the x-axis between 07/23/14 and 08/27/14 in (a), "*" denotes dates for which no rain was collected, and "N/D" indicates non-detect samples. Note (b) and (c) included interpolated values for dates 30 July 2014, 6 August 2014, 13 August 2014, and 20 August 2014 using the method in Section 2.6. The white horizontal line in (c) indicates the annual mean flux.

3.4 DRY DEPOSITION TRACE METAL FLUXES - EASTERN SHORE

The dry fluxes of soluble aluminum (Al_S) in the fine fraction were lower than those for dry coarse Al_S throughout the time series, and ranged from 2.65 x 10^{-3} to 25.2 x 10^{-3} µmol/m^2/d in summer, 0.875 x 10^{-3} to 13.8 x 10^{-3} µmol/m^2/d in fall, 0.958 x 10^{-3} to 4.09 x 10^{-3} µmol/m^2/d in winter, and 1.68 x 10^{-3} to 21.4 x 10^{-3} µmol/m^2/d in spring (Table 12).The dry flux of coarse Al_S ranged from 0.0501 to 0.347 µmol/m^2/d in summer, 0.0219 to 0.325 µmol/m^2/d in fall, 0.0138 to 0.0637 µmol/m^2/d in winter, and 0.0274 to 0.592 µmol/m^2/d in spring (Table 12 and Figure 21a). The dry deposition fluxes for fine and coarse Al_S were relatively high on 9 July 2014, 3 September 2014, 10 September 2014, and 13 May 2014 (Figure 21a).

The dry flux of fine total aerosol aluminum (Al_T) ranged from 0.092 to 0.692 µmol/m^2/d in summer, 0.035 to 0.565 µmol/m^2/d in fall, 0.032 to 0.257 µmol/m^2/d in winter, and 0.036 to 0.504 µmol/m^2/d in spring (Table 13 and Figure 21b). The overall mean dry flux of coarse Al_T (4.32 ± 3.44 µmol/m^2/d) was more than 40 times greater than the dry flux of coarse Al_S (0.105 ± 0.108 µmol/m^2/d) (Tables 12 and 13). The dry flux of coarse Al_T ranged from 2.26 to 17.1 µmol/m^2/d in summer, 1.91 to 12.4 µmol/m^2/d in fall, 0.914 to 3.77 µmol/m^2/d in winter, and 1.78 to 17.7 µmol/m^2/d in spring, and the overall mean coarse Al_T flux (4.32 ± 3.44 µmol/m^2/d) was more than 20 times greater than the overall mean dry fine Al_T flux (0.176 ± 0.135 µmol/m^2/d) (Table 13 and Figure 21b). The dry Al_T fluxes for both size fractions were elevated on 9 July 2014, 3 September 2014, and 13 May 2015 (Figure 21b).

The fractional solubility of aerosol aluminum (%Al_S) for both size fractions was roughly equal, with overall mean fractional solubilities of ~2.9% and ~2.3% calculated for the fine and coarse size fractions, respectively (Table 14 and Figure 21c). The fine %Al_S ranged from 2.08 to 5.48 % in summer, 0.553 to 7.36 % in fall, 1.02 to 4.61 % in winter, and 1.28 to 11.8 % in spring (Table 14 and Figure 21c). The coarse %Al_S ranged from 1.63 to 3.90 % in summer, 0.390 to 6.92 % in fall, 1.14 to 5.22 % in winter, and 0.870 to 5.22 % in spring (Table 14 and Figure 21c).

Table 12. Mean (± standard deviation) dry deposition fluxes of soluble trace metals (μmol/m^2/d) from Eastern Shore samples (the seasonal range of dry soluble fluxes for trace metals is provided in parentheses).

Trace metal	Size fraction	Summer 2014	Fall 2014	Winter 2014-2015	Spring 2015	Overall mean
Al	<1 μm	$7.82 \times 10^{-3} \pm 7.08 \times 10^{-3}$ (2.65×10^{-3}-25.2×10^{-3})	$3.90 \times 10^{-3} \pm 3.89 \times 10^{-3}$ (0.875×10^{-3}-13.8×10^{-3})	$2.29 \times 10^{-3} \pm 0.804 \times 10^{-3}$ (0.958×10^{-3}-4.09×10^{-3})	$5.30 \times 10^{-3} \pm 5.08 \times 10^{-3}$ (1.68×10^{-3}-21.4×10^{-3})	$4.72 \times 10^{-3} \pm 4.91 \times 10^{-3}$
	>1 μm	0.155 ± 0.0936 (0.0501-0.347)	0.0852 ± 0.104 (0.0219-0.325)	0.0455 ± 0.0149 (0.0138-0.0637)	0.137 ± 0.142 (0.0274-0.592)	0.105 ± 0.108
Ti	<1 μm	$4.16 \times 10^{-5} \pm 1.76 \times 10^{-5}$ (0-6.38×10^{-5})	$2.22 \times 10^{-5} \pm 1.95 \times 10^{-5}$ (0-5.42×10^{-5})	$3.55 \times 10^{-5} \pm 1.32 \times 10^{-5}$ (0-5.02×10^{-5})	$2.05 \times 10^{-5} \pm 2.37 \times 10^{-5}$ (0-5.66×10^{-5})	$2.88 \times 10^{-5} \pm 2.07 \times 10^{-5}$
	>1 μm	$1.24 \times 10^{-4} \pm 2.62 \times 10^{-4}$ (0- 6.50×10^{-4})	$0.579 \times 10^{-4} \pm 2.09 \times 10^{-4}$ (0-7.53×10^{-4})	— —	$0.483 \times 10^{-4} \pm 1.87 \times 10^{-4}$ (0-7.25×10^{-4})	$0.543 \times 10^{-4} \pm 1.85 \times 10^{-4}$
V	<1 μm	$5.24 \times 10^{-4} \pm 1.67 \times 10^{-4}$ (2.82×10^{-4}-8.73×10^{-4})	$3.79 \times 10^{-4} \pm 1.62 \times 10^{-4}$ (2.23×10^{-4}-7.08×10^{-4})	$3.19 \times 10^{-4} \pm 2.02 \times 10^{-4}$ (0.955×10^{-4}-6.93×10^{-4})	$2.61 \times 10^{-4} \pm 1.77 \times 10^{-4}$ (0.895×10^{-4}-7.11×10^{-4})	$3.58 \times 10^{-4} \pm 1.96 \times 10^{-4}$
	>1 μm	$14.0 \times 10^{-4} \pm 4.39 \times 10^{-4}$ (6.40×10^{-4}-19.7×10^{-4})	$9.03 \times 10^{-4} \pm 5.60 \times 10^{-4}$ (3.46×10^{-4}-19.4×10^{-4})	$9.77 \times 10^{-4} \pm 4.16 \times 10^{-4}$ (3.20×10^{-4}-17.5×10^{-4})	$9.45 \times 10^{-4} \pm 4.30 \times 10^{-4}$ (4.73×10^{-4}-16.7×10^{-4})	$10.3 \times 10^{-4} \pm 4.85 \times 10^{-4}$
Cr	<1 μm	$4.24 \times 10^{-5} \pm 1.09 \times 10^{-5}$ (2.31×10^{-5}-6.22×10^{-5})	$3.77 \times 10^{-5} \pm 0.818 \times 10^{-5}$ (1.96×10^{-5}-5.10×10^{-5})	$4.42 \times 10^{-5} \pm 1.02 \times 10^{-5}$ (3.14×10^{-5}-5.87×10^{-5})	$4.49 \times 10^{-5} \pm 3.25 \times 10^{-5}$ (1.68×10^{-5}-15.1×10^{-5})	$4.23 \times 10^{-5} \pm 1.93 \times 10^{-5}$
	>1 μm	$3.97 \times 10^{-4} \pm 1.22 \times 10^{-4}$ (2.65×10^{-4}-6.97×10^{-4})	$2.51 \times 10^{-4} \pm 1.56 \times 10^{-4}$ (0-5.34×10^{-4})	$3.10 \times 10^{-4} \pm 0.701 \times 10^{-4}$ (2.12×10^{-4}-4.08×10^{-4})	$3.73 \times 10^{-4} \pm 1.24 \times 10^{-4}$ (2.24×10^{-4}-6.21×10^{-4})	$3.31 \times 10^{-4} \pm 1.3 \times 10^{-4}$
Mn	<1 μm	$4.67 \times 10^{-4} \pm 2.04 \times 10^{-4}$ (1.38×10^{-4}-8.12×10^{-4})	$5.47 \times 10^{-4} \pm 2.39 \times 10^{-4}$ (1.66×10^{-4}-9.42×10^{-4})	$4.04 \times 10^{-4} \pm 1.74 \times 10^{-4}$ (1.48×10^{-4}-7.01×10^{-4})	$5.27 \times 10^{-4} \pm 2.75 \times 10^{-4}$ (1.96×10^{-4}-9.66×10^{-4})	$4.91 \times 10^{-4} \pm 2.31 \times 10^{-4}$
	>1 μm	$20.3 \times 10^{-3} \pm 9.55 \times 10^{-3}$ (9.03×10^{-3}-43.1×10^{-3})	$18.9 \times 10^{-3} \pm 9.24 \times 10^{-3}$ (9.00×10^{-3}-42.7×10^{-3})	$11.8 \times 10^{-3} \pm 8.10 \times 10^{-3}$ (4.51×10^{-3}-34.8×10^{-3})	$19.3 \times 10^{-3} \pm 13.7 \times 10^{-3}$ (8.89×10^{-3}-61.4×10^{-3})	$17.6 \times 10^{-3} \pm 10.7 \times 10^{-3}$
Fe	<1 μm	$3.73 \times 10^{-3} \pm 1.07 \times 10^{-3}$ (1.83×10^{-3}-5.83×10^{-3})	$2.63 \times 10^{-3} \pm 1.04 \times 10^{-3}$ (1.42×10^{-3}-5.34×10^{-3})	$1.83 \times 10^{-3} \pm 0.552 \times 10^{-3}$ (1.01×10^{-3}-2.76×10^{-3})	$2.68 \times 10^{-3} \pm 1.43 \times 10^{-3}$ (1.16×10^{-3}-5.82×10^{-3})	$2.67 \times 10^{-3} \pm 1.24 \times 10^{-3}$
	>1 μm	$38.5 \times 10^{-3} \pm 11.9 \times 10^{-3}$ (22.5×10^{-3}-61.1×10^{-3})	$20.8 \times 10^{-3} \pm 16.2 \times 10^{-3}$ (9.23×10^{-3}-69.2×10^{-3})	$13.9 \times 10^{-3} \pm 5.76 \times 10^{-3}$ (3.56×10^{-3}-23.0×10^{-3})	$28.4 \times 10^{-3} \pm 15.9 \times 10^{-3}$ (9.62×10^{-3}-64.9×10^{-3})	$24.9 \times 10^{-3} \pm 15.7 \times 10^{-3}$
Co	<1 μm	$9.97 \times 10^{-6} \pm 2.67 \times 10^{-6}$ (5.55×10^{-6}-14.7×10^{-6})	$6.09 \times 10^{-6} \pm 3.08 \times 10^{-6}$ (0-12.3×10^{-6})	$6.00 \times 10^{-6} \pm 2.42 \times 10^{-6}$ (2.42×10^{-6}-9.89×10^{-6})	$5.63 \times 10^{-6} \pm 3.48 \times 10^{-6}$ (1.92×10^{-6}-13.3×10^{-6})	$6.71 \times 10^{-6} \pm 3.34 \times 10^{-6}$
	>1 μm	$1.95 \times 10^{-4} \pm 1.28 \times 10^{-4}$ (0.744×10^{-4}-5.36×10^{-4})	$1.06 \times 10^{-4} \pm 0.936 \times 10^{-4}$ (0-3.30×10^{-4})	$0.818 \times 10^{-4} \pm 0.359 \times 10^{-4}$ (0.336×10^{-4}-1.61×10^{-4})	$1.66 \times 10^{-4} \pm 1.32 \times 10^{-4}$ (0.662×10^{-4}-6.08×10^{-4})	$1.36 \times 10^{-4} \pm 1.11 \times 10^{-4}$
Ni	<1 μm	$13.9 \times 10^{-5} \pm 3.37 \times 10^{-5}$ (7.63×10^{-5}-18.2×10^{-5})	$8.65 \times 10^{-5} \pm 4.86 \times 10^{-5}$ (0-16.7×10^{-5})	$9.08 \times 10^{-5} \pm 5.43 \times 10^{-5}$ (0-17.2×10^{-5})	$9.59 \times 10^{-5} \pm 8.21 \times 10^{-5}$ (3.34×10^{-5}-32.4×10^{-5})	$10.1 \times 10^{-5} \pm 3.13 \times 10^{-5}$
	>1 μm	$2.86 \times 10^{-4} \pm 6.10 \times 10^{-4}$ (0-16.2×10^{-4})	$1.33 \times 10^{-4} \pm 3.26 \times 10^{-4}$ (0-8.93×10^{-4})	$4.17 \times 10^{-4} \pm 4.42 \times 10^{-4}$ (0-9.54×10^{-4})	$9.38 \times 10^{-4} \pm 7.93 \times 10^{-4}$ (0-22.8×10^{-4})	$4.73 \times 10^{-4} \pm 6.44 \times 10^{-4}$
Cu	<1 μm	$3.21 \times 10^{-4} \pm 1.01 \times 10^{-4}$ (1.80×10^{-4}-4.80×10^{-4})	$3.61 \times 10^{-4} \pm 1.46 \times 10^{-4}$ (1.47×10^{-4}-7.53×10^{-4})	$3.78 \times 10^{-4} \pm 1.07 \times 10^{-4}$ (1.97×10^{-4}-5.93×10^{-4})	$4.07 \times 10^{-4} \pm 3.11 \times 10^{-4}$ (1.30×10^{-4}-14.3×10^{-4})	$1.95 \times 10^{-4} \pm 3.71 \times 10^{-4}$
	>1 μm	$7.56 \times 10^{-3} \pm 3.33 \times 10^{-3}$ (4.09×10^{-3}-15.0×10^{-3})	$6.34 \times 10^{-3} \pm 1.79 \times 10^{-3}$ (4.35×10^{-3}-10.4×10^{-3})	$9.24 \times 10^{-3} \pm 5.36 \times 10^{-3}$ (3.01×10^{-3}-20.7×10^{-3})	$7.96 \times 10^{-3} \pm 2.48 \times 10^{-3}$ (3.23×10^{-3}-11.5×10^{-3})	$7.77 \times 10^{-3} \pm 3.45 \times 10^{-3}$

Table 12. Continued.

Trace metal	Size fraction	Summer 2014	Fall 2014	Winter 2014-2015	Spring 2015	Overall mean
Zn	<1 µm	$1.94 \times 10^{-3} \pm 0.709 \times 10^{-3}$ (0.937×10^{-3}-3.34×10^{-3})	$1.81 \times 10^{-3} \pm 0.734 \times 10^{-3}$ (0.861×10^{-3}-3.33×10^{-3})	$2.77 \times 10^{-3} \pm 0.848 \times 10^{-3}$ (1.35×10^{-3}-4.00×10^{-3})	$2.52 \times 10^{-3} \pm 2.65 \times 10^{-3}$ (0.684×10^{-3}-11.7×10^{-3})	$2.28 \times 10^{-3} \pm 1.60 \times 10^{-3}$
	>1 µm	$17.6 \times 10^{-3} \pm 6.60 \times 10^{-3}$ (9.51×10^{-3}-33.6×10^{-3})	$19.2 \times 10^{-3} \pm 4.84 \times 10^{-3}$ (11.4×10^{-3}-24.1×10^{-3})	$25.2 \times 10^{-3} \pm 7.84 \times 10^{-3}$ (10.8×10^{-3}-34.6×10^{-3})	$21.9 \times 10^{-3} \pm 6.94 \times 10^{-3}$ (11.8×10^{-3}-32.6×10^{-3})	$21.0 \times 10^{-3} \pm 6.93 \times 10^{-3}$
Cd	<1 µm	$7.84 \times 10^{-6} \pm 2.19 \times 10^{-6}$ (5.17×10^{-6}-12.2×10^{-6})	$13.2 \times 10^{-6} \pm 7.72 \times 10^{-6}$ (4.74×10^{-6}-35.6×10^{-6})	$17.7 \times 10^{-6} \pm 8.18 \times 10^{-6}$ (7.05×10^{-6}-37.3×10^{-6})	$12.9 \times 10^{-6} \pm 5.43 \times 10^{-6}$ (3.93×10^{-6}-20.5×10^{-6})	$13.1 \times 10^{-6} \pm 7.06 \times 10^{-6}$
	>1 µm	$5.98 \times 10^{-5} \pm 2.08 \times 10^{-5}$ (3.73×10^{-5}-9.56×10^{-5})	$8.40 \times 10^{-5} \pm 9.71 \times 10^{-5}$ (0-37.7×10^{-5})	$8.34 \times 10^{-5} \pm 4.03 \times 10^{-5}$ (2.94×10^{-5}-16.9×10^{-5})	$6.86 \times 10^{-5} \pm 2.62 \times 10^{-5}$ (3.02×10^{-5}-12.8×10^{-5})	$7.44 \times 10^{-5} \pm 5.47 \times 10^{-5}$
Sb	<1 µm	$4.94 \times 10^{-5} \pm 1.58 \times 10^{-5}$ (2.51×10^{-5}-7.10×10^{-5})	$7.31 \times 10^{-5} \pm 2.76 \times 10^{-5}$ (2.39×10^{-5}-11.1×10^{-5})	$8.90 \times 10^{-5} \pm 5.39 \times 10^{-5}$ (3.30×10^{-5}-22.6×10^{-5})	$5.35 \times 10^{-5} \pm 2.65 \times 10^{-5}$ (1.04×10^{-5}-10.4×10^{-5})	$6.65 \times 10^{-5} \pm 3.65 \times 10^{-5}$
	>1 µm	$1.27 \times 10^{-4} \pm 0.410 \times 10^{-4}$ (0.799×10^{-4}-2.12×10^{-4})	$1.47 \times 10^{-4} \pm 0.517 \times 10^{-4}$ (0.848×10^{-4}-2.42×10^{-4})	$2.04 \times 10^{-4} \pm 1.20 \times 10^{-4}$ (0.512×10^{-4}-4.68×10^{-4})	$1.41 \times 10^{-4} \pm 0.637 \times 10^{-4}$ (0.572×10^{-4}-2.66×10^{-4})	$1.55 \times 10^{-4} \pm 0.779 \times 10^{-4}$
Pb	<1 µm	$0.781 \times 10^{-4} \pm 0.268 \times 10^{-4}$ (0.302×10^{-4}-1.12×10^{-4})	$1.04 \times 10^{-4} \pm 0.349 \times 10^{-4}$ (0.363×10^{-4}-1.52×10^{-4})	$1.60 \times 10^{-4} \pm 1.51 \times 10^{-4}$ (0.410×10^{-4}-6.03×10^{-4})	$1.07 \times 10^{-4} \pm 0.491 \times 10^{-4}$ (0.435×10^{-4}-1.78×10^{-4})	$1.13 \times 10^{-4} \pm 0.840 \times 10^{-4}$
	>1 µm	$2.64 \times 10^{-4} \pm 1.05 \times 10^{-4}$ (0.939×10^{-4}-4.64×10^{-4})	$2.79 \times 10^{-4} \pm 0.944 \times 10^{-4}$ (1.53×10^{-4}-5.04×10^{-4})	$4.09 \times 10^{-4} \pm 2.21 \times 10^{-4}$ (1.05×10^{-4}-8.99×10^{-4})	$3.52 \times 10^{-4} \pm 1.57 \times 10^{-4}$ (1.33×10^{-4}-6.52×10^{-4})	$3.29 \times 10^{-4} \pm 1.60 \times 10^{-4}$

Table 13. Mean (± standard deviation) dry deposition flux of total aerosol trace metals from Eastern Shore samples (the seasonal range of dry fluxes for total trace metals is provided in parentheses).

Trace metal	Size fraction	Summer 2014 (μmol/m^2/d)	Fall 2014 (μmol/m^2/d)	Winter 2014-2015 (μmol/m^2/d)	Spring 2015 (μmol/m^2/d)	Overall mean flux (μmol/m^2/d)	Overall mean flux (mmol/m^2/yr)	Overall mean total flux fine+coarse (mmol/m^2/yr)	Overall total deposition flux fine+coarse (mg/m^2/yr)
Al	<1 μm	0.227 ± 0.180 (0.0920 -0.692)	0.180 ± 0.135 (0.0347-0.565)	0.107 ± 0.0840 (0.0322-0.257)	0.194 ± 0.125 (0.0363-0.504)	0.176 ± 0.135	64.2×10^{-3}	1.64	44.3
	>1 μm	6.05 ± 4.15 (2.26-17.1)	4.29 ± 2.79 (1.91-12.4)	2.09 ± 0.873 (0.914-3.77)	5.32 ± 3.93 (1.78-17.7)	4.32 ± 3.44	1.58		
Ti	<1 μm	$10.2 \times 10^{-3} \pm 7.86 \times 10^{-3}$ (2.74×10^{-3}-29.0×10^{-3})	$8.61 \times 10^{-3} \pm 6.62 \times 10^{-3}$ (1.43×10^{-3}-28.2×10^{-3})	$5.01 \times 10^{-3} \pm 4.48 \times 10^{-3}$ (1.24×10^{-3}-14.5×10^{-3})	$8.78 \times 10^{-3} \pm 5.53 \times 10^{-3}$ (1.76×10^{-3}-19.4×10^{-3})	$8.11 \times 10^{-3} \pm 6.23 \times 10^{-3}$	2.96×10^{-3}	72.7×10^{-3}	3.48
	>1 μm	0.269 ± 0.178 (95.3×10^{-3}-730×10^{-3})	0.199 ± 0.112 (86.4×10^{-3}-474×10^{-3})	0.0967 ± 0.0423 (39.5×10^{-3}-166×10^{-3})	0.222 ± 0.150 (72.5×10^{-3}-664×10^{-3})	0.191 ± 0.140	69.7×10^{-3}		
V	<1 μm	$8.50 \times 10^{-4} \pm 2.33 \times 10^{-4}$ (4.32×10^{-4}-11.5×10^{-4})	$6.29 \times 10^{-4} \pm 2.67 \times 10^{-4}$ (2.06×10^{-4}-11.2×10^{-4})	$5.62 \times 10^{-4} \pm 2.66 \times 10^{-4}$ (1.60×10^{-4}-9.26×10^{-4})	$5.27 \times 10^{-4} \pm 2.74 \times 10^{-4}$ (1.25×10^{-4}-11.3×10^{-4})	$6.30 \times 10^{-4} \pm 2.81 \times 10^{-4}$	2.30×10^{-4}	2.45×10^{-3}	0.125
	>1 μm	$8.15 \times 10^{-3} \pm 3.70 \times 10^{-3}$ (3.15×10^{-3}-14.7×10^{-3})	$5.63 \times 10^{-3} \pm 2.52 \times 10^{-3}$ (2.94×10^{-3}-12.7×10^{-3})	$4.41 \times 10^{-3} \pm 1.31 \times 10^{-3}$ (1.54×10^{-3}-6.21×10^{-3})	$6.70 \times 10^{-3} \pm 3.50 \times 10^{-3}$ (2.52×10^{-3}-14.1×10^{-3})	$6.09 \times 10^{-3} \pm 3.19 \times 10^{-3}$	2.22×10^{-3}		
Cr	<1 μm	$4.70 \times 10^{-5} \pm 8.94 \times 10^{-5}$ (0-24.7×10^{-5})	$5.43 \times 10^{-5} \pm 10.4 \times 10^{-5}$ (0-25.9×10^{-5})	$10.3 \times 10^{-5} \pm 24.0 \times 10^{-5}$ (0-64.8×10^{-5})	$0.0510 \times 10^{-5} \pm 1.36 \times 10^{-5}$ (0-4.32×10^{-5})	$4.97 \times 10^{-5} \pm 13.6 \times 10^{-5}$	1.81×10^{-5}	2.27×10^{-4}	0.0118
	>1 μm	$1.40 \times 10^{-3} \pm 2.07 \times 10^{-3}$ (0-6.30×10^{-3})	$1.03 \times 10^{-3} \pm 2.59 \times 10^{-3}$ (0-8.29×10^{-3})	— —	$0.0922 \times 10^{-3} \pm 0.345 \times 10^{-3}$ (0-1.29×10^{-3})	$0.573 \times 10^{-3} \pm 1.68 \times 10^{-3}$	0.209×10^{-3}		
Mn	<1 μm	$14.9 \times 10^{-4} \pm 7.32 \times 10^{-4}$ (6.29×10^{-4}-29.6×10^{-4})	$18.1 \times 10^{-4} \pm 8.53 \times 10^{-4}$ (4.62×10^{-4}-35.4×10^{-4})	$14.0 \times 10^{-4} \pm 6.58 \times 10^{-4}$ (5.51×10^{-4}-25.0×10^{-4})	$17.4 \times 10^{-4} \pm 7.63 \times 10^{-4}$ (5.67×10^{-4}-28.5×10^{-4})	$16.3 \times 10^{-4} \pm 7.50 \times 10^{-4}$	5.95×10^{-4}	15.5×10^{-3}	0.851
	>1 μm	$46.1 \times 10^{-3} \pm 20.1 \times 10^{-3}$ (23.7×10^{-3}-97.0×10^{-3})	$43.8 \times 10^{-3} \pm 16.9 \times 10^{-3}$ (23.2×10^{-3}-80.7×10^{-3})	$30.8 \times 10^{-3} \pm 18.1 \times 10^{-3}$ (13.2×10^{-3}-81.2×10^{-3})	$45.8 \times 10^{-3} \pm 24.5 \times 10^{-3}$ (0-115×10^{-3})	$40.8 \times 10^{-3} \pm 21.2 \times 10^{-3}$	14.9×10^{-3}		

Table 13. Continued.

Trace metal	Size fraction	Summer 2014 (μmol/m^2/d)	Fall 2014 (μmol/m^2/d)	Winter 2014-2015 (μmol/m^2/d)	Spring 2015 (μmol/m^2/d)	Overall mean flux (μmol/m^2/d)	Overall mean flux (mmol/m^2/yr)	Overall mean total flux fine+coarse (mmol/m^2/yr)	Overall total deposition flux fine+coarse (mg/m^2/yr)
Fe	<1 μm	$61.6 \times 10^{-3} \pm 42.3 \times 10^{-3}$ (25.0×10^{-3}-16.8×10^{-3})	$54.5 \times 10^{-3} \pm 31.2 \times 10^{-3}$ (13.3×10^{-3}-131×10^{-3})	$38.0 \times 10^{-3} \pm 21.3 \times 10^{-3}$ (16.4×10^{-3}-76.5×10^{-3})	$60.4 \times 10^{-3} \pm 33.7 \times 10^{-3}$ (11.4×10^{-3}-13.3×10^{-3})	$53.7 \times 10^{-3} \pm 3.29 \times 10^{-3}$	19.6×10^{-3}	0.512	28.6
	>1 μm	1.71 ± 0.934 (0.862-4.16)	1.36 ± 0.681 (0.896-3.42)	0.816 ± 0.264 (0.429-1.15)	1.64 ± 0.943 (0.614-4.52)	1.35 ± 0.827	0.493		
Co	<1 μm	$3.53 \times 10^{-5} \pm 1.48 \times 10^{-5}$ (1.71×10^{-5}-6.67×10^{-5})	$3.17 \times 10^{-5} \pm 1.46 \times 10^{-5}$ (1.33×10^{-5}-6.14×10^{-5})	$2.77 \times 10^{-5} \pm 1.04 \times 10^{-5}$ (0.967×10^{-5}-4.24×10^{-5})	$2.64 \times 10^{-5} \pm 1.20 \times 10^{-5}$ (0.575×10^{-5}-4.83×10^{-5})	$2.99 \times 10^{-5} \pm 1.30 \times 10^{-5}$	1.09×10^{-5}	2.33×10^{-4}	13.7×10^{-3}
	>1 μm	$7.67 \times 10^{-4} \pm 4.13 \times 10^{-4}$ (3.72×10^{-4}-18.4×10^{-4})	$5.96 \times 10^{-4} \pm 2.78 \times 10^{-4}$ (3.57×10^{-4}-14.4×10^{-4})	$3.94 \times 10^{-4} \pm 1.71 \times 10^{-4}$ (0.212×10^{-4}-6.65×10^{-4})	$7.31 \times 10^{-4} \pm 3.97 \times 10^{-4}$ (2.84×10^{-4}-19.3×10^{-4})	$6.08 \times 10^{-4} \pm 3.56 \times 10^{-4}$	2.22×10^{-4}		
Ni	<1 μm	$5.24 \times 10^{-4} \pm 1.16 \times 10^{-4}$ (4.04×10^{-4}-8.11×10^{-4})	$4.01 \times 10^{-4} \pm 1.93 \times 10^{-4}$ (1.58×10^{-4}-6.81×10^{-4})	$4.09 \times 10^{-4} \pm 2.04 \times 10^{-4}$ (1.41×10^{-4}-7.52×10^{-4})	$2.60 \times 10^{-4} \pm 1.17 \times 10^{-4}$ (0.832×10^{-4}-4.73×10^{-4})	$3.85 \times 10^{-4} \pm 1.84 \times 10^{-4}$	1.41×10^{-4}	1.44×10^{-3}	84.3×10^{-3}
	>1 μm	$4.16 \times 10^{-3} \pm 1.57 \times 10^{-3}$ (2.32×10^{-3}-8.13×10^{-3})	$3.73 \times 10^{-3} \pm 1.53 \times 10^{-3}$ (2.36×10^{-3}-8.42×10^{-3})	$3.34 \times 10^{-3} \pm 1.28 \times 10^{-3}$ (1.44×10^{-3}-5.72×10^{-3})	$3.38 \times 10^{-3} \pm 1.79 \times 10^{-3}$ (1.51×10^{-3}-7.79×10^{-3})	$3.55 \times 10^{-3} \pm 1.61 \times 10^{-3}$	1.30×10^{-3}		
Cu	<1 μm	$7.27 \times 10^{-4} \pm 1.90 \times 10^{-4}$ (4.18×10^{-4}-9.76×10^{-4})	$9.53 \times 10^{-4} \pm 4.29 \times 10^{-4}$ (3.59×10^{-4}-17.5×10^{-4})	$10.5 \times 10^{-4} \pm 4.13 \times 10^{-4}$ (5.23×10^{-4}-19.5×10^{-4})	$8.14 \times 10^{-4} \pm 3.14 \times 10^{-4}$ (2.53×10^{-4}-11.8×10^{-4})	$8.88 \times 10^{-4} \pm 3.64 \times 10^{-4}$	3.24×10^{-4}	7.70×10^{-3}	0.489
	>1 μm	$17.6 \times 10^{-3} \pm 5.62 \times 10^{-3}$ (12.5×10^{-3}-31.9×10^{-3})	$17.7 \times 10^{-3} \pm 4.93 \times 10^{-3}$ (10.6×10^{-3}-29.0×10^{-3})	$25.1 \times 10^{-3} \pm 15.2 \times 10^{-3}$ (8.78×10^{-3}-57.6×10^{-3})	$21.7 \times 10^{-3} \pm 11.3 \times 10^{-3}$ (9.26×10^{-3}-54.9×10^{-3})	$20.2 \times 10^{-3} \pm 10.8 \times 10^{-3}$	7.37×10^{-3}		

Table 13. Continued.

Trace metal	Size fraction	Summer 2014 (µmol/m^2/d)	Fall 2014 (µmol/m^2/d)	Winter 2014-2015 (µmol/m^2/d)	Spring 2015 (µmol/m^2/d)	Overall mean flux (µmol/m^2/d)	Overall mean flux (mmol/m^2/yr)	Overall mean total flux fine+coarse (mmol/m^2/yr)	Overall total deposition flux fine+coarse (mg/m^2/yr)
Zn	<1 µm	$2.56 \times 10^{-3} \pm 0.591 \times 10^{-3}$ (1.88×10^{-3}-4.04×10^{-3})	$3.49 \times 10^{-3} \pm 1.45 \times 10^{-3}$ (1.79×10^{-3}-6.43×10^{-3})	$5.06 \times 10^{-3} \pm 1.31 \times 10^{-3}$ (2.58×10^{-3}-6.95×10^{-3})	$3.41 \times 10^{-3} \pm 1.42 \times 10^{-3}$ (1.34×10^{-3}-6.47×10^{-3})	$3.66 \times 10^{-3} \pm 1.51 \times 10^{-3}$	1.34×10^{-3}	14.7×10^{-3}	0.959
	>1 µm	$31.5 \times 10^{-3} \pm 10.3 \times 10^{-3}$ (22.5×10^{-3}-52.3×10^{-3})	$39.9 \times 10^{-3} \pm 22.2 \times 10^{-3}$ (20.3×10^{-3}-103×10^{-3})	$41.5 \times 10^{-3} \pm 14.3 \times 10^{-3}$ (18.2×10^{-3}-64.7×10^{-3})	$35.1 \times 10^{-3} \pm 12.6 \times 10^{-3}$ (12.1×10^{-3}-51.8×10^{-3})	$36.5 \times 10^{-3} \pm 16.4 \times 10^{-3}$	13.3×10^{-3}		
Cd	<1 µm	$1.36 \times 10^{-5} \pm 0.506 \times 10^{-5}$ (0.736×10^{-5}-2.59×10^{-5})	$2.09 \times 10^{-5} \pm 1.37 \times 10^{-5}$ (0.570×10^{-5}-5.95×10^{-5})	$3.17 \times 10^{-5} \pm 1.49 \times 10^{-5}$ (1.31×10^{-5}-6.32×10^{-5})	$1.82 \times 10^{-5} \pm 0.777 \times 10^{-5}$ (0.717×10^{-5}-3.40×10^{-5})	$2.12 \times 10^{-5} \pm 1.26 \times 10^{-5}$	0.774×10^{-5}	4.64×10^{-5}	5.22×10^{-3}
	>1 µm	$1.29 \times 10^{-4} \pm 0.538 \times 10^{-4}$ (641×10^{-4}-2.56×10^{-4})	$1.05 \times 10^{-4} \pm 0.288 \times 10^{-4}$ (0.703×10^{-4}-1.78×10^{-4})	$1.09 \times 10^{-4} \pm 33.9 \times 10^{-4}$ (0.491×10^{-4}-1.60×10^{-4})	$0.946 \times 10^{-4} \pm 0.336 \times 10^{-4}$ (0.441×10^{-4}-1.57×10^{-4})	$1.06 \times 10^{-4} \pm 0.408 \times 10^{-4}$	0.387×10^{-4}		
Sb	<1 µm	$1.55 \times 10^{-4} \pm 0.606 \times 10^{-4}$ (0.748×10^{-4}-2.60×10^{-4})	$1.76 \times 10^{-4} \pm 0.550 \times 10^{-4}$ (0.842×10^{-4}-2.49×10^{-4})	$1.98 \times 10^{-4} \pm 1.24 \times 10^{-4}$ (0.780×10^{-4}-5.19×10^{-4})	$1.12 \times 10^{-4} \pm 0.589 \times 10^{-4}$ (0.166×10^{-4}-2.43×10^{-4})	$1.58 \times 10^{-4} \pm 0.835 \times 10^{-4}$	0.577×10^{-4}	6.09×10^{-4}	68.7×10^{-3}
	>1 µm	$21.7 \times 10^{-4} \pm 6.99 \times 10^{-4}$ (8.73×10^{-4}-28.7×10^{-4})	$18.6 \times 10^{-4} \pm 4.91 \times 10^{-4}$ (14.0×10^{-4}-33.6×10^{-4})	$14.8 \times 10^{-4} \pm 9.07 \times 10^{-4}$ (5.19×10^{-4}-32.3×10^{-4})	$8.32 \times 10^{-4} \pm 3.12 \times 10^{-4}$ (2.67×10^{-4}-12.8×10^{-4})	$15.1 \times 10^{-4} \pm 8.11 \times 10^{-4}$	5.51×10^{-4}		
Pb	<1 µm	$1.99 \times 10^{-4} \pm 0.652 \times 10^{-4}$ (0.985×10^{-4}-3.39×10^{-4})	$2.84 \times 10^{-4} \pm 1.20 \times 10^{-4}$ (0.699×10^{-4}-4.41×10^{-4})	$4.53 \times 10^{-4} \pm 3.60 \times 10^{-4}$ (1.69×10^{-4}-15×10^{-4})	$2.83 \times 10^{-4} \pm 1.06 \times 10^{-4}$ (1.31×10^{-4}-4.38×10^{-4})	$3.07 \times 10^{-4} \pm 2.11 \times 10^{-4}$	1.12×10^{-4}	6.85×10^{-4}	0.142
	>1 µm	$15.8 \times 10^{-4} \pm 8.25 \times 10^{-4}$ (8.34×10^{-4}-37.0×10^{-4})	$15.7 \times 10^{-4} \pm 3.56 \times 10^{-4}$ (12.1×10^{-4}-23.3×10^{-4})	$16.4 \times 10^{-4} \pm 6.98 \times 10^{-4}$ (7.14×10^{-4}-32.5×10^{-4})	$16.1 \times 10^{-4} \pm 4.87 \times 10^{-4}$ (8.16×10^{-4}-23.8×10^{-4})	$15.7 \times 10^{-4} \pm 6.15 \times 10^{-4}$	5.73×10^{-4}		

Table 14. Mean (± standard deviation) fractional solubility of trace metals (%) from Eastern Shore aerosol samples (the seasonal range of the fractional solubility for each trace metal is provided in parentheses).

Trace metal	Size fraction	Summer 2014	Fall 2014	Winter 2014-2015	Spring 2015	Overall mean
Al	<1 μm	3.41 ± 1.23 (2.08-5.48)	2.35 ± 1.74 (0.553-7.36)	2.90 ± 1.26 (1.02-4.61)	3.14 ± 2.71 (1.28-11.8)	2.93 ± 1.90
	>1 μm	2.64 ± 0.793 (1.63-3.90)	1.87 ± 1.64 (0.393-6.92)	2.46 ± 1.24 (1.14-5.22)	2.30 ± 1.46 (0.871-5.22)	2.34 ± 1.31
Ti	<1 μm	0.505 ± 0.324 (0-1.05)	0.309 ± 0.285 (0-0.841)	1.19 ± 0.947 (0-3.22)	0.254 ± 0.393 (0-1.46)	0.543 ± 0.653
	>1 μm	0.0285 ± 0.0669 (0-0.205)	0.0122 ± 0.0440 (0-0.158)	— —	0.0140 ± 0.0543 (0-0.210)	0.0134 ± 0.0477
V	<1 μm	63.0 ± 14.1 (37.6-79.4)	62.5 ± 15.5 (37.0-100)	55.4 ± 13.3 (35.4-76.0)	50.4 ±15.8 (26.2-78.7)	57.2 ± 15.4
	>1 μm	19.4 ± 7.01 (5.95-31.5)	15.9 ± 6.45 (6.24-27.9)	22.2 ± 6.86 (11.7-39.2)	13.8 ± 6.19 (6.56-23.9)	17.8 ± 6.81
Cr	<1 μm	1.95 ± 6.17 (0-19.5)	1.64 ± 5.92 (0-21.4)	0.726 ± 2.51 (0-8.71)	6.67 ± 25.8 (0-100)	2.99 ± 14.6
	>1 μm	11.5 ± 15.5 (0-38.3)	0.472 ± 1.70 (0-6.13)	— —	2.56 ± 9.93 (0-38.5)	3.25 ± 9.65
Mn	<1 μm	31.8 ± 6.17 (21.9-41.7)	31.2 ± 5.00 (20.4-41.3)	29.5 ± 5.76 (21.1-41.4)	30.3 ± 6.64 (20.6-42.4)	30.6 ± 5.82
	>1 μm	43.4 ± 4.27 (38.2-52.5)	42.7 ± 7.20 (29.1-53.3)	37.5 ± 7.71 (25.9-53.1)	38.8 ± 13.5 (27.1-53.4)	41.3 ± 7.4
Fe	<1 μm	7.31 ± 2.52 (2.90-10.9)	5.97 ± 3.23 (1.38-14.6)	6.07 ± 3.14 (2.09-11.1)	5.48 ± 3.51 (2.14-14.1)	6.11 ± 3.15
	>1 μm	2.47 ± 0.688 (1.15-3.19)	1.50 ± 0.634 (0.578-2.99)	1.80 ± 0.867 (0.714-3.50)	1.68 ± 0.844 (0.859-3.11)	1.86 ± 0.788
Co	<1 μm	29.9 ± 5.97 (21.4-40.5)	20.5 ± 9.64 (0-35.2)	23.1 ± 8.25 (8.40-35.7)	21.9 ± 8.30 (14.4-44.5)	23.4 ± 8.72
	>1 μm	24.6 ± 2.84 (20.0-29.2)	17.3 ± 11.3 (0-38.4)	25.7 ± 23.8 (12.3-100)	20.5 ± 8.47 (13.0-33.4)	22.2 ± 13.6

Table 14. Continued.

Trace metal	Size fraction	Summer 2014	Fall 2014	Winter 2014-2015	Spring 2015	Overall mean
Ni	<1 µm	26.6 ± 4.46 (17.5-34.4)	19.9 ± 12.7 (0-43.7)	21.2 ± 8.02 (0-28.3)	35.2 ± 16.0 (19.7-76.7)	26.1 ± 13.1
	>1 µm	5.03 ± 11.6 (0-35.0)	2.43 ± 6.29 (0-20.9)	11.3 ± 12.1 (0-27.4)	25.3 ± 28.7 (0-89.5)	12.2 ± 19.9
Cu	<1 µm	44.5 ± 8.41 (26.1-53.2)	39.7 ± 8.09 (23.9-55.2)	38.4 ± 9.45 (27.1-54.1)	47.4 ± 17.0 (29.6-100)	42.7 ± 12.1
	>1 µm	42.1 ± 8.74 (28.5-55.7)	36.6 ± 7.42 (19.4-50.4)	38.5 ± 12.1 (25.1-60.9)	36.3 ± 14.1 (15.8-53.8)	38.9 ± 9.66
Zn	<1 µm	73.7 ± 17.7 (49.7-100)	53.4 ± 14.7 (37.8-98.3)	54.7 ± 8.44 (38.6-67.9)	60.2 ± 12.9 (47.7-100)	59.8 ± 15.2
	>1 µm	56.5 ± 11.9 (33.0-72.6)	53.4 ± 12.4 (23.2-72.8)	62.0 ± 11.3 (43.7-81.1)	59.9 ± 22.9 (38.2-97.4)	59.2 ± 13.7
Cd	<1 µm	59.4 ± 8.72 (47.1-72.1)	63.0 ± 14.6 (41.1-100)	59.2 ± 14.9 (16.1-70.5)	70.4 ± 10.9 (47.6-100)	63.6 ± 13.1
	>1 µm	50.3 ± 18.2 (25.5-82.6)	53.8 ± 32.0 (0-100)	71.2 ± 13.3 (47.5-100)	64.6 ± 19.4 (48.7-79.5)	61.7 ± 21.4
Sb	<1 µm	33.4 ± 8.59 (24.4-49.4)	41.8 ± 10.7 (21.1-66.9)	45.5 ± 6.50 (36.6-60.3)	49.9 ± 11.5 (29.1-68.6)	43.4 ± 11.1
	>1 µm	6.50 ± 3.12 (3.23-14.2)	7.99 ± 2.35 (4.61-12.3)	14.3 ± 4.06 (9.05-21.3)	15.8 ± 5.60 (11.7-24.3)	11.8 ± 5.43
Pb	<1 µm	40.1 ± 10.8 (18.6-54.7)	40.3 ± 19.3 (23.5-100)	33.4 ± 6.47 (24.3-41.8)	36.9 ± 6.70 (24.9-50.4)	37.6 ± 11.9
	>1 µm	18.9 ± 7.56 (5.76-27.8)	18.1 ± 5.59 (9.57-29.8)	24.2 ± 6.90 (12.1-37.1)	19.0 ± 7.28 (9.5-31.1)	20.4 ± 6.51

(a) Aerosol soluble aluminum from Eastern Shore samples

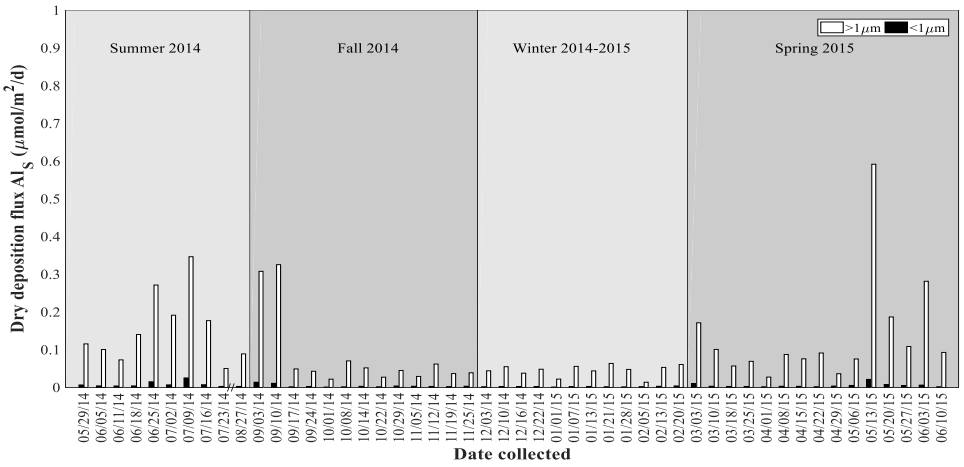

(b) Aerosol total aluminum from Eastern Shore samples

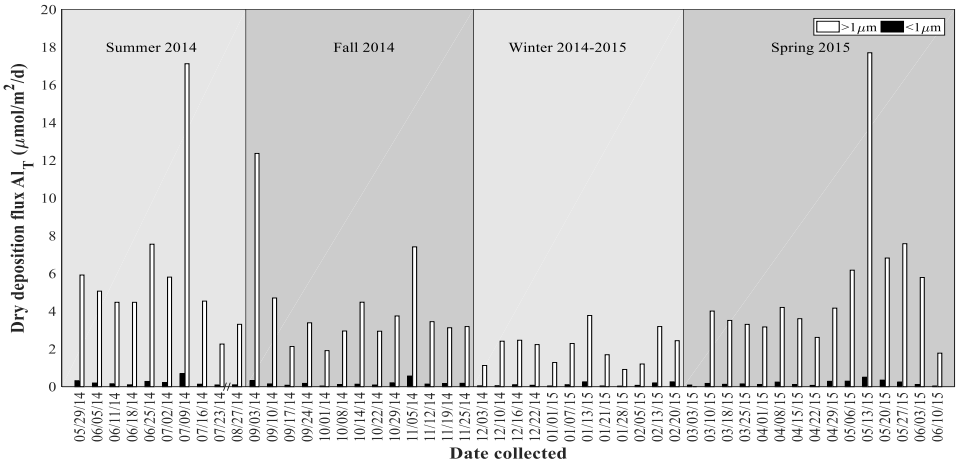

(c) Aerosol aluminum fractional solubility from Eastern Shore samples

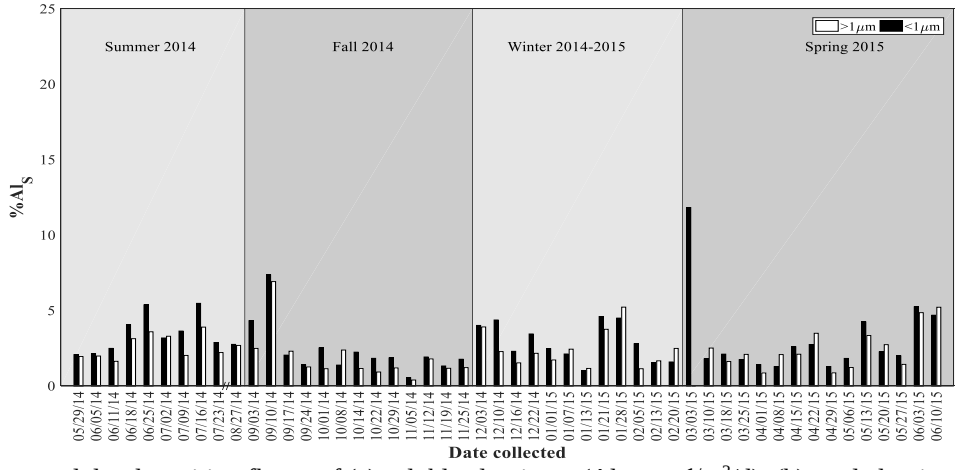

Figure 21. Seasonal dry deposition fluxes of (a) soluble aluminum (Al_S, μmol/m^2/d), (b) total aluminum (Al_T, μmol/m^2/d), and (c) fractional solubility (%Al_S) for weekly collected Eastern Shore samples. "//" indicates the break in the x-axis between 07/23/14 and 08/27/14.

The smoothed data and residuals show that the flux of dry fine Al_S remained relatively low throughout the time series (Figures 22a and 23a), whereas the flux of dry coarse Al_S was often above the overall mean during summer and spring, and below this mean during fall and winter (Figure 22a). The dry Al_T fluxes and the dry Al_S fluxes for both size fractions followed a similar seasonal pattern (Figures 23a and 23b). The fractional solubility for both size fractions was consistently below 15 % (Figure 21c) and showed no clear seasonal trend (Figures 22c and 23c).

(a) Aerosol soluble aluminum from Eastern Shore samples - smoothed

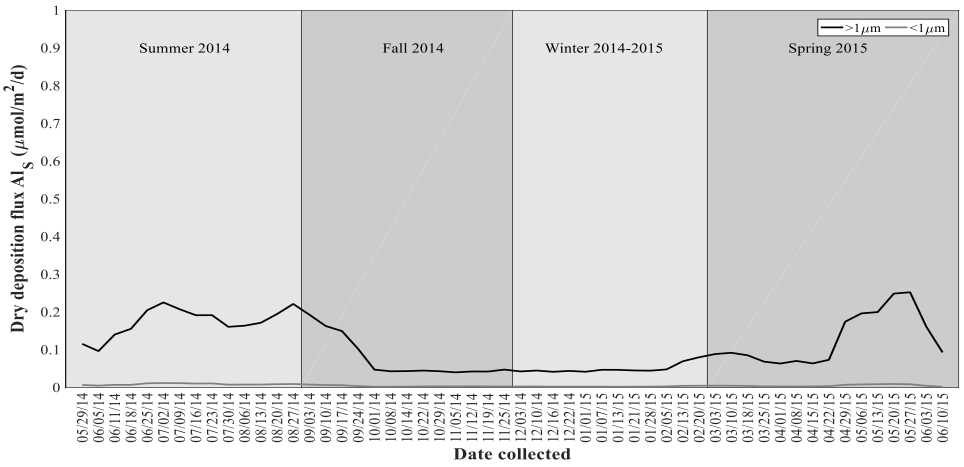

(b) Aerosol total aluminum from Eastern Shore samples - smoothed

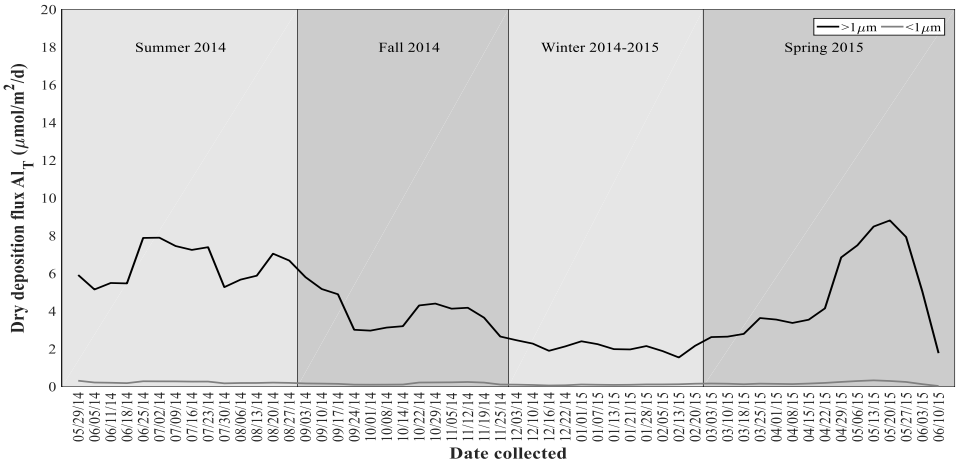

(c) Aerosol aluminum fractional solubility from Eastern Shore samples - smoothed

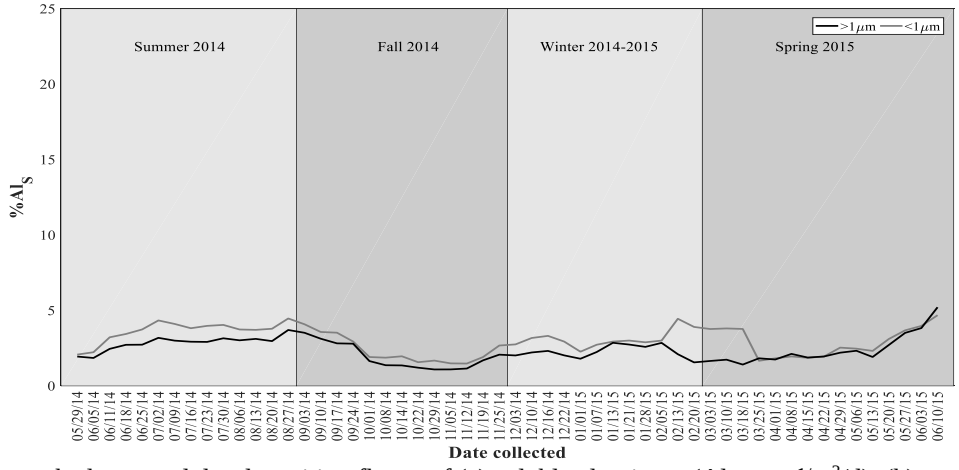

Figure 22. Smoothed seasonal dry deposition fluxes of (a) soluble aluminum (Al_S, μmol/m^2/d), (b) total aluminum (Al_T, μmol/m^2/d), and (c) fractional solubility (%Al_S) for weekly collected Eastern Shore samples. Note that data were interpolated for dates 30 July 2014, 6 August 2014, 13 August 2014, and 20 August 2014 using the method in Section 2.6.

(a) Aerosol soluble aluminum from Eastern Shore samples - residuals

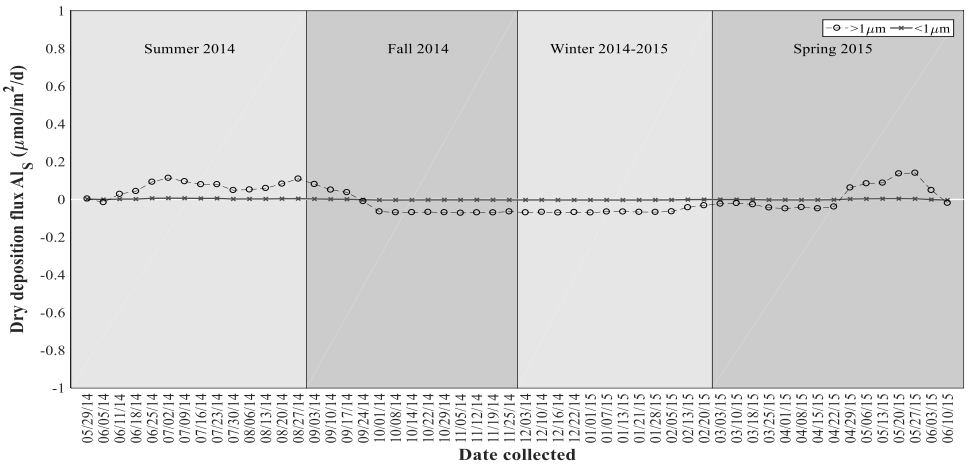

(b) Aerosol total aluminum from Eastern Shore samples - residuals

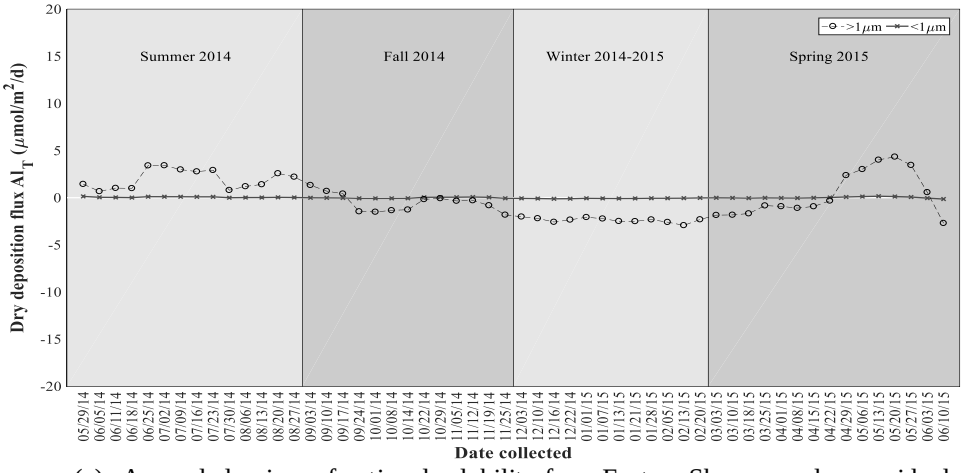

(c) Aerosol aluminum fractional solubility from Eastern Shore samples - residuals

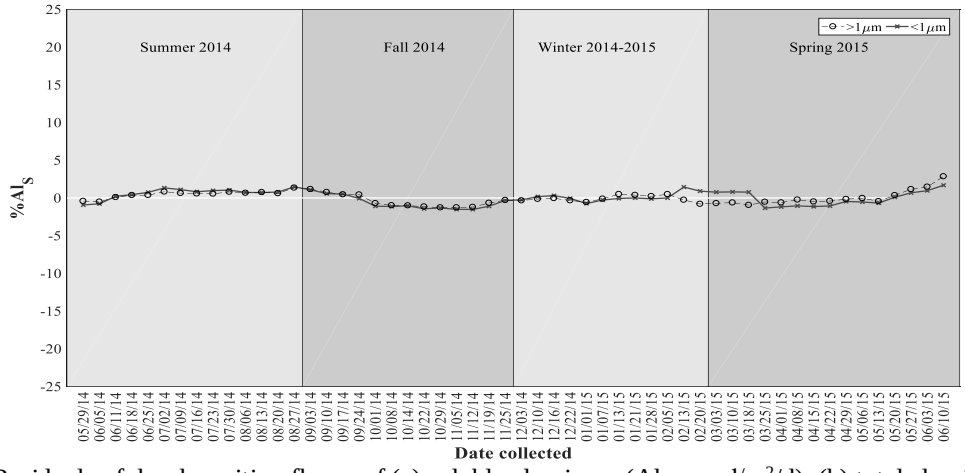

Figure 23. Residuals of dry deposition fluxes of (a) soluble aluminum (Al_S, μmol/m^2/d), (b) total aluminum (Al_T, μmol/m^2/d), and (c) fractional solubility (%Al_S) for weekly collected Eastern Shore samples. Note that data were interpolated for dates 30 July 2014, 6 August 2014, 13 August 2014, and 20 August 2014 using the method in Section 2.6. The white horizontal line indicates the annual mean.

There were statistically significant differences in the seasonal mean dry fine Al_S fluxes, as the mean dry fine Al_S flux for summer ($7.82 \times 10^{-3} \pm 7.08 \times 10^{-3}$ µmol/m^2/d) was significantly greater ($p = 0.0033$, $df = 49$, $F = 5.28$) than those for both fall ($3.90 \times 10^{-3} \pm 3.89 \times 10^{-3}$ µmol/m^2/d) and winter ($2.29 \times 10^{-3} \pm 0.804 \times 10^{-3}$ µmol/m^2/d) (Table 12), as determined by a one-way ANOVA and a multiple comparison test. The mean dry coarse Al_S flux for summer (0.155 ± 0.094 µmol/m^2/d) was also found to be significantly greater ($p = 0.0033$, $df = 49$, $F = 5.28$) than those for fall (0.085 ± 0.104 µmol/m^2/d) and winter (0.046 ± 0.015 µmol/m^2/d) (Table 12), and the mean dry coarse Al_S flux for spring (0.137 ± 0.142 µmol/m^2/d) was significantly greater ($p = 0.0033$, $df = 49$, $F = 5.28$) than that for winter (0.0455 ± 0.0149 µmol/m^2/d) (Table 12), as confirmed by a one-way ANOVA and a multiple comparison test. The results of a two-sample t-test confirmed that the overall mean dry coarse Al_S flux (0.105 ± 0.108 µmol/m^2/d) was significantly greater ($p < 0.0001$, $df = 53.3$, $tstat = 19.2$) than the overall mean dry fine Al_S flux ($4.72 \times 10^{-3} \pm 4.91 \times 10^{-3}$ µmol/m^2/d) (Table 12).

The means of the dry fine Al_T fluxes for the four seasons were not significantly different ($p = 0.182$, $df = 49$, $F = 0.1822$). However, the median dry coarse Al_T fluxes for summer (4.80×10^{-3} µmol/m^2/d), fall (3.39 , $\times 10^{-3}$ µmol/m^2/d), and spring (4.09×10^{-3} µmol/m^2/d) were found to be significantly greater ($p = 0.0002$, $df = 48$, chi-sq = 19.42) than the median dry coarse Al_T flux for winter (2.26×10^{-3} µmol/m^2/d), as determined by a Kruskal-Wallis test and a multiple comparison test. The overall mean dry coarse Al_T flux (4.32 ± 3.44 µmol/m^2/d) was significantly greater ($p < 0.0001$, $tstat = 24.4$, $df = 97$) than the overall mean dry fine Al_T flux (0.176 ± 0.135 µmol/m^2/d) (Table 13), as determined by a two-sample t-test. There were no significant differences for the seasonal means of both coarse $\%Al_S$ ($p = 0.1043$, $df = 48$, $F = 2.17$) and fine $\%Al_S$ ($p = 0.1638$, $df = 49$, $F = 1.78$), as well as for the overall mean $\%Al_S$ for the two size fractions ($p < 0.0001$, $df = 97$, $tstat = 24.4103$).

Concentrations were quantifiable for more than more than 50% of the dry fine soluble titanium (Ti_S) samples, for which fluxes ranged from below the level of quantification to 6.38 x 10^{-5} µmol/m^2/d in summer, below the level of quantification to 5.42 x 10^{-5} µmol/m^2/d in fall, below the level of quantification to 5.02 x 10^{-5} µmol/m^2/d in winter, and below the level of quantification to 5.66 x 10^{-5} µmol/m^2/d in spring (Table 12 and Figure 24a). However, dry coarse Ti_S was quantifiable for only 4 samples, which were collected on 25 June 2014, 9 July 2014, 3 September 2014, and 20 May 2015 (Table 12 and Figure 24a). The dry flux of coarse Ti_S flux ranged from below the level of quantification to 6.50 x 10^{-4} µmol/m^2/d in summer, below the level of quantification to 7.53 x 10^{-4} µmol/m^2/d in fall, and below the level of quantification to 7.25 x 10^{-4} µmol/m^2/d in spring (Table 12 and Figure 24a). Data are not available for winter, as Ti_S concentrations in those samples were below the detection limit of 0.28 µg L^{-1} (Figure 24a and Table 3).

The dry fine total flux of titanium (Ti_T) was consistently lower than the dry coarse Ti_T flux, and ranged from 2.74 x 10^{-3} to 29.0 x 10^{-3} µmol/m^2/d in summer, 1.43 x 10^{-3} to 28.2 x 10^{-3} µmol/m^2/d in fall, 1.24 x 10^{-3} to 14.5 x 10^{-3} µmol/m^2/d in winter, and 1.76 x 10^{-3} to 19.4 x 10^{-3} µmol/m^2/d in spring (Table 13 and Figure 24b). The dry coarse Ti_T ranged from 95.3 x 10^{-3} to 730 x 10^{-3} µmol/m^2/d in summer, 86.4 x 10^{-3} to 474 x 10^{-3}µmol/m^2/d in fall, 39.5 x 10^{-3} to 166 x 10^{-3} µmol/m^2/d in winter, and 72.5 x 10^{-3} to 664 x 10^{-3} µmol/m^2/d in spring (Table 13 and Figure 24b). The dry flux of Ti_T for both fine and coarse size fractions peaked on 9 July 2014, 3 September 2014, 5 November 2014, and 13 May 2015 (Figure 24b).

The overall mean fine %Ti_S (0.543 ± 0.653 %) was greater than the overall mean coarse %Ti_S (0.0134 ± 0.0477 %) and ranged from below the level of quantification to 1.05 % in summer, below the level of quantification to 0.840 % in fall, below the level of quantification to 3.22 % in winter, and below the level of quantification to 1.46 % in spring (Table 14). Data were only available for 3 samples for coarse %Ti_S, which were collected on 25 June 2014, 3 September 2014, and 20 May 2015 (Figure 24a). The coarse %Ti_S ranged from below the level of quantification to 0.205 % in summer, below the level of quantification to 0.158% in fall, and below the level of quantification to 0.210 % in spring (Figure 24c). Data were not available for coarse %Ti_S during winter (Figure 24c), with Ti_s below detection.

(a) Aerosol soluble titanium from Eastern Shore samples

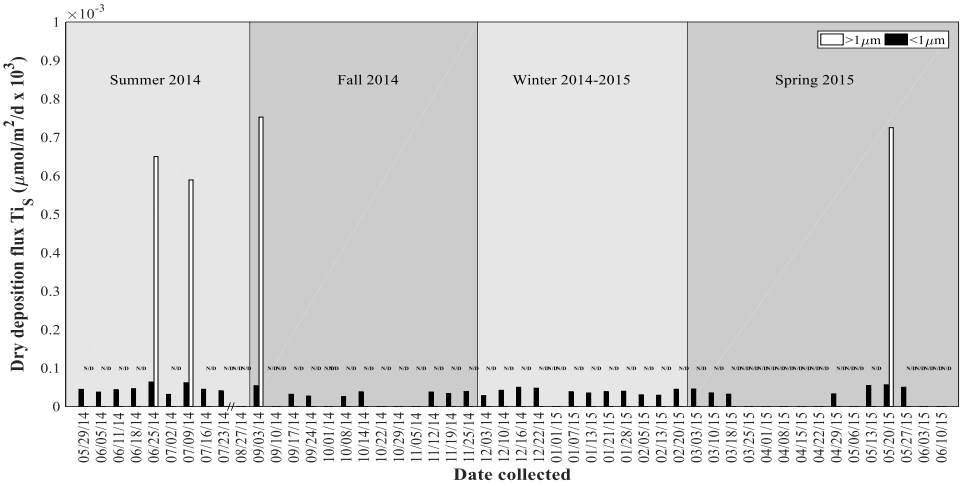

(b) Aerosol total titanium from Eastern Shore samples

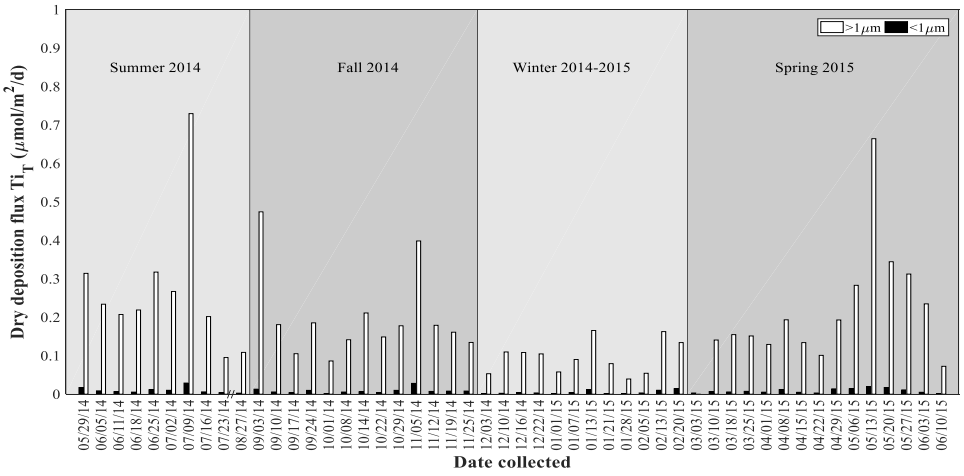

(c) Aerosol titanium fractional solubility from Eastern Shore samples

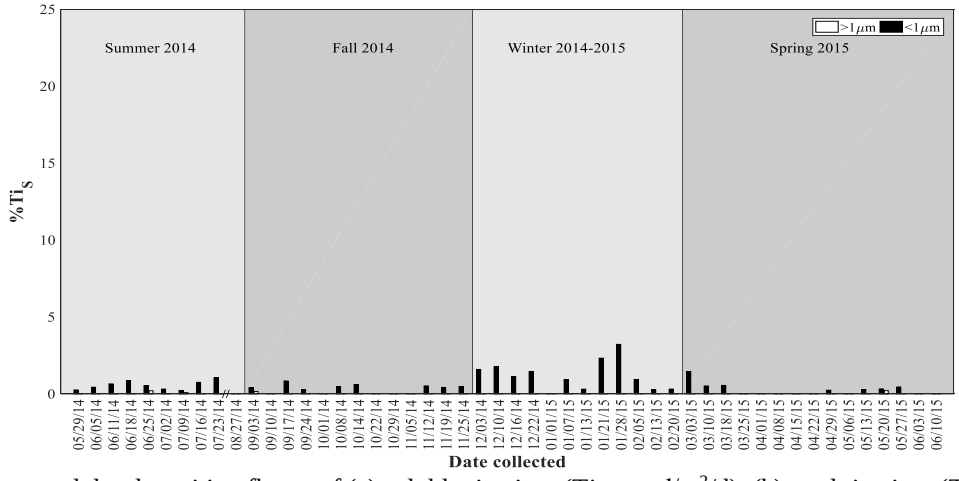

Figure 24. Seasonal dry deposition fluxes of (a) soluble titanium (Ti_S, μmol/m^2/d), (b) total titanium (Ti_T, μmol/m^2/d), and (c) fractional solubility (%Ti_S) for weekly collected Eastern Shore samples. "//" indicates the break in the x-axis between 07/23/14 and 08/27/14, "*" denotes dates for which no rain was collected and "N/D" indicates samples for which Ti was below the detection limit.

The smoothed data and residuals show that the dry fluxes for fine Ti_S remained relatively constant throughout the time series (Figures 25a and 26a). The dry coarse Ti_S flux data were limited to only 4 samples for the time series, as most samples were below the detection limit of 0.28 µg L^{-1} (Table 3 and Figure 24a). The smoothed data and residuals show that both dry fine Ti_T remained relatively constant throughout the time series (Figure 25b). However, dry coarse Ti_T was above the overall mean during summer and spring, and below this mean during winter (Figure 26b). The dry fluxes for coarse Ti_T remained near the overall mean during most of fall (Figure 26b). Titanium in both aerosol size fractions was relatively insoluble, as $\%Ti_S$ values were consistently below 5% throughout the time series (Figure 24c). The $\%Ti_S$ for both size fractions varied little from the overall mean throughout the time series (Figures 25c and 26c).

(a) Aerosol soluble titanium from Eastern Shore samples - smoothed

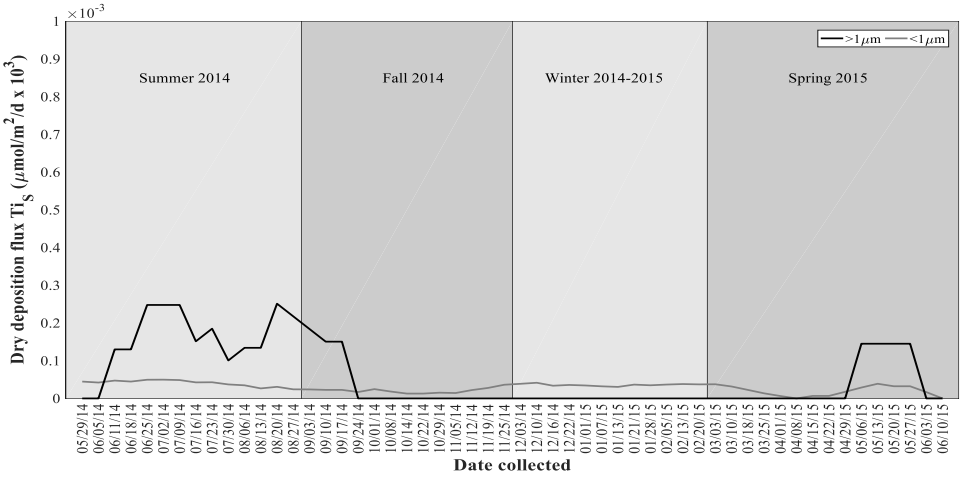

(b) Aerosol total titanium from Eastern Shore samples - smoothed

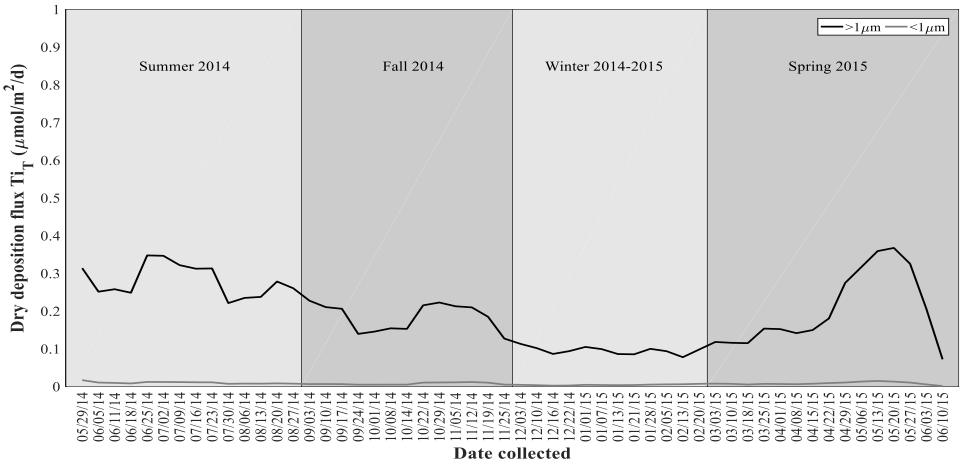

(c) Aerosol titanium fractional solubility from Eastern Shore samples - smoothed

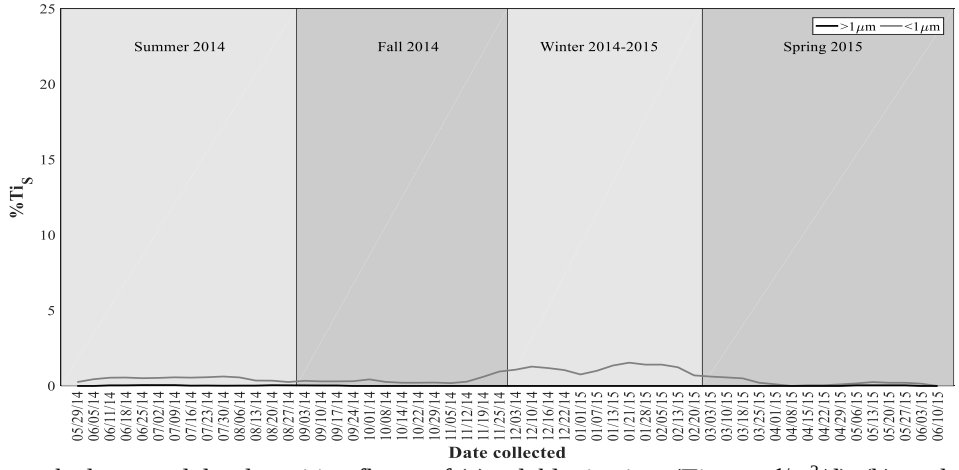

Figure 25. Smoothed seasonal dry deposition fluxes of (a) soluble titanium (Ti_S, μmol/m^2/d), (b) total titanium (Ti_T, μmol/m^2/d), and (c) fractional solubility (%Ti_S) for weekly collected Eastern Shore samples. Note that data were interpolated for dates 30 July 2014, 6 August 2014, 13 August 2014, and 20 August 2014 using the method in Section 2.6.

(a) Aerosol soluble titanium from Eastern Shore samples - residuals

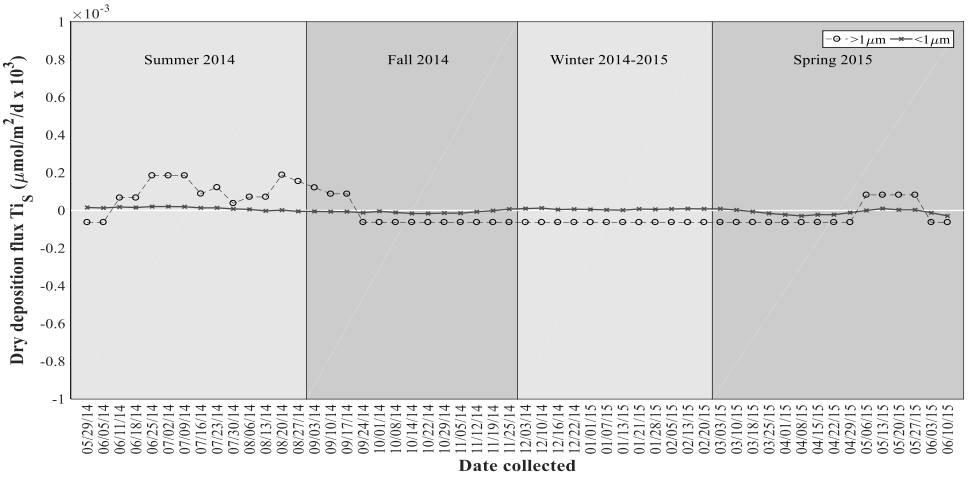

(b) Aerosol total titanium from Eastern Shore samples - residuals

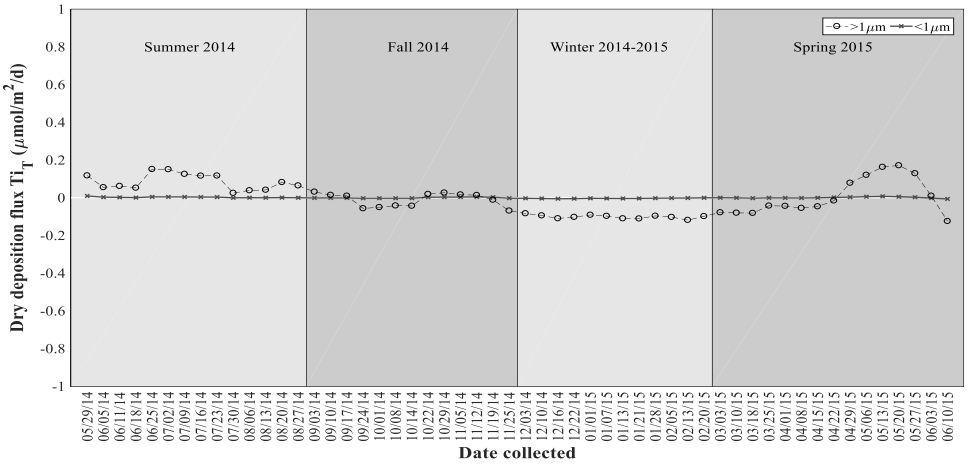

(c) Aerosol titanium fractional solubility from Eastern Shore samples - residuals

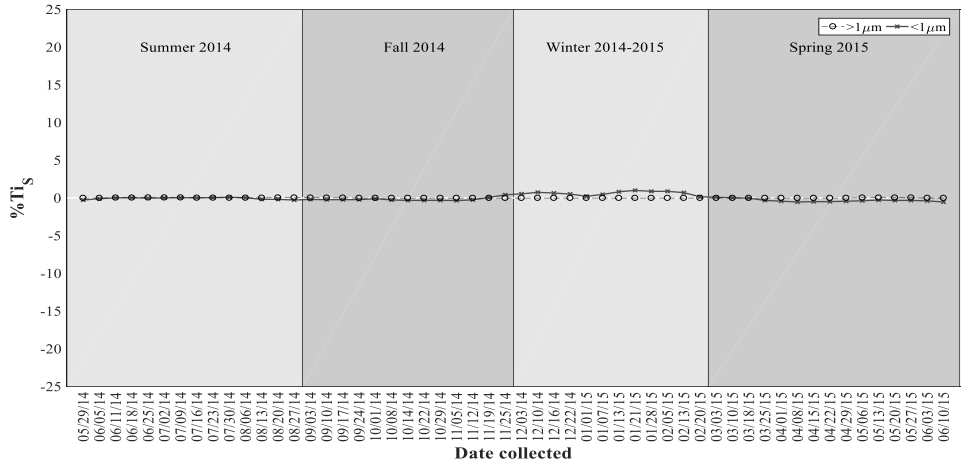

Figure 26. Residuals of dry deposition fluxes of (a) soluble titanium (Ti_S, μmol/m^2/d), (b) total titanium (Ti_T, μmol/m^2/d), and (c) fractional solubility (%Ti_S) for weekly collected Eastern Shore samples. Note that data were interpolated for dates 30 July 2014, 6 August 2014, 13 August 2014, and 20 August 2014 using the method in Section 2.6. The white horizontal line indicates the annual mean.

There were no statistically significant differences in the mean dry Ti_S fluxes for the four seasons for both fine ($p = 0.0996$, $df = 34$, $F = 2.27$) and coarse ($p = 0.3605$, $df = 3$, $F = 0.3605$) fractions. However, the overall mean dry coarse Ti_S flux ($0.543 \times 10^{-4} \pm 1.85 \times 10^{-4}$ µmol/m^2/d) was significantly greater ($p < 0.0001$, $df = 6.59$, $tstat = 41.7$) than the overall mean dry fine Ti_S flux ($2.28 \times 10^{-5} \pm 2.07 \times 10^{-5}$ µmol/m^2/d) (Table 12), as determined by a two-sample t-test.

The median dry coarse Ti_T fluxes for summer (0.227 µmol/m^2/d), fall (0.178 µmol/m^2/d), and spring (0.174 µmol/m^2/d) were found to be significantly greater ($p = 0.0009$, $df = 48$, $F = 16.49$) than the median dry coarse Ti_T flux for winter (0.0975 µmol/m^2/d) (Table 13), using a Kruskal-Wallis test. There were no significant seasonal differences for fine $\%Ti_S$ ($p = 0.0341$, $df = 34$, $F = 3.27$). The sample size of coarse $\%Ti_S$ ($n = 4$) was insufficient for use in statistical analyses. There were no significant differences in the overall mean $\%Ti_S$ for the two size fractions ($p = 0.0005$, $df = 37$, $tstat = -3.8044$).

The dry flux of soluble vanadium (V_S) in the fine fraction ranged from 2.82 x 10^{-4} to 8.73 x 10^{-4} µmol/m^2/d in summer, 2.23 x 10^{-4} to 7.08 x 10^{-4} µmol/m^2/d in fall, 0.955 x 10^{-4} to 6.93 x 10^{-4} µmol/m^2/d in winter, and 0.895 x 10^{-4} to 7.11 x 10^{-4} µmol/m^2/d in spring (Table 12 and Figure 27a). The dry flux of coarse V_S ranged from 6.40 x 10^{-4} to 19.7 x 10^{-4} µmol/m^2/d in summer, 3.46 x 10^{-4} to 19.4 x 10^{-4} µmol/m^2/d in fall, 3.20 x 10^{-4} to 17.5 x 10^{-4} µmol/m^2/d in winter, and 4.73 x 10^{-4} to 16.7 x 10^{-4} µmol/m^2/d in spring (Table 12 and Figure 27a). The lowest fluxes for dry coarse V_S occurred during the fall (Figure 27a), and the overall mean dry coarse V_S flux (10.3 x 10^{-4} ± 4.85 x 10^{-4} µmol/m^2/d) was more than twice that for fine V_S (3.58 x 10^{-4} ± 1.96 x 10^{-4} µmol/m^2/d) (Table 12).

The dry total vanadium (V_T) in the fine fraction ranged from 4.32 x 10^{-4} to 11.5 x 10^{-4} µmol/m^2/d in summer, 2.06 x 10^{-4} to 11.2 x 10^{-4} µmol/m^2/d in fall, 1.60 x 10^{-4} to 9.26 x 10^{-4} µmol/m^2/d in winter, and 1.25 x 10^{-4} to 11.3 x 10^{-4} µmol/m^2/d in spring (Table 13 and Figure 27b). The dry flux coarse V_T ranged from 3.15 x 10^{-3} to 14.7 x 10^{-3} µmol/m^2/d in summer, 2.94 x 10^{-3} to 12.7 x 10^{-3} µmol/m^2/d in fall, 1.54 x 10^{-3} to 6.21 x 10^{-3} µmol/m^2/d in winter, and 2.52 x 10^{-3} to 14.1 x 10^{-3} µmol/m^2/d in spring (Table 13 and Figure 27b). The overall mean dry flux for coarse V_T (6.09 x 10^{-3} ± 3.19 x 10^{-3} µmol/m^2/d) was roughly an order of magnitude greater than that for fine V_T (6.30 x 10^{-4} ± 2.81 x 10^{-4} µmol/m^2/d) (Table 13).

The fractional solubility of aerosol vanadium (%V_S) was greater for the fine fraction throughout the time series (Figure 27c). The coarse %V_S ranged from 5.95 to 31.5 % in summer, 6.24 to 27.9 % in fall, 11.7 to 39.2 % in winter, and 6.56 to 23.9 % in spring (Table 14 and Figure 27c). The fine %V_S ranged from 37.6 to 79.4 % in summer, 37.0 to 100 % in fall, 35.4 to 76.0 % in winter, and 26.2 to 78.7 % in spring (Table 14 and Figure 27c). The overall mean fine %V_S was more than twice that for coarse %V_S (Table 14).

(a) Aerosol soluble vanadium from Eastern Shore samples

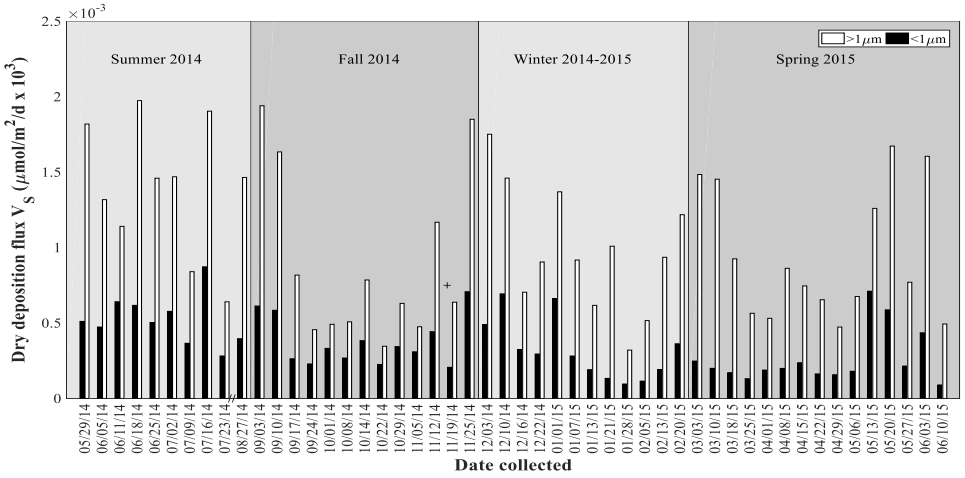

(b) Aerosol total vanadium from Eastern Shore samples

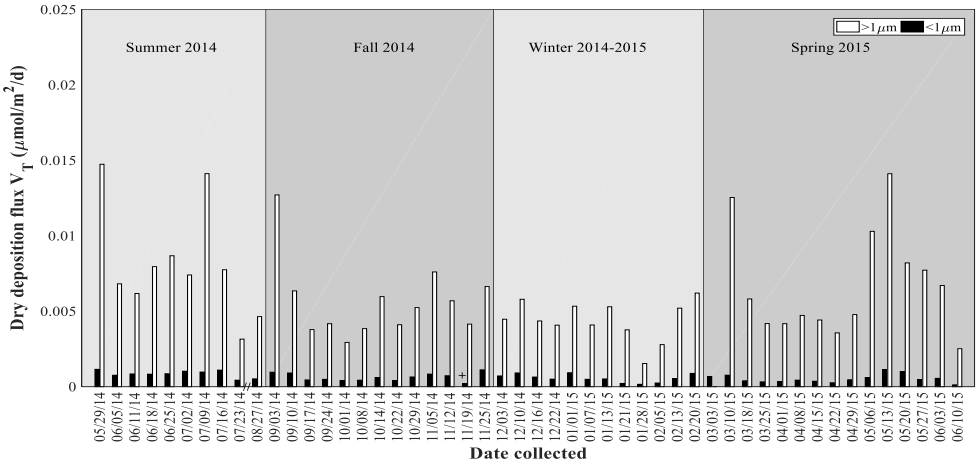

(c) Aerosol fractional solubility vanadium from Eastern Shore samples

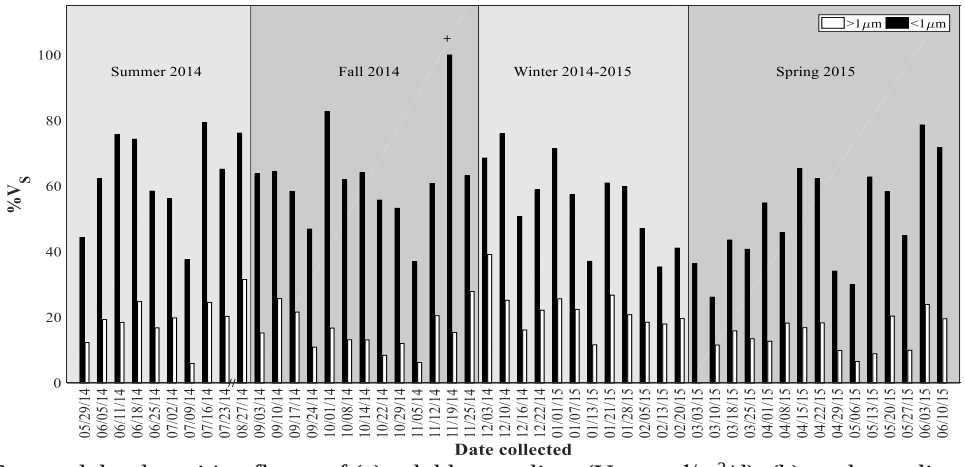

Figure 27. Seasonal dry deposition fluxes of (a) soluble vanadium (V_S, μmol/m²/d), (b) total vanadium (V_T, μmol/m²/d), and (c) fractional solubility (%V_S) for weekly collected Eastern Shore samples. "//" indicates the break in the x-axis between 07/23/14 and 08/27/14, "+" denotes samples for which the soluble flux was set to equal the total flux as mentioned in Section 2.6.

The smoothed data and residuals show that the flux of dry coarse and fine V_S followed similar trends throughout the time series (Figures 28a and 29a). The fluxes of dry coarse and fine V_S were typically above the overall mean during summer, and below this mean for during fall, winter, and spring (Figure 29a). The smoothed data and residuals show that the flux of dry coarse V_T was typically above the overall mean during summer and spring, and mostly below this mean during the fall and winter (Figures 28b and 29b). The smoothed data and residuals show that the flux of coarse and fine $\%V_S$ followed similar trends throughout the time series, with highest values in late fall and late spring, and minima in late winter to early spring (Figures 28c and 29c).

(a) Aerosol soluble vanadium from Eastern Shore samples - smoothed

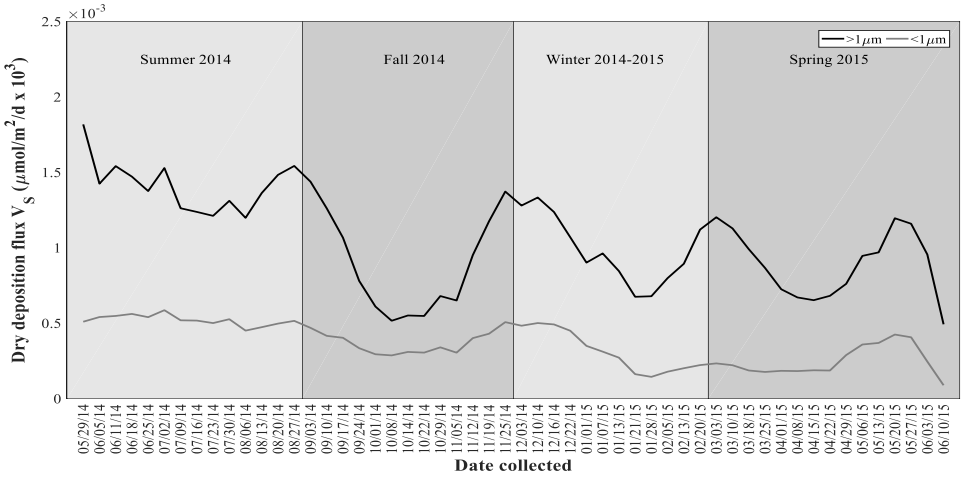

(b) Aerosol total vanadium from Eastern Shore samples - smoothed

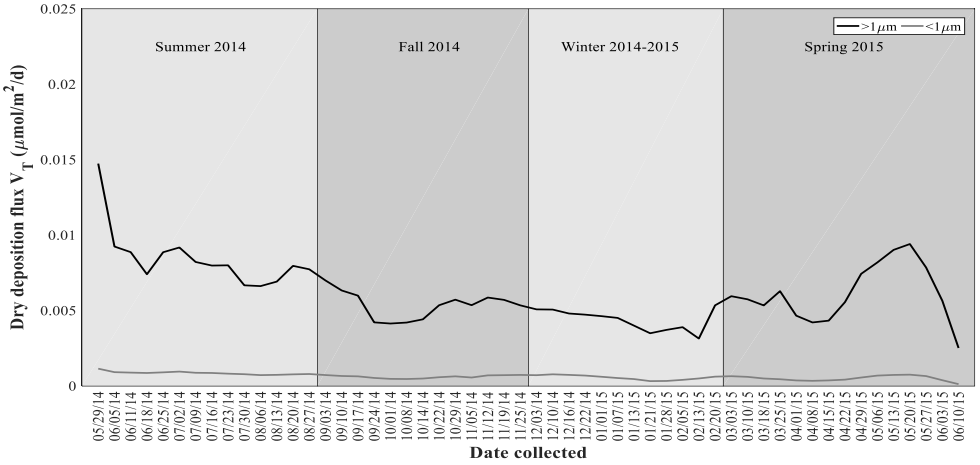

(c) Aerosol fractional solubility vanadium from Eastern Shore samples - smoothed

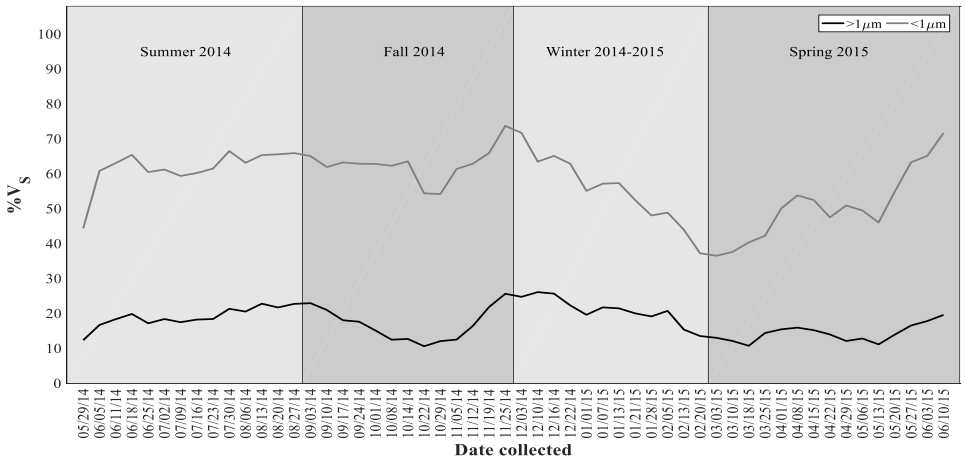

Figure 28. Smoothed seasonal dry deposition fluxes of (a) soluble vanadium (V_S, μmol/m²/d), (b) total vanadium (V_T, μmol/m²/d), and (c) fractional solubility (% V_S) for weekly collected Eastern Shore samples. Note that data were interpolated for dates 30 July 2014, 6 August 2014, 13 August 2014, and 20 August 2014 using the method in Section 2.6

(a) Aerosol soluble vanadium from Eastern Shore samples - residuals

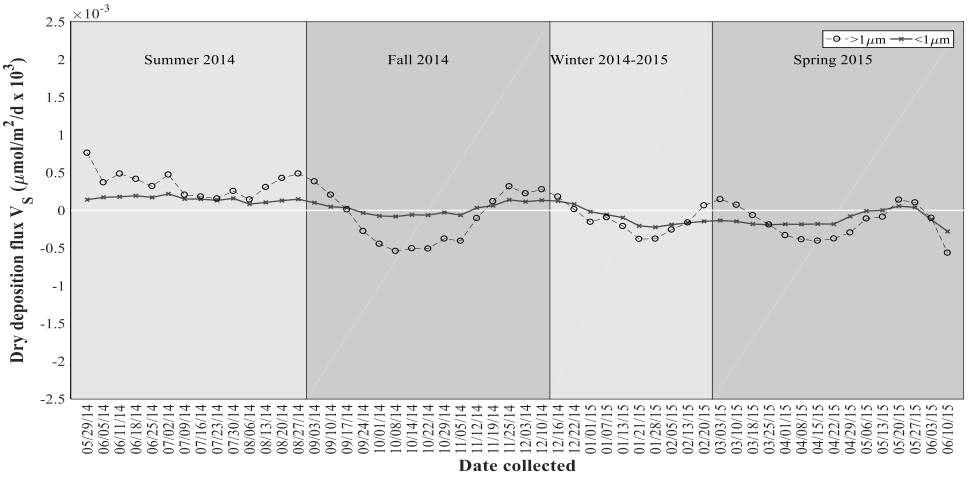

(b) Aerosol total vanadium from Eastern Shore samples - residuals

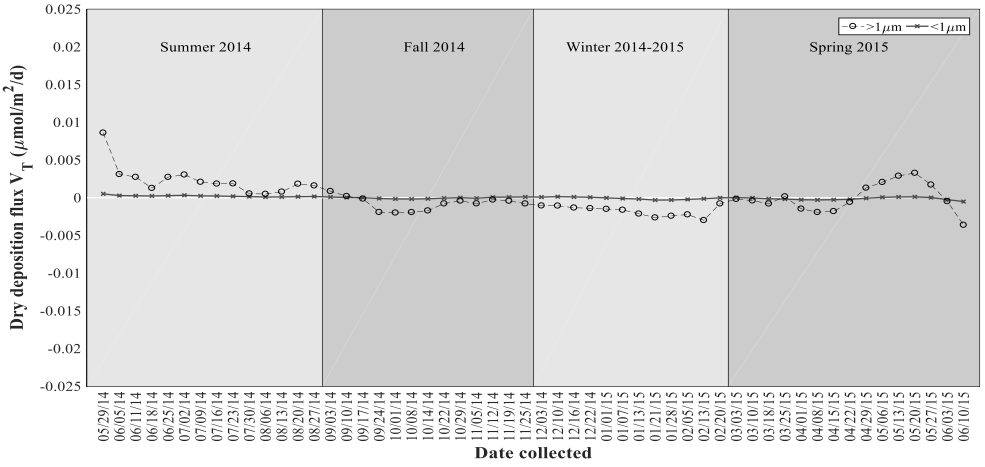

(c) Aerosol fractional solubility vanadium in Eastern Shore samples - residuals

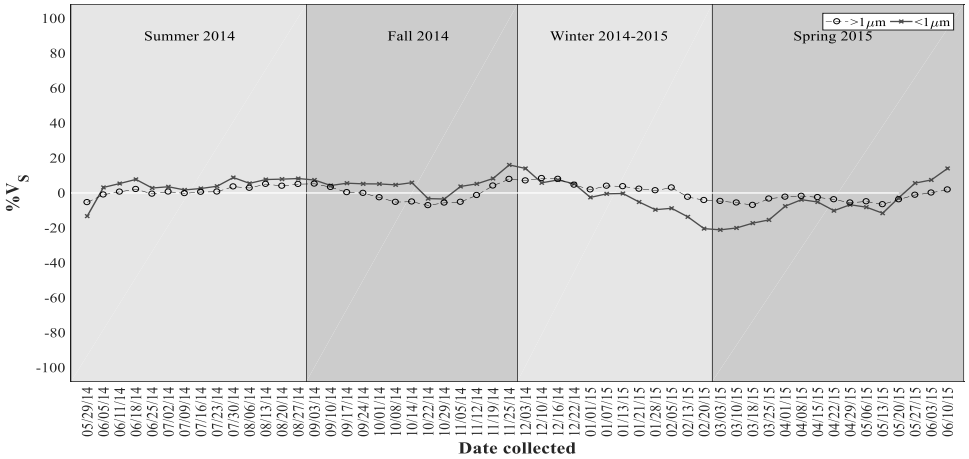

Figure 29. Residuals of dry deposition fluxes of (a) soluble vanadium (V_S, μmol/m²/d), (b) total vanadium (V_T, μmol/m²/d), and (c) fractional solubility (%V_S) for weekly collected Eastern Shore samples. Note that data were interpolated for dates 30 July 2014, 6 August 2014, 13 August 2014, and 20 August 2014 using the method in Section 2.6. The white horizontal line indicates the annual mean.

The mean dry fine V_S flux for summer ($5.25 \times 10^{-4} \pm 1.67 \times 10^{-4}$ µmol/m^2/d) was significantly greater ($p = 0.0021$, df = 49, F = 5.71) from those for both winter ($3.19 \times 10^{-4} \pm 2.02 \times 10^{-4}$ µmol/m^2/d) and spring ($2.61 \times 10^{-4} \pm 1.77 \times 10^{-4}$ µmol/m^2/d), using a one-way ANOVA and a multiple comparison test. However, the median dry coarse V_S fluxes for the four seasons were not significantly different ($p = 0.0609$, df = 49, chi-sq = 7.37), as determined by a Kruskal-Wallis test. The median flux of dry coarse V_S was found to be significantly greater ($p < 0.0001$, zval = 7.22) than the median dry fine V_S flux, using a Wilcoxon rank sum test.

The mean dry fine V_T flux for summer ($8.50 \times 10^{-4} \pm 2.33 \times 10^{-4}$ µmol/m^2/d) was found to be significantly greater ($p = 0.0266$, df = 49, F= 3.36) than that for spring ($5.27 \times 10^{-4} \pm 2.74 \times 10^{-4}$ µmol/m^2/d) (Table 13), using a one-way ANOVA and a multiple comparison test. The median dry coarse V_T flux of summer (7.58×10^{-3} µmol/m^2/d) was significantly greater ($p = 0.0227$, df = 48, chi-sq= 9.56) than that for winter (4.41×10^{-3} µmol/m^2/d), as determined by a Kruskal-Wallis test and a multiple comparison test. The overall mean dry coarse flux of V_T ($6.09 \times 10^{-3} \pm 3.19 \times 10^{-3}$ µmol/m^2/d) was significantly greater than the overall mean dry fine V_T ($6.30 \times 10^{-4} \pm 2.81 \times 10^{-4}$ µmol/m^2/d) (Table 13), as determined by a two-sample t-test.

There were no significant differences in the seasonal mean fine $\%V_S$ ($p = 0.1042$, df = 49, F = 2.17). However, the mean dry coarse $\%V_S$ for winter (22.2 ± 6.86 %) was found to be significantly greater ($p = 0.035$, df = 48, F= 3.12) than the mean dry coarse $\%V_S$ for spring (13.8 ± 6.19 %), using a one-way ANOVA and a multiple comparison test. The overall mean fine $\%V_S$ (57.2 ± 15.4 %) was found to be significant greater ($p < 0.0001$, df = 49.5, tstat = -29.2) than the overall mean dry coarse $\%V_S$ (17.8 ± 6.81 %) (Table 14), using a two-sample t-test.

The dry flux of soluble chromium (Cr_S) in the fine fraction ranged from 2.31 x 10^{-5} to 6.22 x 10^{-5} µmol/m^2/d in summer, 1.96 x 10^{-5} to 5.10 x 10^{-5} µmol/m^2/d in fall, 3.14 x 10^{-5} to 5.87 x 10^{-5} µmol/m^2/d in winter, and 1.68 x 10^{-5} to 15.1 x 10^{-5} µmol/m^2/d in spring (Table 12 and Figure 30a). The dry flux of coarse soluble chromium (Cr_S) ranged from 2.65 x 10^{-4} to 6.97 x 10^{-4} µmol/m^2/d in summer, below the level of quantification to 5.34 x 10^{-4} µmol/m^2/d in fall, 2.12 x 10^{-4} to 4.08 x 10^{-4} µmol/m^2/d in winter, and 2.24 x 10^{-4} to 6.21 x 10^{-4} µmol/m^2/d in spring, and was consistently greater than the dry flux of fine Cr_S throughout the time series (Table 12 and Figure 30a).

Data are not available for more than 50% of the samples for the dry flux of total chromium (Cr_T), as total concentrations in those digest samples were below the detection limit of 0.035 µg L^{-1} (Table 3 and Figure 30b). The samples for which dry Cr_T flux data are available were collected mainly during summer (Figure 30b). The dry fine Cr_T flux was ranged from below the level of quantification to 2.47 x 10^{-4} µmol/m^2/d in summer, below the level of quantification to 2.59 x 10^{-4} µmol/m^2/d in fall, below the level of quantification to 64.8 x 10^{-5} µmol/m^2/d in winter, and below the level of quantification to 4.32 x 10^{-5} µmol/m^2/d in spring (Table 13 and Figure 30b). The dry coarse Cr_T flux ranged from below the level of quantification to 6.30 x 10^{-3} µmol/m^2/d in summer, below the level of quantification to 8.29 x 10^{-3} µmol/m^2/d in fall, and below the level of quantification to 1.29 x 10^{-3} µmol/m^2/d in spring (Table 13 and Figure 30b). The overall mean dry coarse Cr_T flux (0.573 x 10^{-3} ± 1.68 x 10^{-3} µmol/m^2/d) was more than an order of magnitude greater than the overall mean dry fine Cr_T flux (4.97 x 10^{-5} ± 13.6 x 10^{-5} µmol/m^2/d) (Table 13 and Figure 30b).

The data for the fractional solubility of chromium (%Cr_S) were limited, as dry Cr_T values were available for only a few samples (Figure 30b). The dry fine %Cr_S ranged from below the level of quantification to 19.5 % in summer, below the level of quantification to 21.4 % in fall, below the level of quantification to 8.71 % in winter, and below the level of quantification to 100 % in spring (Table 14 and Figure 30c). The dry coarse %Cr_S ranged from below the level of quantification to 38.3 % in summer, below the level of quantification to 6.13 % in fall, and below the level of quantification to 38.5 % in spring (Table 14 and Figure 30c).

(a) Aerosol soluble chromium from Eastern Shore samples

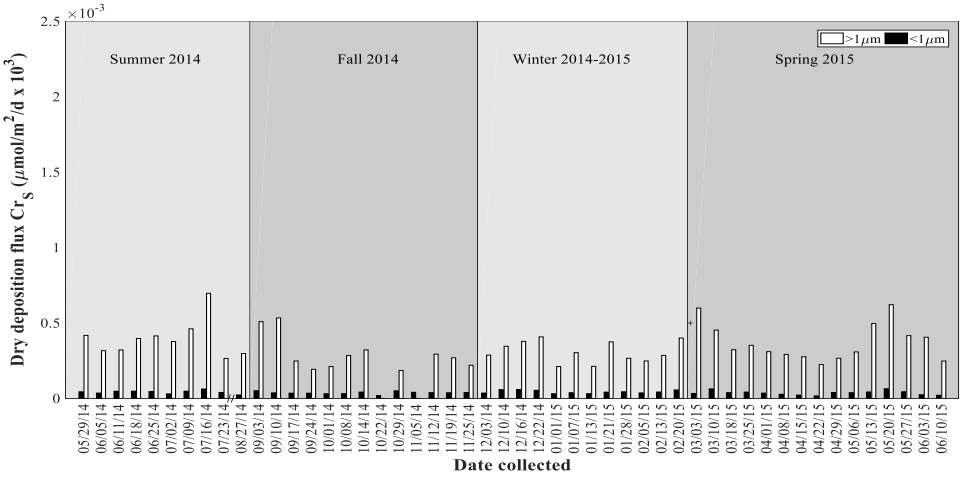

(b) Aerosol total chromium from Eastern Shore samples

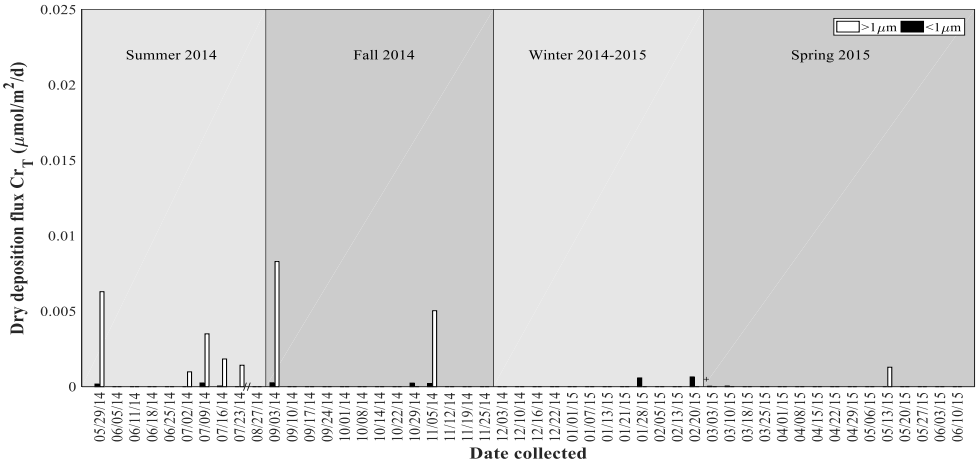

(c) Aerosol chromium fractional solubility from Eastern Shore samples

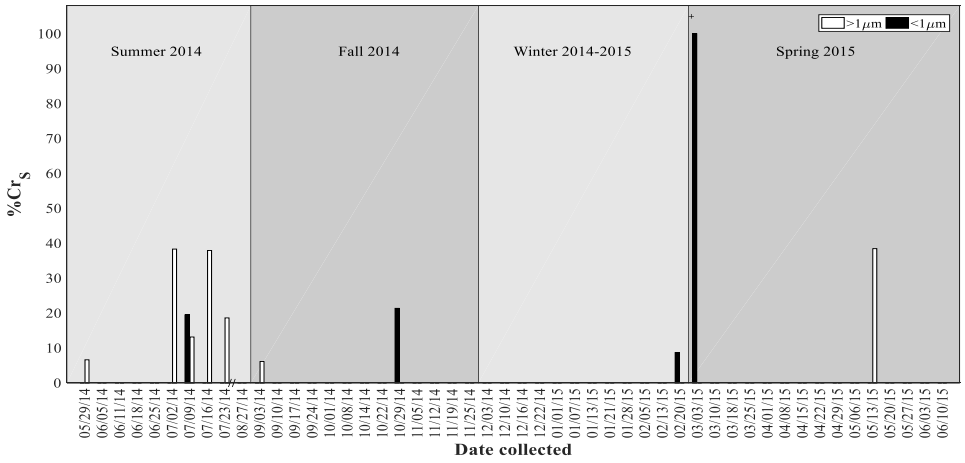

Figure 30. Seasonal dry deposition fluxes of (a) soluble chromium (Cr_S, μmol/m^2/d), (b) total chromium (Cr_T, μmol/m^2/d), and (c) fractional solubility (%Cr_S) for weekly collected Eastern Shore samples. "//" indicates the break in the x-axis between 07/23/14 and 08/27/14, "+" denotes samples for which the soluble flux was set to equal the total flux as mentioned in Section 2.6.

The smoothed data and residuals show that the flux of both fine and coarse Cr_S show little variation throughout the time series (Figures 31a and 32a). Due to the limited data, it cannot be determined how the dry flux of Cr_T (Figures 31b and 32b) and $\%Cr_S$ (Figures 31c and 32c), for both size fractions, changed over time.

(a) Aerosol soluble chromium from Eastern Shore samples - smoothed

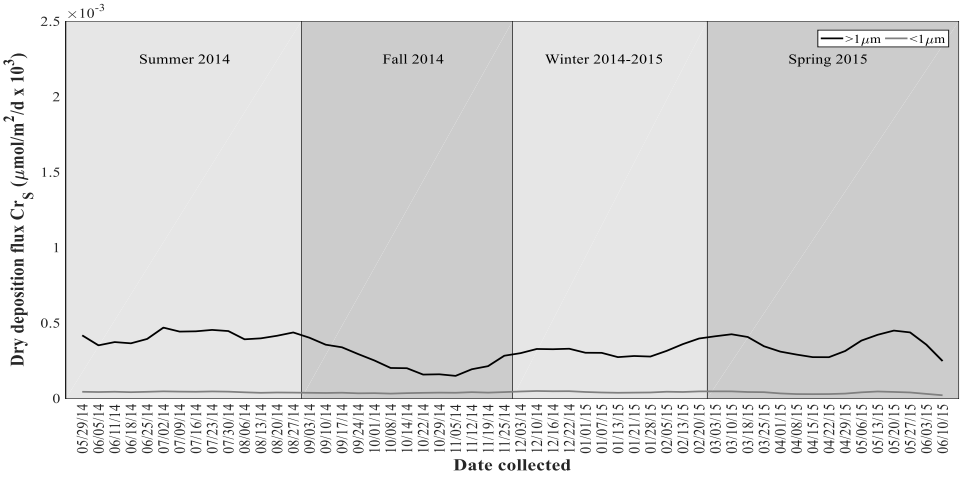

(b) Aerosol total chromium from Eastern Shore samples - smoothed

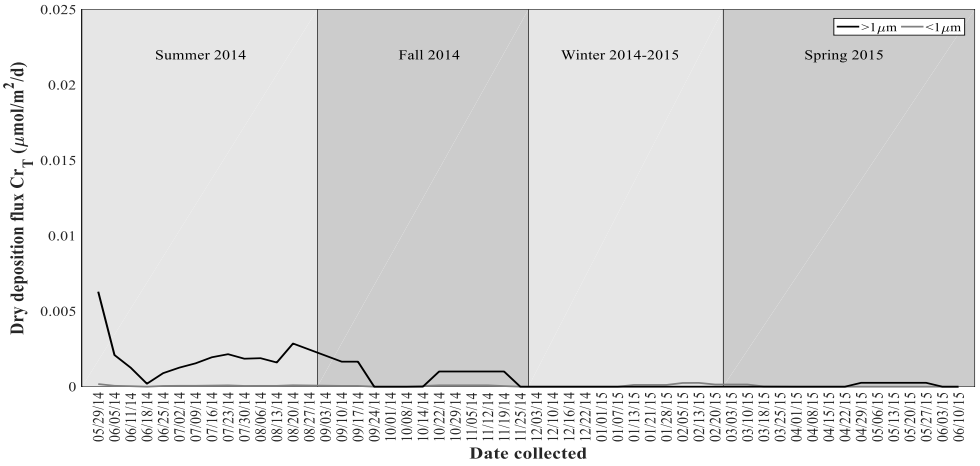

(c) Aerosol chromium fractional solubility from Eastern Shore samples - smoothed

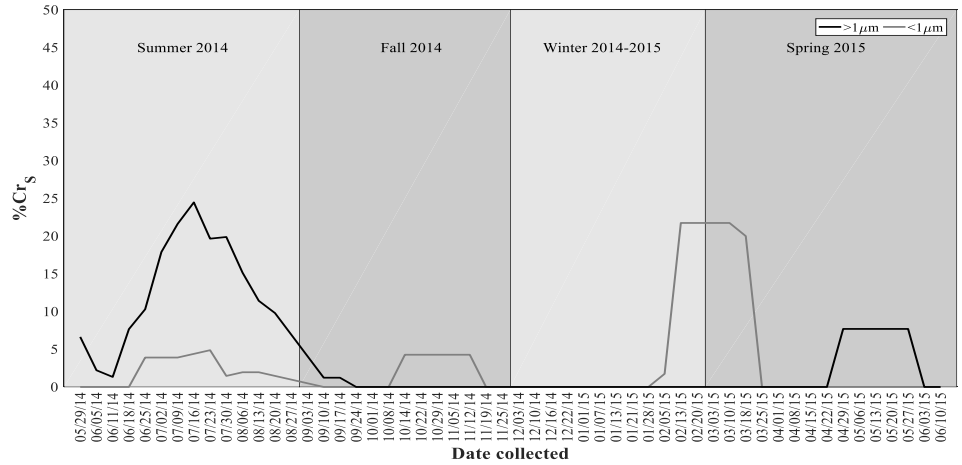

Figure 31. Smoothed seasonal dry deposition fluxes of (a) soluble chromium (Cr_S, μmol/m^2/d), (b) total chromium (Cr_T, μmol/m^2/d), and (c) fractional solubility (%Cr_S) for weekly collected Eastern Shore samples. Note that data were interpolated for dates 30 July 2014, 6 August 2014, 13 August 2014, and 20 August 2014 using the method in Section 2.6.

(a) Aerosol soluble chromium in Eastern Shore samples - residuals

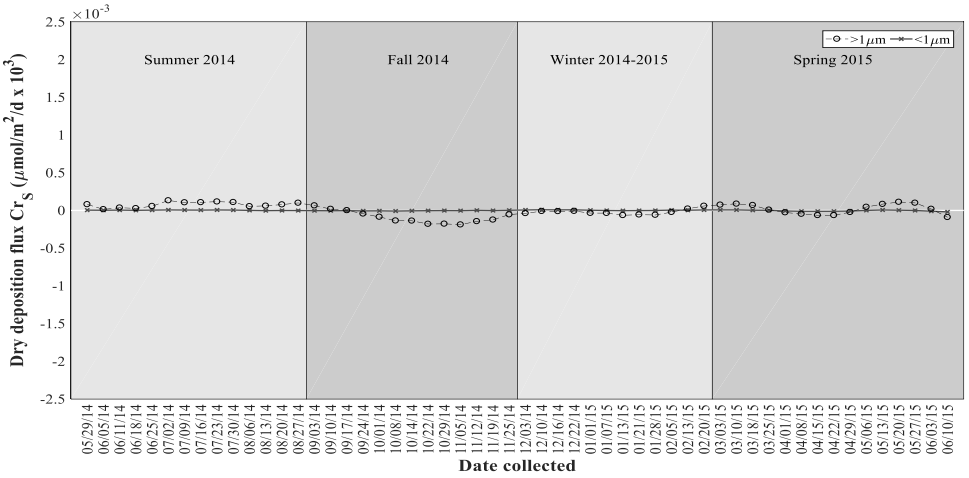

(b) Aerosol total chromium in Eastern Shore samples - residuals

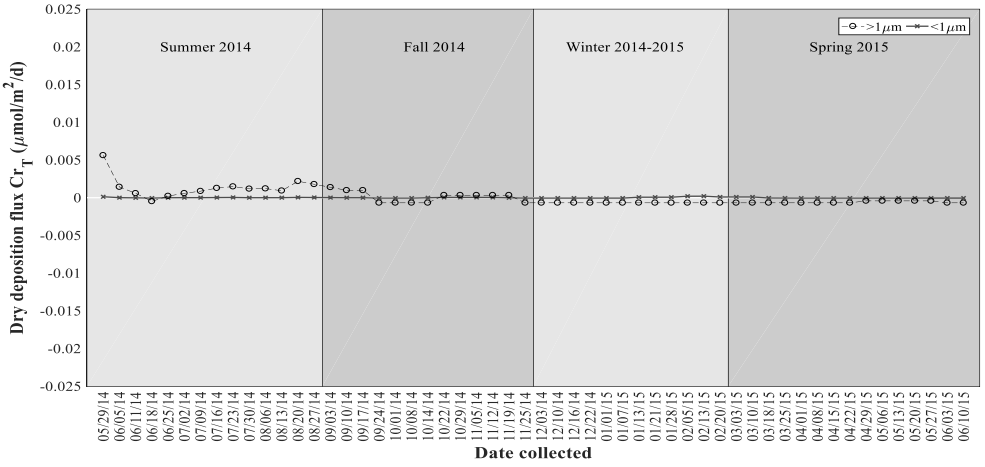

(c) Aerosol chromium fractional solubility in Eastern Shore samples - residuals

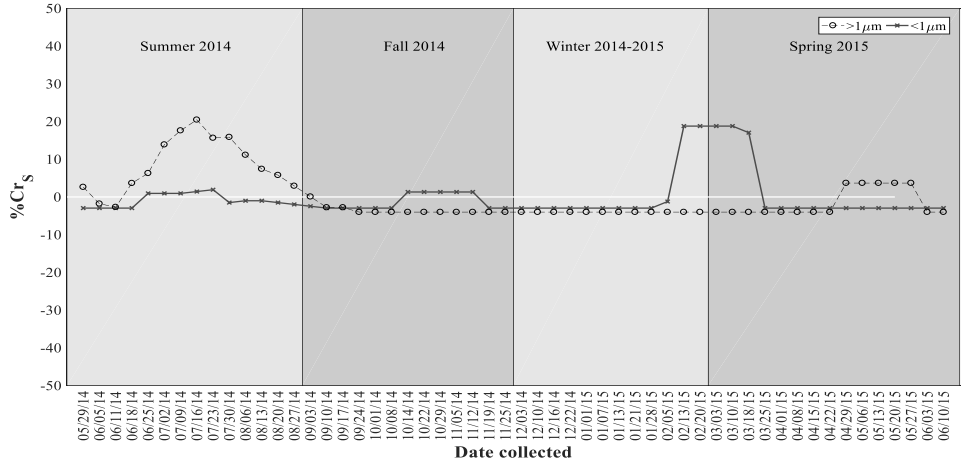

Figure 32. Residuals of dry deposition fluxes of (a) soluble chromium (Cr_S, μmol/m^2/d), (b) total chromium (Cr_T, μmol/m^2/d), and (c) fractional solubility (%Cr_S) for weekly collected Eastern Shore samples. Note that data were interpolated for dates 30 July 2014, 6 August 2014, 13 August 2014, and 20 August 2014 using the method in Section 2.6. The white horizontal line indicates the annual mean.

Both the median dry fine Cr_S fluxes and the mean dry fluxes of coarse Cr_S fluxes were not significantly different between seasons (fine: p = 0.435, df = 49, chi-sq = 2.7, coarse: p = 0.0633, df = 47, F = 2.61). However, the overall median dry fluxes for fine and coarse Cr_S were found to be significantly different (p < 0.0001, zval = 8.53), using a Wilcoxon rank sum test.

The data for dry Cr_T were limited, with only a few samples in each size fraction above the detection limit of 0.035 μg L^{-1} (Table 3 and Figure 30b), and therefore statistical analyses were limited. The mean dry fine Cr_T flux for winter ($10.3 \times 10^{-5} \pm 24.0 \times 10^{-5}$ μmol/m^2/d) was found to be significantly greater (p = 0.0004, df = 9, chi-sq = 32) than those for summer ($4.70 \times 10^{-5} \pm 8.94 \times 10^{-5}$ μmol/m^2/d), fall ($5.43 \times 10^{-5} \pm 10.4 \times 10^{-5}$ μmol/m^2/d), and spring ($0.0510 \times 10^{-5} \pm 1.36 \times 10^{-5}$ μmol/m^2/d) (Table 13), using a one-way ANOVA and a multiple comparison test. However, the mean dry fluxes of coarse Cr_T for the four seasons were not significantly different (p = 0.1512, df = 7, F = 2.82). A two-sample t-test showed that the overall mean dry coarse Cr_T flux ($0.573 \times 10^{-3} \pm 1.68 \times 10^{-3}$ μmol/m^2/d) was significantly greater (p < 0.0001, df = 16, tstat = 6.41) than the overall mean dry fine Cr_T flux ($4.97 \times 10^{-5} \pm 13.6 \times 10^{-5}$ μmol/m^2/d) (Table 14).

The sample size for dry fine $\%Cr_S$ (n = 4) was insufficient for use in statistical tests. The mean dry coarse $\%Cr_S$ for the four seasons were not significantly different (p = 0.3124, df = 6, F = 1.58). The overall mean $\%Cr_S$ was not significantly different for the two size fractions (p = 0.576, tstat = -0.581).

The dry flux of soluble manganese (Mn_S) in the fine fraction was consistently lower than the dry flux of coarse Mn_S throughout the time series, and ranged from 1.38 x 10^{-4} to 8.12 x 10^{-4} µmol/m^2/d in summer, 1.66 x 10^{-4} to 9.42 x 10^{-4} µmol/m^2/d in fall, 1.48 x 10^{-4} to 7.01 x 10^{-4} µmol/m^2/d in winter, and 1.96 x 10^{-4} to 9.66 x 10^{-4} µmol/m^2/d in spring (Table 12 and Figure 33a). The dry flux of coarse Mn_S ranged from 9.03 x 10^{-3} to 43.1 x 10^{-3} µmol/m^2/d in summer, 9.00 x 10^{-3} to 42.7 x 10^{-3} µmol/m^2/d in fall, 4.51 x 10^{-3} to 34.8 x 10^{-3} µmol/m^2/d in winter, and 8.89 x 10^{-3} to 61.4 x 10^{-3} µmol/m^2/d in spring (Table 12 and Figure 33a). There were 5 weeks (9 July 2014, 3 September, 14 October 2014, 10 December 2014, 13 May 2015, and 27 May 2015) with elevated dry fluxes of coarse Mn_S (Figure 33a).

The dry fine total manganese (Mn_T) flux ranged from 6.29 x 10^{-4} to 29.6 x 10^{-4} µmol/m^2/d in summer, 4.62 x 10^{-4} to 35.4 x 10^{-4} µmol/m^2/d in fall, 5.51 x 10^{-4} to 25.0 x 10^{-4} µmol/m^2/d in winter, and 5.67 x 10^{-4} to 28.5 x 10^{-4} µmol/m^2/d in spring (Table 13 and Figure 33b). The overall mean dry coarse Mn_T flux (40.8 x 10^{-3} ± 21.2 x 10^{-3} µmol/m^2/d) was more than twice the overall mean dry coarse Mn_S flux (17.6 x 10^{-3} ± 10.7 x 10^{-3} µmol/m^2/d), and the dry coarse Mn_T flux ranged from 23.7 x 10^{-3} to 97.0 x 10^{-3} µmol/m^2/d in summer, 23.2 x 10^{-3} to 80.7 x 10^{-3} µmol/m^2/d in fall, 13.2 x 10^{-3} to 81.2 x 10^{-3} µmol/m^2/d in winter, and below the level of quantification to 115 x 10^{-3} µmol/m^2/d in spring (Table 13 and Figure 33b).

The aerosol fractional solubility was relatively high for both size fractions (Figure 33c). The dry fine fractional solubility of manganese (%Mn_S) ranged from 21.9 to 41.7 % in summer, 20.4 to 41.3% in fall, 21.1 to 41.4 % in winter, and 20.6 to 42.4% in spring (Table 14 and Figure 33c). The coarse %Mn_S ranged from 38.2 to 52.5 % in summer, 29.1 to 53.3 % in fall, 25.9 to 53.1 % in winter, and 27.1 to 53.4 % in spring (Table 14 and Figure 33c).

(a) Aerosol soluble manganese from Eastern Shore samples

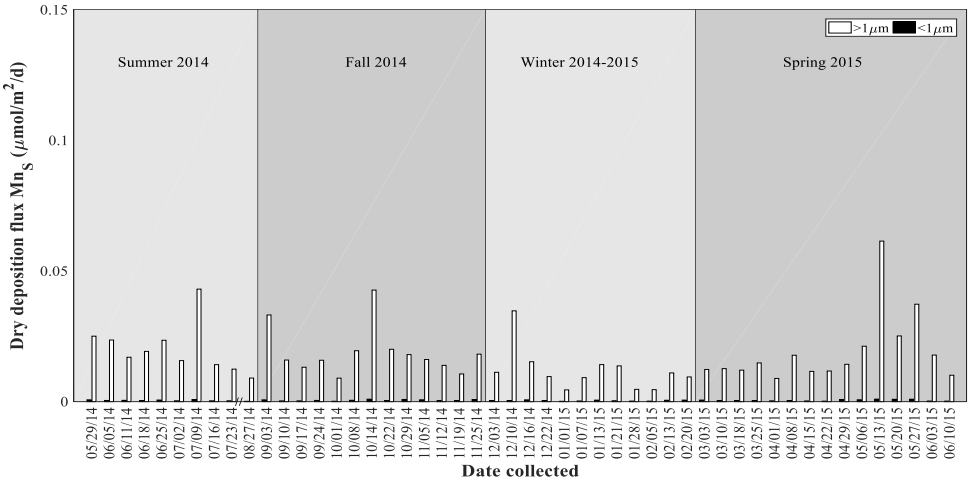

(b) Aerosol total manganese from Eastern Shore samples

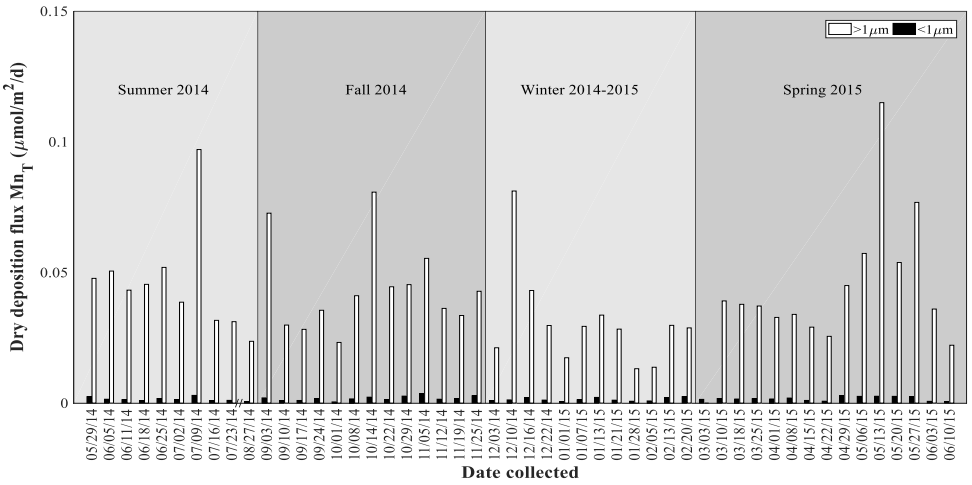

(c) Aerosol manganese fractional solubility from Eastern Shore samples

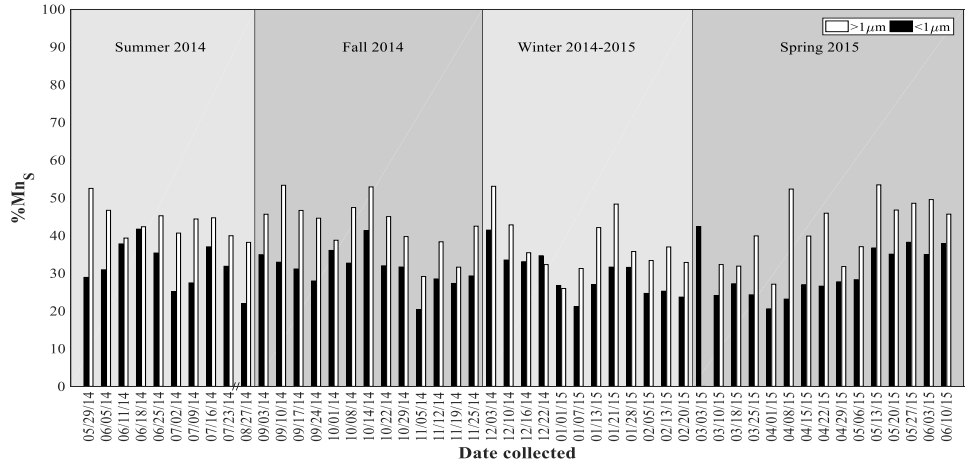

Figure 33. Seasonal dry deposition fluxes of (a) soluble manganese (Mn_S, μmol/m^2/d), (b) total manganese (Mn_T, μmol/m^2/d), and (c) fractional solubility (%Mn_S) for weekly collected Eastern Shore samples. "//" indicates the break in the x-axis between 07/23/14 and 08/27/14.

The smoothed data and residuals plots show that the flux of dry fine Mn_S remained relatively constant throughout the time series (Figures 34a and 35a). The flux of dry coarse Mn_S was above the overall mean at the end of the spring, but remained near this mean for the preceding seasons (Figure 35a). The dry fine Mn_T flux remained little changed throughout the time series, whereas the dry coarse Mn_T flux was below the overall mean during winter and early spring, and above the mean during late spring (Figure 35b). The fractional solubility for both size fractions was roughly equal (Figure 33c), and varied little throughout the time series (Figures 34c and 35c).

(a) Aerosol soluble manganese from Eastern Shore samples - smoothed

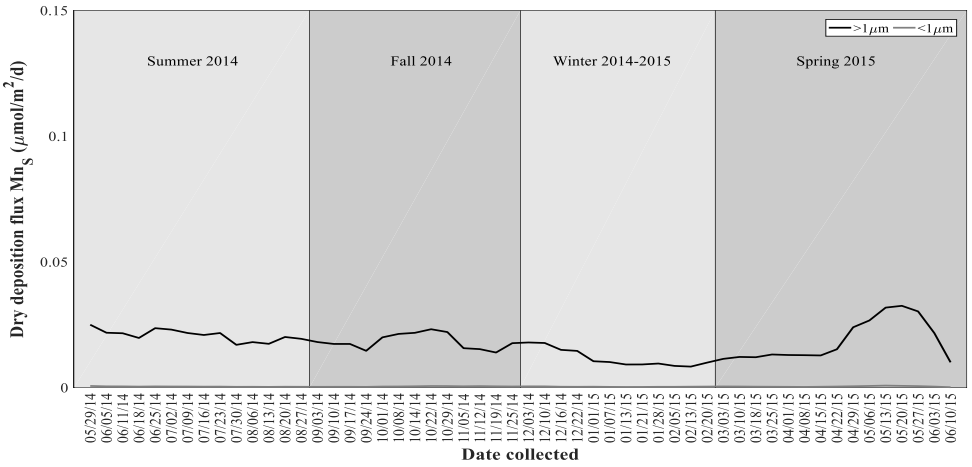

(b) Aerosol total manganese from Eastern Shore samples - smoothed

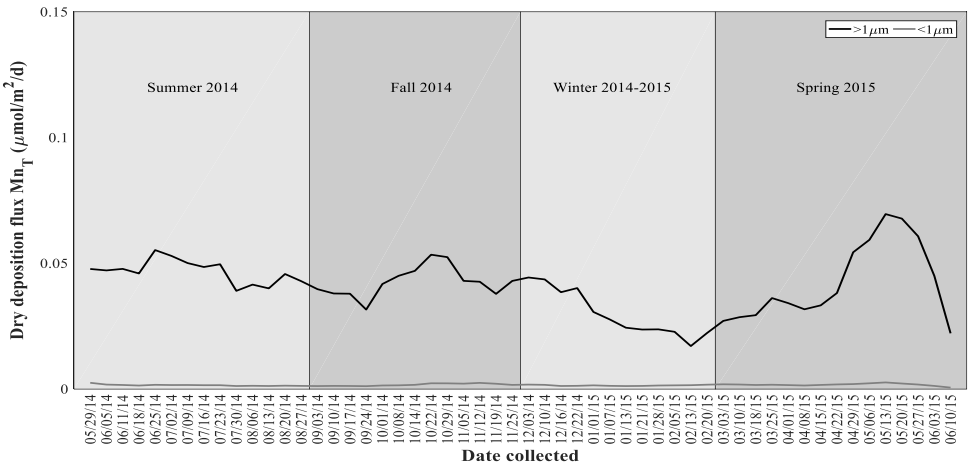

(c) Aerosol manganese fractional solubility from Eastern Shore samples - smoothed

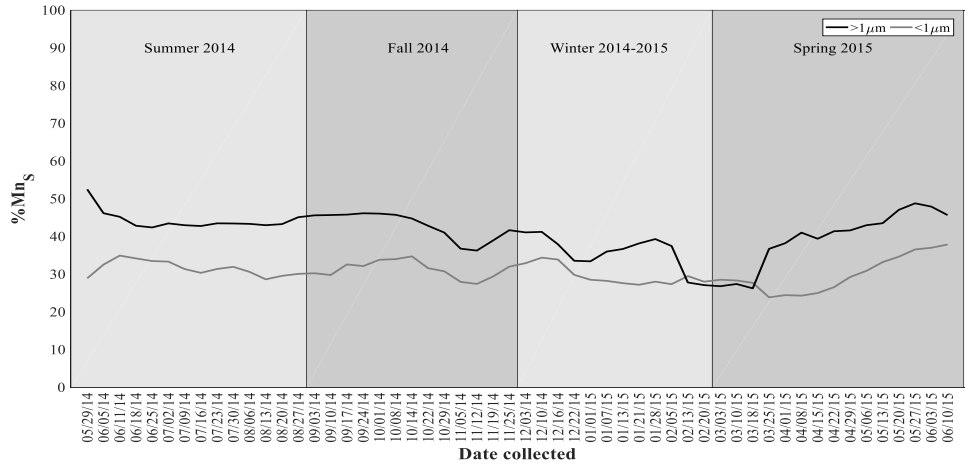

Figure 34. Smoothed seasonal dry deposition fluxes of (a) soluble manganese (Mn_S, μmol/m^2/d), (b) total manganese (Mn_T, μmol/m^2/d), and (c) fractional solubility (%Mn_S) for weekly collected Eastern Shore samples. Note that data were interpolated for dates 30 July 2014, 6 August 2014, 13 August 2014, and 20 August 2014 using the method in Section 2.6.

(a) Aerosol soluble manganese from Eastern Shore samples - residuals

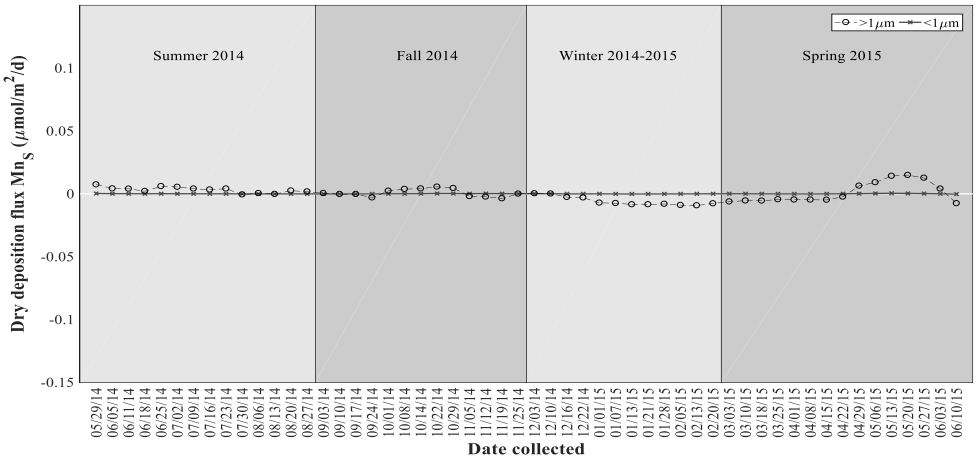

(b) Aerosol total manganese from Eastern Shore samples - residuals

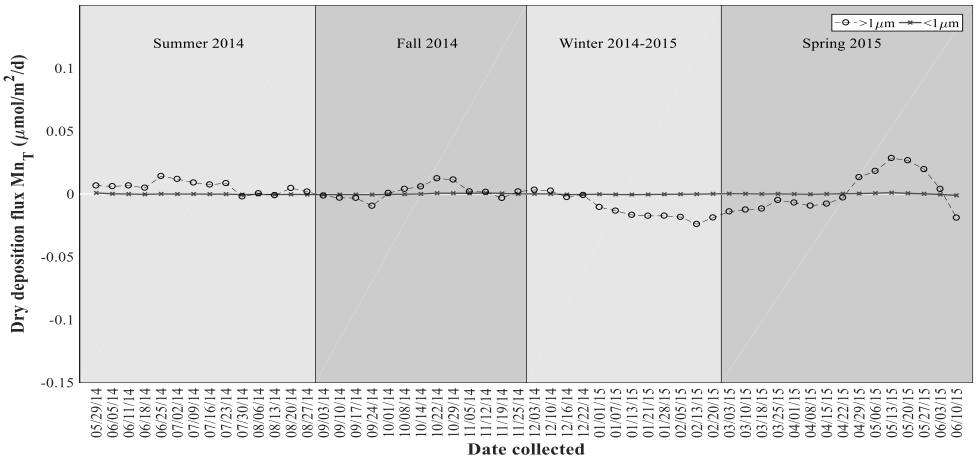

(c) Aerosol manganese fractional solubility from Eastern Shore samples - residuals

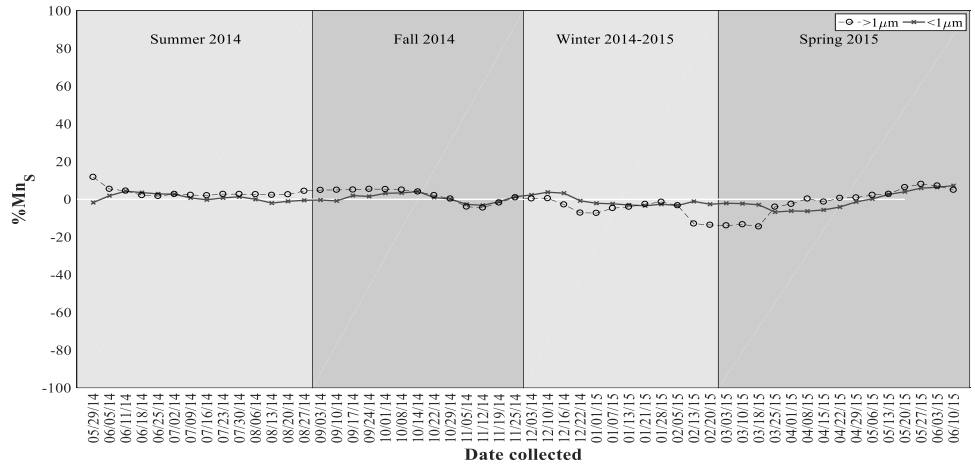

Figure 35. Residuals of dry deposition fluxes of (a) soluble manganese (Mn_S, μmol/m^2/d), (b) total manganese (Mn_T, μmol/m^2/d), and (c) fractional solubility (%Mn_S) for weekly collected Eastern Shore samples. Note that data were interpolated for dates 30 July 2014, 6 August 2014, 13 August 2014, and 20 August 2014 using the method in Section 2.6. The white horizontal line indicates the annual mean.

The mean dry fluxes of fine Mn_S for the four seasons were not significantly different. However, the mean dry coarse Mn_S fluxes for both summer ($20.3 \times 10^{-3} \pm 9.55 \times 10^{-3}$ μmol/m^2/d) and fall ($18.9 \times 10^{-3} \pm 9.24 \times 10^{-3}$ μmol/m^2/d) were significantly greater ($p = 0.0132$, $df = 49$, $F = 3.99$) than that for winter ($11.8 \times 10^{-3} \pm 8.10 \times 10^{-3}$ μmol/m^2/d) (Table 12), using a one-way ANOVA and a multiple comparison test. The overall mean dry flux of coarse Mn_S ($17.6 \times 10^{-3} \pm 10.7 \times 10^{-3}$ μmol/m^2/d) was found to be significantly greater ($p < 0.0001$, $df = 49.3$, $tstat = -20.80$) than the overall mean dry flux of fine Mn_S ($4.91 \times 10^{-4} \pm 2.31 \times 10^{-4}$ μmol/m^2/d) (Table 12), using a two-sample t-test.

The seasonal mean dry Mn_T fluxes for both fine ($p = 0.4952$, $df = 49$, $F = 0.81$) and coarse ($p = 0.2122$, $df = 48$, $F = 1.56$) size fractions were not significantly different. However, the overall mean dry coarse Mn_T flux ($40.8 \times 10^{-3} \pm 21.2 \times 10^{-3}$ μmol/m^2/d) was found to be significantly greater ($p < 0.0001$, $df = 49.1$, $tstat = -11.7$) than the overall mean fine Mn_T ($1.63 \times 10^{-3} \pm 0.750 \times 10^{-3}$ μmol/m^2/d) (Table 13), using a two-sample t-test.

There were no significant differences in the seasonal means of both fine ($p = 0.7879$, $df = 49$, $F = 0.35$) and coarse ($p = 0.1805$, $df = 48$, $F = 1.7$) $\%Mn_S$. A two-sample t-test showed that the overall mean coarse $\%Mn_S$ (41.3 ± 7.40 %) was significantly greater ($p < 0.0001$, $df = 55.9$, $tstat = -32.2$) than the overall mean fine $\%Mn_S$ (30.6 ± 5.82 %) (Table 14).

The dry flux of soluble iron (Fe_S) in the fine fraction ranged from 1.83 x 10^{-3} to 5.83 x 10^{-3} µmol/m^2/d in summer, 1.42 x 10^{-3} to 5.34 x 10^{-3} µmol/m^2/d in fall, 1.01 x 10^{-3} to 2.76 x 10^{-3} µmol/m^2/d in winter, and 1.16 x 10^{-3} to 5.82 x 10^{-3} µmol/m^2/d in spring (Table 12 and Figure 36a). The dry flux of coarse Fe_S ranged from 22.5 x 10^{-3} to 61.1 x 10^{-3} µmol/m^2/d in summer, 9.23 x 10^{-3} to 69.2 x 10^{-3} µmol/m^2/d in fall, 3.56 x 10^{-3} to 23.0 x 10^{-3} µmol/m^2/d in winter, and 9.62 x 10^{-3} to 64.9 x 10^{-3} µmol/m^2/d in spring (Table 12 and Figure 36a). Both the dry fine and coarse Fe_S fluxes were elevated during summer and spring, compared to fall and winter (Figure 36a).

The dry flux of both fine and coarse total iron (Fe_T) flux peaked on 9 July 2014, 3 September 2014, and 13 May 2015 (Figure 36b). The dry fine Fe_T flux ranged from 25.0 x 10^{-3} to 16.8 x 10^{-3} µmol/m^2/d in summer, 13.3 x 10^{-3} to 131 x 10^{-3} µmol/m^2/d in fall, 16.4 x 10^{-3} to 76.5 x 10^{-3} µmol/m^2/d in winter, and 11.4 x 10^{-3} to 13.3 x 10^{-3} µmol/m^2/d in spring (Table 13 and Figure 36b). The dry coarse Fe_T flux ranged from 0.862 to 4.16 µmol/m^2/d in summer, 0.896 to 3.42 µmol/m^2/d in fall, 0.429 to 1.15 µmol/m^2/d in winter, and 0.614 to 4.52 µmol/m^2/d in spring (Table 13 and Figure 21b).

The aerosol fractional solubility of iron (%Fe_S) was greater for the fine fraction throughout the time series (Figure 36c). The dry fine %Fe ranged from 2.90 to 10.9 % in summer, 1.38 to 14.6 % in fall, 2.09 to 11.1 % in winter, and 2.14 to 14.1% in spring (Table 14 and Figure 36c), and the overall mean fine %Ti_S (6.11 ± 3.15 %) was approximately 3 times greater than the overall mean coarse %Fe_S (1.86 ± 0.788 %). The coarse %Fe_S ranged from 1.15 to 3.19 % in summer, 0.578 to 2.99 % in fall, 0.714 to 3.50 % in winter, and 0.859 to 3.11 % in spring (Table 14 and Figure 36c).

(a) Aerosol soluble iron from Eastern Shore samples

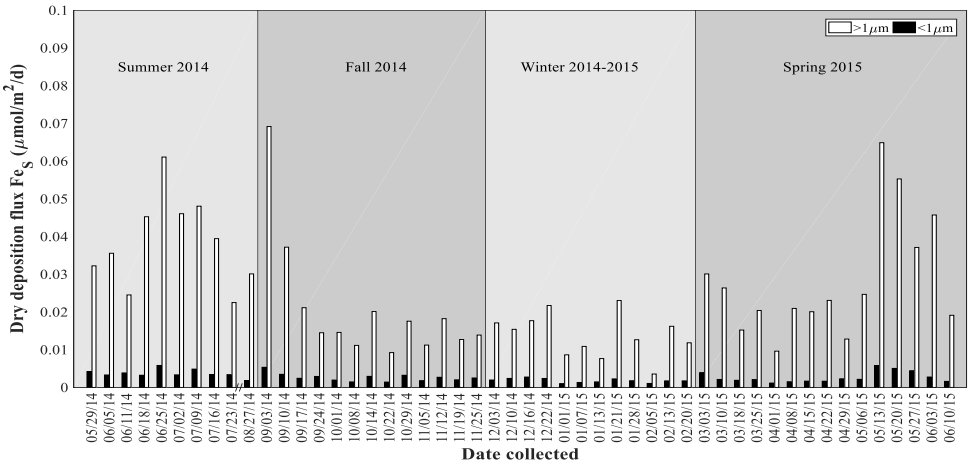

(b) Aerosol total iron from Eastern Shore samples

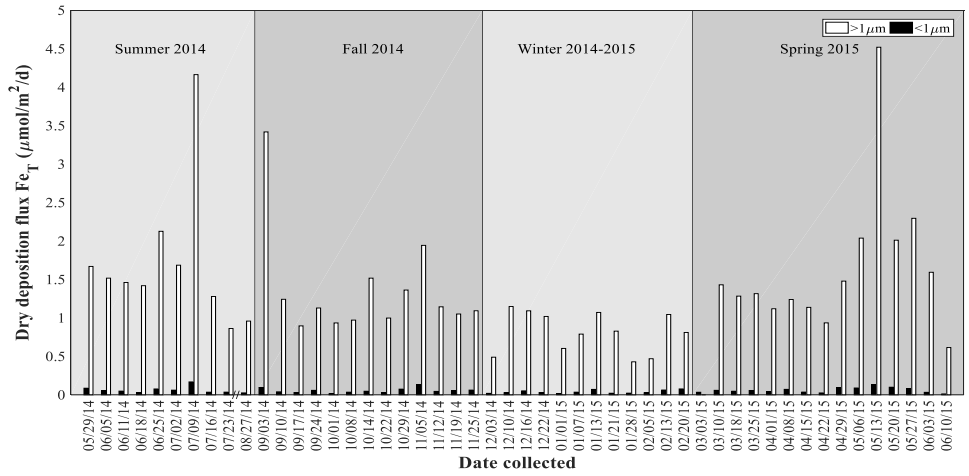

(c) Aerosol iron fractional solubility from Eastern Shore samples

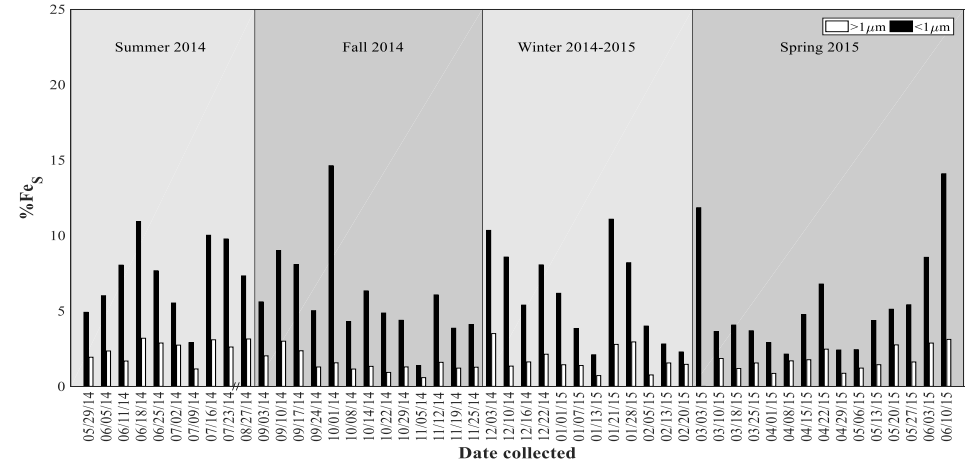

Figure 36. Seasonal dry deposition fluxes of (a) soluble iron (Fe_S, μmol/m^2/d), (b) total iron (Fe_T, μmol/m^2/d), and (c) fractional solubility (%Fe_S) for weekly collected Eastern Shore samples. "//" indicates the break in the x-axis between 07/23/14 and 08/27/14.

The smoothed data and residuals plots show that the dry fine Fe_S flux remained relatively constant throughout the time series (Figure 37a and Figure 38a), whereas the dry coarse Fe_S flux was above the overall mean during summer and some of the spring, and mostly below this mean during fall and winter (Figure 38a). The smoothed data and residuals plots show that the dry flux of fine Fe_T remained nearly constant throughout the time series (Figures 37b and 38b), whereas the dry flux of coarse Fe_T was above the overall mean during summer and later spring, and below this mean during late fall and winter (Figure 38b). The smoothed data and residuals plots show that the dry flux of coarse $\%Fe_S$ remained little changed throughout the time series (Figures 37c and 38c), whereas the dry flux of fine $\%Fe_S$ was mostly above the overall mean during summer and early fall, and below this mean during early spring (Figure 38c).

(a) Aerosol soluble iron from Eastern Shore samples - smoothed

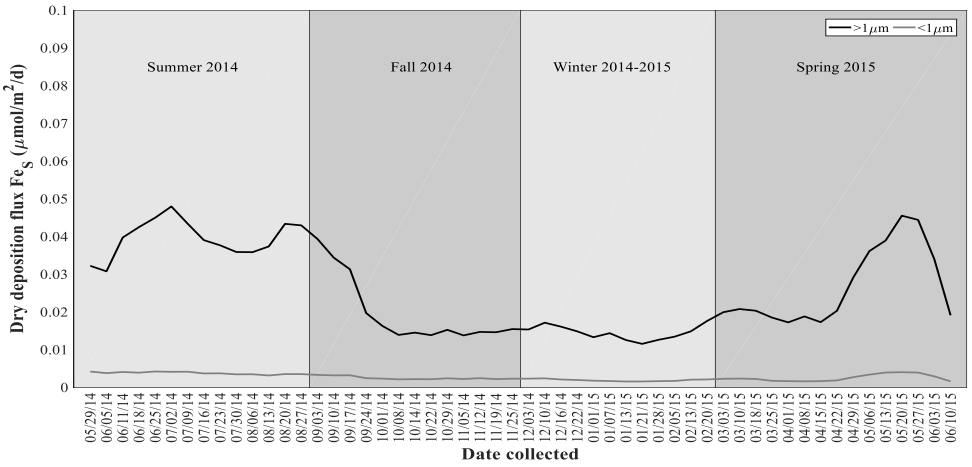

(b) Aerosol total iron from Eastern Shore samples - smoothed

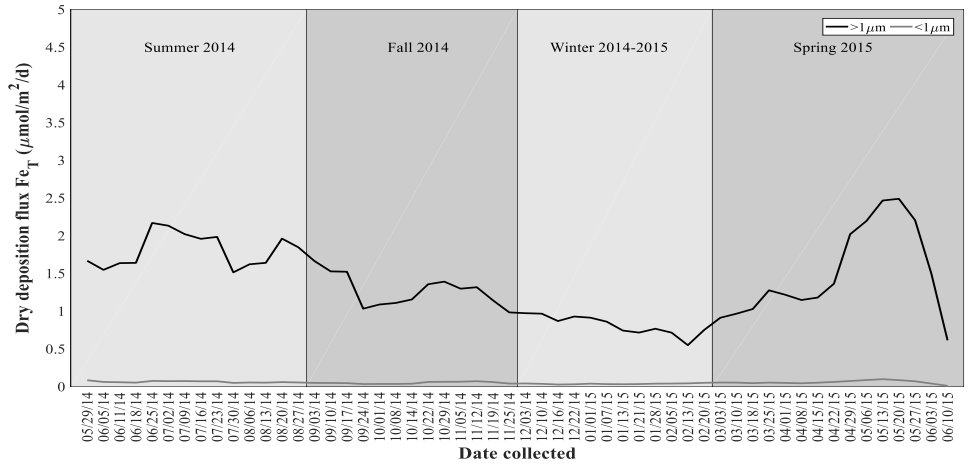

(c) Aerosol iron fractional solubility from Eastern Shore samples - smoothed

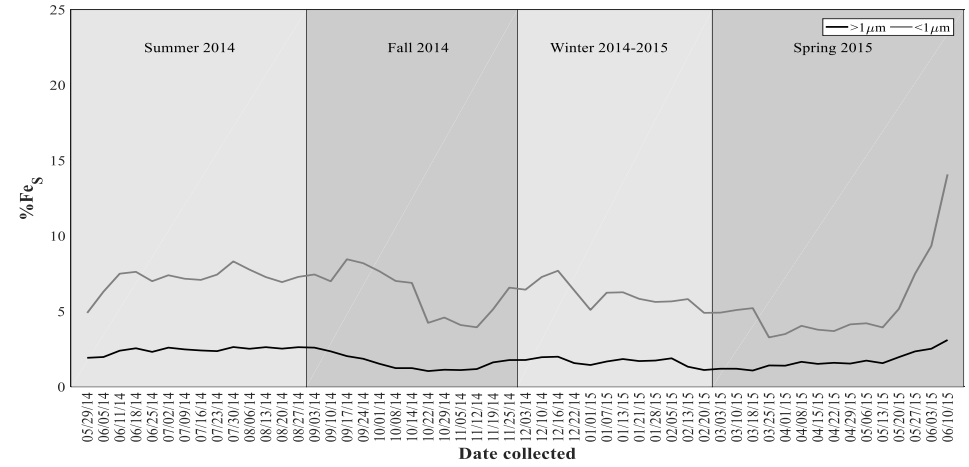

Figure 37. Smoothed seasonal dry deposition fluxes of (a) soluble iron (Fe_S, μmol/m²/d), (b) total iron (Fe_T, μmol/m²/d), and (c) fractional solubility ($\%Fe_S$) for weekly collected Eastern Shore samples. Note that data were interpolated for dates 30 July 2014, 6 August 2014, 13 August 2014, and 20 August 2014 using the method in Section 2.6.

(a) Aerosol soluble iron from Eastern Shore samples - residuals

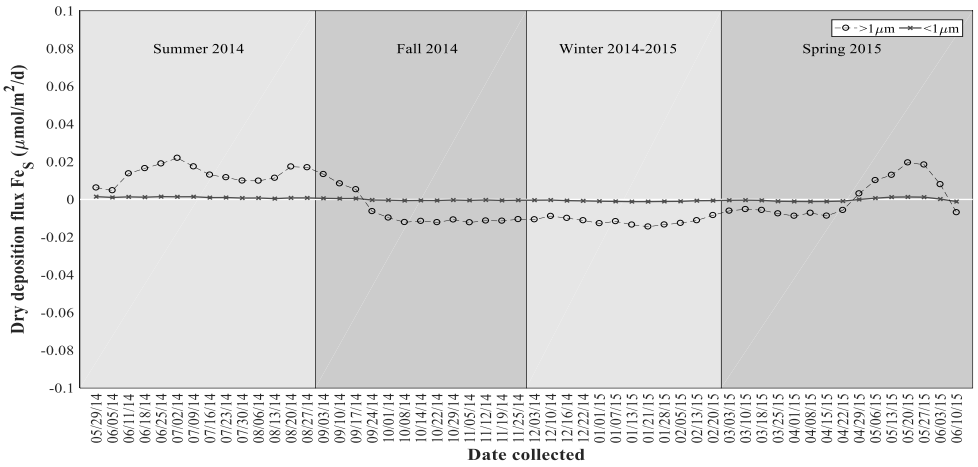

(b) Aerosol total iron from Eastern Shore samples - residuals

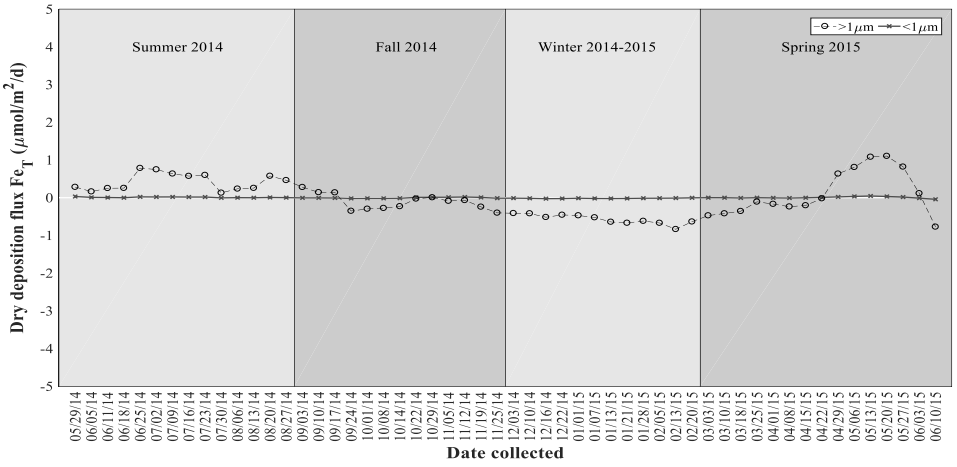

(c) Aerosol iron fractional solubility from Eastern Shore samples - residuals

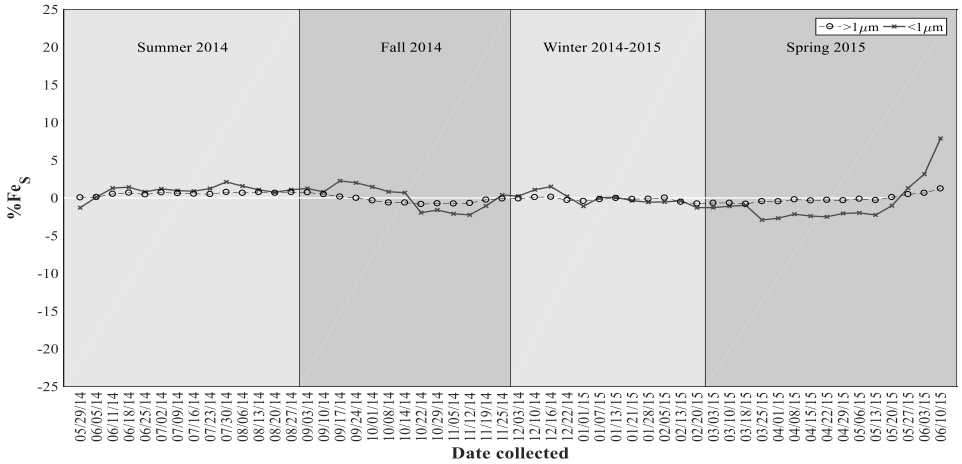

Figure 38. Smoothed seasonal dry deposition fluxes of (a) soluble iron (Fe_S, μmol/m^2/d), (b) total iron (Fe_T, μmol/m^2/d), and (c) fractional solubility (%Fe_S) for weekly collected Eastern Shore samples. Note that data were interpolated for dates 30 July 2014, 6 August 2014, 13 August 2014, and 20 August 2014 using the method in Section 2.6. The white horizontal line indicates the annual mean.

The mean dry fine Fe_S flux for summer ($3.73 \times 10^{-3} \pm 1.07 \times 10^{-3}$ µmol/m^2/d) was significantly greater ($p = 0.0011$, df = 49, F = 6.36) than the mean dry fine Fe_S flux for winter ($1.83 \times 10^{-3} \pm 0.552 \times 10^{-3}$ µmol/m^2/d) (Table 12), as determined by a one-way ANOVA and a multiple comparison test. The mean dry coarse Fe_S flux for summer ($38.5 \times 10^{-3} \pm 11.9 \times 10^{-3}$ µmol/m^2/d) was found to be significantly greater ($p < 0.0001$, df = 49, F = 9.75) than those for fall ($20.8 \times 10^{-3} \pm 16.2 \times 10^{-3}$ µmol/m^2/d) and winter ($13.9 \times 10^{-3} \pm 5.76 \times 10^{-3}$ µmol/m^2/d) (Table 12), and the mean dry coarse Fe_S flux for both spring ($28.4 \times 10^{-3} \pm 15.9 \times 10^{-3}$ µmol/m^2/d) and summer ($38.5 \times 10^{-3} \pm 11.9 \times 10^{-3}$ µmol/m^2/d) were both significantly greater ($p < 0.0001$, df = 49, F = 9.75) than the mean dry coarse Fe_S flux for winter ($13.9 \times 10^{-3} \pm 5.76 \times 10^{-3}$ µmol/m^2/d) (Table 12), using a one-way ANOVA and a multiple comparison test. A two-sample t-test indicated that the overall mean flux of dry coarse Fe_S ($24.9 \times 10^{-3} \pm 15.7 \times 10^{-3}$ µmol/m^2/d) was significantly greater ($p < 0.0001$, df = 62.0, tstat = 38.0) than the overall mean dry fine Fe_S flux ($2.67 \times 10^{-3} \pm 1.24 \times 10^{-3}$ µmol/m^2/d) (Table 12).

There were no significant differences in the mean dry fine Fe_T fluxes for the four seasons ($p = 0.2713$, df = 49, F = 1.35). However, the median dry coarse Fe_T fluxes for summer (1.49 µmol/m^2/d) and spring (1.37 µmol/m^2/d) were significantly greater ($p = 0.0004$, df = 48, chi-sq = 18.03) than the median dry coarse Fe_T flux for winter (0.819 µmol/m^2/d) (Table 13), using a Kruskal-Wallis test and a multiple comparison test. The overall mean dry coarse Fe_T flux (1.35 ± 0.827 µmol/m^2/d) was significantly greater ($p < 0.0001$, df = 97, tstat =30.5) than the overall mean dry fine Fe_T flux ($53.7 \times 10^{-3} \pm 32.9 \times 10^{-3}$ µmol/m^2/d) (Table 13), using a two-sample t-test.

The mean fine $\%Fe_S$ values for the four seasons were not significantly different ($p = 0.2713$, df = 49, F = 1.35). The mean coarse $\%Fe_S$ for summer (2.47 ± 0.688 %) was found to be significantly greater ($p = 0.0345$, df = 48, F = 3.14) than that for fall (1.50 ± 0.634 %) (Table 14), using a one-way ANOVA and Kruskal-Wallis test. A two-sample t-test indicated that the overall mean fine $\%Fe_S$ (6.11 ± 3.15 %) was significantly greater ($p < 0.0001$, df = 79.5, tstat = -12.2) than the overall mean coarse $\%Fe_S$ (1.86 ± 0.788%) (Table 14).

The dry flux of soluble cobalt (Co_S) in the fine fraction ranged from 5.55 x 10^{-6} to 14.7 x 10^{-6} µmol/m^2/d in summer, below the level of quantification to 12.3 x 10^{-6} µmol/m^2/d in fall, 2.42 x 10^{-6} to 9.89 x 10^{-6} µmol/m^2/d in winter, and 1.92 x 10^{-6} to 13.3 x 10^{-6} µmol/m^2/d in spring (Table 12 and Figure 39a). The dry flux of coarse Co_S ranged from 0.744 x 10^{-4} to 5.36 x 10^{-4} µmol/m^2/d in summer, below the level of quantification to 3.30 x 10^{-4} µmol/m^2/d in fall, 0.336 x 10^{-4} to 1.61 x 10^{-4} µmol/m^2/d in winter, and 0.662 x 10^{-4} to 6.08 x 10^{-4} µmol/m^2/d in spring (Table 12 and Figure 39a). The Co_S concentrations were below the detection limit of 0.003 µg L^{-1} (Table 3) on 22 October 2014, 29 October 2014, and 5 November 2014 (Figure 39a).

The overall mean total cobalt (Co_T) flux in the coarse fraction (6.08 x 10^{-4} ± 3.56 x 10^{-4} µmol/m^2/d) was ~20 times greater than the overall mean fine Co_T flux (2.99 x 10^{-5} ± 1.30 x 10^{-5} µmol/m^2/d) (Table 13 and Figure 39c), and ranged from 3.72 x 10^{-4} to 18.4 x 10^{-4} µmol/m^2/d in summer, 3.57 x 10^{-4} to 4.14 x 10^{-4} µmol/m^2/d in fall, 0.212 x 10^{-4} to 6.65 x 10^{-4} µmol/m^2/d in winter, and 2.84 x 10^{-4} to 19.3 x 10^{-4} µmol/m^2/d in spring (Table 13 and Figure 39b).The dry flux of fine Co_T ranged from 1.71 x 10^{-5} to 6.67 x 10^{-5} µmol/m^2/d in summer, 1.33 x 10^{-5} to 6.14 x 10^{-5} µmol/m^2/d in fall, 0.967 x 10^{-5} to 4.24 x 10^{-5} µmol/m^2/d in winter, and 0.575 x 10^{-5} to 4.83 x 10^{-5} µmol/m^2/d in spring (Table 13 and Figure 39b).

The aerosol fractional solubility of cobalt (%Co_S) was roughly equal for both size fractions throughout the time series (Figure 39c and Table 14). The fine %Co_S ranged from 21.4 to 40.5 % in summer, below the level of quantification to 35.2 % in fall, 8.40 to 35.7 % in winter, and 14.4 to 44.5 % in spring (Table 14 and Figure 39c). The coarse %Co_S ranged from 20.0 to 29.2% in summer, below the level of quantification to 38.4 % in fall, 12.3 to 100% in winter, and 13.0 to 33.4% in spring (Table 14 and Figure 39c).

(a) Aerosol soluble cobalt from Eastern Shore samples

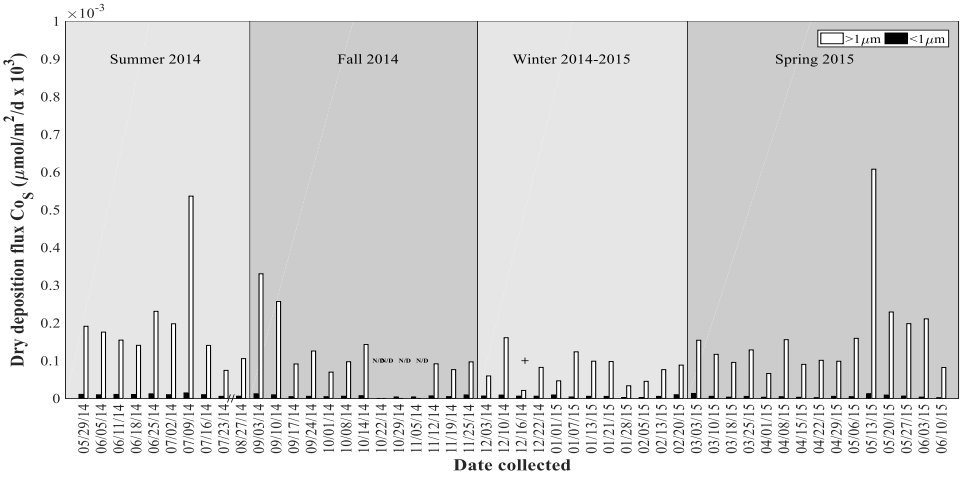

(b) Aerosol total cobalt from Eastern Shore samples

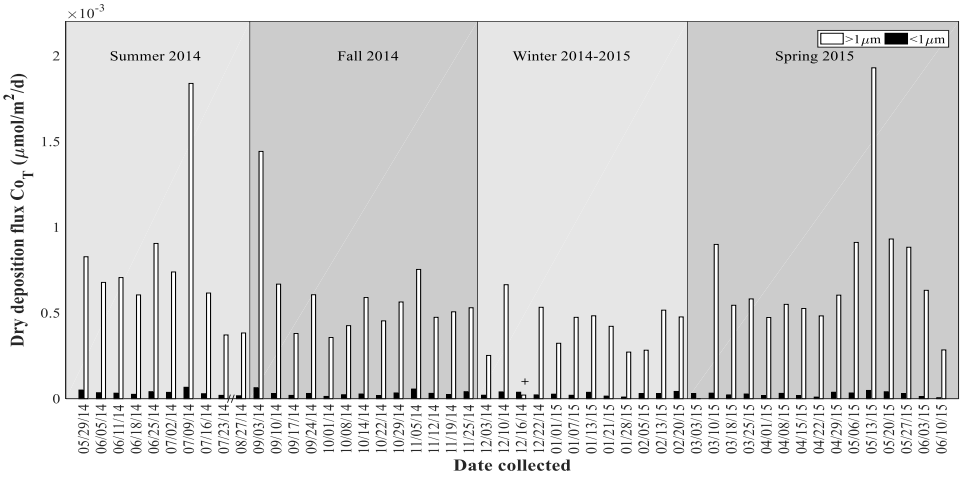

(c) Aerosol cobalt fractional solubility from Eastern Shore samples

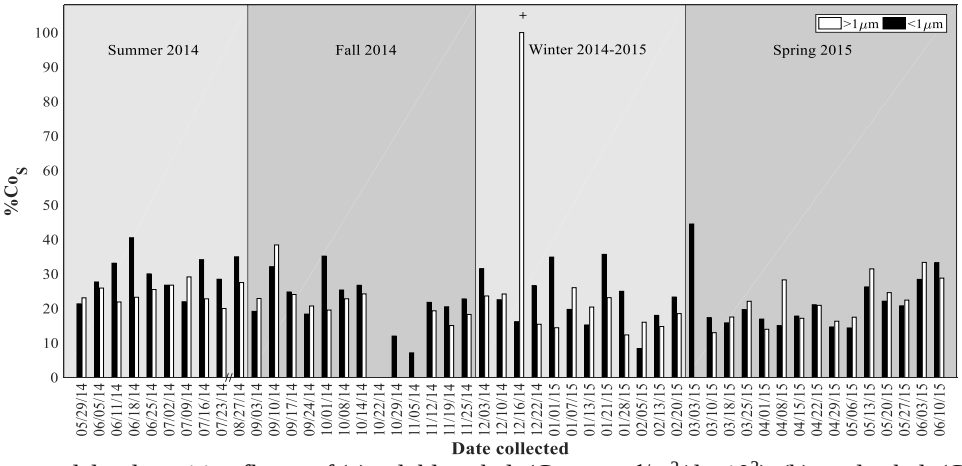

Figure 39. Seasonal dry deposition fluxes of (a) soluble cobalt (Co_S, µmol/m^2/d x 10^3), (b) total cobalt (Co_T, µmol/m^2/d x 10^3), and (c) fractional solubility (%Co_S) for weekly collected Eastern Shore samples. "//" indicates the break in the x-axis between 07/23/14 and 08/27/14, "N/D" indicates samples which are non-detect and "+" denotes samples for which the soluble flux was set to equal the total flux as mentioned in Section 2.6.

The smoothed data and residuals plots show that the dry flux of fine Co_S varied little throughout the time series (Figures 40a and 41a), whereas the dry flux of coarse Co_S was above the overall mean during summer and late spring, and mostly below this mean during fall and winter (Figure 41a). The smoothed data and residuals plots show that the dry flux of fine Co_T remained relatively constant throughout the time series (Figures 40b and 41b), whereas the dry flux of coarse Co_T was above the overall mean during summer and late spring, and below this mean during late fall and winter (Figure 41b). The fine and coarse $\%Co_S$ were mostly similar throughout the time series (Figures 40c and 41c), although there was a relative maximum in coarse %Cos in early winter.

(a) Aerosol soluble cobalt from Eastern Shore samples - smoothed

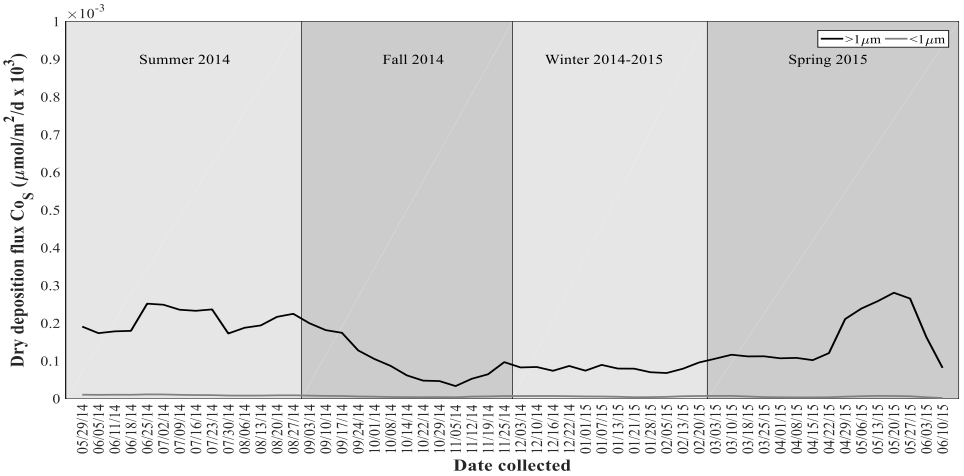

(b) Aerosol total cobalt from Eastern Shore samples - smoothed

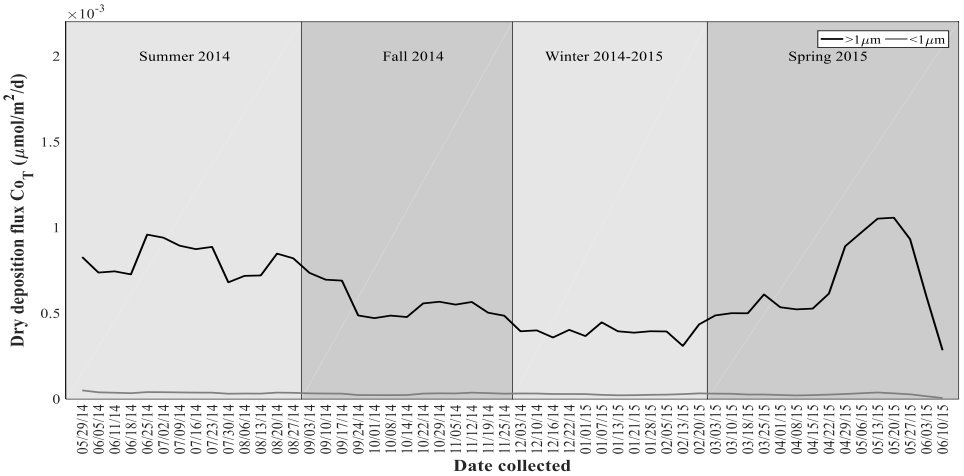

(c) Aerosol cobalt fractional solubility from Eastern Shore samples - smoothed

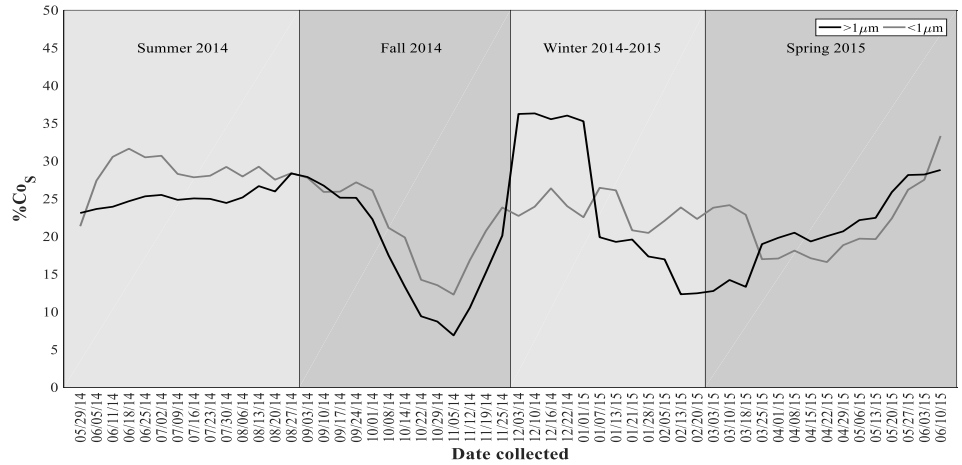

Figure 40. Smoothed seasonal dry deposition fluxes of (a) soluble cobalt (Co_S, μmol/m^2/d x 10^3), (b) total cobalt (Co_T, μmol/m^2/d x 10^3), and (c) fractional solubility (%Co_S) for weekly collected Eastern Shore samples. Note that data were interpolated for dates 30 July 2014, 6 August 2014, 13 August 2014, and 20 August 2014 using the method in Section 2.6. The horizontal white line in (c) indicates the annual mean.

(a) Aerosol soluble cobalt from Eastern Shore samples - residuals

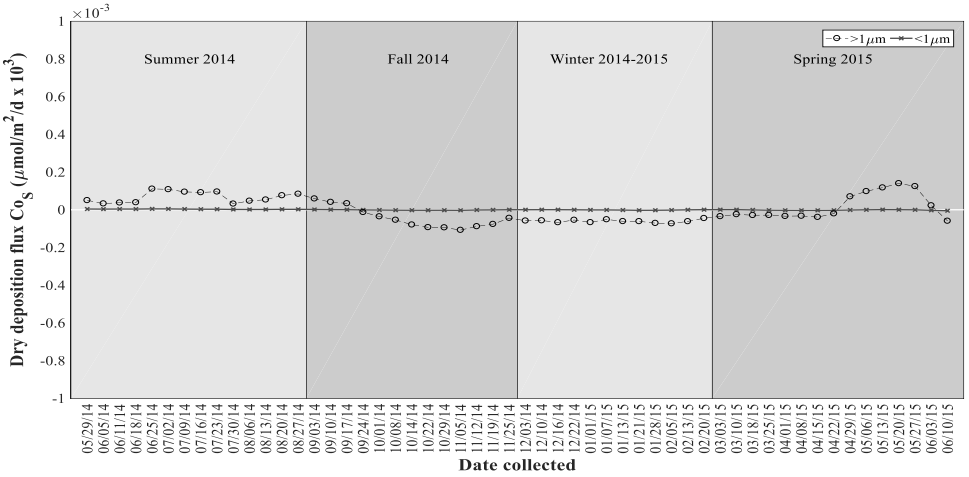

(b) Aerosol total cobalt from Eastern Shore samples - residuals

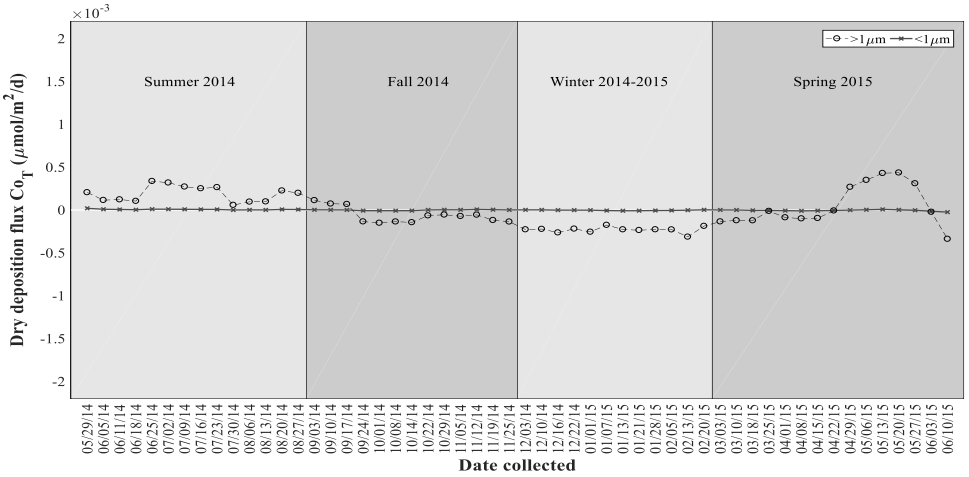

(c) Aerosol cobalt fractional solubility from Eastern Shore samples - residuals

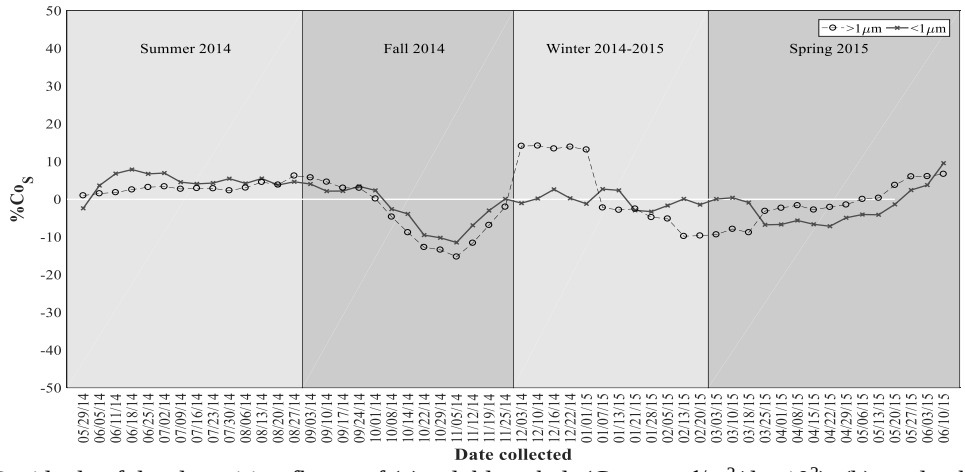

Figure 41. Residuals of dry deposition fluxes of (a) soluble cobalt (Co_S, μmol/m^2/d x 10^3), (b) total cobalt (Co_T, μmol/m^2/d x 10^3), and (c) fractional solubility (%Co_S) for weekly collected Eastern Shore samples. Note that data were interpolated for dates 30 July 2014, 6 August 2014, 13 August 2014, and 20 August 2014 using the method in Section 2.6. The white horizontal line indicates the annual mean.

The mean summer dry fine Co_S flux ($9.97 \times 10^{-6} \pm 2.67 \times 10^{-6}$ µmol/m^2/d) was significantly greater ($p = 0.0046$, $df = 48$, $F = 4.98$) than those for both winter ($6.09 \times 10^{-6} \pm 2.42 \times 10^{-6}$ µmol/m^2/d) and spring ($5.63 \times 10^{-6} \pm 3.48 \times 10^{-6}$ µmol/m^2/d), using a one-way ANOVA and a multiple comparison test. The mean dry coarse Co_S flux for summer ($1.95 \times 10^{-4} \pm 1.28 \times 10^{-4}$ µmol/m^2/d) was significantly greater ($p = 0.003$, $df = 46$, $F = 5.42$) than the mean dry coarse Co_S flux for fall ($1.06 \times 10^{-4} \pm 0.936 \times 10^{-4}$ µmol/m^2/d), as determined by a one-way ANOVA and a multiple comparison test. The mean dry coarse Co_S fluxes for summer ($1.95 \times 10^{-4} \pm 1.28 \times 10^{-4}$ µmol/m^2/d) and spring ($1.66 \times 10^{-4} \pm 1.32 \times 10^{-4}$ µmol/m^2/d) were both found to be significantly greater ($p = 0.003$, $df = 46$, $F = 5.42$) than the mean dry coarse Co_S flux for winter ($0.818 \times 10^{-4} \pm 0.359 \times 10^{-4}$ µmol/m^2/d), using a one-way ANOVA and a multiple comparison test (Table 12). A two-sample t-test indicated that the overall mean dry coarse Co_S flux ($1.36 \times 10^{-4} \pm 1.11 \times 10^{-4}$ µmol/m^2/d) was significantly greater ($p < 0.0001$, $df = 94$, $tstat = 26.9396$) than the overall mean dry fine Co_S flux ($6.71 \times 10^{-6} \pm 3.34 \times 10^{-6}$ µmol/m^2/d) (Table 12 and Figure 39a).

The means of the fine Co_T flux for the four seasons were not significantly different ($p = 0.3452$, $df = 49$, $F = 1.13$). However, the median dry coarse Co_T fluxes for summer and spring were found to be significantly greater ($p = 0.0038$, $df = 48$, $F = 13.44$) than that for winter, using a Kruskal-Wallis test and a multiple comparison test. A Wilcoxon rank sum test indicated that the median coarse Co_T flux was significantly greater ($p < 0.0001$, $zval = 8.32$) than the median fine Co_T flux.

There were no significant differences in the medians of fine $\%Co_S$ ($p = 0.0799$, $df = 48$, $F = 2.4$) or the means of coarse $\%Co_S$ ($p = 0.2291$, $df = 45$, $chi\text{-}sq = 4.32$) for the four seasons. A Wilcoxon rank sum test showed that the medians of fine and coarse $\%Co_S$ were not significantly different ($p = 0.390$, $zval = -0.860$).

Although the dry fluxes of soluble nickel (Ni_S) in the fine fraction were lower than those for dry coarse Ni_S, the fine fraction was more soluble than the coarse (Figure 42a and Table 3), with > 50% of the dry coarse Ni_S samples yielding concentrations of Ni_S below the detection limit of 0.081 µg L^{-1} (Figure 42a and Table 3). The dry fine Ni_S flux ranged from 7.63 x 10^{-5} to 18.2 x 10^{-5} µmol/m^2/d in summer, below the level of quantification to 16.7 x 10^{-5} µmol/m^2/d in fall, below the level of quantification to 17.2 x 10^{-5} µmol/m^2/d in winter, and 3.34 x 10^{-5} to 32.4 x 10^{-5} µmol/m^2/d in spring (Table 12 and Figure 42a). The dry flux of coarse Ni_S ranged from below the level of quantification to 16.2 x 10^{-4} µmol/m^2/d in summer, below the level of quantification to 8.93 x 10^{-4} µmol/m^2/d in fall, below the level of quantification to 9.54 x 10^{-4} µmol/m^2/d in winter, and below the level of quantification to 22.8 x 10^{-4} µmol/m^2/d in spring (Table 12 and Figure 42a).

The dry total nickel (Ni_T) flux in the fine fraction ranged from 4.04 x 10^{-4} to 8.11 x 10^{-4} µmol/m^2/d in summer, 1.58 x 10^{-4} to 6.81 x 10^{-4} µmol/m^2/d in fall, 1.41 x 10^{-4} to 7.52 x 10^{-4} µmol/m^2/d in winter, and 0.832 x 10^{-4} to 4.73 x 10^{-4} µmol/m^2/d in spring (Table 13 and Figure 42b). The overall mean dry coarse Ni_T (3.55 x 10^{-3} ± 1.61 x 10^{-3} µmol/m^2/d) was ~10 times greater than the overall mean dry fine Ni_T (3.85 x 10^{-4} ± 1.84 x 10^{-4} µmol/m^2/d) (Table 13). The dry flux of coarse Ni_T ranged from 2.32 x 10^{-3} to 8.13 x 10^{-3} µmol/m^2/d in summer, 2.36 x 10^{-3} to 8.42 x 10^{-3} µmol/m^2/d in fall, 1.44 x 10^{-3} to 5.72 x 10^{-3} µmol/m^2/d in winter, and 1.51 x 10^{-3} to 7.79 x 10^{-3} µmol/m^2/d in spring (Table 13 and Figure 42b).

Although both the dry fine Ni_S and dry fine Ni_T fluxes throughout the time series were lower than those for the coarse fraction, the aerosol fractional solubility of nickel (%Ni_S) was similar for both size fractions (Table 14 and Figure 42c). The dry fine %Ni_S ranged from 17.5 to 34.4 % in summer, below the level of quantification to 43.7 % in fall, below the level of quantification to 28.3 % in winter, and 19.7 to 76.7 % in spring, and the coarse %Ni_S ranged from below the level of quantification to 35.0 % in summer, below the level of quantification to 20.9 % in fall, below the level of quantification to 27.4 % in winter, and below the level of quantification to 89.5 % in spring (Table 14 and Figure 42c).

(a) Aerosol soluble nickel from Eastern Shore samples

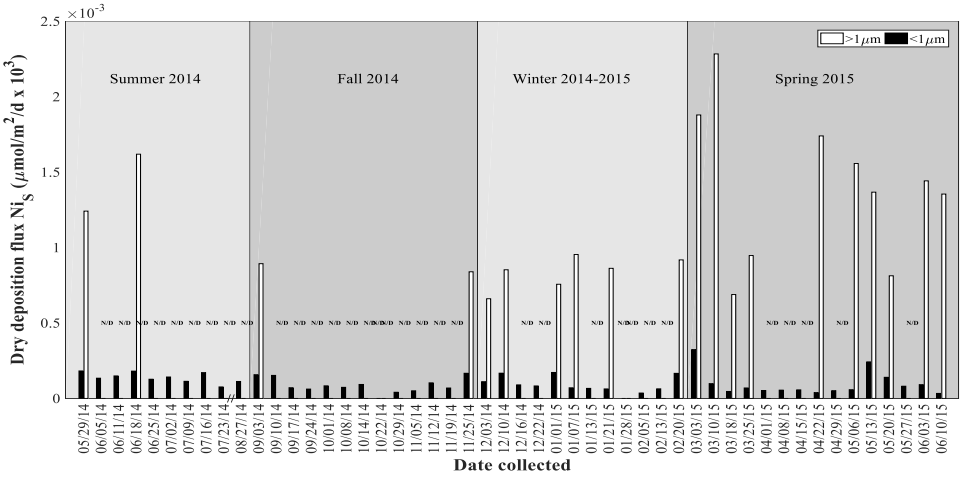

(b) Aerosol total nickel from Eastern Shore samples

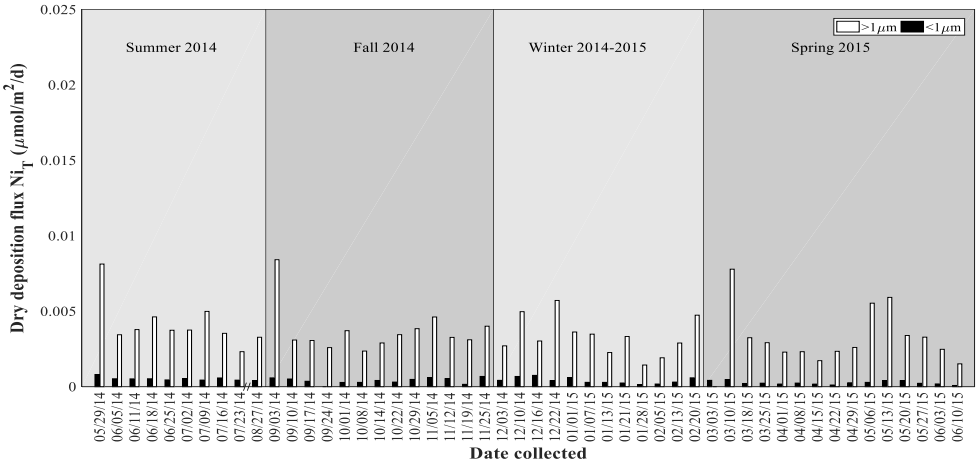

(c) Aerosol fractional solubility nickel from Eastern Shore samples

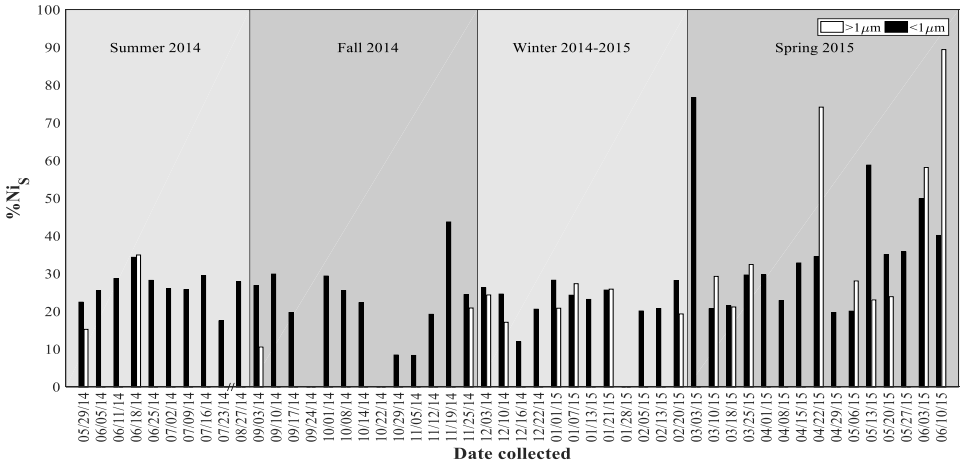

Figure 42. Seasonal dry deposition fluxes of (a) soluble nickel (Ni_S, μmol/m^2/d x 10^3), (b) total nickel (Ni_T, μmol/m^2/d), and (c) fractional solubility (%Ni_S) for weekly collected Eastern Shore samples. "//" indicates the break in the x-axis between 07/23/14 and 08/27/14 and "N/D" indicates samples which are non-detect.

The smoothed data and residuals plots show that the dry flux of fine Ni_S varied little throughout the time series (Figures 43a and 44a). The dry flux of coarse Ni_S was mostly above the overall mean during spring, and below this mean during summer and fall (Figure 43a). During the winter, the dry flux of coarse Ni_S did not vary far from the overall mean, except in late winter (Figure 43a). The smoothed data and residuals plots show that the dry flux of fine Ni_T remained nearly constant throughout the time series and did not deviate far from the overall mean (Figures 43b and 44a). The fine and coarse $\%Ni_S$ were roughly equal throughout the time series, except in late spring (Figure 41c). The smoothed data and residuals show that the $\%Ni_S$ for both size fractions increased above the overall mean in late spring (Figures 43c and 44c).

(a) Aerosol soluble nickel from Eastern Shore samples - smoothed

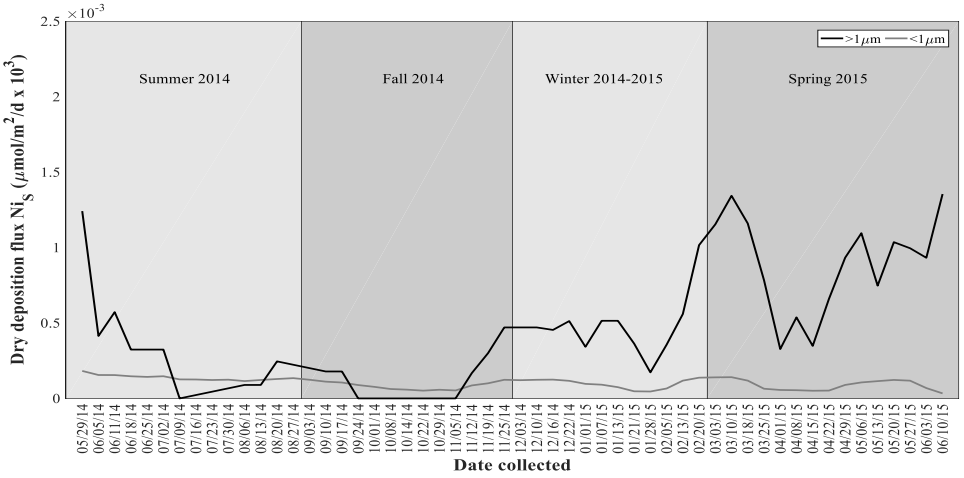

(b) Aerosol total nickel from Eastern Shore samples - smoothed

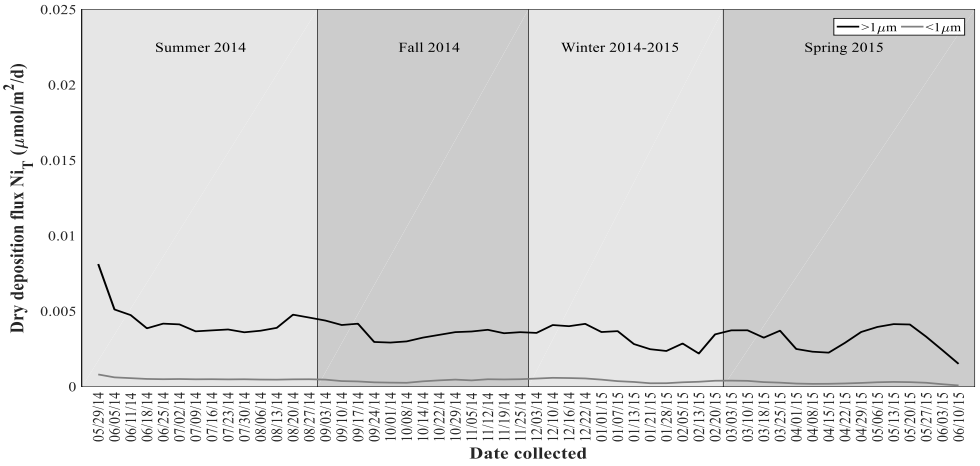

(c) Aerosol nickel fractional solubility from Eastern Shore samples - smoothed

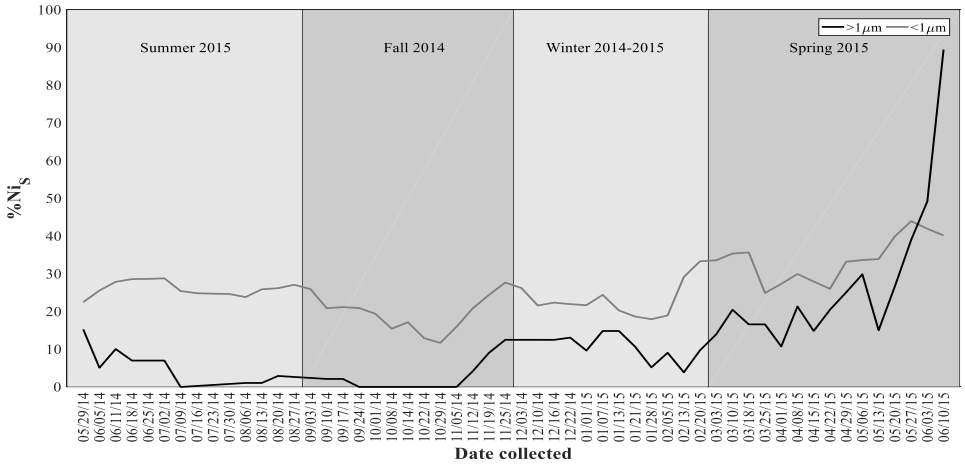

Figure 43. Seasonal dry deposition fluxes of (a) soluble nickel (Ni_S, μmol/m^2/d x 10^3), (b) total nickel (Ni_T, μmol/m^2/d), and (c) fractional solubility (%Ni_S) for weekly collected Eastern Shore samples. Note that data were interpolated for dates 30 July 2014, 6 August 2014, 13 August 2014, and 20 August 2014 using the method in Section 2.6.

(a) Aerosol soluble nickel from Eastern Shore samples - residuals

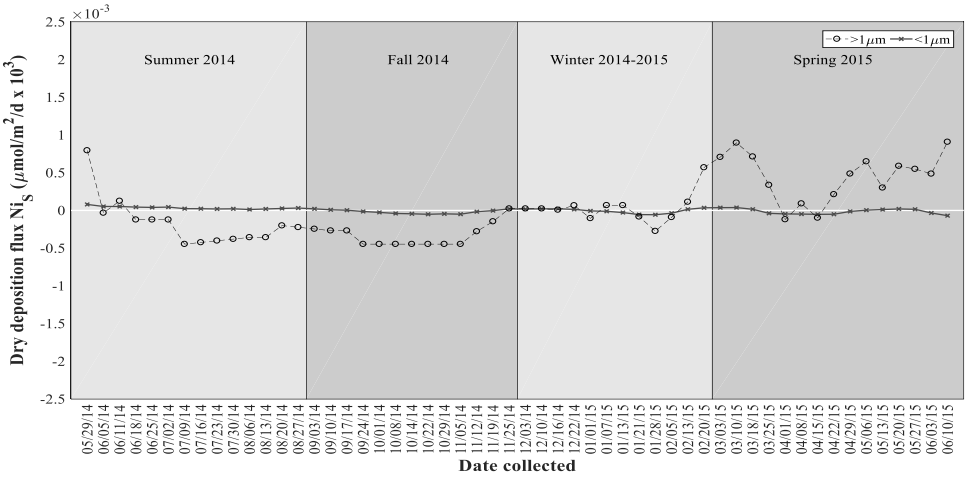

(b) Aerosol total nickel from Eastern Shore samples - residuals

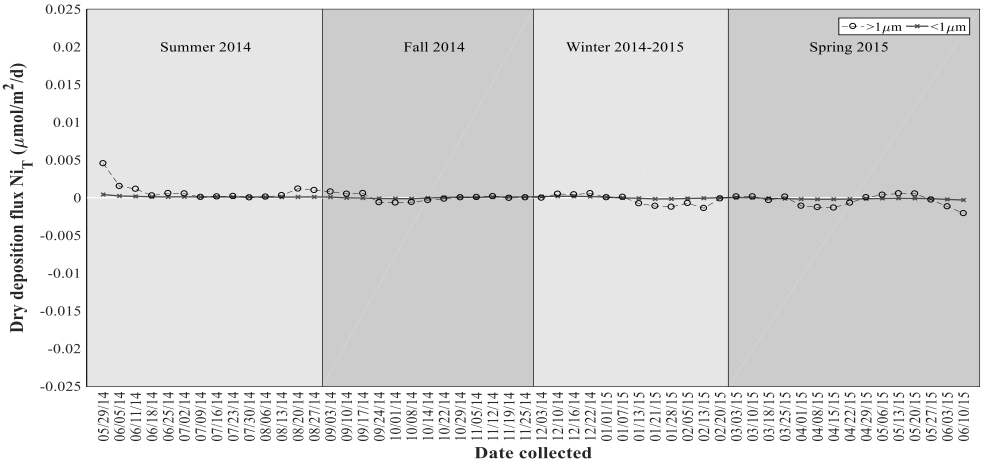

(c) Aerosol nickel fractional solubility from Eastern Shore samples - residuals

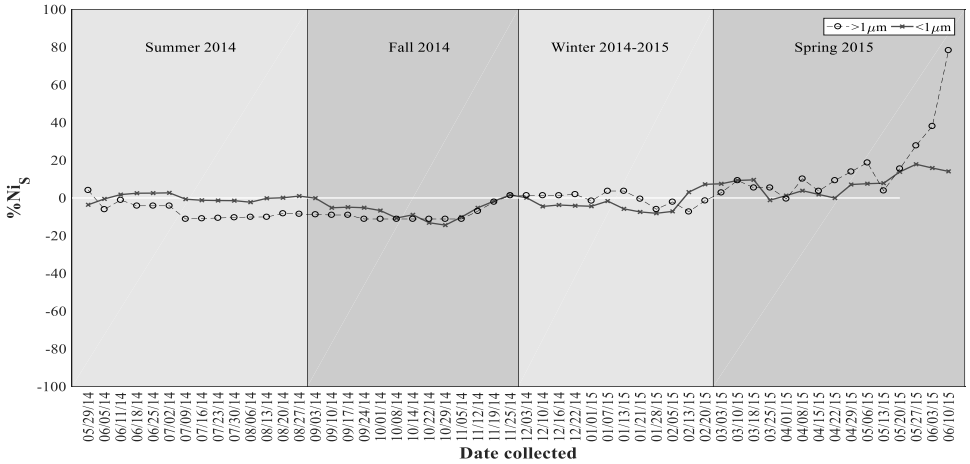

Figure 44. Residuals of dry deposition fluxes of (a) soluble nickel (Ni_S, μmol/m^2/d x 10^3), (b) total nickel (Ni_T, μmol/m^2/d), and (c) fractional solubility (%Ni_S) for weekly collected Eastern Shore samples. Note that data were interpolated for dates 30 July 2014, 6 August 2014, 13 August 2014, and 20 August 2014 using the method in Section 2.6. The white horizontal line indicates the annual mean.

The mean dry fine Ni_S flux for summer ($13.9 \times 10^{-5} \pm 3.37 \times 10^{-5}$ µmol/m^2/d) was found to be significantly greater ($p = 0.0544$, df = 47, F = 2.74) than that for winter ($9.08 \times 10^{-5} \pm 5.43 \times 10^{-5}$ µmol/m^2/d) (Table 12), using a one-way ANOVA and a multiple comparison test. The mean dry coarse Ni_S flux for the spring ($9.38 \times 10^{-4} \pm 7.93 \times 10^{-4}$ µmol/m^2/d) was found to be significantly greater ($p = 0.0274$, df = 19, F = 3.96) than that for winter ($4.17 \times 10^{-4} \pm 4.42 \times 10^{-4}$ µmol/m^2/d) (Table 12), using a one-way ANOVA and a multiple comparison test. The overall mean dry flux of coarse Ni_S ($4.73 \times 10^{-4} \pm 6.44 \times 10^{-4}$ µmol/m^2/d) was significantly greater ($p < 0.0001$, df = 66, tstat = 19.2) than that for fine Ni_S ($10.1 \times 10^{-5} \pm 3.13 \times 10^{-5}$ µmol/m^2/d) (Table 12), as determined by a two-sample t-test. Many dry coarse Ni_S samples contained Ni concentrations below the detection limit of 0.081 µg L^{-1} (Table 3 and Figure 42a).

The median dry fine Ni_T flux for summer (5.53×10^{-4} µmol/m^2/d) was significantly greater ($p = 0.0008$, df = 48, F = 6.62) from those for fall (4.15×10^{-4} µmol/m^2/d) and spring (2.34×10^{-4} µmol/m^2/d), as determined by a Kruskal-Wallis test and a multiple comparison test. However, the mean dry coarse Ni_T fluxes for the four seasons were found to be not significantly different ($p = 0.5868$, df = 48, F = 0.65), using a one-way ANOVA. A two-sample t-test indicated that the overall mean coarse Ni_T flux ($3.55 \times 10^{-3} \pm 1.61 \times 10^{-3}$ µmol/m^2/d) was significantly greater ($p < 0.0001$, df = 88.9, tstat = 24.4) than the overall mean dry fine Ni_T flux ($3.85 \times 10^{-4} \pm 1.84 \times 10^{-4}$ µmol/m^2/d) (Table 13).

There were no significant differences in the medians of fine $\%Ni_S$ ($p = 0.052$, df = 46, chi-sq = 7.73), as determined by a Kruskal-Wallis test. The means of coarse $\%Ni_S$ for the four seasons were also not significantly different ($p = 0.065$, df = 18, F = 2.98), as determined by a one-way ANOVA. A Wilcoxon rank sum test determined that the median $\%Ni_S$ for the two size fractions were not significantly different ($p = 0.077$, zval = -0.2832).

The dry flux of soluble copper (Cu_S) in the fine fraction ranged from 1.80 x 10^{-4} to 4.80 x 10^{-4} µmol/m^2/d in summer, 1.47 x 10^{-4} to 7.53 x 10^{-4} µmol/m^2/d in fall, 1.97 x 10^{-4} to 5.93 x 10^{-4} µmol/m^2/d in winter, and 1.30 x 10^{-4} to 14.3 x 10^{-4} µmol/m^2/d in spring (Table 12). The dry flux of coarse Cu_S ranged from 4.09 x 10^{-3} to 15 x 10^{-3} µmol/m^2/d in summer, 4.35 x 10^{-3} to 10.4 x 10^{-3} µmol/m^2/d in fall, 3.01 x 10^{-3} to 20.7 x 10^{-3} µmol/m^2/d in winter, and 3.23 x 10^{-3} to 11.5 x 10^{-3} µmol/m^2/d in spring (Table 12 and Figure 45a). The fluxes of dry coarse Cu_S were elevated during winter, while dry Cu_S fluxes for all other seasons were less variable (Table 12 and Figure 45a).

The dry total copper (Cu_T) flux in the fine fraction ranged from 4.18 x 10^{-4} to 9.76 x 10^{-4} µmol/m^2/d in summer, 3.59 x 10^{-4} to 17.5 x 10^{-4} µmol/m^2/d in fall, 5.23 x 10^{-4} to 19.5 x 10^{-4} µmol/m^2/d in winter, and 2.53 x 10^{-4} to 11.8 x 10^{-4} µmol/m^2/d in spring (Table 13 and Figure 45b). The dry flux of Cu_T ranged from 12.5 x 10^{-3} to 31.9 x 10^{-3} µmol/m^2/d in summer, 10.6 x 10^{-3} to 29.0 x 10^{-3} µmol/m^2/d in fall, 8.78 x 10^{-3} to 57.6 x 10^{-3} µmol/m^2/d in winter, and 9.26 x 10^{-3} to 54.9 x 10^{-3} µmol/m^2/d in spring (Table 13 and Figure 45b). The overall mean dry coarse Cu_T flux (20.2 x 10^{-3} ± 10.8 x 10^{-3} µmol/m^2/d) was roughly 20 times greater than the overall mean dry fine Cu_T flux (8.88 x 10^{-4} ± 3.64 x 10^{-4} µmol/m^2/d).

The aerosol fractional solubility of copper (%Cu_S) was mostly similar for both size fractions throughout the time series (Figure 45c). The fine %Cu_S ranged from 26.1 to 53.2 % in summer, 23.9 to 55.2 % in fall, 27.1 to 54.1 % in winter, and 29.6 to 100 % in spring (Table 14 and Figure 45c). The coarse %Cu_S ranged from 28.5 to 55.7 % in summer, 19.4 to 50.4 % in fall, 25.1 to 60.9 % in winter, and below the level of quantification to 53.8 % in spring (Table 14 and Figure 45c).

(a) Aerosol soluble copper from Eastern Shore samples

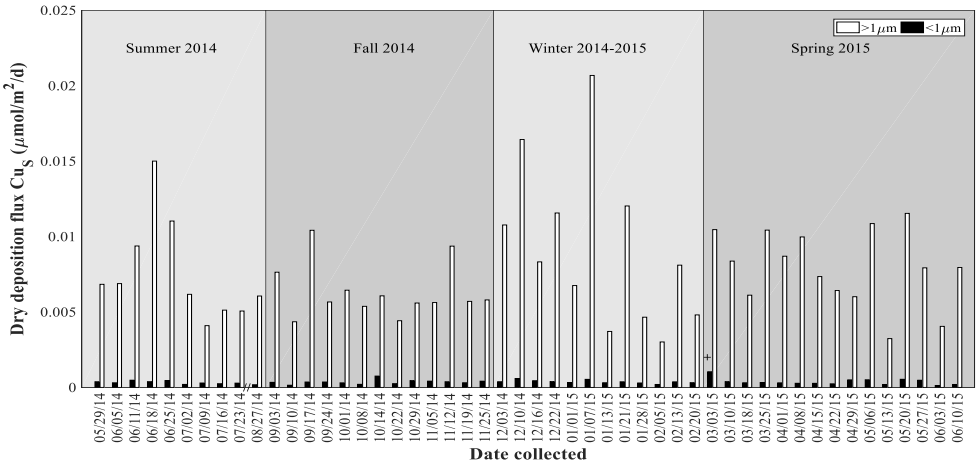

(b) Aerosol total copper from Eastern Shore samples

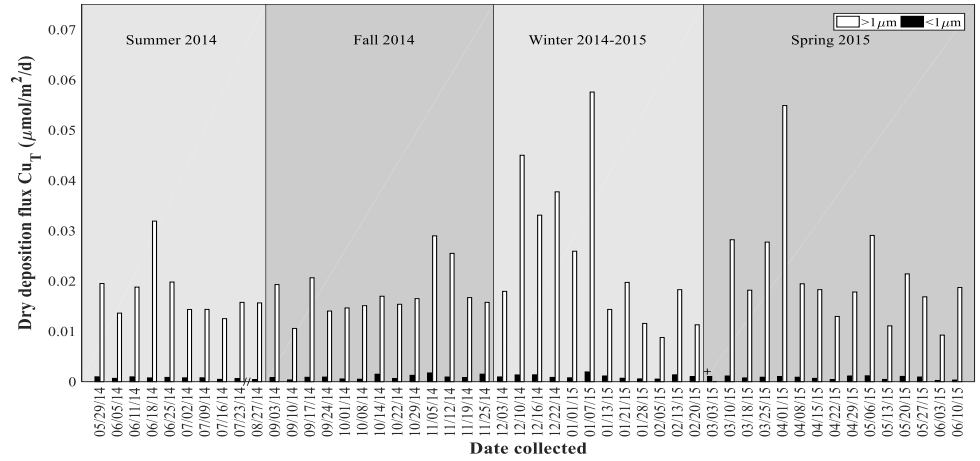

(c) Aerosol copper fractional solubility from Eastern Shore samples

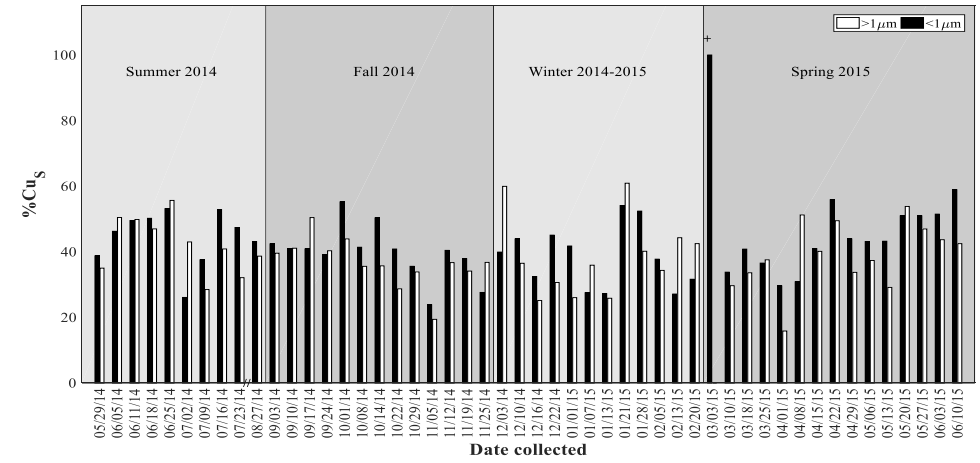

Figure 45. Seasonal dry deposition fluxes of (a) soluble copper (Cu_S, μmol/m^2/d), (b) total copper (Cu_T, μmol/m^2/d), and (c) fractional solubility (%Cu_S) for weekly collected Eastern Shore samples. "//" indicates the break in the x-axis between 07/23/14 and 08/27/14 and "+" indicates samples for which the soluble flux was set to equal the total flux as mentioned in Section 2.6.

The smoothed data and residuals plots show that the dry flux of fine Cu_S varied little throughout the time series (Figures 46a and 47a). The dry flux of coarse Cu_S was above the overall mean at the start of summer and during early winter (Figure 47a). During the latter part of summer, and throughout fall, the dry flux of coarse Cu_S remained below the overall mean (Figure 47a). The dry flux of coarse Cu_T was above the overall mean during the early winter and early spring (Figure 47b). The smoothed data and residuals plots show that the dry flux of fine Cu_T remained nearly constant throughout the time series (Figures 46b and 47b). The fine and coarse $\%Cu_S$ values were mostly similar (Figure 45c). The smoothed data and residuals show that the fine and coarse $\%Cu_S$ varied little during the time series (Figures 46c and 47c).

(a) Aerosol soluble copper from Eastern Shore samples - smoothed

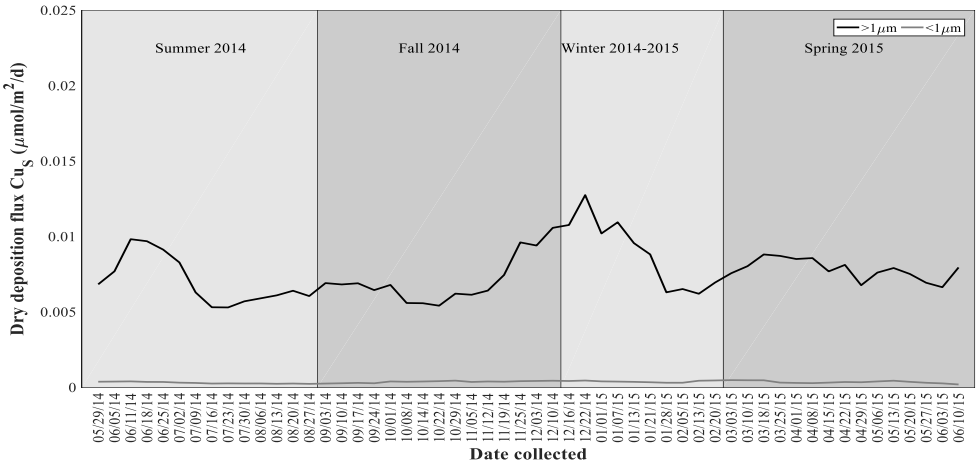

(b) Aerosol total copper from Eastern Shore samples - smoothed

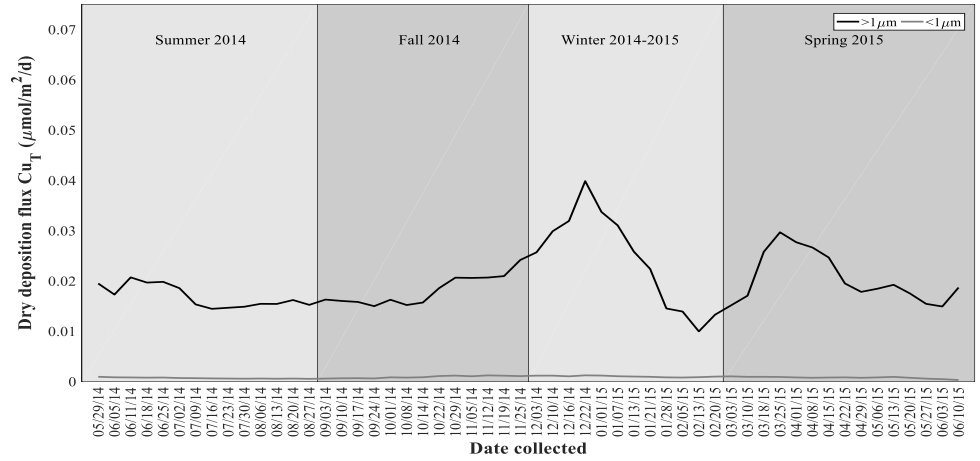

(c) Aerosol copper fractional solubility from Eastern Shore samples - smoothed

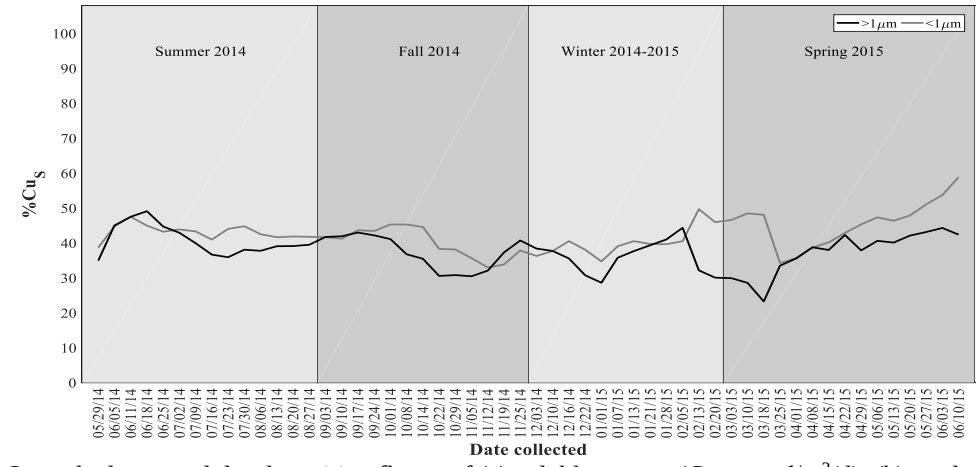

Figure 46. Smoothed seasonal dry deposition fluxes of (a) soluble copper (Cu_S, μmol/m^2/d), (b) total copper (Cu_T, μmol/m^2/d), and (c) fractional solubility (%Cu_S) for weekly collected Eastern Shore samples. Note that data were interpolated for dates 30 July 2014, 6 August 2014, 13 August 2014, and 20 August 2014 using the method in Section 2.6.

(a) Aerosol soluble copper from Eastern Shore samples - residuals

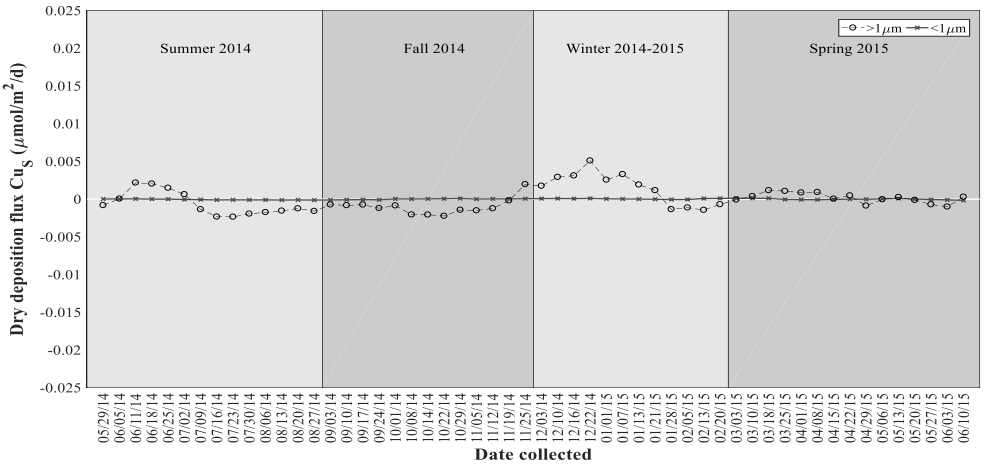

(b) Aerosol total copper from Eastern Shore samples - residuals

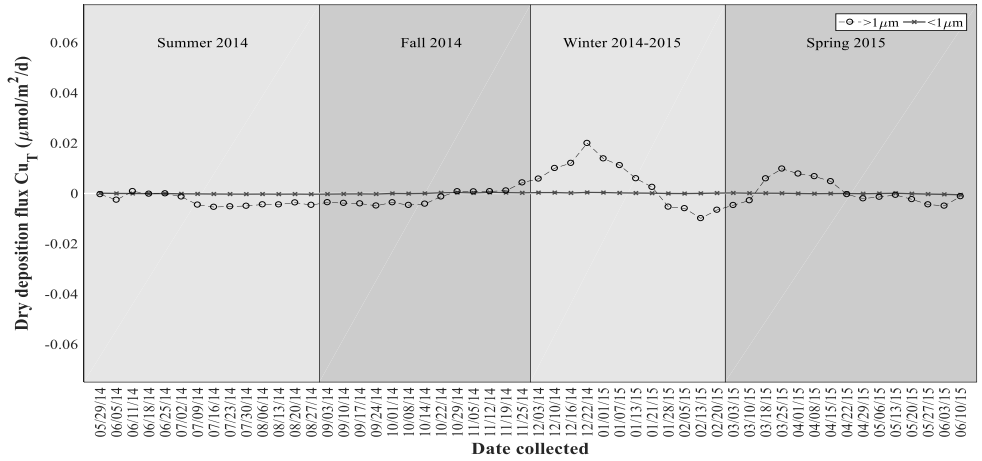

(c) Aerosol copper fractional solubility from Eastern Shore samples - residuals

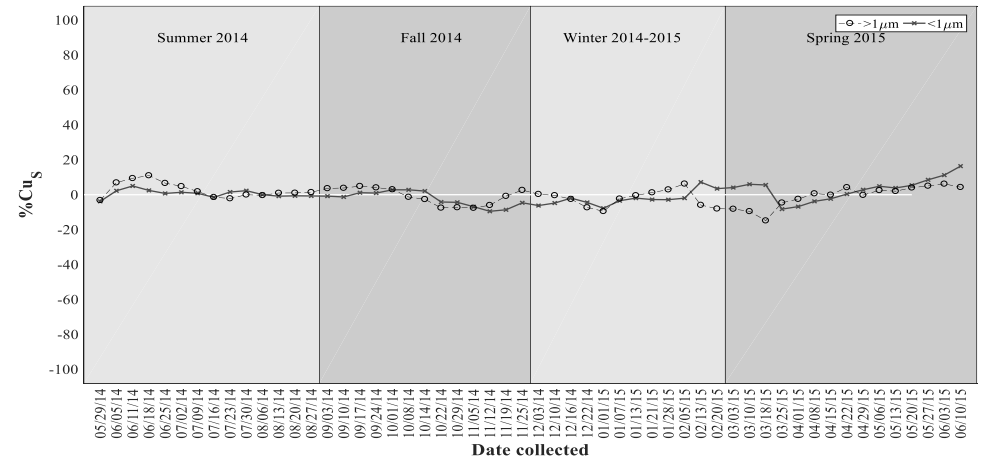

Figure 47. Residuals of dry deposition fluxes of (a) soluble copper (Cu_S, μmol/m^2/d), (b) total copper (Cu_T, μmol/m^2/d), and (c) fractional solubility (%Cu_S) for weekly collected Eastern Shore samples. Note that data were interpolated for dates 30 July 2014, 6 August 2014, 13 August 2014, and 20 August 2014 using the method in Section 2.6. The white horizontal line indicates the annual mean.

There were no significant differences between the mean dry fine Cu_S fluxes ($p = 0.8092$, $df = 49$, $F = 0.32$) and the mean dry coarse Cu_S fluxes ($p = 0.5238$, $df = 49$, $F = 0.76$) for the four seasons. However, a two-sample t-test indicated that the overall mean dry coarse Cu_S flux ($7.77 \times 10^{-3} \pm 3.45 \times 10^{-3}$ μmol/m^2/d) was significantly greater ($p < 0.0001$, $df = 62.5$, $tstat = 37.5$) than the overall mean dry fine Cu_S flux ($1.95 \times 10^{-4} \pm 3.71 \times 10^{-4}$ μmol/m^2/d) (Table 12).

There were no significant differences between the means of the dry fine Cu_T fluxes ($p = 0.1524$, $df = 49$, $F = 1.84$) and between the medians of the dry coarse Cu_T fluxes ($p = 0.576$, $df = 48$, $F = 1.98$) for the four seasons. The overall mean dry coarse Cu_T flux ($20.2 \times 10^{-3} \pm 10.8 \times 10^{-3}$ μmol/m^2/d) was found to be significantly greater ($p < 0.0001$, $df = 48.4$, $tstat = -26.4$) than the overall mean dry fine Cu_T flux ($8.88 \times 10^{-4} \pm 3.64 \times 10^{-4}$ μmol/m^2/d) (Table 13), using a two-sample t-test.

There were no significant differences between the medians of fine $\%Cu_S$ ($p = 0.2221$, $df = 49$, $F = 4.39$) and between the means of coarse $\%Cu_S$ ($p = 0.6518$, $df = 48$, $F = 0.55$) for the four seasons. A Wilcoxon rank sum test indicated that median $\%Cu_S$ was not significantly different for the two size fractions ($p = 0.0871$, $zval = -1.711$).

The dry flux of soluble zinc (Zn_S) in the fine fraction ranged from 0.937 x 10^{-3} to 3.34 x 10^{-3} µmol/m^2/d in summer, 0.861 x 10^{-3} to 3.33 x 10^{-3} µmol/m^2/d in fall, 1.35 x 10^{-3} to 4.00 x 10^{-3} µmol/m^2/d in winter, and 0.684 x 10^{-3} to 11.7 x 10^{-3} µmol/m^2/d in spring (Table 12 and Figure 48a). The dry flux of coarse Zn_S ranged from 9.51 x 10^{-3} to 33.6 x 10^{-3} µmol/m^2/d in summer, 11.4 x 10^{-3} to 24.1 x 10^{-3} µmol/m^2/d in fall, 10.8 x 10^{-3} to 34.6 x 10^{-3} µmol/m^2/d in winter, and 11.8 x 10^{-3} to 32.6 x 10^{-3} µmol/m^2/d in spring (Table 12 and Figure 48a). The overall mean coarse Zn_S flux (21.0 x 10^{-3} ± 6.93 x 10^{-3} µmol/m^2/d) was roughly 10 times greater than the overall mean fine Zn_S flux (2.28 x 10^{-3} ± 1.60 x 10^{-3} µmol/m^2/d) (Table 12).

The dry flux of total zinc (Zn_T) in the fine fraction ranged from 1.88 x 10^{-3} to 4.04 x 10^{-3} µmol/m^2/d in summer, 1.79 x 10^{-3} to 6.43 x 10^{-3} µmol/m^2/d in fall, 2.58 x 10^{-3} to 6.95 x 10^{-3} µmol/m^2/d in winter, and 1.34 x 10^{-3} to 6.47 x 10^{-3} µmol/m^2/d in spring (Table 13 and Figure 48b). The dry flux of coarse Zn_T ranged from 22.5 x 10^{-3} to 52.3 x 10^{-3} µmol/m^2/d in summer, 20.3 x 10^{-3} to 103 x 10^{-3} µmol/m^2/d in fall, 18.2 x 10^{-3} to 64.7 x 10^{-3} µmol/m^2/d in winter, and 12.1 x 10^{-3} to 51.8 x 10^{-3} µmol/m^2/d in spring (Table 13 and Figure 48b).

The aerosol fractional solubility of zinc (%Zn_S) was high and similar for both size fractions throughout the time series (Table 14 and Figure 48c). The fine %Zn_S ranged from 49.7 to 100 % in summer, 37.8 to 98.3 % in fall, 38.6 to 67.9 % in winter, and 47.7 to 100 % in spring (Table 14 and Figure 48c). The coarse (%Zn_S) ranged from 33.0 to 72.6 % in summer, 23.2 to 72.8 % in fall, 43.7 to 81.1 % in winter, and 38.2 to 97.4 % in spring (Table 14 and Figure 48c).

(a) Aerosol soluble zinc from Eastern Shore samples

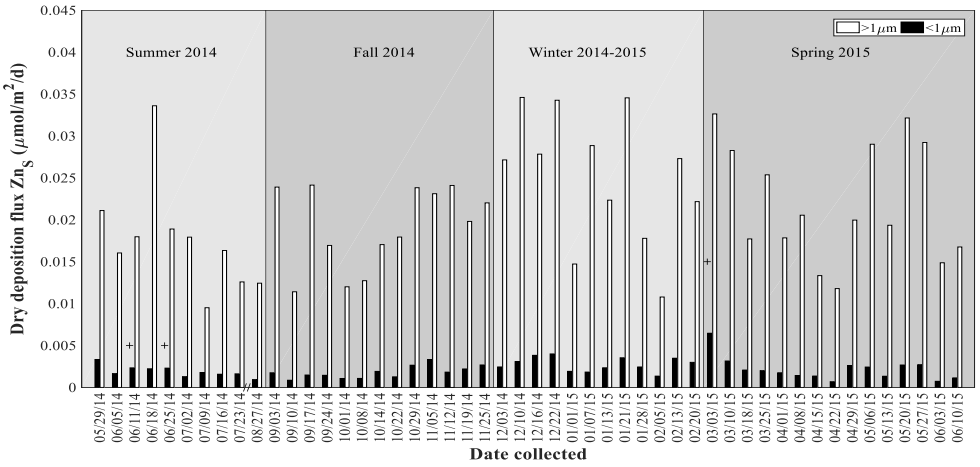

(b) Aerosol total zinc from Eastern Shore samples

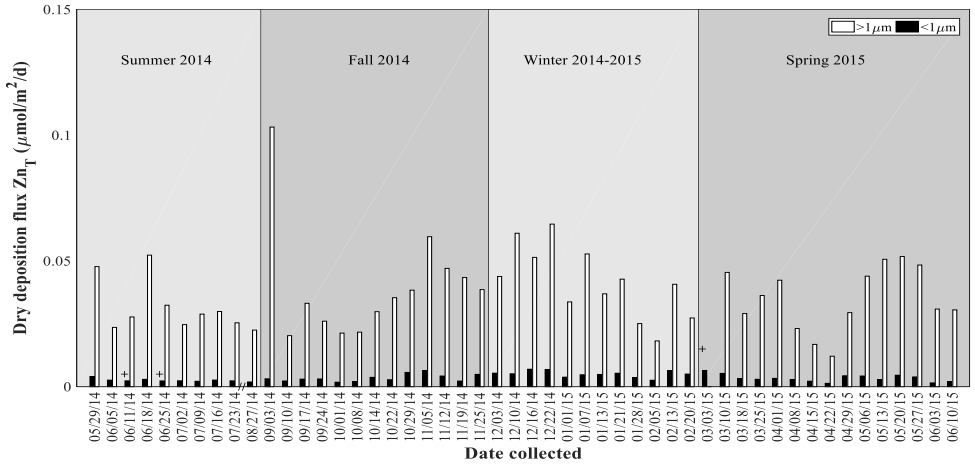

(c) Aerosol zinc fractional solubility from Eastern Shore samples

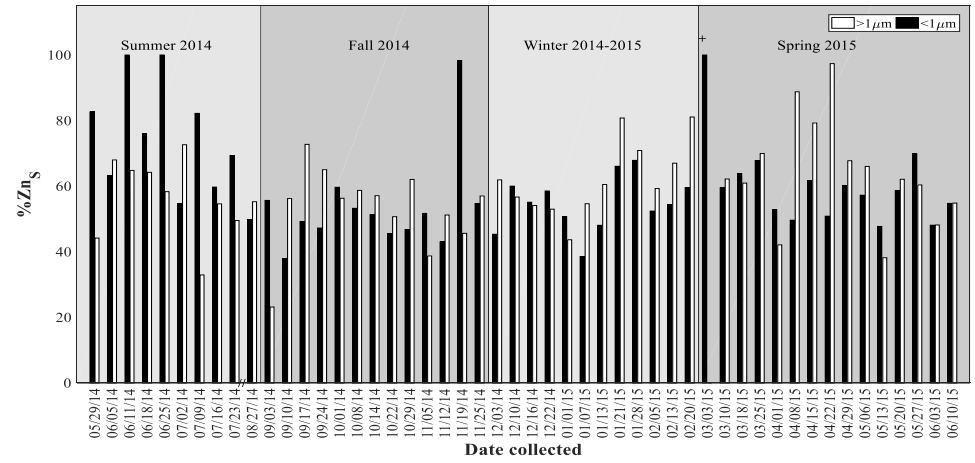

Figure 48. Seasonal dry deposition fluxes of (a) soluble zinc (Zn_S, μmol/m^2/d), (b) total zinc (Zn_T, μmol/m^2/d), and (c) fractional solubility (%Zn_S) for weekly collected Eastern Shore samples. "//" indicates the break in the x-axis between 07/23/14 and 08/27/14 and "+" indicates samples for which the soluble flux was set to equal the total flux as mentioned in Section 2.6

The smoothed data and residuals show that the dry flux of fine Zn_S displayed little variation throughout the time series (Figures 49a and 50a). The dry flux of coarse Zn_S was mostly above the overall mean during the winter and remained near this mean during the other seasons (Figure 50a). The smoothed data and residuals plots show that the dry flux of fine Zn_S remained relatively constant throughout the time series (Figures 49b and 50b), whereas the dry flux of coarse Zn_T was above the overall mean during the winter and remained close to this mean during the other seasons (Figure 50b). The dry Zn_T flux and dry Zn_S flux for both size fractions followed similar seasonal patterns (Figures 49a and 49b). The dry fine and coarse $\%Zn_S$ were similar throughout the time series (Figure 48c). The smoothed data and residuals show that the fine and coarse $\%Zn_S$ were greater during early summer and late spring (Figures 49c and 50c).

(a) Aerosol soluble zinc from Eastern Shore samples - smoothed

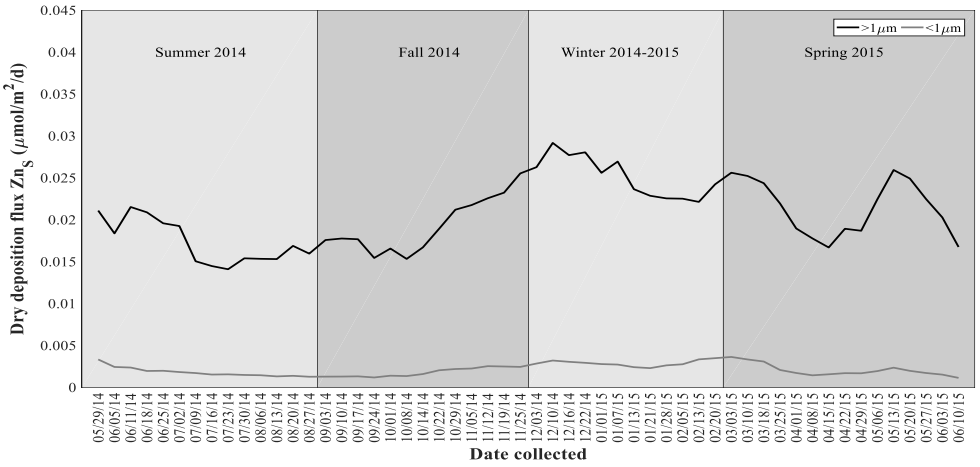

(b) Aerosol total zinc from Eastern Shore samples - smoothed

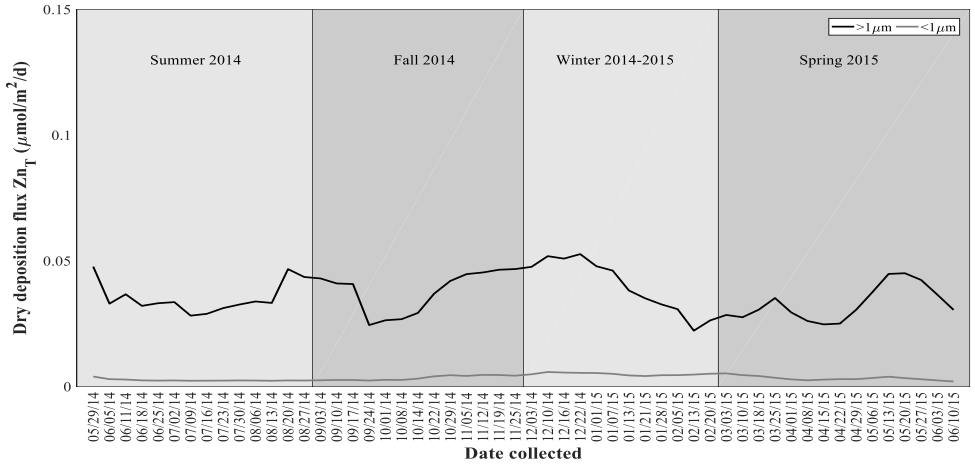

(c) Aerosol zinc fractional solubility from Eastern Shore samples - smoothed

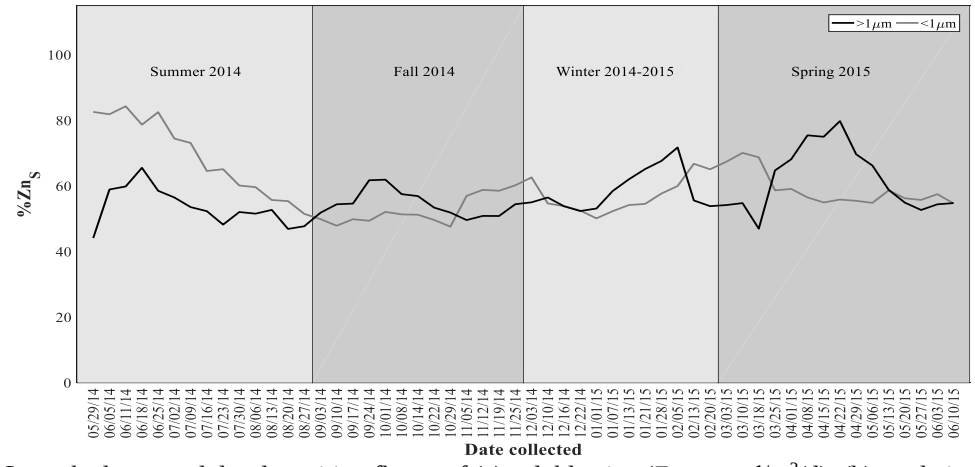

Figure 49. Smoothed seasonal dry deposition fluxes of (a) soluble zinc (Zn_S, μmol/m²/d), (b) total zinc (Zn_T, μmol/m²/d), and (c) fractional solubility (%Zn_S) for weekly collected Eastern Shore samples. Note that data were interpolated for dates 30 July 2014, 6 August 2014, 13 August 2014, and 20 August 2014 using the method in Section 2.6.

(a) Aerosol soluble zinc from Eastern Shore samples - residuals

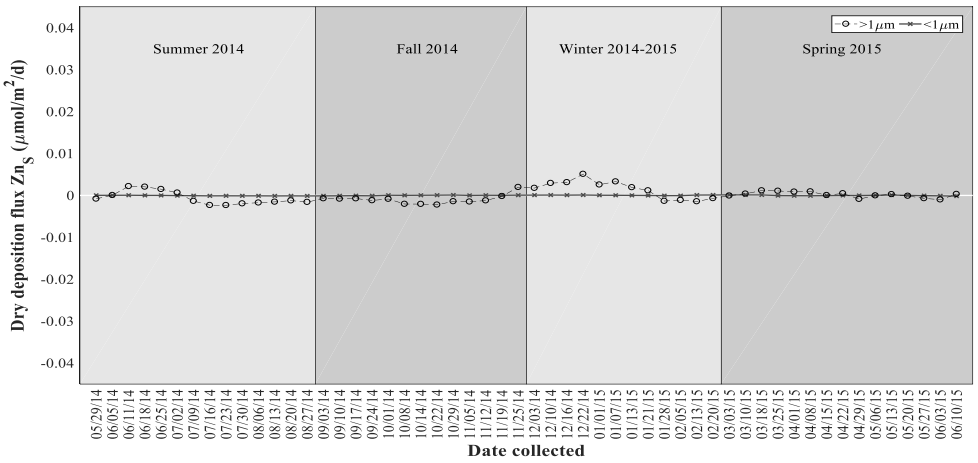

(b) Aerosol total zinc from Eastern Shore samples - residuals

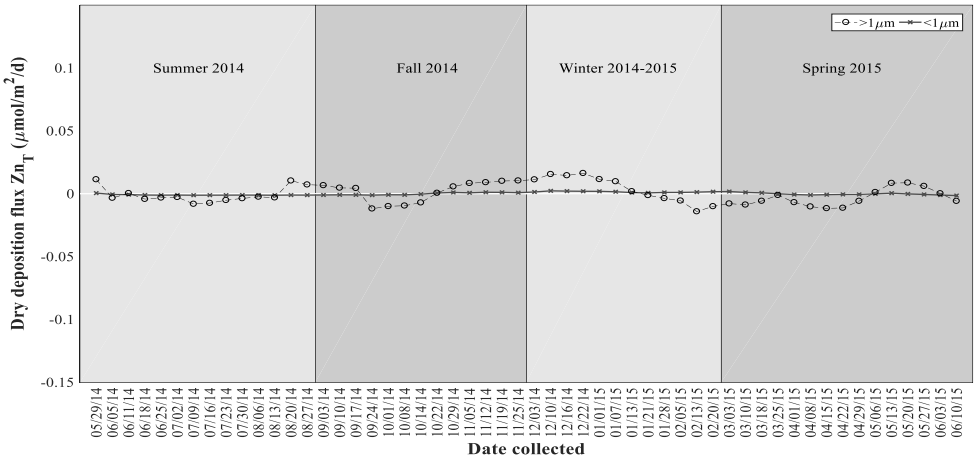

(c) Aerosol zinc fractional solubility from Eastern Shore samples - residuals

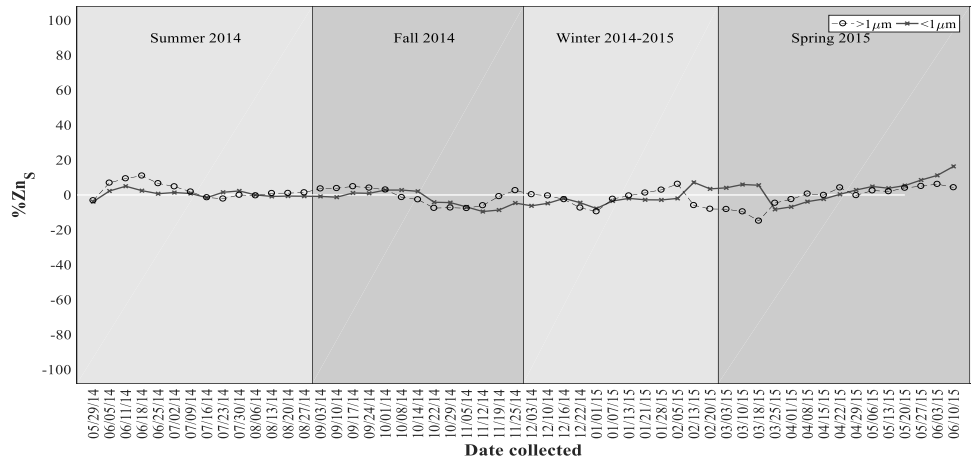

Figure 50. Residuals of dry deposition fluxes of (a) soluble zinc (Zn_S, μmol/m²/d), (b) total zinc (Zn_T, μmol/m²/d), and (c) fractional solubility (%Zn_S) for weekly collected Eastern Shore samples. Note that data were interpolated for dates 30 July 2014, 6 August 2014, 13 August 2014, and 20 August 2014 using the method in Section 2.6. The white horizontal line indicates the annual mean flux.

The median dry fine Zn_S flux for spring (2.00×10^{-3} µmol/m^2/d) was significantly different ($p < 0.0001$, df = 49, chi-sq = 34.2) from those for summer (1.72×10^{-3} µmol/m^2/d) , fall (1.75×10^{-3} µmol/m^2/d), and winter (2.72×10^{-3} µmol/m^2/d), as determined by a Kruskal-Wallis test and a multiple comparison test. The means of the dry coarse Zn_S flux for the four seasons were not significantly different ($p = 0.0619$, df = 49, F = 2.62). A two-sample t-test indicated that the overall mean dry coarse Zn_S flux ($21.0 \times 10^{-3} \pm 6.93 \times 10^{-3}$µmol/m^2/d) was significantly greater ($p < 0.0001$, df = 49.3, tstat = 40.0) than the overall mean dry fine Zn_S flux ($2.28 \times 10^{-3} \pm 1.60 \times 10^{-3}$ µmol/m^2/d).

The mean dry fine Zn_T flux for winter ($5.06 \times 10^{-3} \pm 1.31 \times 10^{-3}$ µmol/m^2/d) was found to be significantly greater ($p = 0.0003$, df = 49, F = 7.53) than those for summer ($2.56 \times 10^{-3} \pm 0.591 \times 10^{-3}$ µmol/m^2/d), fall ($3.49 \times 10^{-3} \pm 1.45 \times 10^{-3}$ µmol/m^2/d), and spring ($3.41 \times 10^{-3} \pm 1.42 \times 10^{-3}$ µmol/m^2/d) (Table 13), using a one-way ANOVA and a multiple comparison test. However, the means of coarse Zn_T flux for the four seasons were not significantly different ($p = 0.4246$, df = 48, F = 0.95). A two-sample t-test indicated that the overall mean dry coarse Zn_T flux ($36.5 \times 10^{-3} \pm 16.4 \times 10^{-3}$ µmol/m^2/d) was significantly greater ($p < 0.0001$, df = 97, tstat = -26.6) than the overall mean dry fine Zn_T flux ($3.66 \times 10^{-3} \pm 1.51 \times 10^{-3}$ µmol/m^2/d) (Table 13).

The median fine $\%Zn_S$ for spring (58.6 %) was significantly greater ($p < 0.0001$, df = 49, F = 114.49) than those for both fall (51.3 %) and winter (54.7 %), but lower than that for summer (72.7 %), as determined using a Kruskal-Wallis test and a multiple comparison test. The medians of the coarse $\%Zn_S$ for the four seasons were not significantly different ($p = 0.2884$, df = 48, chi-sq =3.76). A Wilcoxon rank sum test indicated that the median $\%Zn_S$ was not significantly different for the two size fractions ($p = 0.469$, zval = 0.7244).

The dry flux of soluble cadmium (Cd_S) in the fine fraction ranged from 5.17 x 10^{-6} to 12.2 x 10^{-6} µmol/m^2/d in summer, 4.74 x 10^{-6} to 35.6 x 10^{-6} µmol/m^2/d in fall, 7.05 x 10^{-6} to 37.3 x 10^{-6} µmol/m^2/d in winter, and 3.93 x 10^{-6} to 20.5 x 10^{-6} µmol/m^2/d in spring (Table 12 and Figure 51a). The dry flux of coarse Cd_S ranged from 3.73 x 10^{-5} to 9.56 x 10^{-5} µmol/m^2/d in summer, below the level of quantification to 37.7 x 10^{-5} µmol/m^2/d in fall, 2.94 x 10^{-5} to 19.6 x 10^{-5} µmol/m^2/d in winter, and 3.02 x 10^{-5} to 12.8 x 10^{-5} µmol/m^2/d in spring (Table 12 and Figure 51a). There were a few weeks during fall (22 October 2014, 29 October 2014, and 5 November 2014) during which dry coarse Cd_S was below the detection limit or drastically lower than those for all other sampling periods (Figure 51a).

The dry flux of total cadmium (Cd_T) in the fine fraction ranged from 0.736 x 10^{-5} to 2.59 x 10^{-5} µmol/m^2/d in summer, 0.570 x 10^{-5} to 5.95 x 10^{-5} µmol/m^2/d in fall, 1.31 x 10^{-5} to 6.32 x 10^{-5} µmol/m^2/d in winter, and 0.717 x 10^{-5} to 3.40 x 10^{-5} µmol/m^2/d in spring (Table 13 and Figure 51b). The dry flux of coarse total cadmium (Cd_T) ranged from 641 x 10^{-4} to 2.56 x 10^{-4} µmol/m^2/d in summer, 0.703 x 10^{-4} to 1.78 x 10^{-4} µmol/m^2/d in fall, 0.491 x 10^{-4} to 1.60 x 10^{-4} µmol/m^2/d in winter, and 0.441 x 10^{-4} to 1.57 x 10^{-4} µmol/m^2/d in spring (Table 13 and Figure 51b).

The aerosol fractional solubility of cadmium (%Cd_S) for both size fractions was relatively high and similar throughout the time series (Figure 51c). The fine %Cd_S ranged from 47.1 to 72.1 % in summer, 41.1 to 100 % in fall, 16.1 to 70.5 % in winter, and 47.6 to 100 % in spring (Table 14 and Figure 51c). The coarse %Cd_S ranged from 25.5 to 82.6 % in summer, below the level of quantification to 100 % in fall, 47.5 to 100 % in winter, and 48.7 to 79.5 % in spring (Table 14 and Figure 51c).

(a) Aerosol cadmium soluble from Eastern Shore samples

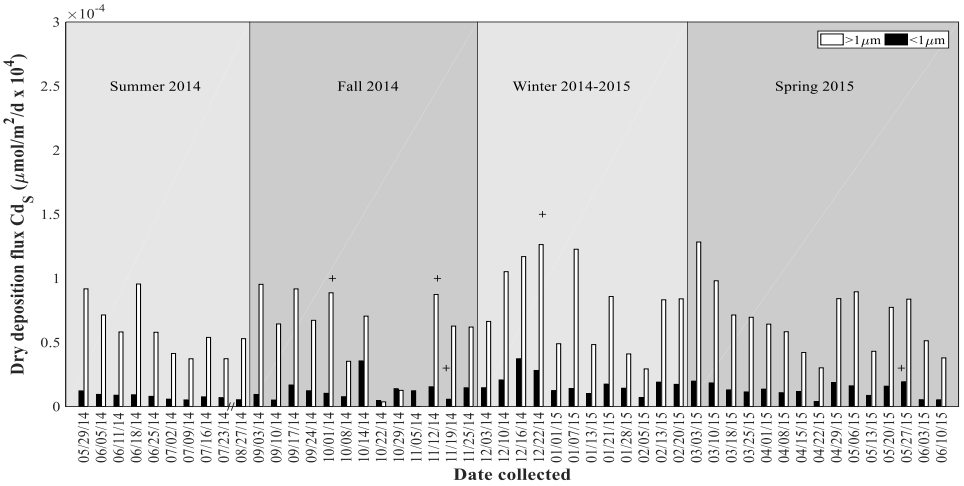

(b) Aerosol total cadmium from Eastern Shore samples

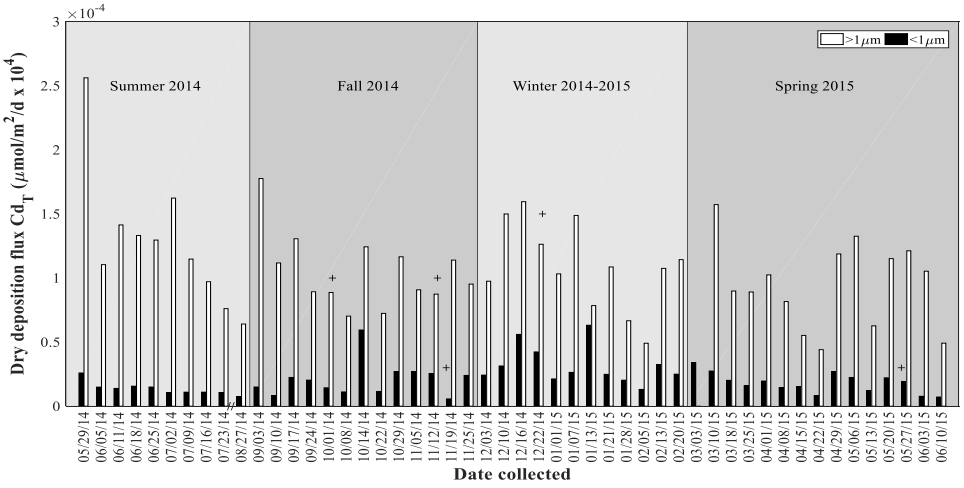

(c) Aerosol cadmium fractional solubility from Eastern Shore samples

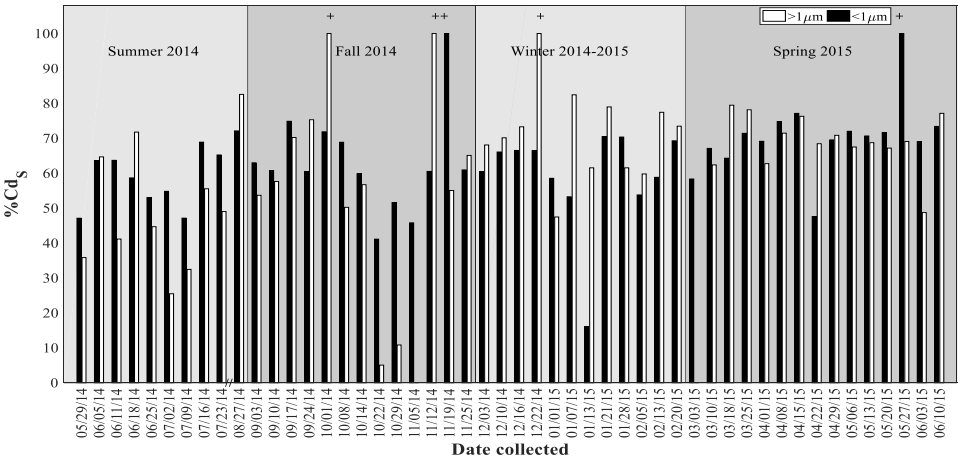

Figure 51. Seasonal dry deposition fluxes of (a) soluble cadmium (Cd_S, μmol/m^2/d), (b) total cadmium (Cd_T, μmol/m^2/d), and (c) fractional solubility (%Cd_S) for weekly collected Eastern Shore samples. "//" indicates the break in the x-axis between 07/23/14 and 08/27/14 and "+" indicates samples for which the soluble flux was set to equal the total flux as mentioned in Section 2.6.

The smoothed data and residuals show that the dry fine Cd_S flux varied little throughout the time series (Figures 52a and Figure 53a). The dry coarse Cd_S flux was above the overall mean during winter and early spring, and mostly below this mean during fall (Figure 53a). During summer, the dry coarse Cd_S flux remained near the overall mean (Figure 53a). The smoothed data and residuals show that the coarse Cd_T flux was above the overall mean in summer, and mostly below the mean in late winter and spring (Figures 52a and Figure 53a). The dry fine Cd_T flux was mainly above the overall mean during winter, and remained close to this mean during other seasons (Figure 53b). The smoothed data and residuals show that the fine and coarse $\%Cd_S$ was relatively low in summer and late fall in comparison to winter (Figures 52c and 53c). The fine and coarse $\%Cd_S$ were mostly similar (Figure 51c).

(a) Aerosol soluble cadmium from Eastern Shore samples - smoothed

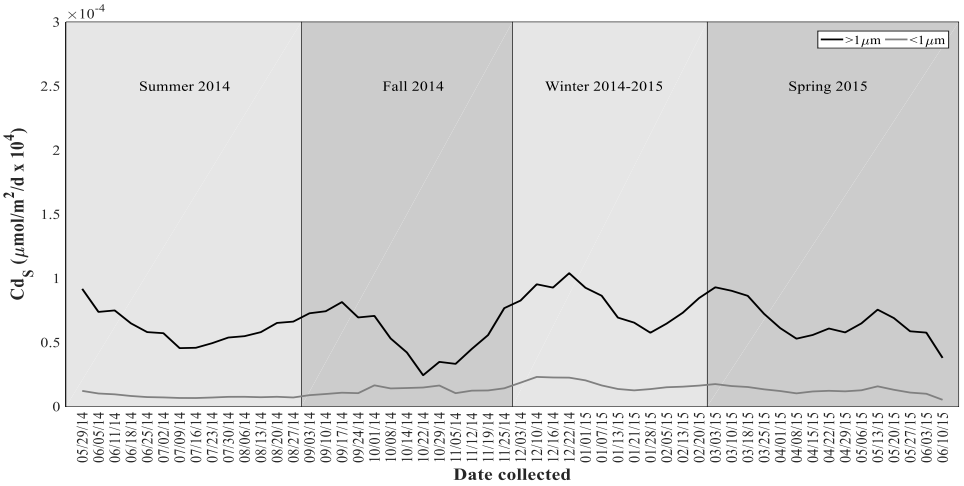

(b) Aerosol total cadmium from Eastern Shore samples - smoothed

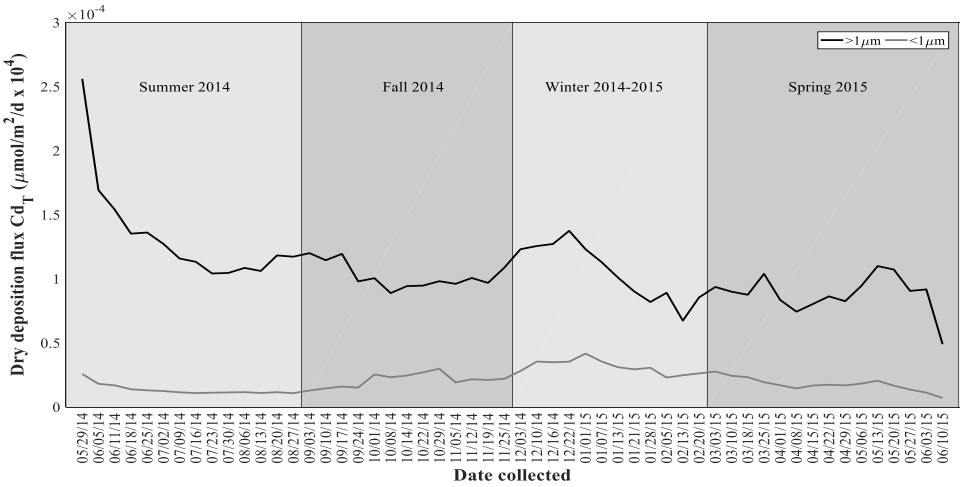

(c) Aerosol cadmium fractional solubility from Eastern Shore samples - smoothed

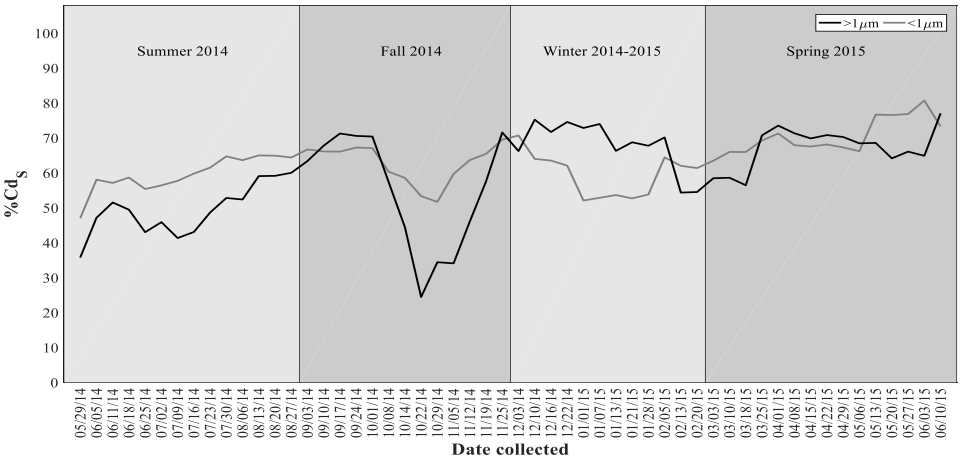

Figure 52. Smoothed seasonal dry deposition fluxes of (a) soluble cadmium (Cd_S, μmol/m^2/d), (b) total cadmium (Cd_T, μmol/m^2/d), and (c) fractional solubility (%Cd_S) for weekly collected Eastern Shore samples. Note that data were interpolated for dates 30 July 2014, 6 August 2014, 13 August 2014, and 20 August 2014 using the method in Section 2.6.

(a) Aerosol soluble cadmium from Eastern Shore samples - residuals

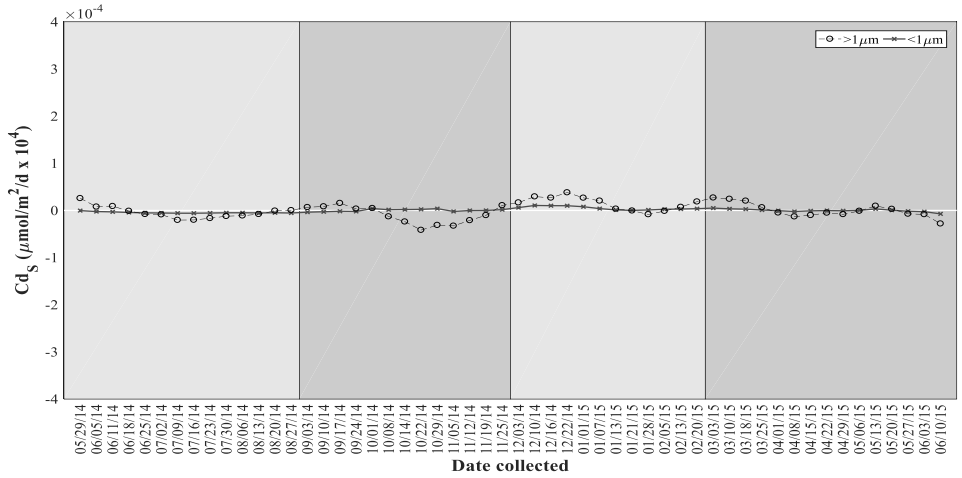

(b) Aerosol total cadmium from Eastern Shore samples - residuals

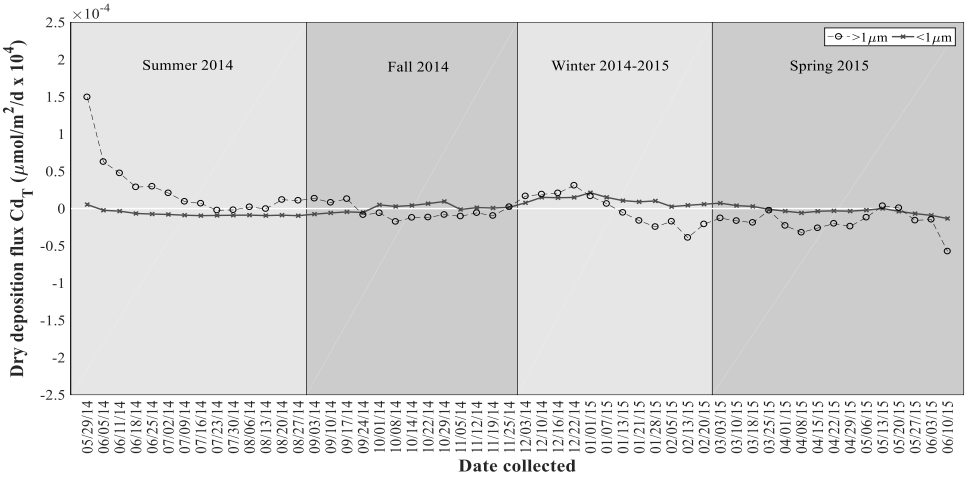

(c) Aerosol cadmium fractional solubility from Eastern Shore samples - residuals

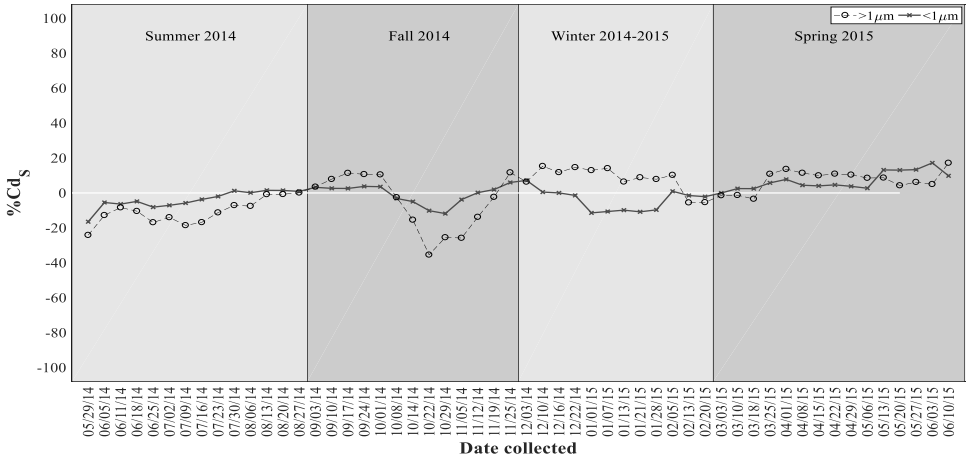

Figure 53. Residuals of dry deposition fluxes of (a) soluble cadmium (Cd_S, μmol/m^2/d), (b) total cadmium (Cd_T, μmol/m^2/d), and (c) fractional solubility (%Cd_S) for weekly collected Eastern Shore samples. Note that data were interpolated for dates 30 July 2014, 6 August 2014, 13 August 2014, and 20 August 2014 using the method in Section 2.6. The white horizontal line indicates the annual mean flux.

The mean dry fine Cd_S flux for winter ($17.7 \times 10^{-6} \pm 8.18 \times 10^{-6}$ µmol/m^2/d) was significantly greater ($p = 0.0048$, df = 49, $F = 4.91$) than that for summer ($7.84 \times 10^{-6} \pm 2.19 \times 10^{-6}$ µmol/m^2/d) (Table 12), as determined by a one-way ANOVA and a multiple comparison test. However, the medians of the dry coarse Cd_S fluxes for the four seasons were not significantly different ($p = 0.5732$, df = 48, chi-sq = 2). A Wilcoxon rank sum test indicated that the median fine and coarse dry Cd_S fluxes for the two size fractions were significantly different ($p < 0.0001$, zval = 8.0098).

The mean dry fine Cd_T flux for winter ($3.17 \times 10^{-5} \pm 1.49 \times 10^{-5}$ µmol/m^2/d) was significantly greater than that for summer ($1.36 \times 10^{-5} \pm 0.506 \times 10^{-5}$ µmol/m^2/d) and spring ($1.82 \times 10^{-5} \pm 0.777 \times 10^{-5}$ µmol/m^2/d) (Table 13). However, the means of the coarse Cd_T fluxes for the four seasons were not significantly different ($p = 0.2315$, df = 48, $F = 1.48$). A two-sample t-test indicated that the overall mean dry coarse Cd_T flux ($1.06 \times 10^{-4} \pm 0.408 \times 10^{-4}$ µmol/m^2/d) was significantly greater ($p < 0.0001$, df = 57.6, tstat = 41.8) than the overall mean fine Cd_S flux ($2.12 \times 10^{-5} \pm 1.26 \times 10^{-5}$ µmol/m^2/d) (Table 13).

The medians of fine $\%Cd_S$ for summer and winter were found to be significantly different ($p = 0.0204$, df = 49, chi-sq = 9.8), using a Kruskal-Wallis test and multiple comparison test. There were no significant differences in the medians of coarse $\%Cd_S$ for the seasons ($p = 0.032$, df = 47, chi-sq = 8.81). A Wilcoxon rank sum test confirmed that the median $\%Cd_S$ values for the two size fractions were not significantly different ($p = 0.061$, zval = 0.515).

The dry flux of soluble antimony (Sb_S) in the fine fraction ranged from 2.51 x 10^{-5} to 7.10 x 10^{-5} µmol/m^2/d in summer, 2.39 x 10^{-5} to 11.1 x 10^{-5} µmol/m^2/d in fall, 3.30 x 10^{-5} to 22.6 x 10^{-5} µmol/m^2/d in winter, and 1.04 x 10^{-5} to 10.4 x 10^{-5} µmol/m^2/d in spring (Table 12 and Figure 54a). The dry flux of soluble antimony (Sb_S) in the coarse fraction ranged from 0.799 x 10^{-4} to 2.12 x 10^{-4} µmol/m^2/d in summer, 0.848 x 10^{-4} to 2.42 x 10^{-4} µmol/m^2/d in fall, 0.512 x 10^{-4} to 4.68 x 10^{-4} µmol/m^2/d in winter, and 0.572 x 10^{-4} to 2.66 x 10^{-4} µmol/m^2/d in spring (Table 12 and Figure 54a). The overall mean dry coarse Sb_S flux (1.55 x 10^{-4} ± 0.779 x 10^{-4} µmol/m^2/d) was roughly twice the overall mean dry fine Sb_S flux (6.65 x 10^{-5} ± 3.65 x 10^{-5} µmol/m^2/d) (Table 12).

The dry fine of total antimony (Sb_T) in the fine fraction ranged from 0.748 x 10^{-4} to 2.60 x 10^{-4} µmol/m^2/d in summer, 0.842 x 10^{-4} to 2.49 x 10^{-4} µmol/m^2/d in fall, 0.780 x 10^{-4} to 5.19 x 10^{-4} µmol/m^2/d in winter, and 0.166 x 10^{-4} to 2.43 x 10^{-4} µmol/m^2/d in spring (Table 13 and Figure 54b). The dry flux of coarse Sb_T ranged from 8.73 x 10^{-4} to 28.7 x 10^{-4} µmol/m^2/d in summer, 14.0 x 10^{-4} to 33.6 x 10^{-4} µmol/m^2/d in fall, 5.19 x 10^{-4} to 32.3 x 10^{-4} µmol/m^2/d in winter, and 2.67 x 10^{-4} to 12.8 x 10^{-4} µmol/m^2/d in spring (Table 13 and Figure 54b).

The aerosol fractional solubility of antimony (%Sb_S) was consistently greater for the fine fraction than for the coarse fraction throughout the time series (Figure 54c). The overall mean fine %Sb_S (43.4 ± 11.1 %) was roughly 3 times greater than the overall mean coarse %Sb_S (11.8 ± 5.43 %) (Table 14). The fine %Sb_S ranged from 24.4 to 49.4 % in summer, 21.1 to 66.9 % in fall, 36.6 to 60.3 % in winter, and 29.1 to 68.6 % in spring (Table 14 and Figure 54c). The coarse %Sb_S ranged from 3.23 to 14.2 % in summer, 4.61 to 12.3 % in fall, 9.05 to 21.3 % in winter, and 11.7 to 24.3 % in spring (Table 14 and Figure 54c).

(a) Aerosol soluble antimony from Eastern Shore samples

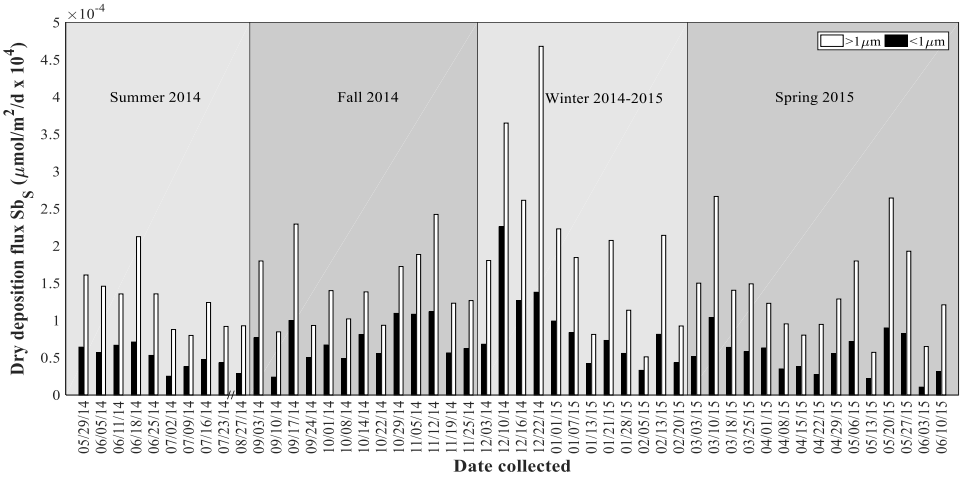

(b) Aerosol total antimony from Eastern Shore samples

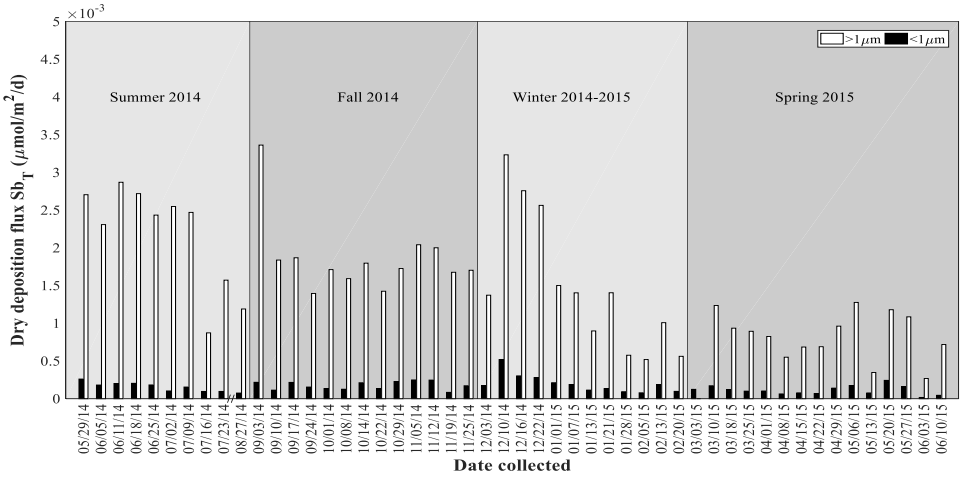

(c) Aerosol fractional solubility antimony from Eastern Shore samples

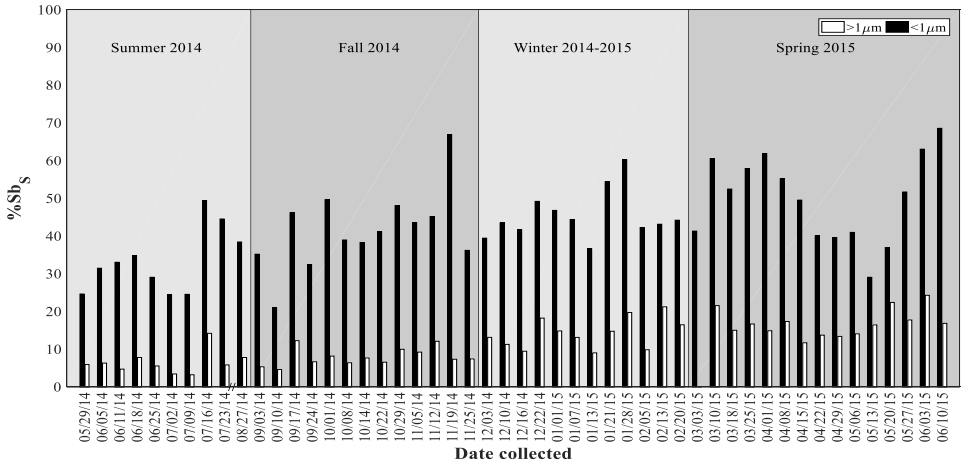

Figure 54. Seasonal dry deposition fluxes of (a) soluble antimony (Sb_S, μmol/m^2/d), (b) total antimony (Sb_T, μmol/m^2/d), and (c) fractional solubility (%Sb_S) for weekly collected Eastern Shore samples. "//" indicates the break in the x-axis between 07/23/14 and 08/27/14.

The smoothed data and residuals show that the dry flux of fine and coarse Sb_S followed a similar pattern throughout the time series (Figures 55a and 56a). The dry flux of fine and coarse Sb_S were both mostly above the overall mean during winter and remained closer to this mean during all other seasons (Figure 56a). The smoothed data and residuals (Figures 55a and 56a) show that the dry flux of fine Sb_T was little changed throughout the time series and remained near the mean flux. The dry flux of coarse Sb_T was above the overall mean during summer, fall, and early winter, and was below this mean during late winter and spring (Figure 56b).

(a) Aerosol soluble antimony from Eastern Shore samples - smoothed

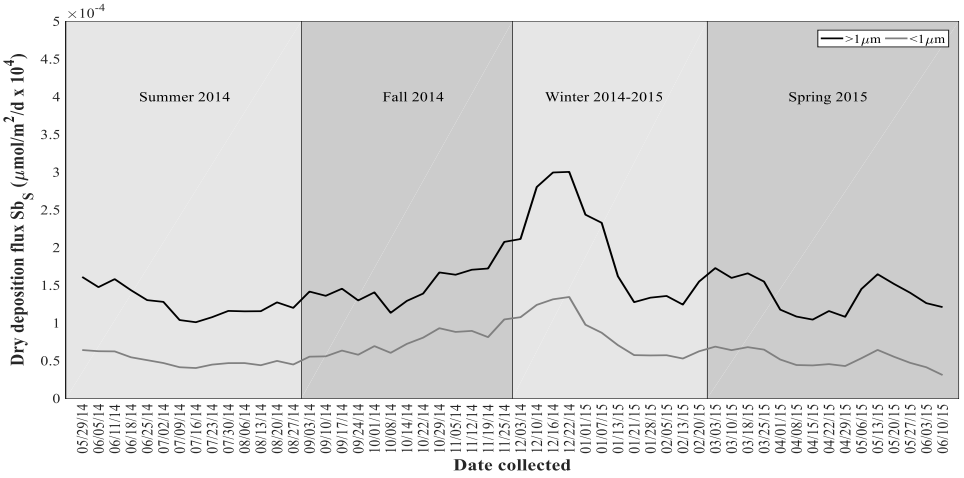

(b) Aerosol total antimony from Eastern Shore samples - smoothed

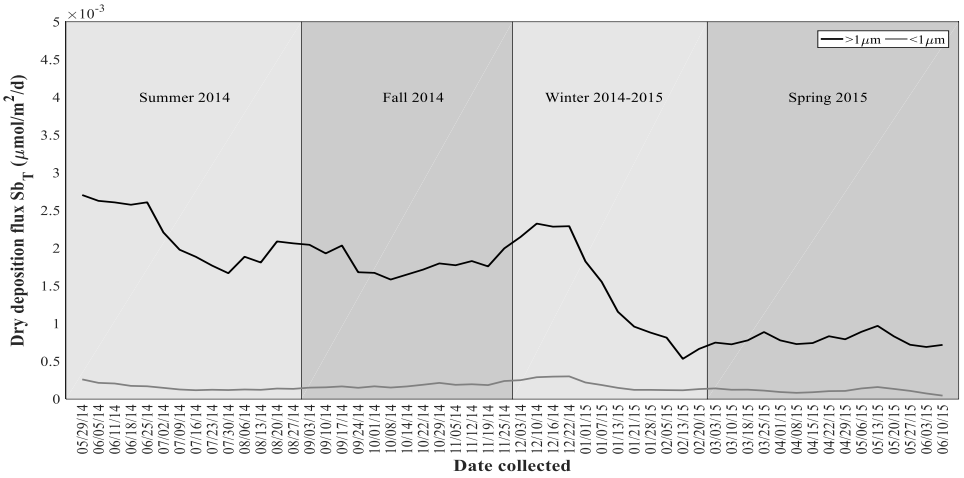

(c) Aerosol antimony fractional solubility from Eastern Shore samples - smoothed

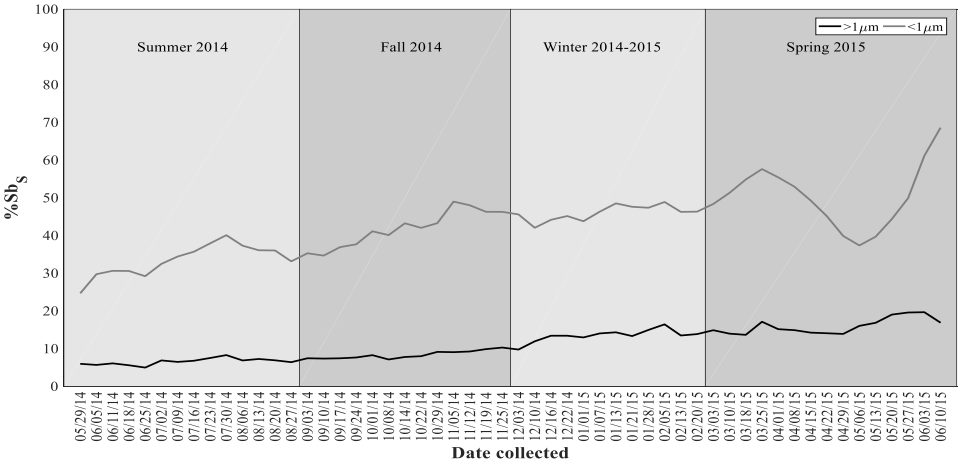

Figure 55. Smoothed seasonal dry deposition fluxes of (a) soluble antimony (Sb_S, μmol/m^2/d), (b) total antimony (Sb_T, μmol/m^2/d), and (c) fractional solubility (%Sb_S) for weekly collected Eastern Shore samples. Note that data were interpolated for dates 30 July 2014, 6 August 2014, 13 August 2014, and 20 August 2014 using the method in Section 2.6.

(a) Aerosol soluble antimony from Eastern Shore samples - residuals

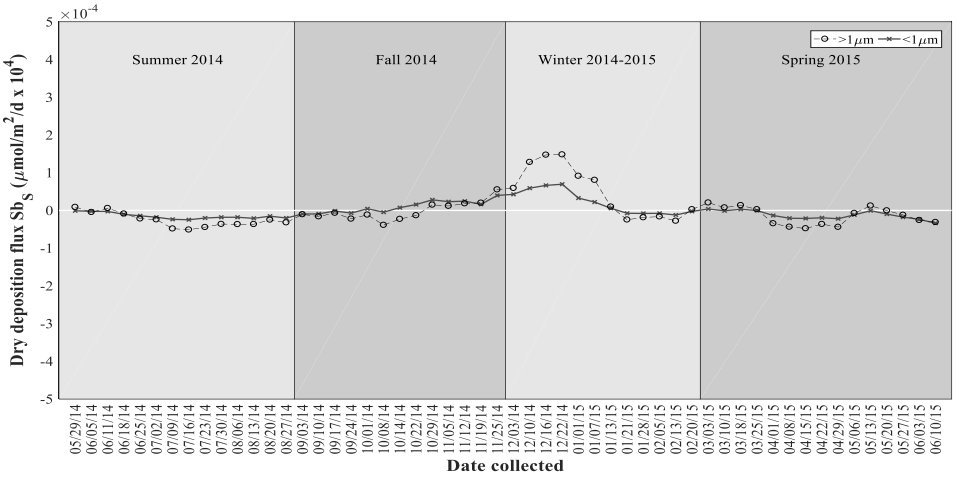

(b) Aerosol total antimony from Eastern Shore samples - residuals

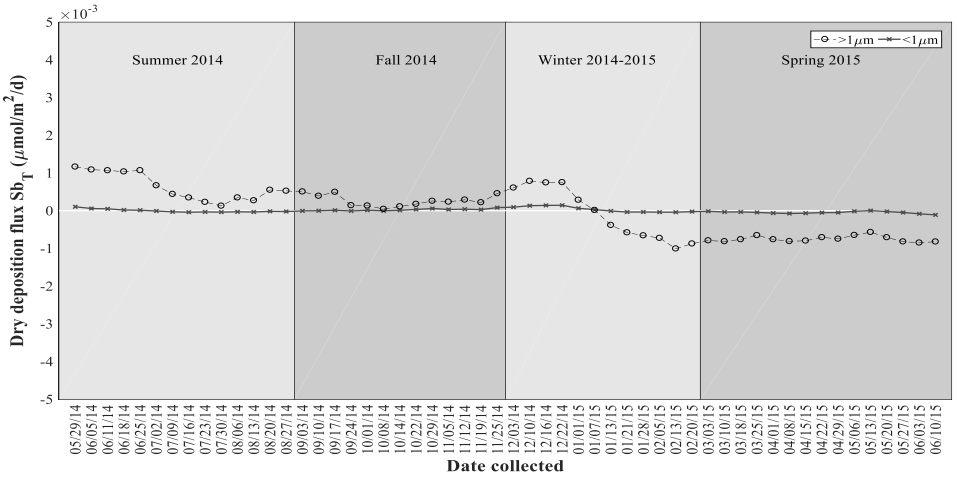

(c) Aerosol antimony fractional solubility from Eastern Shore samples - residuals

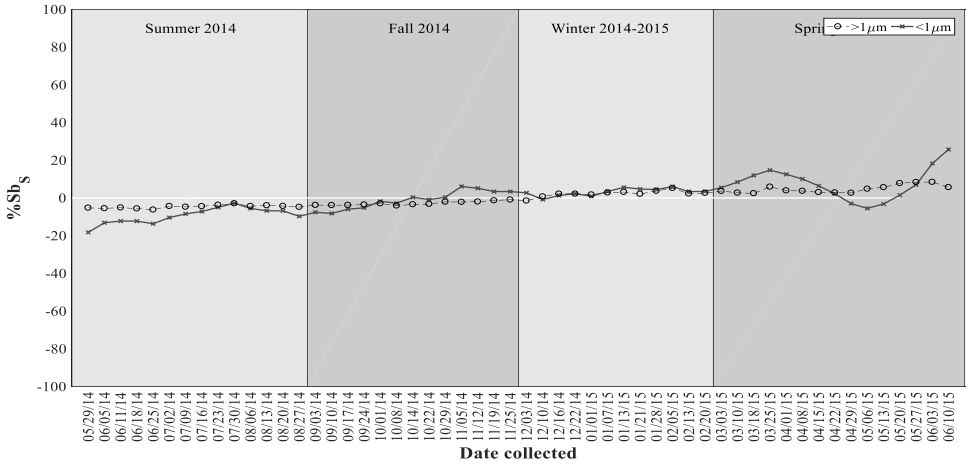

Figure 56. Residuals of dry deposition fluxes of (a) soluble antimony (Sb_S, μmol/m^2/d), (b) total antimony (Sb_T, μmol/m^2/d), and (c) fractional solubility (%Sb_S) for weekly collected Eastern Shore samples. Note that data were interpolated for dates 30 July 2014, 6 August 2014, 13 August 2014, and 20 August 2014 using the method in Section 2.6. The white horizontal line indicates the annual mean flux.

There were no significant differences between the means of the dry fine Sb_S fluxes ($p = 0.0269$, $df = 49$, $F = 3.35$) and between the means of the dry coarse Sb_S fluxes ($p = 0.344$, $df = 49$, $F = 1.14$) for the four seasons. The overall mean dry coarse Sb_S flux ($1.55 \times 10^{-4} \pm 0.779 \times 10^{-4}$ μmol/m^2/d) was found to be significantly greater ($p < 0.0001$, $df = 49.1$, $tstat = -57.8$) than the overall mean dry fine Sb_S flux ($6.65 \times 10^{-5} \pm 3.65 \times 10^{-5}$) (Table 12).

The mean dry fine Sb_T flux in fall ($1.76 \times 10^{-4} \pm 0.550 \times 10^{-4}$ μmol/m^2/d) was found to be significantly greater ($p = 0.02$, $df = 49$, $F = 3.61$) than that for winter ($1.98 \times 10^{-4} \pm 1.24 \times 10^{-4}$ μmol/m^2/d) (Table 13), using a one-way ANOVA and a multiple comparison test. The median dry coarse Sb_T summer flux (2.45×10^{-3} μmol/m^2/d) was significantly greater ($p < 0.0001$, $df = 48$, $F = 1.14$) than that for fall (1.73×10^{-3} μmol/m^2/d), as determined by a Kruskal-Wallis test and a multiple comparison test. A two-sample t-test indicated that the overall mean dry coarse Sb_T flux ($15.1 \times 10^{-4} \pm 8.11 \times 10^{-4}$ μmol/m^2/d) was significantly greater ($p < 0.0001$, $df = 48.1$, $tstat = -47.5$) than the overall mean fine Sb_T flux ($1.58 \times 10^{-4} \pm 0.835 \times 10^{-4}$ μmol/m^2/d) (Table 13).

The means of fine $\%Sb_S$ for both winter (45.5 ± 6.50 %) and spring (49.9 ± 11.5 %) were significantly greater than that for summer (33.4 ± 8.59 %) (Table 14), as determined by a one-way ANOVA and a multiple comparison test. A two-sample t-test indicated that the overall mean fine $\%Sb_S$ (43.4 ± 11.1 %) was significantly greater ($p < 0.0001$, $tstat = -18.0629$) than the overall mean coarse $\%Sb_S$ (11.8 ± 5.43 %) (Table 14). The means of coarse $\%Sb_S$ for both winter (14.3 ± 4.06 %) and spring (15.8 ± 5.60 %) were found to be significantly greater ($p < 0.0001$, $df = 48$, $F = 30.02$) than those for summer (6.50 ± 3.12 %) and fall (7.99 ± 2.35 %) (Table 14), using a one-way ANOVA and a multiple comparison test.

The dry flux of soluble lead (Pb_S) in the fine fraction ranged from 0.302 x 10^{-4} to 1.12 x 10^{-4} µmol/m^2/d in summer, 0.363 x 10^{-4} to 1.52 x 10^{-4} µmol/m^2/d in fall, 0.410 x 10^{-4} to 6.03 x 10^{-4} µmol/m^2/d in winter, and 0.435 x 10^{-4} to 1.78 x 10^{-4} µmol/m^2/d in spring (Table 12 and Figure 57a). The dry flux of coarse Pb_S ranged from 0.939 x 10^{-4} to 4.64 x 10^{-4} µmol/m^2/d in summer, 1.53 x 10^{-4} to 5.04 x 10^{-4} µmol/m^2/d in fall, 1.05 x 10^{-4} to 8.99 x 10^{-4} µmol/m^2/d in winter, and 1.33 x 10^{-4} to 6.52 x 10^{-4} µmol/m^2/d in spring (Table 12 and Figure 57a). Both dry fine and coarse Pb_S peaked on 16 December 2014 (Figure 57a).

The dry flux of total lead (Pb_T) in the fine fraction ranged from 0.985 x 10^{-4} to 3.39 x 10^{-4} µmol/m^2/d in summer, 0.699 x 10^{-4} to 4.41 x 10^{-4} µmol/m^2/d in fall, 1.69 x 10^{-4} to 15.0 x 10^{-4} µmol/m^2/d in winter, and 1.31 x 10^{-4} to 4.38 x 10^{-4} µmol/m^2/d in spring (Table 13 and Figure 57b). The dry flux of coarse Pb_T ranged from 8.34 x 10^{-4} to 37.0 x 10^{-4} µmol/m^2/d in summer, 12.1 x 10^{-4} to 23.3 x 10^{-4} µmol/m^2/d in fall, 7.14 x 10^{-4} to 32.5 x 10^{-4} µmol/m^2/d in winter, and 8.16 x 10^{-4} to 23.8 x 10^{-4} µmol/m^2/d in spring (Table 13 and Figure 57b). Both fine and coarse Pb_T fluxes were also elevated on 16 December 2014 (Figure 57b).

The aerosol fractional solubility of lead (%Pb_S) was relatively high for both size fractions throughout the time series (Figure 57c). The overall mean fine %Pb_S (37.6 ± 11.9 %) was higher than the overall mean coarse %Pb_S (20.4 ± 6.51 %), and ranged from 18.6 to 54.7 % in summer, 23.5 to 100 % in fall, 24.3 to 41.8 % in winter, and 24.9 to 50.4 % in spring (Table 14 and Figure 57c). The coarse %Pb_S ranged from 5.76 to 27.8 % in summer, 9.57 to 29.8 % in fall, 12.1 to 37.1 % in winter, and 9.5 to 31.1% in spring (Table 14 and Figure 57c).

(a) Aerosol soluble lead from Eastern Shore samples

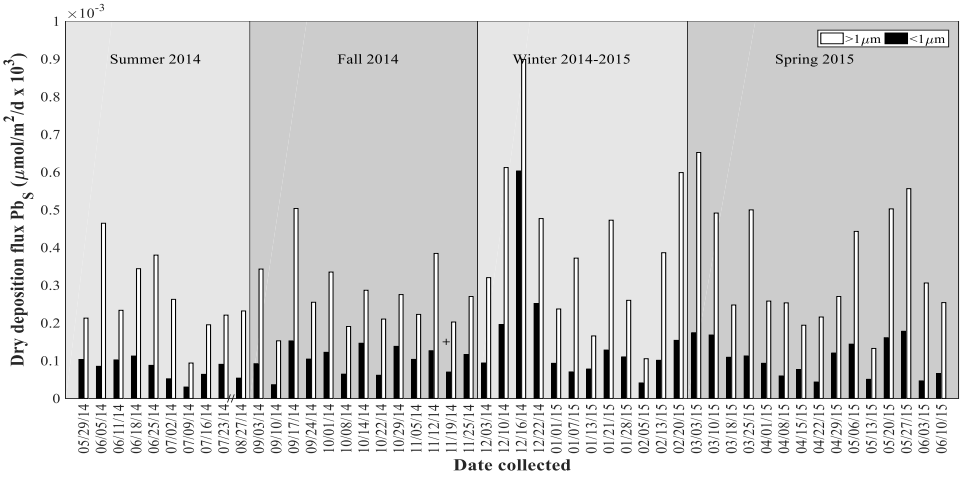

(b) Aerosol total lead from Eastern Shore samples

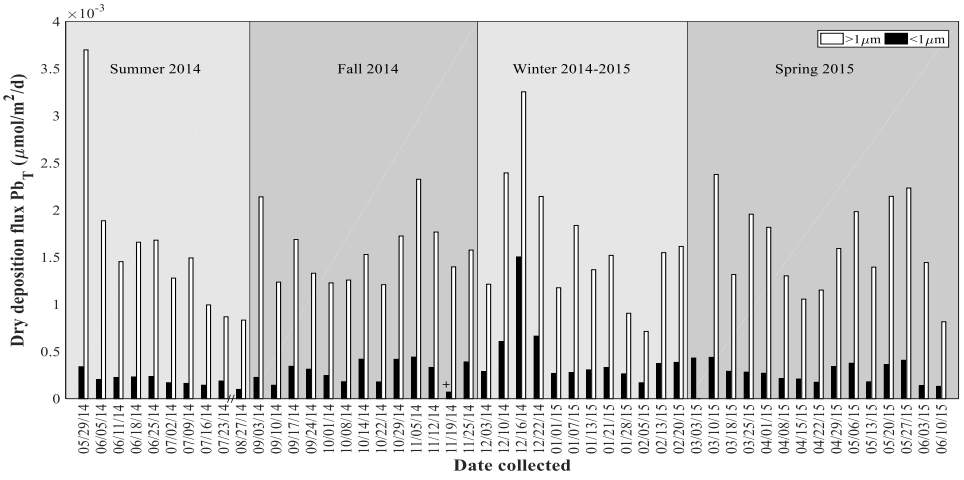

(c) Aerosol lead fractional solubility from Eastern Shore samples

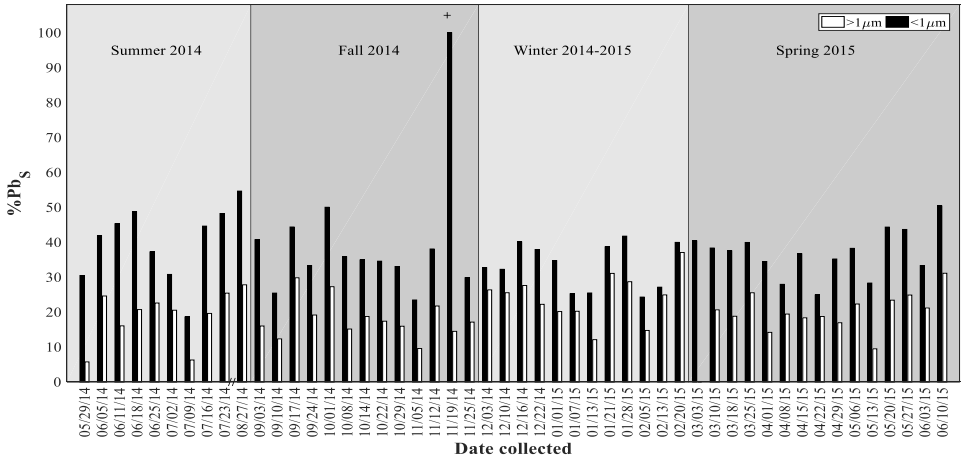

Figure 57. Seasonal dry deposition fluxes of (a) soluble lead (Pb_S, μmol/m^2/d), (b) total lead (Pb_T, μmol/m^2/d), and (c) fractional solubility (%Pb_S) for weekly collected Eastern Shore samples. "//" indicates the break in the x-axis between 07/23/14 and 08/27/14 and "+" indicates samples for which the soluble flux was set to equal the total flux as mentioned in Section 2.6.

The smoothed data and residuals plots show that the dry flux of fine and coarse Pb_S followed similar patterns throughout the time series (Figures 58a and 59a). The dry flux of fine and coarse Pb_S were both above the overall mean during winter and early spring, but remained consistently near or below this mean during other seasons (Figure 59a). The smoothed data and residuals show that the dry Pb_T flux for both size fractions was above the overall mean during early summer and early winter (Figures 58b and 59b). The smoothed data and residuals show that the fine and coarse $\%Pb_S$ followed mostly similar patterns throughout the time series (Figures 58c and 59c). Both fine and coarse $\%Pb_S$ remained at or close to the overall mean throughout the time series, except during early summer, late fall, and late spring (Figure 59c).

(a) Aerosol soluble lead from Eastern Shore samples - smoothed

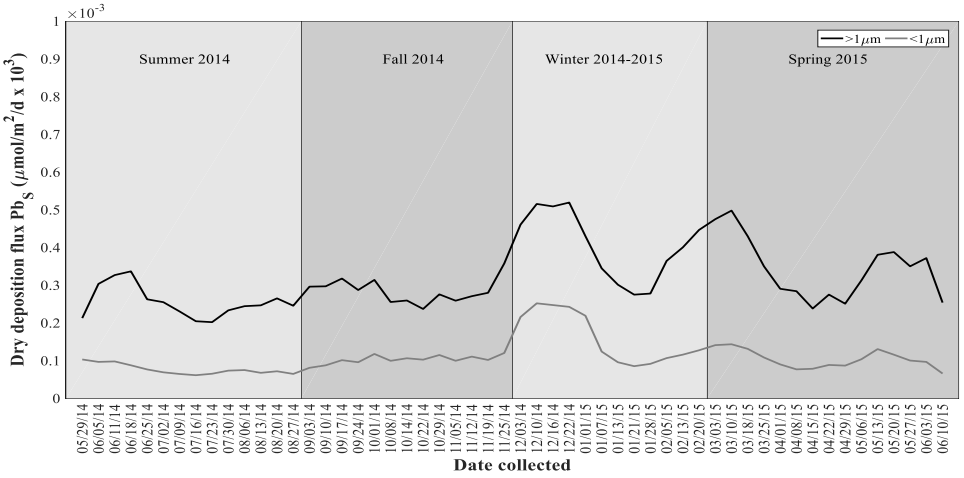

(b) Aerosol total lead from Eastern Shore samples - smoothed

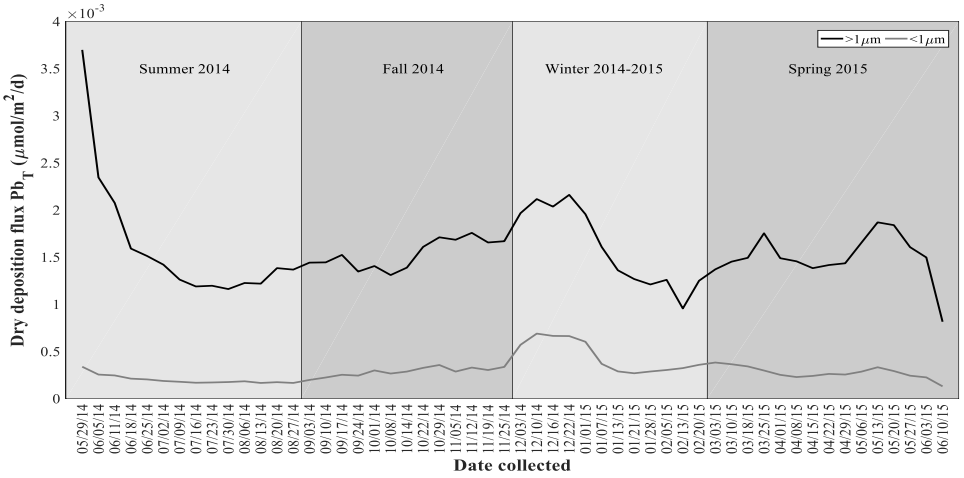

(c) Aerosol lead fractional solubility from Eastern Shore samples - smoothed

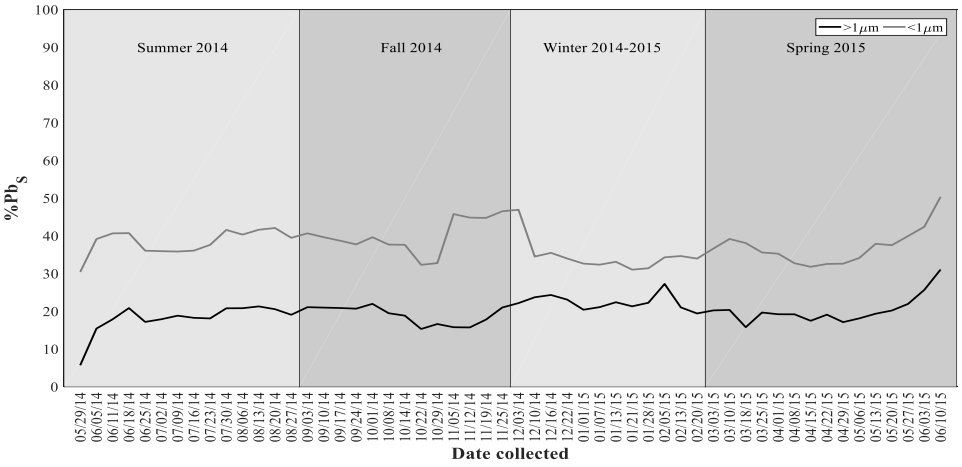

Figure 58. Smoothed seasonal dry deposition fluxes of (a) soluble lead (Pb_S, μmol/m^2/d), (b) total lead (Pb_T, μmol/m^2/d), and (c) fractional solubility (%Pb_S) for weekly collected Eastern Shore samples. Note that data were interpolated for dates 30 July 2014, 6 August 2014, 13 August 2014, and 20 August 2014 using the method in Section 2.6

(a) Aerosol soluble lead from Eastern Shore samples - residuals

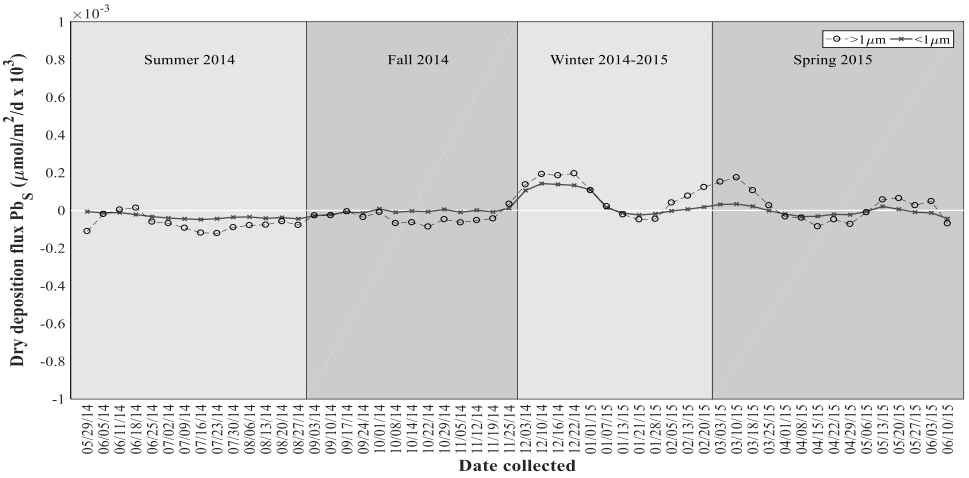

(b) Aerosol total lead from Eastern Shore samples - residuals

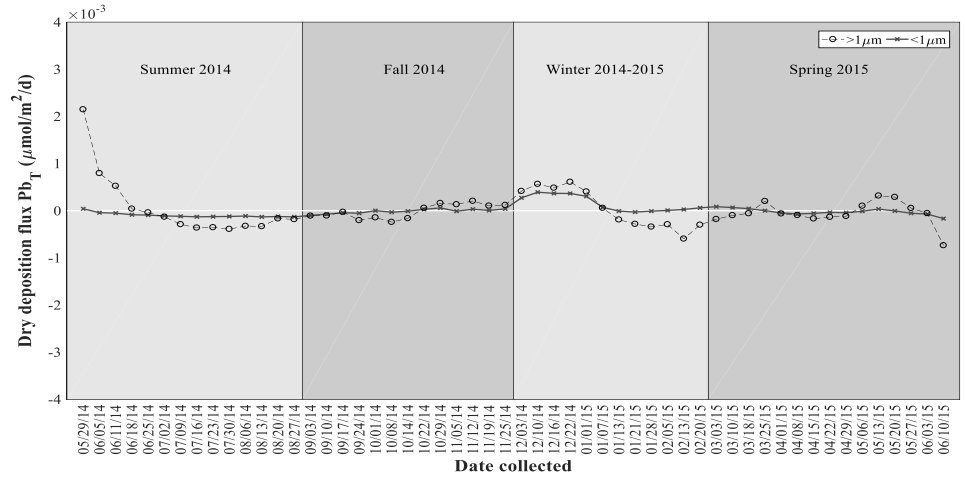

(c) Aerosol lead fractional solubility from Eastern Shore samples - residuals

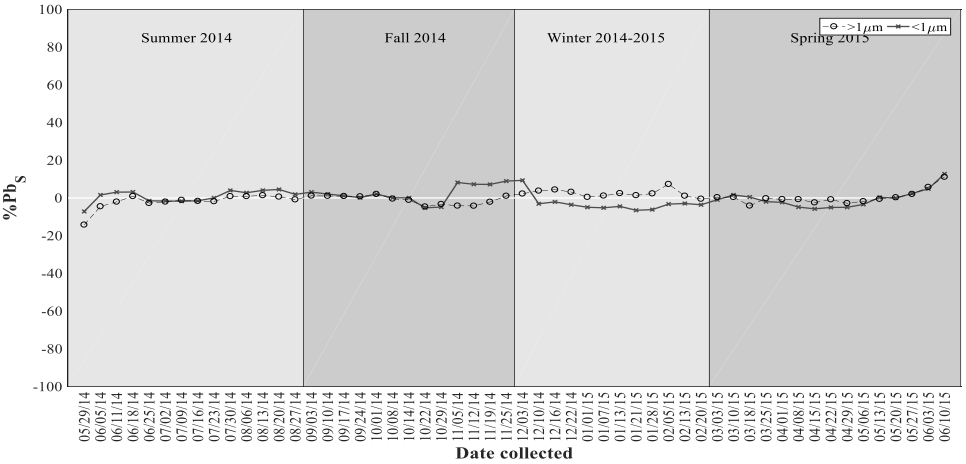

Figure 59. Residuals of dry deposition fluxes of (a) soluble lead (Pb_S, μmol/m^2/d), (b) total lead (Pb_T, μmol/m^2/d), and (c) fractional solubility (%Pb_S) for weekly collected Eastern Shore samples. Note that data were interpolated for dates 30 July 2014, 6 August 2014, 13 August 2014, and 20 August 2014 using the method in Section 2.6. The white horizontal line indicates the annual mean flux.

There were no significant differences between the means of the dry fine Pb_S flux ($p = 0.1664$, $df = 49$, $F = 1.77$) and between the means of dry coarse Pb_S flux ($p = 0.2146$, $df = 49$, $F = 1.55$) for the four seasons. The overall mean flux of coarse Pb_S ($3.29 \times 10^{-4} \pm 1.60 \times 10^{-4}$ μmol/m^2/d) was significantly greater ($p < 0.0001$, $df = 50.2$, $tstat = 41.8$) than the overall mean flux of fine Pb_S flux ($1.13 \times 10^{-4} \pm 0.840 \times 10^{-4}$ μmol/m^2/d) (Table 12), as determined by a two-sample t-test.

The mean dry fine Pb_T flux for winter ($4.53 \times 10^{-4} \pm 3.60 \times 10^{-4}$ μmol/m^2/d) was found to be significantly greater ($p = 0.0166$, $df = 49$, $F = 3.78$) than that for summer ($1.99 \times 10^{-4} \pm 0.652 \times 10^{-4}$ μmol/m^2/d) (Table 13), using a one-way ANOVA and a multiple comparison test. The medians of dry coarse Pb_T for the four seasons were not significantly different ($p = 0.9314$, $df = 48$, $F = 0.44$). A two-sample t-test indicated that the overall mean coarse Pb_T flux ($15.7 \times 10^{-4} \pm 6.15 \times 10^{-4}$ μmol/m^2/d) was significantly greater ($p < 0.0001$, $df = 53.3$, $tstat = 38.6$) than that for dry fine Pb_S ($3.07 \times 10^{-4} \pm 2.11 \times 10^{-4}$ μmol/m^2/d) (Table 13).

The mean fine $\%Pb_S$ for summer (40.1 ± 10.8 %) was significantly different from those for winter (33.4 ± 6.47 %) and spring (36.9 ± 6.70 %) (Table 14). The medians of coarse $\%Pb_S$ were not significantly different for the four seasons ($p = 0.0891$, $df = 48$, $chi\text{-}sq = 6.51$). A Wilcoxon rank sum test indicated that there was a significant difference in the median $\%Pb_S$ values for the two size fractions ($p < 0.0001$, $zval = -8.00$).

The Eastern Shore dry deposition data show that the flux of soluble trace metals was greater for the coarse particles than for fine particles in all seasons (Table 12). The dry flux of soluble Ti was below the detection limit 0.28 μg L^{-1} (Table 3) during winter (Table 12), and data obtained for the total flux showed that this season had the lowest flux of dry coarse Ti (Table 13). Dry deposition was the dominant aeolian flux of all trace metals, except for Cr, Ni, and Cd (Table 15). Wet deposition accounted for almost all atmospheric Ni delivered to the Eastern Shore site (Table 15). The total-dissolvable wet deposition samples may underestimate trace metal concentrations since rainwater samples were only acidified to pH 1.7 with ultrapure HCl, whereas more aggressive acid-digestion would have been more efficient at dissolving particulate material in the sample, yielding higher trace metal concentrations.

Table 15. Comparison of wet (total-dissolvable) and total dry deposition fluxes for trace metals at the Eastern Shore field station ($mg/m^2/yr$).

Trace metal	Dry deposition flux ($mg/m^2/yr$)	Wet deposition flux ($mg/m^2/yr$)	Estimated total (wet+dry) flux ($mg/m^2/yr$)	Estimated wet deposition percentage of total (%)
Al	44.3	11.4	55.7	20.5
Ti	3.48	0.224	3.70	6.04
V	0.125	0.0483	0.173	27.9
Cr	0.0118	0.0304	0.0422	72.0
Mn	0.851	0.403	1.25	32.1
Fe	28.6	7.57	36.2	20.9
Co	0.0137	0.00469	0.0183	25.5
Ni	0.0843	7.50	7.58	98.9
Cu	0.489	0.0974	0.586	16.6
Zn	0.959	0.487	1.45	33.7
Cd	0.00522	0.00927	0.0145	64.0
Sb	0.0687	0.0219	0.091	24.2
Pb	0.142	0.0321	0.174	18.4

3.5 EMPIRICAL ORTHOGONAL FUNCTION ANALYSIS OF AEROSOL TOTAL TRACE METAL FLUXES

An EOF analysis was conducted using the dry total trace metal fluxes estimated from aerosol samples collected from the Eastern Shore site. The first five EOF modes were significant as eigenvalues of 0.442, 0.202, 0.0946, 0.0603, and 0.0438 were obtained. These modes represent 44.2%, 20.2%, 9.5%, 6.0%, and 4.4% of the total variance, respectively.

The EOF mode 1 accounted for 44.2 % of the total variance. Thirteen variables (50% of the variables) were associated with EOF mode 1 (Figure 60a and Appendix G). These variables were the dry fluxes of total fine Ti, coarse Ti, fine V, coarse V, fine Fe, coarse Fe, fine Co, coarse Co, fine Al, coarse Al, fine Mn, coarse Mn, and coarse Ni. Both size fractions of these trace metals exhibited this pattern, except for Ni, for which EOF mode 1 only explained the variance of the dry total flux for the coarse fraction. The eigenfunction values for all EOF mode 1 trace metal variables (dry fine Ti, coarse Ti, fine V, coarse V, fine Fe, coarse Fe, fine Co, coarse Co, fine Al, coarse Al, fine Mn, coarse Mn, and coarse Ni) were positive, indicating that the total fluxes of these variables increased above the mean during the sample periods identified by the flux time mode plot (Figure 60b). The dry total fluxes of all EOF mode 1 trace metal variables increased above the mean four times during the time series, on 9 July 2014, 3 September 2014, 5 November 2014, and 13 May 2015 (Figure 60b), suggesting that these aerosol trace metal variables have similar sources.

Five-day NOAA HYSPLIT air mass back trajectories (AMBTs) (Figure 61 a-d) for the Eastern Shore field station indicated that air masses sampled on 9 July 2014, 3 September 2014, 5 November 2014, and 13 May 2015 were likely influenced by aeolian dust transported across the North Atlantic during Saharan dust events (Figure 61a and b) or agricultural activities in the continental U.S. (Figure 61c and d). The AMBTs for 9 July 2014, 3 September 2014, and 13 May 2015 (Figure 61 a and b) were consistent with the transport of Saharan dust across the North Atlantic, which typically occurs during the warmer summer months (~May-September) [Jickells et al., 1999; Kaufman et al., 2005; Tian et al., 2008; Sholkovitz et al., 2009]. The Saharan mineral dust is transported westward across the North Atlantic by

prevailing easterly winds [Jickells et al., 2005; Ussher et al., 2013], and sometimes north by the anticyclone over the Azores [Kaufman et al., 2005]. The seasonal migration of the Intertropical Convergence Zone (ITCZ) influences the latitudinal region of maximum dust transport [Shelley et al., 2017], as this zone shifts northwards from between 0° and 10°N during the Northern Hemisphere winter to between 10° and 20°N during the Northern Hemisphere summer [Moulin et al., 1997; Jickells, 1999; Barrett et al., 2012]. The northward migration of the ITCZ coupled with the occurrence of Bermuda-Azores high pressure systems guides the pulses of Saharan dust across the North Atlantic [Jickells, 1999; Tian et al., 2008] during the warmer months. The AMBT for 5 November 2014 suggests that the air mass sampled passed through the southeastern U.S. before arriving at the Eastern Shore field station (Figure 61c), and was thus likely influenced by regional agricultural aerosol sources. The southeastern U.S. has been recognized as an area of intensive agricultural activity [Franzluebbers, 2005], and dry pasture soils could become entrained in the atmosphere during periods of limited vegetation coverage [Mahowald et al., 2005].

(a)

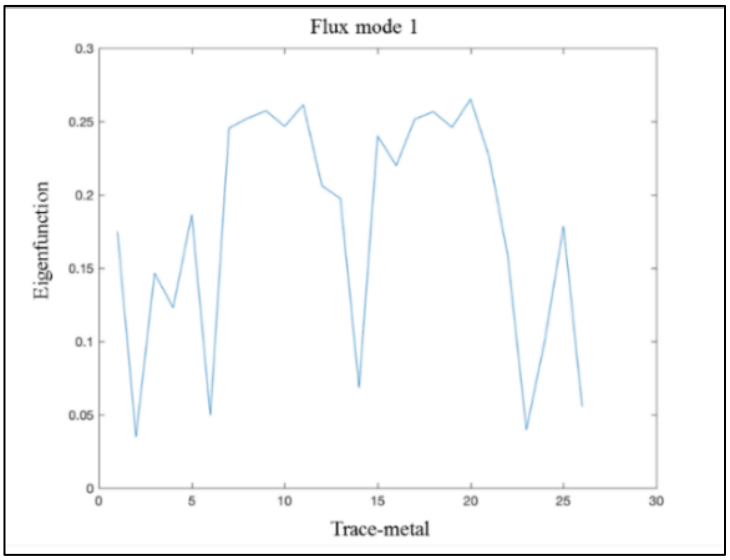

(b)

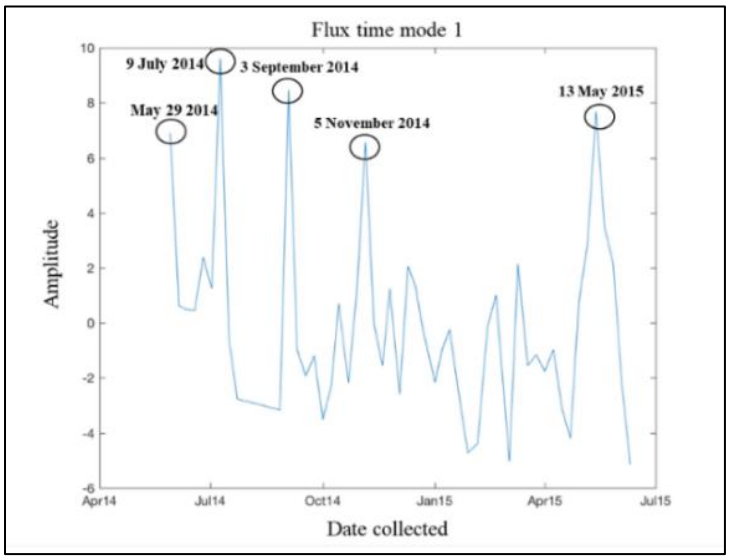

Figure 60. (a) Variance of dry total fluxes for trace metal variables associated with EOF mode 1 and (b) temporal patterns of dry deposition flux data for EOF mode 1 for Eastern Shore samples. The dates during which the dry flux of trace metals associated with this EOF mode increased are circled.

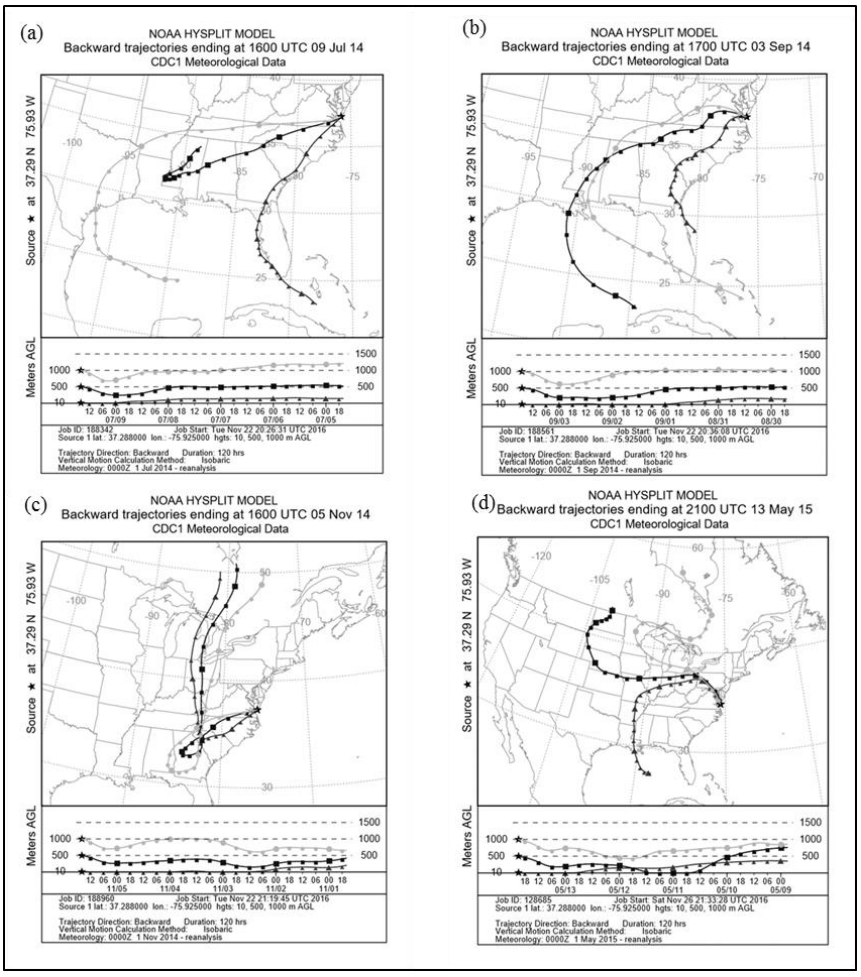

Figure 61. Five-day air mass back trajectory analyses (NOAA HYSPLIT model) with arrival heights of 10 m, 500 m, and 1000 m for the Eastern Shore field station samples collected on (a) 9 July 2014, (b) 3 September 2014, (c) 5 November 2014, and (d) 13 May 2015. These dates were associated with increases in the dry total flux of EOF mode 1 trace metals.

The trace metals associated with EOF mode 1 were likely influenced by both North African (Saharan dust) and continental North American air masses (Figure 61 a-d). These trace metals were primarily elements typically enriched in crustal material (Ti, Fe, Co, Mn, and Al) [Scudlark et al., 1994; Wu et al., 1994; Chester et al., 1999; Spokes et al., 2001; Morel and Price, 2003; Jickells et al., 2016]. The origins of atmospheric V are less readily constrained, as this element has both natural and anthropogenic sources [Duce and Hoffman, 1976]. The natural sources of V include crustal weathering and volcanic debris, while combustion of fossil fuels releases anthropogenic V [Duce and Hoffman, 1976;

Pacyna and Pacyna, 2001; Tian et al., 2008]. Both V and Ni are enriched in oil combustion products [Wu et al., 1994; Pacyna and Pacyna, 2001; Sholkovitz et al., 2009].

The enrichment factors (EFs) calculated for EOF mode 1 trace metal variables further suggest that the peaks in the total fluxes observed on 9 July 2014, 3 September 2014, 5 November 2014, and 13 May 2015 were predominantly due to crustal sources, as EFs <10 were obtained for all EOF mode 1 trace metal variables during these periods (Tables 16 and 17). The EFs for those four weeks for total fine Ti (1.98, 1.94, 2.36, and 1.82), coarse Ti (2.02, 1.81, 2.54, and 1.78), fine Mn (1.16, 1.70, 1.70, and 1.42), coarse Mn (1.51, 1.60, 2.03, and 1.76), fine Fe (1.15, 1.41, 1.10, and 1.25), coarse Fe (1.15, 1.31, 1.24, and 1.21), fine Co (1.69, 3.50, 1.74, and 1.67), and coarse Co (1.88, 2.04, 1.78, and 1.90) (Appendix H) were near unity, indicating that terrigenous material was the dominant aerosol source. The EFs for total fine V (3.54, 7.57, 3.72, and 5.66), coarse V (2.08, 2.59, 2.58, and 2.01), and coarse Ni (2.54, 5.92, 5.42, and 2.91) on 9 July 2014, 3 September 2014, 5 November 2014, and 13 May 2015 were somewhat higher, but still <10 indicating crustal sources possibly augmented by combustion emissions (Appendix H).

Box plots show that the EFs for EOF mode 1 trace metal variables were mostly between 1 and 10 throughout the time series (Figure 62 and Appendix H). The overall mean and seasonal mean EFs for fine and coarse Ti, Mn, Fe, and Co were below 5 (Tables 16 and 17). The overall mean and seasonal mean EFs for coarse V and Ni were ~3.5-9.4 (Tables 16 and 17). However, for fine V the overall mean and seasonal mean EFs were somewhat higher at ~8-20 (Tables 16 and 17). The difference in the EFs for fine and coarse V likely reflects the relative contributions of anthropogenic and natural sources to each size fraction, with the anthropogenic material enriched in the finer size fraction.

(a)

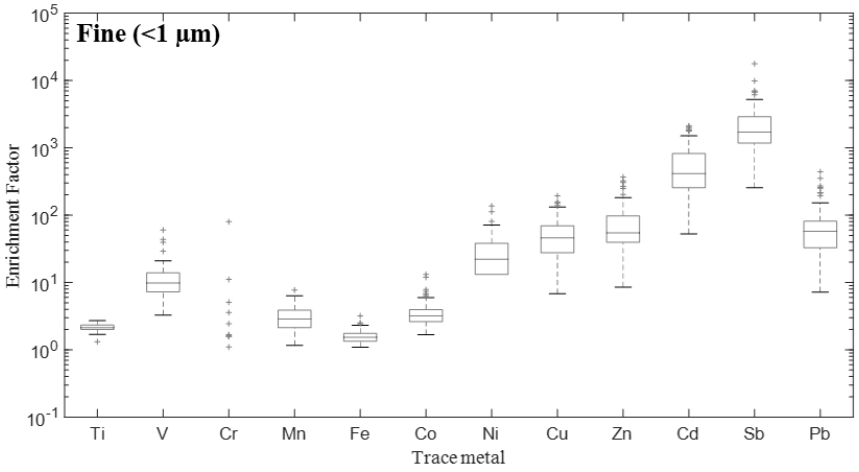

(b)

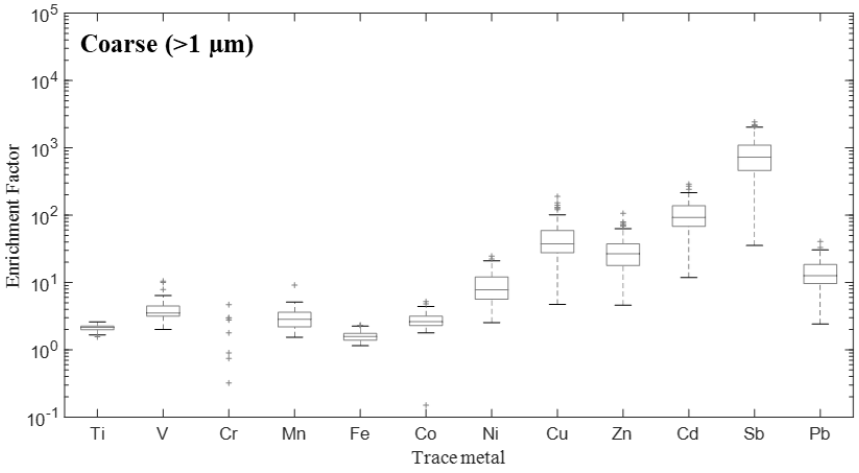

Figure 62. Box plots of enrichment factors (EFs; normalized to Al) for (a) fine (<1 µm) and (b) coarse (>1 µm) fractions of total Ti, V, Cr, Mn, Fe, Co, Ni, Cu, Zn, Cd, Sb, and Pb from Eastern Shore aerosol samples. The center line of each box is the median EF, and the bottom and top edges of the box represent the 25th and 75th percentiles, respectively. The whiskers extend to the highest and lowest data points that are not considered outliers and outliers are indicated by the '+' symbol.

Table 16. Mean (± standard deviation) and range (in parentheses) enrichment factors for total trace metal concentrations in Eastern Shore fine (<1 μm) aerosol samples.

	Ti	V	Cr	Mn	Fe	Co
Summer 2014	2.11 ± 0.354	12.3 ± 5.43	0.560 ± 0.931	2.05 ± 0.554	1.35 ± 0.181	3.18 ± 0.771
	(1.32 - 2.60)	(3.54 – 21.0)	(0 - 2.44)	(1.16 - 3.12)	(1.15 - 1.79)	(1.69 - 4.45)
Fall 2014	2.25 ± 0.238	11.6 ± 6.68	0.792 ± 1.67	3.16 ± 1.02	1.54 ± 0.21	3.62 ± 1.15
	(1.85 - 2.71)	(3.26 - 29.1)	(0 - 5.09)	(1.64 - 4.70)	(1.10 - 1.84)	(1.74 - 6.72)
Winter 2014 - 2015	2.09 ± 0.240	20.2 ± 17.6	7.57 ± 22.9	4.48 ± 1.75	1.98 ± 0.557	6.25 ± 3.47
	(1.82 - 2.66)	(5.04 - 60.1)	(0 – 80.0)	(2.31 - 7.74)	(1.30 - 3.20)	(2.54 - 13.1)
Spring 2015	2.13 ± 0.211	8.04 ± 3.97	0.185 ± 0.500	2.79 ± 0.870	1.53 ± 0.175	2.69 ± 1.03
	(1.70 - 2.39)	(4.06 - 19.6)	(0 - 1.68)	(1.42 - 4.46)	(1.25 - 1.81)	(1.67 - 5.97)
Overall mean	2.15 ± 0.259	12.7 ± 10.5	2.19 ± 11.3	3.14 ± 1.39	1.60 ± 0.382	3.89 ± 2.32

	Ni	Cu	Zn	Cd	Sb	Pb
Summer 2014	27.8 ± 12.7	32.0 ± 14.8	43.0 ± 21.5	266 ± 127	1620 ± 898	36.4 ± 18.6
	(5.54 - 45.8)	(8.50 - 57.3)	(8.54 - 79.9)	(52.8 - 520)	(403 - 3676)	(7.20 - 70.7)
Fall 2014	26.4 ± 17.8	52.0 ± 29.9	67.6 ± 32.8	548 ± 458	2510 ± 1770	69.8 ± 55.3
	(0 - 71.3)	(18.3 - 120)	(26.9 - 141)	(119 - 1505)	(794 - 7023)	(13.5 - 216)
Winter 2014 - 2015	51.6 ± 40.5	105 ± 53.9	198 ± 112	1380 ± 688	5510 ± 4780	190 ± 133
	(9.74 - 137)	(29.3 - 193)	(51.9 - 370)	(324 - 2104)	(684 - 17775)	(35.6 - 442)
Spring 2015	14.5 ± 8.91	41.2 ± 21.7	66.1 ± 50.0	420 ± 291	1300 ± 671	60.3 ± 35.6
	(7.11 - 42.1)	(6.81 - 89.8)	(15.2 - 202)	(81.3 - 1296)	(225 - 2563)	(10.9 - 152)
Overall mean	29.2 ± 26.2	57.5 ± 42.6	93.5 ± 86.6	653 ± 604	2690 ± 2990	89.0 ± 92.2

Table 17. Mean (± standard deviation) and range (in parentheses) enrichment factors for total trace metal concentrations in Eastern Shore coarse (>1 μm) aerosol samples.

	Ti	V	Cr	Mn	Fe	Co
Summer 2014	2.10 ± 0.25	3.71 ± 1.21	1.09 ± 1.58	2.31 ± 0.657	1.42 ± 0.173	2.34 ± 0.309
	(1.56 - 2.51)	(2.08 - 6.27)	(0 - 4.68)	(1.54 - 3.74)	(1.15 - 1.80)	(1.88 - 2.87)
Fall 2014	2.52 ± 0.252	3.57 ± 0.731	0.457 ± 1.16	3.12 ± 0.948	1.61 ± 0.291	2.62 ± 0.436
	(1.81 - 2.59)	(2.58 - 5.24)	(0 - 2.99)	(1.60 - 4.89)	(1.24 - 2.31)	(1.78 - 3.26)
Winter 2014 - 2015	2.18 ± 0.187	5.82 ± 2.25	–	4.12 ± 1.78	1.94 ± 0.335	3.60 ± 1.36
	(1.86 - 2.60)	(3.53 - 10.5)	–	(2.42 - 9.13)	(1.34 - 2.31)	(0.150 - 5.20)
Spring 2015	2.00 ± 0.206	3.50 ± 1.38	0.0229 ± 0.0860	2.55 ± 0.492	1.55 ± 0.189	2.61 ± 0.544
	(1.66 - 2.39)	(2.01 - 7.87)	(0 - 0.321)	(1.69 - 3.38)	(1.21 - 1.88)	(1.90 - 3.92)
Overall mean	2.13 ± 0.240	4.13 ± 1.73	0.350 ± 0.978	3.04 ± 1.26	1.64 ± 0.312	2.80 ± 0.891
	Ni	Cu	Zn	Cd	Sb	Pb
Summer 2014	7.10 ± 2.69	28.4 ± 15.2	17.9 ± 8.57	84.2 ± 33.9	778 ± 331	9.45 ± 4.45
	(2.54 - 11.9)	(6.33 - 53.8)	(4.60 - 31.9)	(22.3 - 144.2)	(260 - 1254)	(2.68 - 19.2)
Fall 2014	8.67 ± 3.33	38.0 ± 16.6	27.5 ± 9.05	98.3 ± 43.0	924 ± 346	13.4 ± 4.90
	(5.45 - 16.9)	(11.8 - 73.1)	(11.8 - 42.5)	(40.8 - 204)	(491 - 1615)	(5.32 - 24.3)
Winter 2014 - 2015	15.4 ± 5.78	98 .1 ± 50.7	60.3 ± 23.4	193 ± 64.3	1400 ± 749	25.8 ± 8.31
	(5.22 - 24.6)	(28.7 - 189)	(26.7 - 106)	(69.3 - 289)	(416 - 2418)	(11.1 - 40.6)
Spring 2015	6.50 ± 3.49	42.9 ± 32.0	21.9 ± 10.7	73.3 ± 29.4	375 ± 184	11.6 ± 4.45
	(2.91 - 16.9)	(4.73 - 131)	(7.81 - 46.9)	(11.8 - 131)	(35.4 - 728)	(2.42 - 18.2)
Overall mean	9.37 ± 5.26	52.1 ± 41.3	32.0 ± 21.6	111 ± 64.4	853 ± 575	15.1 ± 8.39

The EOF mode 2 accounted for 20.2 % of the total variance. Eight variables were associated with EOF mode 2 (Figure 63a and Appendix G). These variables were the dry total fluxes of coarse Al, fine Pb, coarse Pb, fine Zn, fine Sb, fine Cd, fine Cu, and coarse Cu. Both size fractions of Cu and Pb were associated with EOF mode 2 (Figure 63a). The EOF mode 2 eigenfunction value for dry coarse Al was positive indicating that the total flux for this variable increased, on 9 July 2014 and 13 May 2015, and decreased on 16 December 2014 (Figure 63b and Appendix H). The eigenfunction values for all other EOF mode 2 trace metal variables were negative (Appendix G), and therefore the total fluxes of these variables changed in the opposite direction to that shown in the flux time mode plot for EOF mode 2 (Figure 63b). The total fluxes for fine Pb, coarse Pb, fine Zn, fine Sb, fine Cd, fine Cu, and coarse Cu declined, on 9 July 2014 and 13 May 2016, and peaked on 16 December 2014 (Appendix H). These results suggest that the source of aerosol coarse Al is likely different from that for all other EOF mode 2 trace metal variables.

Five-day NOAA HYSPLIT AMBTs for the Eastern Shore field station suggest that trace metal variables for EOF mode 2 were more closely associated with continental North America air masses than trace metal variables associated with EOF mode 1 (Figure 64 a-c). The trace metal variables associated with EOF mode 2 were likely influenced by anthropogenic emissions, as air masses sampled on 9 July 2014, 13 May 2016, and 16 December 2014 were associated with continental North American air masses. Sources of aerosol Zn include biomass burning, fossil fuel combustion, power generation, metal mining, and steel galvanization [Spokes et al., 2001; Pacyna and Pacyna, 2001]. Zinc, Cd, Sb, and Pb are emitted from incinerators [Wu et al., 1994]. Antimony is released from the combustion of coal in electric power plants [Pacyna and Pacyna, 2001; Zhou et al., 2015], nonferrous metal production, steel production, waste incineration, and vehicle brake wear [Zhou et al., 2015; Sanchez et al., 2017]. Both Cd and Pb are emitted by motor vehicles [Wu et al., 1994]. Although crustal dust is the dominant source of aerosol Al, this element also is released from coal combustion [Wu et al., 1994].

The EFs for total fine Pb (7.20, 442, and 10.9), coarse Pb (2.68, 40.6, and 2.42), fine Cu (8.50, 99.0, and 6.81), coarse Cu (6.33, 101, and 4.72), fine Sb (403, 5220, and 272) and fine Cd (52.8, 1790,

and 81.3), on 9 July 2014, 13 May 2015, and 16 December 2014, respectively, were relatively low when the total flux decreased below the mean, on 9 July 2014 and 13 May 2015, and relatively high when the total flux peaked above the mean, on 16 December 2014 (Appendix H). This suggests that aerosol sources for 9 July 2014 and 13 May 2015 were different from that of 16 December 2014. All seasonal mean EFs, except that for coarse Pb during summer, were >10, indicating that aerosol samples were likely enriched with anthropogenic emissions containing EOF mode 2 trace metals (Tables 16 and 17). The mean EF for coarse Pb during summer was 9.45 ± 4.45, close to 10. The range of EFs for coarse Pb varied widely from 2.68 to 19.2 (Tables 16 and 17). The overall mean EFs for all EOF mode 2 trace metal variables were >10 (Tables 16 and 17), indicating that anthropogenic emissions contributed to the maxima of these trace metal variables.

(a)

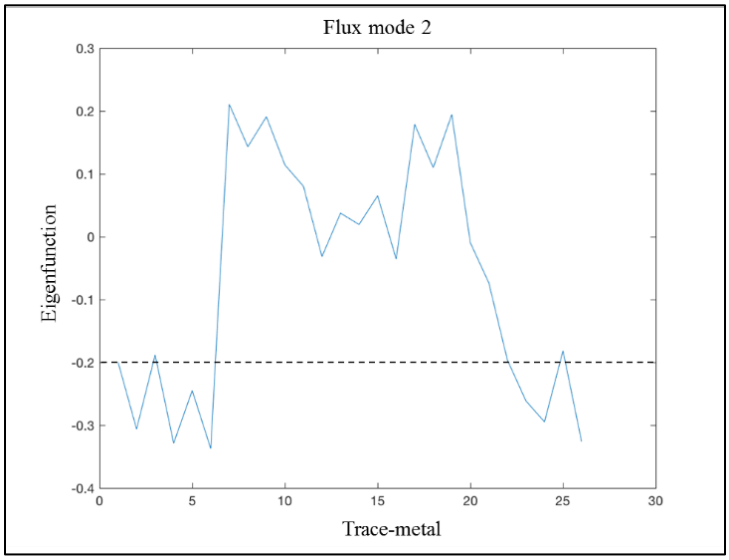

(b)

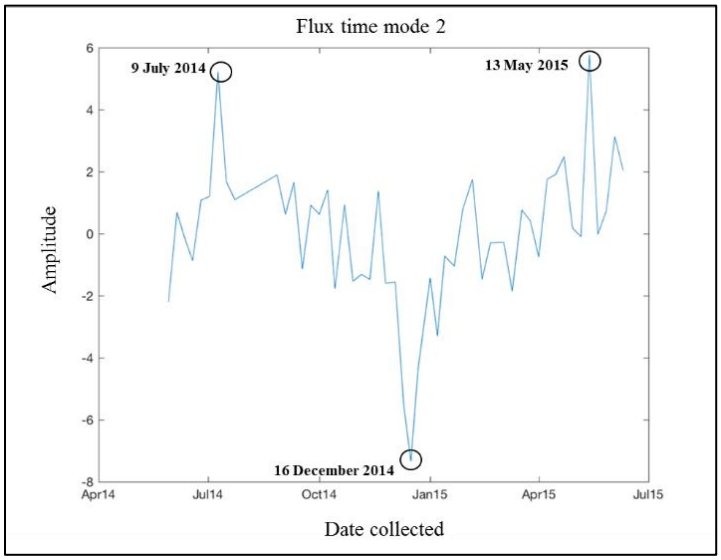

Figure 63. (a) Variance of dry total fluxes for trace metal variables associated with EOF mode 2 and (b) temporal patterns of total dry deposition flux data for EOF mode 2 for Eastern Shore samples. The dates during which the dry flux of trace metals associated with this EOF mode peaked and declined are circled.

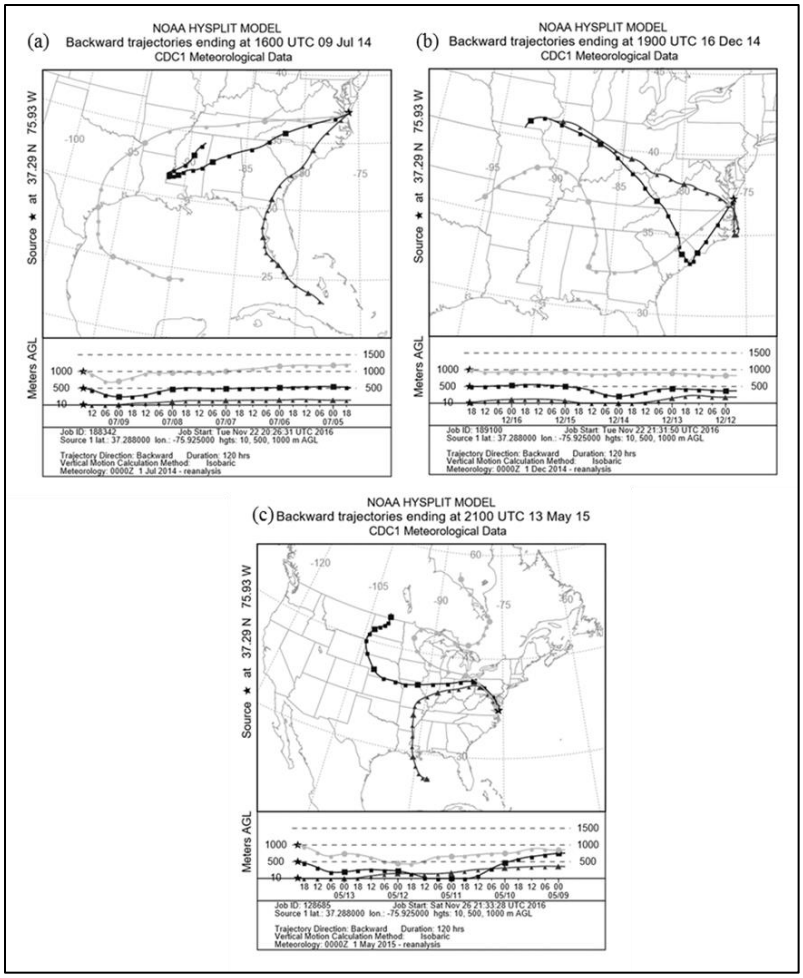

Figure 64. Five-day air mass back trajectory analyses (NOAA HYSPLIT model) with arrival heights of 10 m, 500 m and 1000 m for the Eastern Shore field station on (a) 9 July 2014, (b) 16 December 2014, and 13 May 2014. These dates were associated with peaks (a, c) and declines (b) in the flux of trace metals in EOF mode 2.

The EOF mode 3 accounted for 9.5% of the total variance. Ten variables were associated with EOF mode 3 (Figure 65a and Appendix G). These variables were the dry total fluxes of fine Al, fine Ti, fine Mn, fine Fe, coarse Ni, fine Cu, fine Zn, fine Cd, coarse Cd, and coarse Sb (Appendix G). Both size fractions of Cd were associated with EOF mode 3. The eigenfunction values for dry fine Al, Ti, Mn, Fe, Cu, Zn, and Cd were positive (Appendix G), indicating that the total fluxes of these trace metal variables peaked above the mean, on 5 November 2014, 13 January 2015, 3 March 2015, and 29 April 2015 (Figure 65b), and declined below the mean on 3 September 2014 and 10 December 2014 (Figure 65b). The eigenfunction values for the dry coarse fraction of Ni, Cd, and Sb were negative (Appendix G), indicating that the total fluxes of these trace metal variables declined below the mean, on 5 November 2014, 13 January 2015, 3 March 2015, and 29 April 2015 (Figure 65b), and peaked above the mean on 3 September 2014 and 10 December 2014 (Figure 65b). This suggests that there were different sources for the two groups of trace metal variables associated with EOF mode 3.

Five-day NOAA HYSPLIT AMBTs for the Eastern Shore field station indicated that air masses sampled during 3 September 2014, 5 November 2014, 10 December 2014, 13 January 2015, 3 March 2015, and 29 April 2015 (Figures 66 a-d and 67 a-b) did not have a common source, and likely contained both crustal and anthropogenic materials, suggesting multiple sources may contribute to the peaks and declines noted for EOF mode 3.

The EFs for the total fluxes of fine Ti, Mn, and Fe were <10, on 3 September 2014, 5 November 2014, 10 December 2014, 13 January 2015, 3 March 2015, and 29 April 2015 (Appendix H), suggesting a predominantly crustal source during these periods. The seasonal means and overall mean EFs for these EOF mode 3 trace metals were <5 (Table 16), further indicating a predominantly crustal source. However, the EFs for the total fluxes of fine Cu, Zn, and Cd were >10 (Appendix H), on 3 September 2014, 5 November 2014, 10 December 2014, 13 January 2015, 3 March 2015, and 29 April 2015 (Appendix H), suggesting anthropogenic sources of these EOF mode 3 trace metal variables during these periods. The seasonal mean and overall mean EFs for fine Cu, Zn, and Cd were >10 (Table 16), also indicated that anthropogenic emissions were a significant source of the dry fine Cu, Zn, and Cd

throughout the sampling period. The EFs for the dry coarse Ni varied widely and were <10, on 5 November 2014, 13 January 2015, and 29 April 2015, when the total flux decreased below the mean but >10, on 10 December 2014, when the total flux increased above the mean (Appendix H). The seasonal mean EFs for dry coarse Ni were <10 for summer, fall, and spring, but >10 during winter (Table 17) suggesting mixed sources. Also, the overall mean EF for dry coarse Ni was <10 (Table 17). The EFs for dry coarse Cd and coarse Sb were consistently >10 (Table 16), indicating that these trace metals were influenced by anthropogenic emissions.

(a)

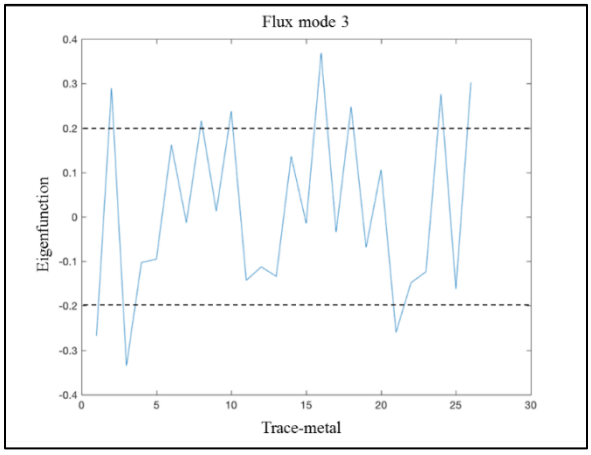

(b)

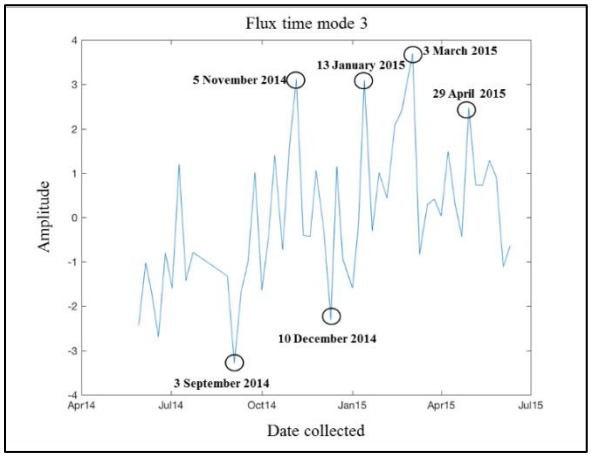

Figure 65. (a) Variance of dry total fluxes for trace metal variables associated with EOF mode 3 and (b) temporal patterns of total dry deposition flux data for EOF mode 3. The dates during which the dry flux of trace metals associated with this EOF mode peaked and declined are circled.

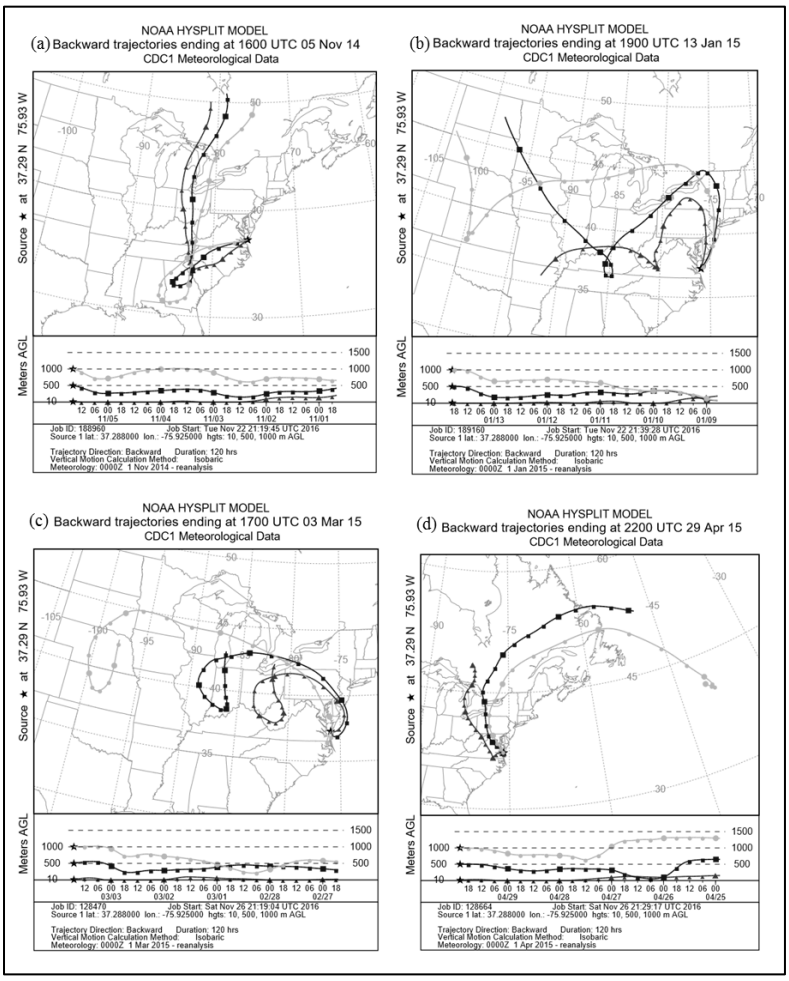

Figure 66. Five-day air mass back trajectory analyses (NOAA HYSPLIT model) with arrival heights of 10 m, 500 m and 1000 m for the Eastern Shore field station on (a) 5 November 2014, (b) 13 January 2015, (c) 3 March 2015, and (d) 29 April 2015. These sample collection dates were associated with elevated fluxes of trace metals in EOF mode 3.

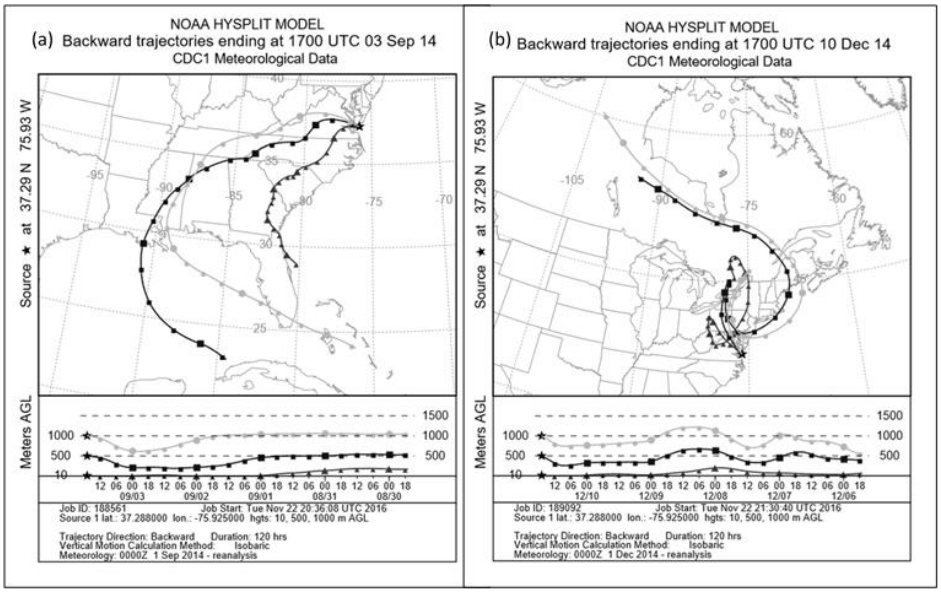

Figure 67. Five-day air mass back trajectory analyses (NOAA HYSPLIT model) with arrival heights of 10 m, 500 m, and 1000 m for the Eastern Shore field station on (a) 3 September 2014 and (b) 10 December 2014. These sample collection dates were associated with declines in fluxes of trace metals in EOF mode 3.

The EOF mode 4 accounted for 6.0% of the variance. Seven variables were associated with EOF mode 4 (Figure 68a and Appendix G). These variables were dry total fluxes of fine V, coarse Cr, fine Cr, coarse Mn, fine Ni, coarse Cu, and coarse Zn. The eigenfunction values of coarse Mn, coarse Cu, and coarse Zn were positive indicating that the dry total fluxes of these trace metal variables peaked above the mean, on 7 January 2015 and 1 April 2015, and declined below the mean, on 20 February 2015 and 3 March 2015 (Appendix G). The eigenfunction values of fine Cr, fine Ni, fine V, and coarse Cr were negative indicating that the dry total fluxes of these variables declined below the mean, on 7 January 2015 and 1 April 2015, and peaked above the mean, on 20 February 2015 and 3 March 2015 (Appendix G). The peaks and declines in the trace metals represented by EOF mode 4 occurred during the winter and spring of 2015. The results suggest that there were different aerosol sources for the two groups of trace metal variables for EOF mode 4.

The NOAA HYSPLIT AMBTs for the Eastern Shore field station suggest that continental North American air masses were sampled, on 7 January 2015, 20 February 2015, 3 March 2015, and 1 April 2015 (Figure 69 a-d). The EFs for dry coarse Mn were ~2 to 3.5, on 7 January 2015, 20 February 2015, 3 March 2015, and 1 April 2015 (Appendix H), indicating that the peaks and declines of this trace metal variable were likely due to crustal sources. However, the EFs of all other EOF mode 4 trace metals do not clearly identify the source of the peaks and declines of these variables, on 7 January 2015, 20 February 2015, 3 March 2015, and 1 April 2015 (Appendix H). The seasonal means and overall mean EFs for dry fine V, fine Ni, coarse Cu, and coarse Zn were >10 (Tables 16 and 17), indicating anthropogenic emissions were the dominant source of these trace metals.

(a)

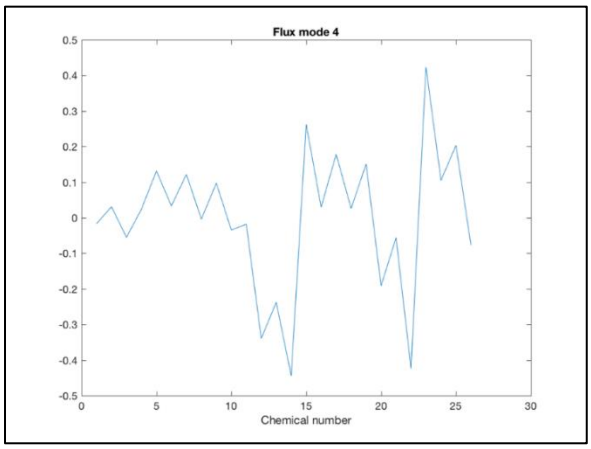

(b)

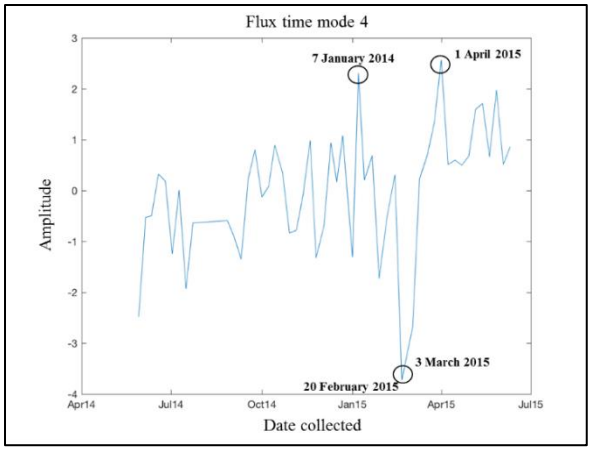

Figure 68. (a) Variance of dry total fluxes for trace metal variables associated with EOF mode 4 and (b) temporal patterns of total dry deposition flux data for EOF mode 4 for Eastern Shore samples. The dates during which the dry flux of trace metals associated with this EOF mode peaked and declined are circled.

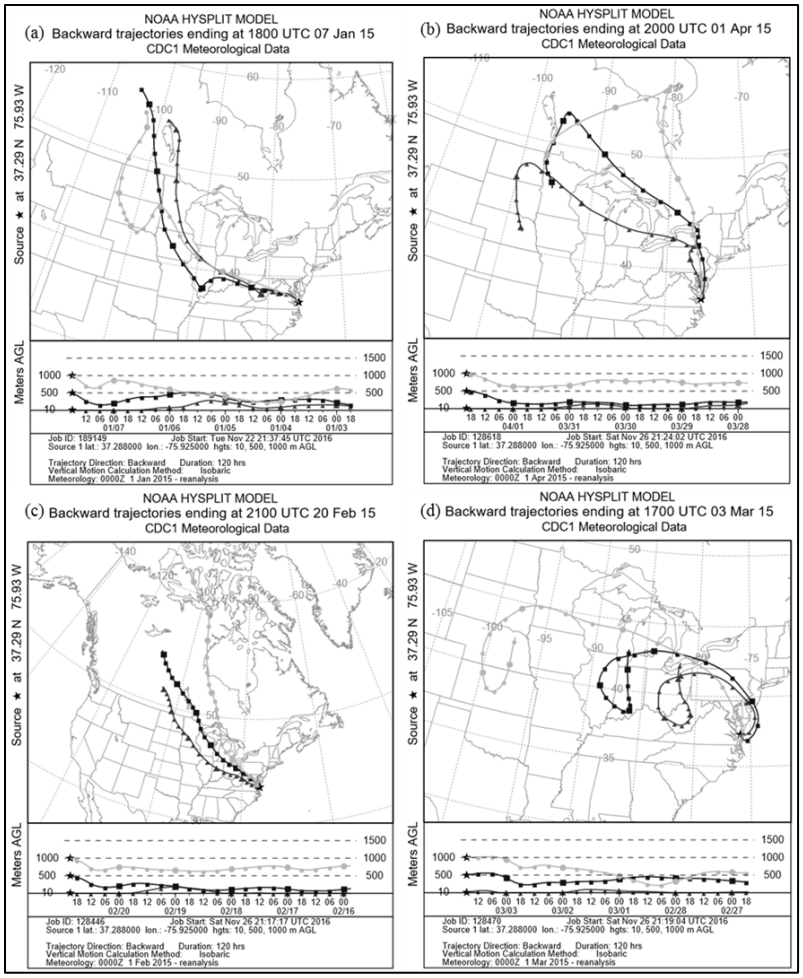

Figure 69. Five-day air mass back trajectory analyses (NOAA HYSPLIT model) with arrival heights of 10 m, 500 m, and 1000 m for the Eastern Shore field station on (a) 7 January 2014, (b) 1 April 2015, (c) 20 February 2015, and (d) 3 March 2015. These dates were associated with peaks and declines in the flux of trace metals in EOF mode 4.

The EOF mode 5 accounted for 4.4% of the total variance. Six variables were associated with EOF mode 5 (Figure 70a). These variables were the dry total fluxes of fine V, coarse Mn, fine Cr, coarse Cr, fine Ni, and coarse Zn. Both size fractions of chromium were associated with EOF mode 5. The eigenfunction values for dry fine Cr, coarse Cr and coarse Zn were positive indicating that the total fluxes of these trace metals peaked above the mean, on 3 September 2014, 5 November 2014, 19 November 2014, 20 February 2015, and 1 April 2015 (Figure 70b), and declined below the mean on 3 March 2015 and 13 May 2015 (Figure 70b). The eigenfunction values for dry fine V, fine N, and coarse Mn were negative indicating that the total fluxes of these trace metals declined below the mean, on 3 September 2014, 5 November 2014, 19 November 2014, 20 February 2015, and 1 April 2015 (Figure 70b), and peaked above the mean on 3 March 2015 and 13 May 2015 (Figure 70b). These results imply that there were different aerosol sources for the two groups of trace metal variables associated with EOF mode 5.

Five-day NOAA HYSPLIT AMBTs indicated that the air masses associated with elevated fluxes of the trace metals represented by EOF mode 5 originated from different source regions (Figure 71 a-e and 72 a-b). The AMBTS indicated that continental North American air masses were sampled on 3 September 2014, 5 November 2014, 19 November 2014, 20 February 2015, 1 April 2015, 3 March 2015, and 13 May 2015 (Figure 71 a-e and 72 a-b). The trace metals associated with this EOF mode are possibly derived from mixed sources, as the seasonal mean and overall mean EFs for fine Cr, coarse Cr, and coarse Mn were <10, but those for coarse Zn, fine V, and fine Ni were >10 (Tables 16 and 17). This indicates that both terrigenous dust and anthropogenic emissions contributed to the observed total dry fluxes of EOF mode 5 trace metals.

(a)

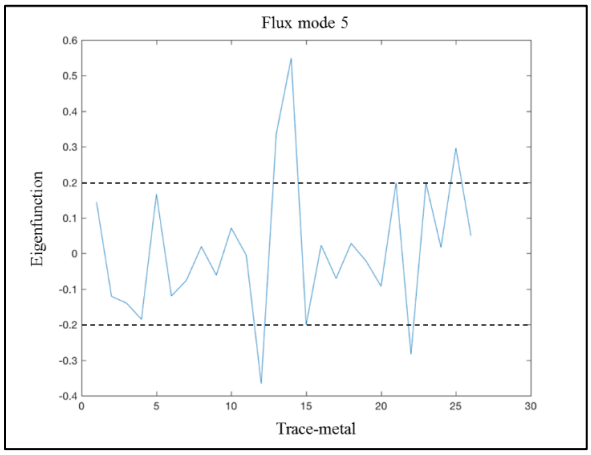

(b)

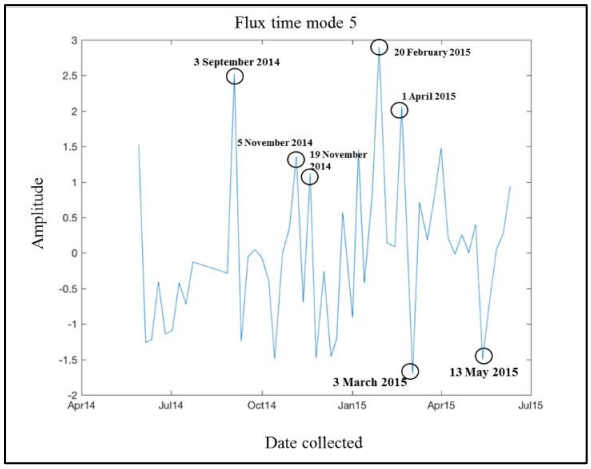

Figure 70. (a) Variance of dry total fluxes for trace metal variables associated with EOF mode 5 and (b) temporal patterns of total dry deposition flux data for EOF mode 5 for Eastern Shore samples. The dates during which the flux of trace metals associated with this EOF mode peaked and declined are circled.

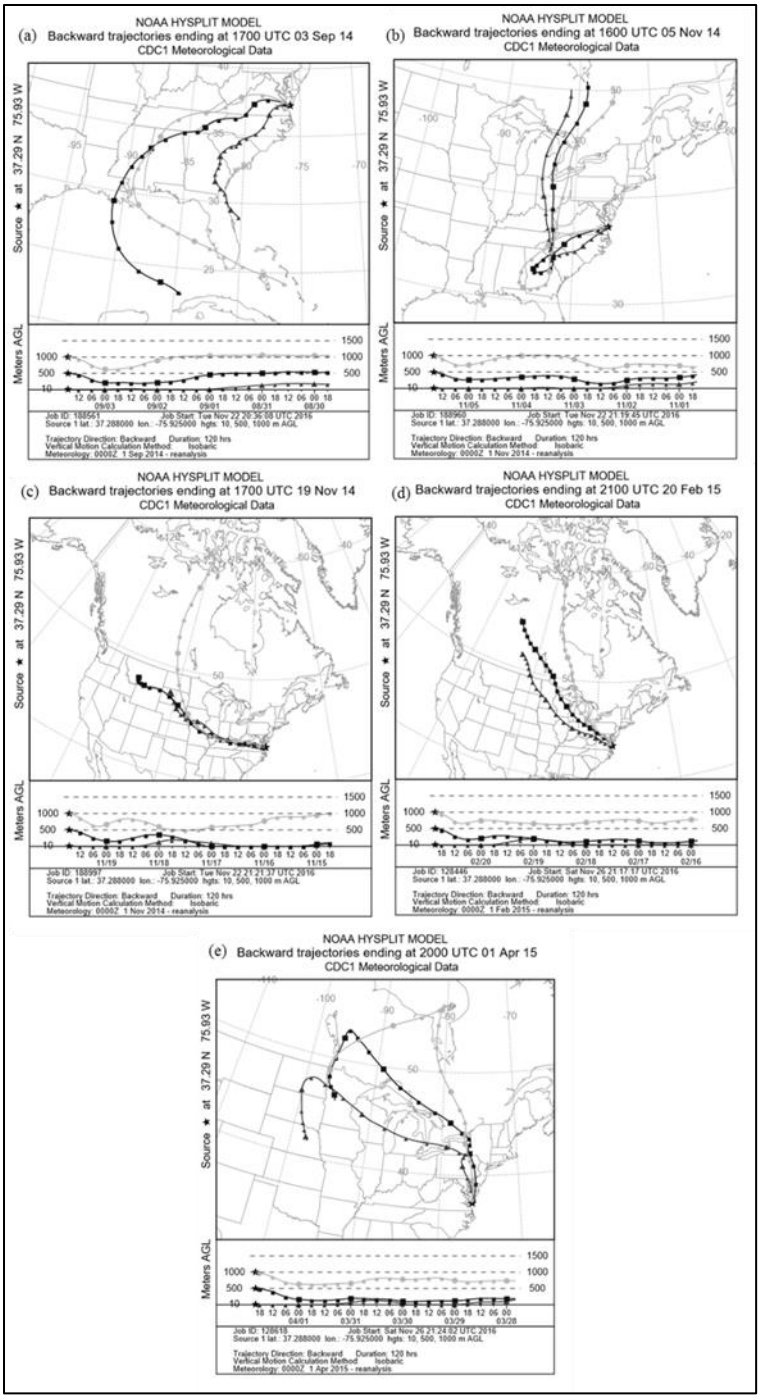

Figure 71. Five-day air mass back trajectory analyses (NOAA HYSPLIT model) with arrival heights of 10 m, 500 m, and 1000 m for the Eastern Shore field station on (a) 3 September 2014, (b) 5 November 2014, (c) 19 November 2014, (d) 20 February 2015, and (e) 1 April 2015. These dates were associated with elevated fluxes of trace metals in EOF mode 5.

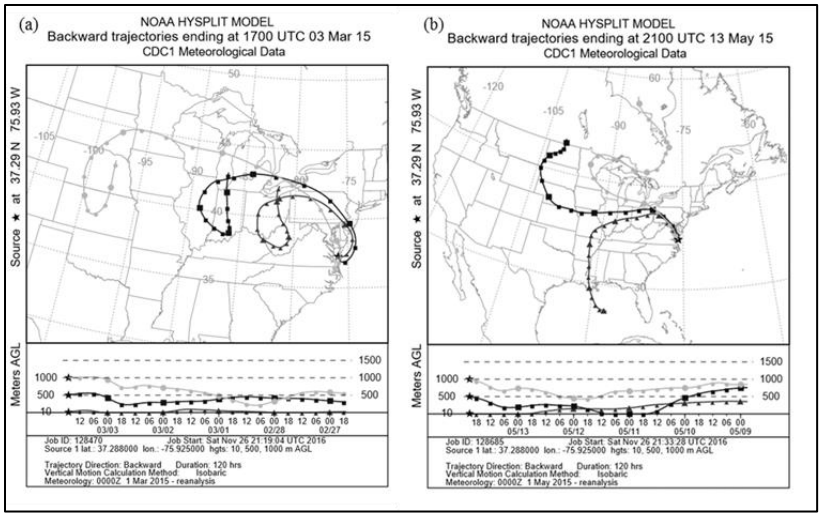

Figure 72. Five-day air mass back trajectory analyses (NOAA HYSPLIT model) with arrival heights of 10 m, 500 m, and 1000 m for the Eastern Shore field station on (a) 3 March 2015 and (b) 13 May 2015. These dates were associated with the decline in the flux of trace metals in EOF mode 5.

3.6 WET DEPOSITION OF SOLUBLE NUTRIENTS IN THE MID-ATLANTIC BIGHT

The soluble nutrient data for event-based rain samples collected during a research cruise in coastal waters of the Mid-Atlantic Bight, at ~200km offshore (see Section 2.3) (Figure 1), were compared to the Eastern Shore summer wet deposition estimates. All wet and dry deposition data referring to the cruise samples are described as "offshore". Wet deposition samples were obtained for a total of 5 offshore rain events. Average wet deposition fluxes were estimated for soluble nutrients in offshore rain samples using the sum of the wet deposition fluxes for the 5 offshore wet deposition samples and the total time period of the cruise (Table 18), however, unlike weekly composite samples collected at the ABCRC, the offshore wet fluxes do not account for periods of no rainfall (Table 18).

The mean concentration of soluble NO_3^- for Eastern Shore weekly composite summer rain samples (20.7 ± 16.0 µM) (Table 18) was 3 times greater than that for the event-based offshore rain samples (6.00 ± 4.48 µM) (Table 18). The mean wet flux of soluble NO_3^- estimated for Eastern Shore summer samples (20.5 ± 14.1 µmol/m^2/d) (Tables 5 and 18) was twice that estimated for offshore samples (10.8 µmol/m^2/d) (Table 18). The mean concentrations of soluble NH_4^+ and PO_4^{3-} for Eastern Shore summer rain samples (NH_4^+ = 52.6 ± 75.1 µM; PO_4^{3-} = 1.00 ± 1.84 µM) (Table 18) were at least 10 times greater than those for offshore rain samples (NH_4^+ = 4.64 ± 5.23 µM; PO_4^{3-} = 0.102 ± 0.122 µM) (Table 18). The mean wet flux of soluble NH_4^+ and PO_4^{3-} estimated for Eastern Shore samples (NH_4^+ = 35.9 ± 33.8 µmol/m^2/d; PO_4^{3-} = 0.718 ± 1.41 µmol/m^2/d) (Tables 5 and 18) was roughly 4 times greater than those estimated for offshore samples (NH_4^+ = 8.1 µmol/m^2/d; PO_4^{3-} = 0.718 ± 1.41 µmol/m^2/d) (Tables 5 and 18). The dominant forms of soluble inorganic N in offshore wet deposition samples was NO_3^- (Table 18), whereas NH_4^+ was the dominant form in Eastern Shore wet deposition (Table 5). The soluble inorganic N: P ratio for offshore wet deposition samples was ~119 and far exceeded the Redfield ratio (16:1), where soluble N only includes NO_3^- and NH_4^+, and soluble P includes only PO_4^{3-}.

Table 18. Comparison of wet deposition data for soluble nutrients for rain samples collected in the coastal waters of the Mid-Atlantic Bight (offshore) and at the Eastern Shore site. Note that wet deposition data presented for the Eastern Shore are for the summer only (for purpose of comparison).

Nutrient	Offshore mean concentration (±standard deviation) (µM)	[a]Offshore mean wet flux (±standard deviation) (µmol/m^2/s)	[b]Offshore estimated mean wet flux (µmol/m^2/d)	Eastern Shore mean wet concentration (±standard deviation) (µM)	Eastern Shore mean wet flux (±standard deviation) (µmol/m^2/d)
NO_3^-	6.00 ± 4.48	$13.3 \times 10^{-3} \pm 11.1 \times 10^{-3}$	10.8	20.7 ± 16.0	20.5 ± 14.1
NH_4^+	4.64 ± 5.23	$8.79 \times 10^{-3} \pm 8.70 \times 10^{-3}$	8.10	52.6 ± 75.1	35.9 ± 33.8
PO_4^{3-}	0.102 ± 0.122	$1.95 \times 10^{-4} \pm 2.84 \times 10^{-4}$	0.159	1.00 ± 1.84	0.718 ± 1.41

[a] Average offshore wet deposition fluxes of soluble nutrients during rainfall. These fluxes are skewed higher and do not account for periods of no rainfall.

[b] Average offshore wet deposition fluxes calculated using the sum of wet deposition fluxes for all offshore rain event samples and the total time period of the cruise. These values were calculated using data from the 5 soluble nutrient rainwater samples collected and assumes that these rain events were representative of the total number of times rainfall occurred over the offshore sampling region during the entire cruise. The calculation of estimated mean wet fluxes of soluble nutrients from offshore rain samples is described in Section 2.6.

(a) Rain soluble nitrate from offshore samples

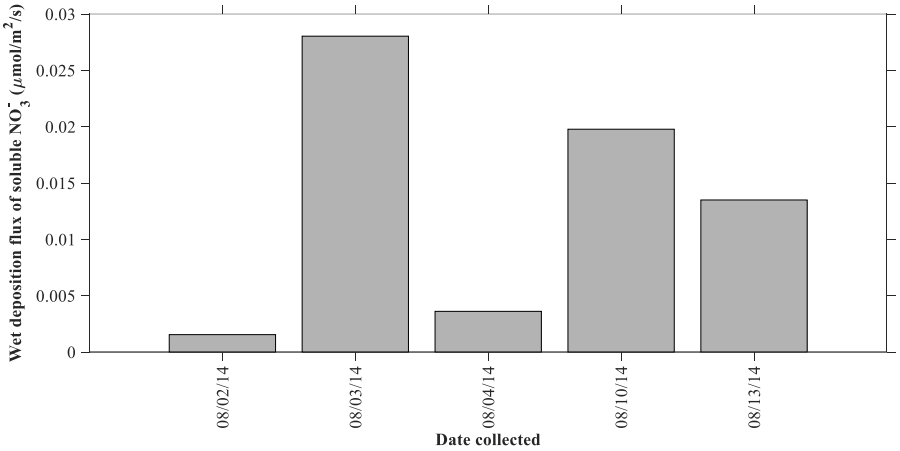

(b) Rain soluble ammonium from offshore samples

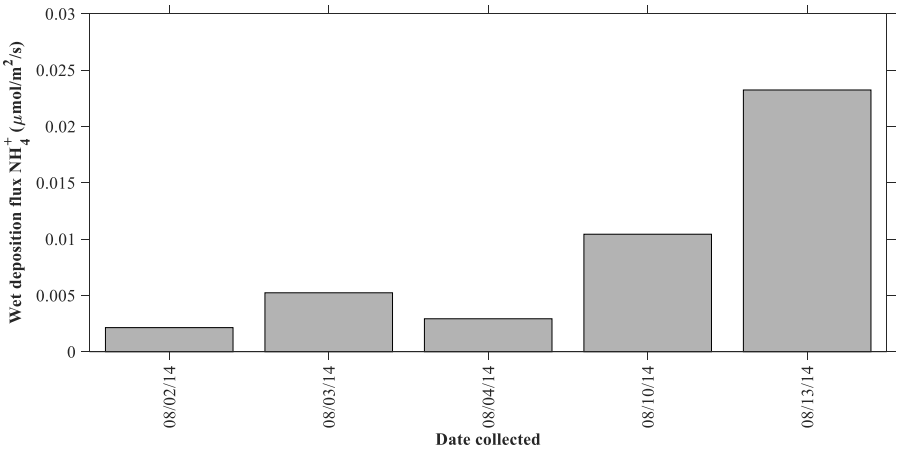

(c) Rain soluble phosphate from offshore samples

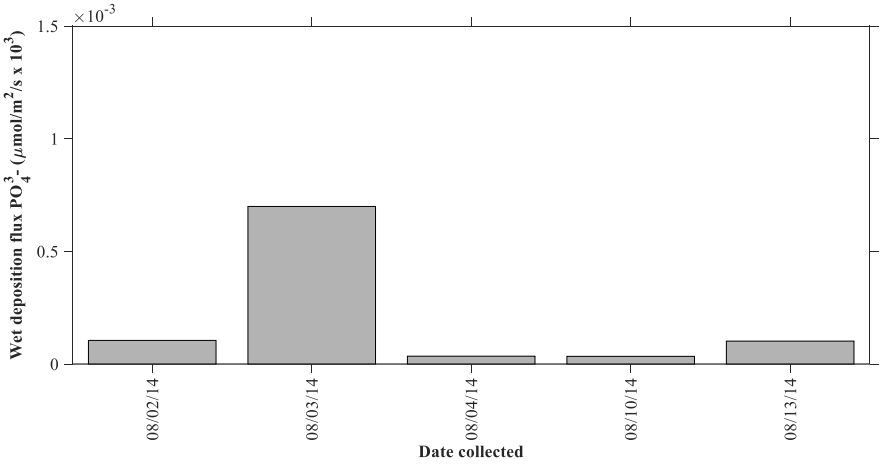

Figure 73. Wet deposition fluxes (μmol/m^2/s) of soluble (a) NO_3^-, (b) NH_4^+, and (c) PO_4^{3-} estimated from rain event-based samples collected in coastal waters of the Mid-Atlantic Bight. The wet deposition fluxes for individual rain events are higher than the mean wet fluxes for the entire cruise period, as these fluxes only account for the periods during which rainfall occurred.

3.7 DRY DEPOSITION OF SOLUBLE NUTRIENTS IN THE MID-ATLANTIC BIGHT

The mean dry deposition fluxes estimated for all three soluble nutrients (NO_3^-, NH_4^+, and PO_4^{3-}) from offshore aerosol samples were greater for the coarse aerosol fraction than for the fine aerosol fraction (Table 19). The mean total (fine+coarse) dry deposition flux of soluble NO_3^- estimated for offshore samples (22.7 μmol/m^2/d) was similar to that from Eastern Shore samples (18.1 μmol/m^2/d) (Tables 6 and 19). However, the mean total (fine+coarse) dry deposition flux of soluble NH_4^+ estimated from offshore samples (6.64 μmol/m^2/d) was approximately one third that for the Eastern Shore site (Table 19). The mean total (fine+coarse) dry soluble PO_4^{3-} flux (0.105 μmol/m^2/d) estimated from offshore aerosol samples was similar to that for the Eastern Shore site (0.0913 μmol/m^2/d) (Table 19). For the offshore area, soluble NO_3^- dominated dry deposition of inorganic N, whereas for the Eastern Shore site the mean total (fine+coarse) dry fluxes of soluble NO_3^- and NH_4^+ were nearly equal (Table 19). The dry atmospheric deposition soluble inorganic N: P ratios for offshore (279) and Eastern Shore samples (~400) both far exceeded the Redfield ratio (16:1), where soluble N includes only NO_3^- and NH_4^+, soluble P includes only PO_4^{3-}.

Table 19. Comparison of mean (± standard deviation) dry deposition fluxes of soluble nutrients (μmol/m^2/d) estimated for offshore and Eastern Shore locations. Note that data presented for the Eastern Shore site are for the summer season only (for purpose of comparison).

Nutrient	Offshore		Offshore	Eastern Shore		Eastern Shore
	< 1μm (μmol/m^2/d)	>1 μm (μmol/m^2/d)	total (fine+coarse) dry flux (μmol/m^2/d)	< 1μm (μmol/m^2/d)	>1 μm (μmol/m^2/d)	total (fine+coarse) dry flux (μmol/m^2/d)
NO_3^-	0.484 ± 0.440	22.2 ± 11.4	22.7	0.377 ± 0.147	17.7 ± 4.53	18.1
NH_4^+	1.75 ± 1.27	4.89 ± 5.67	6.64	3.19 ± 0.600	15.2 ± 7.35	18.4
PO_4^{3-}	0.0225 ± 0.0193	0.0820 ± 0.0907	0.105	$4.45 \times 10^{-3} \pm 1.85 \times 10^{-3}$	0.0868 ± 0.0363	0.0913

(a) Aerosol soluble nitrate from offshore samples

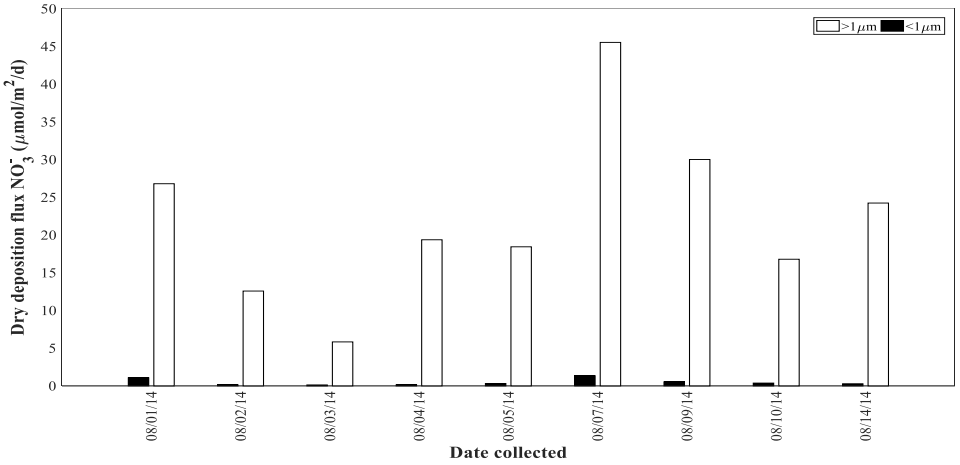

(b) Aerosol soluble ammonium from offshore samples

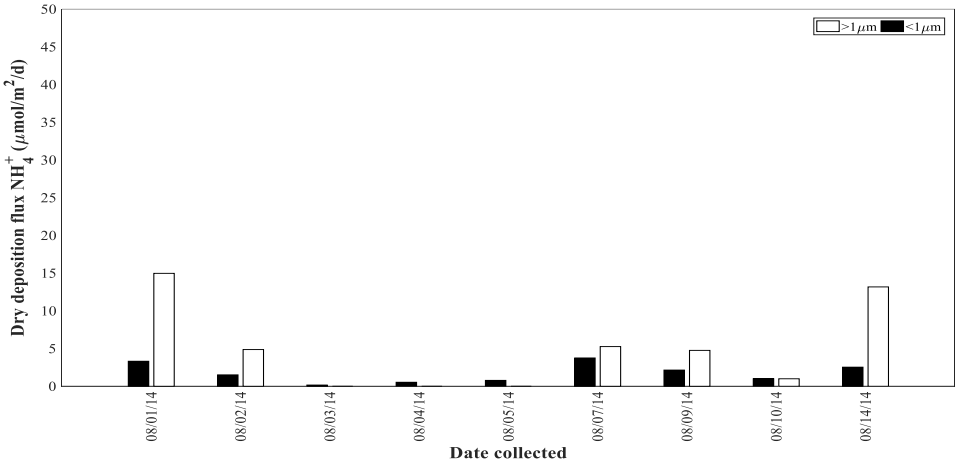

(c) Aerosol soluble phosphate from offshore samples

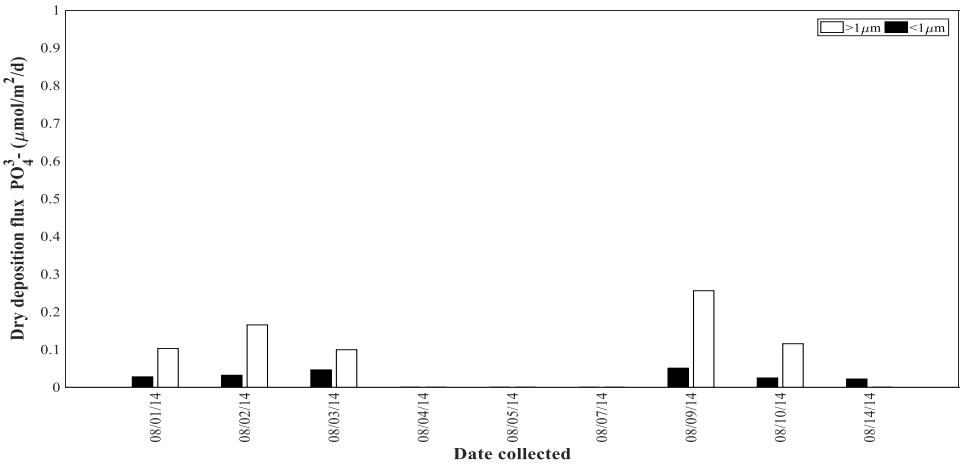

Figure 74. Dry deposition flux (μmol/m^2/s) of soluble (a) NO_3^-, (b) NH_4^+, and (c) PO_4^{3-} estimated from offshore aerosol samples collected in coastal waters of the Mid-Atlantic Bight.

3.8 WET DEPOSITION TOTAL-DISSOLVABLE TRACE METALS IN THE MID-ATLANTIC BIGHT

The concentrations of total-dissolvable trace metals in offshore rain samples were lower than those in Eastern Shore wet deposition, except for Cd, for which the concentrations at sea was ~3 times higher than those on land (Table 19). The concentrations of total-dissolvable Ni and Pb in offshore samples were relatively close to values measured in Eastern Shore rain samples (Table 19). Total-dissolvable Fe and Al concentrations in offshore wet deposition samples were ~16 to 17 times lower than for Eastern Shore rain samples. The volume of rain collected on 10 August 2014 (~1.8 L) was approximately twice that collected on both 4 August 2014 (~1 L) and 13 August 2014 (0.75 L). The volume of rain collected did not appear to be directly related to the magnitude of the flux of soluble trace metals, that is, larger or smaller calculated fluxes were not associated with higher or rain lower volumes (Figure 75 a-d). Chromium, Co, Ni, Zn, and Cd wet deposition fluxes were highest for the 4 August 2014 (Figure 75 a-d) event, whereas Mn, Fe, Cu, Sb, and Pb fluxes were highest for the 10 August 2014 event (Figure 75 a and d). Titanium and V wet deposition fluxes were only marginally greater for the 10 August 2014 sample (Figure 75). Aluminum was the only trace metal that showed the greatest wet deposition flux for the 13 August 2014 event (Figure 75 a).

Additional calculations were performed to estimate the average daily wet deposition fluxes of total-dissolvable trace metals in the coastal North Atlantic to compare the offshore wet flux data to that for the Eastern Shore, which averages wet deposition over ~weekly periods. These flux calculations assumed that the 3 rain events, for which total-dissolvable trace metal samples were collected, were representative of the composition and frequency of rainfall received by the study region during the entire cruise period. A detailed description of the calculation of these estimated fluxes is provided in Section 2.6. These wet fluxes are the means estimated using the wet deposition data from all 3 rain events and are lower than the event-specific wet deposition fluxes reported in $\mu mol/m^2/s$ (Table 20), which are the mean wet fluxes during rainfall and do not account for periods of no rainfall. The time-averaged wet fluxes of total-dissolvable Zn, Cd, and Pb were nearly equal for both the offshore and Eastern Shore sites (Table

20). However, the wet deposition fluxes of total-dissolvable crustal trace metals Al, Ti, Mn, and Fe were around 50 times, 10 times, 10 times, and 20 times greater, respectively, for the Eastern Shore site (Table 20). The wet deposition flux of TDNi was over 600 times greater for the Eastern Shore site than for the offshore location (Table 20). Eastern Shore wet deposition fluxes of total-dissolvable V, Cr, Co, Cu, and Sb were around 3 to 8 times greater than those for the offshore location.

Table 20. Comparison of mean (± standard deviation) wet deposition concentrations and fluxes of total-dissolvable trace metals from offshore and Eastern Shore samples. Note that data presented for the Eastern Shore are for the summer season only (for purpose of comparison).

Trace metal	Offshore wet deposition concentration (mean ± standard deviation) (µM)	[a]Offshore wet deposition flux (mean ± standard deviation) (µmol/m^2/s)	[b]Estimated offshore wet deposition flux (µmol/m^2/d)	Eastern Shore wet deposition concentration (mean ± standard deviation) (µM)	Eastern Shore wet deposition flux (mean ± standard deviation) (µmol/m^2/d)
Al	2.69 ± 2.50	$10.7 \times 10^{-5} \pm 7.50 \times 10^{-5}$	0.0553	47.5 ± 103	2.70 ± 6.35
Ti	0.0607 ± 0.0365	$2.66 \times 10^{-6} \pm 1.56 \times 10^{-6}$	1.49×10^{-3}	0.718 ± 1.10	$21.7 \times 10^{-3} \pm 38.3 \times 10^{-3}$
V	0.0343 ± 0.221	$14.9 \times 10^{-7} \pm 9.80 \times 10^{-7}$	0.842×10^{-3}	0.155 ± 0.170	$4.89 \times 10^{-3} \pm 6.17 \times 10^{-3}$
Cr	0.0153 ± 0.0123	$5.70 \times 10^{-7} \pm 3.99 \times 10^{-7}$	0.309×10^{-3}	0.0758 ± 0.105	$2.20 \times 10^{-3} \pm 3.48 \times 10^{-3}$
Mn	0.113 ± 0.0448	$4.79 \times 10^{-6} \pm 3.11 \times 10^{-6}$	2.75×10^{-3}	1.24 ± 1.47	$41.0 \times 10^{-3} \pm 62.7 \times 10^{-3}$
Fe	1.63 ± 0.724	$6.24 \times 10^{-5} \pm 3.87 \times 10^{-5}$	0.0366	25.7 ± 46.6	0.721 ± 1.41
Co	$3.42 \times 10^{-3} \pm 2.08 \times 10^{-3}$	$12.1 \times 10^{-8} \pm 5.96 \times 10^{-8}$	0.663×10^{-4}	0.0196 ± 0.0301	$5.28 \times 10^{-4} \pm 8.86 \times 10^{-4}$
Ni	0.0802 ± 0.0958	$2.64 \times 10^{-6} \pm 2.80 \times 10^{-6}$	0.00145	0.0912 ± 0.103	0.939 ± 2.02
Cu	0.0819 ± 0.0215	$2.93 \times 10^{-6} \pm 1.43 \times 10^{-6}$	1.68×10^{-3}	0.254 ± 0.218	$5.73 \times 10^{-3} \pm 6.32 \times 10^{-3}$
Zn	2.04 ± 2.49	$5.59 \times 10^{-5} \pm 6.19 \times 10^{-5}$	30.4×10^{-3}	1.15 ± 0.973	$27.4 \times 10^{-3} \pm 31.8 \times 10^{-3}$
Cd	$18.7 \times 10^{-3} \pm 22.4 \times 10^{-3}$	$3.46 \times 10^{-7} \pm 3.71 \times 10^{-7}$	1.89×10^{-4}	$6.51 \times 10^{-3} \pm 5.52 \times 10^{-3}$	$0.982 \times 10^{-4} \pm 1.21 \times 10^{-4}$
Sb	$16.5 \times 10^{-3} \pm 8.00 \times 10^{-3}$	$3.04 \times 10^{-7} \pm 1.55 \times 10^{-7}$	1.70×10^{-4}	0.0608 ± 0.0517	$7.67 \times 10^{-4} \pm 8.43 \times 10^{-4}$
Pb	0.0473 ± 0.0267	$4.11 \times 10^{-6} \pm 2.88 \times 10^{-6}$	23.5×10^{-4}	0.0617 ± 0.0500	$4.98 \times 10^{-4} \pm 7.44 \times 10^{-4}$

[a] Average offshore wet deposition fluxes of acid-soluble trace metals during rainfall. These fluxes are skewed higher and do not account for periods of no rainfall.

[b] Average offshore wet deposition fluxes calculated using the sum of wet deposition fluxes for all offshore rain event samples and the total time period of the cruise. These values were calculated using data from the 3 total-dissolvable trace metal rainwater samples collected and assumes these rain events were representative of the total number of times rainfall occurred over the offshore study region during the entire cruise period. The calculation of estimated mean wet fluxes of total-dissolvable trace metals from offshore rain samples is described in Section 2.6.

(a) Rain total-dissolvable aluminum, iron, and zinc from offshore samples

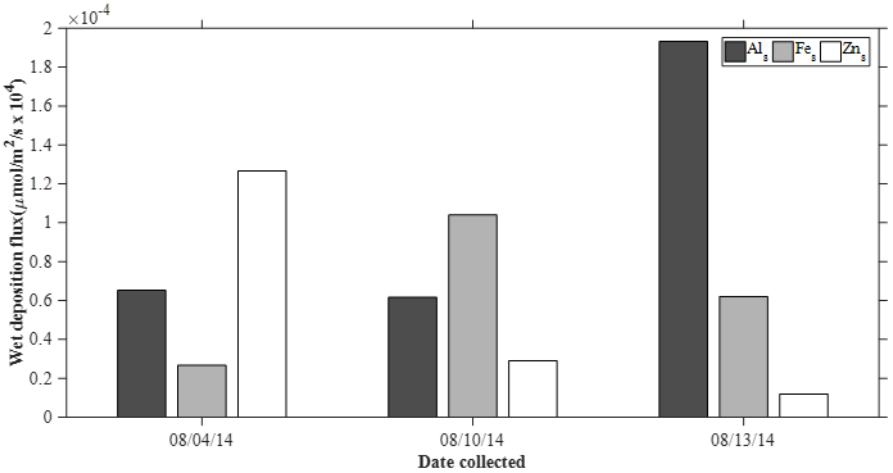

(b) Rain total-dissolvable titanium, vanadium, and chromium from offshore samples

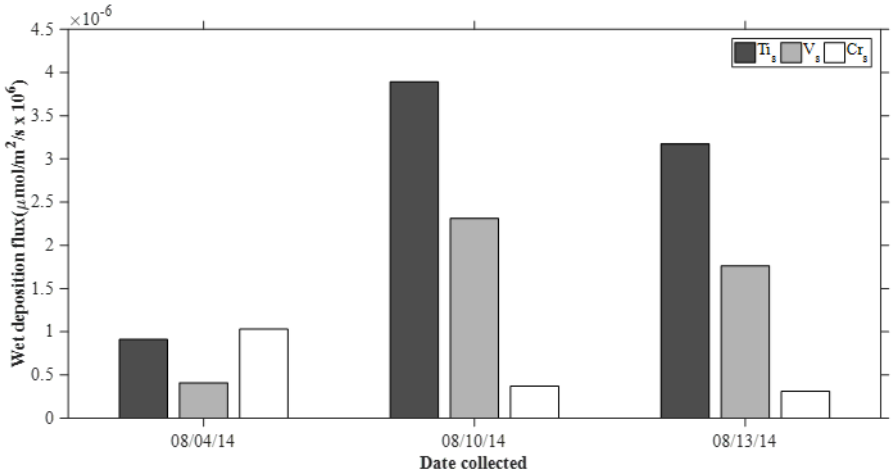

(c) Rain total-dissolvable manganese, cobalt, and nickel from offshore samples

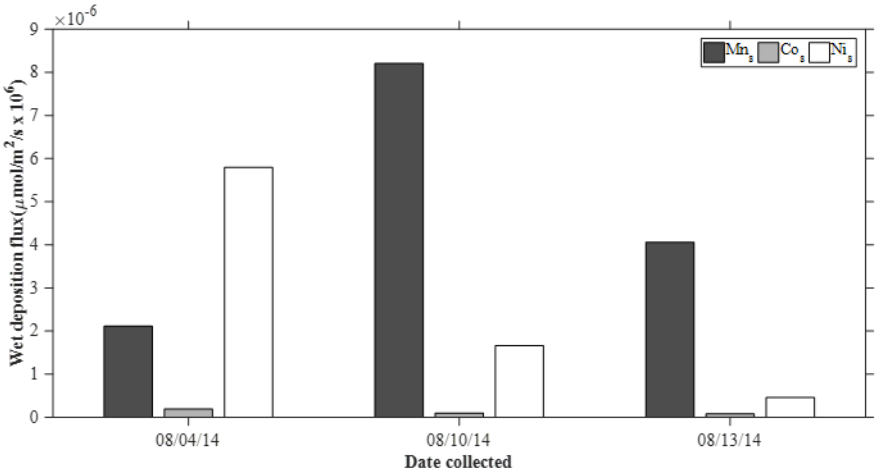

Figure 75. Wet deposition (µmol/m^2/s) of total-dissolvable (a) Al, Fe, and Zn, (b) Ti, V, and Cr, (c) Mn, Co, and Ni, and (d) Cu, Cd, Sb, and Pb for event-based offshore samples. The wet deposition fluxes of total-dissolvable trace metals for individual rain events (shown here) are higher than the mean wet fluxes for the entire cruise period, as these fluxes only account for the time during which rainfall occurred.

(d) Rain total-dissolvable copper, cadmium, antimony, and lead from offshore samples

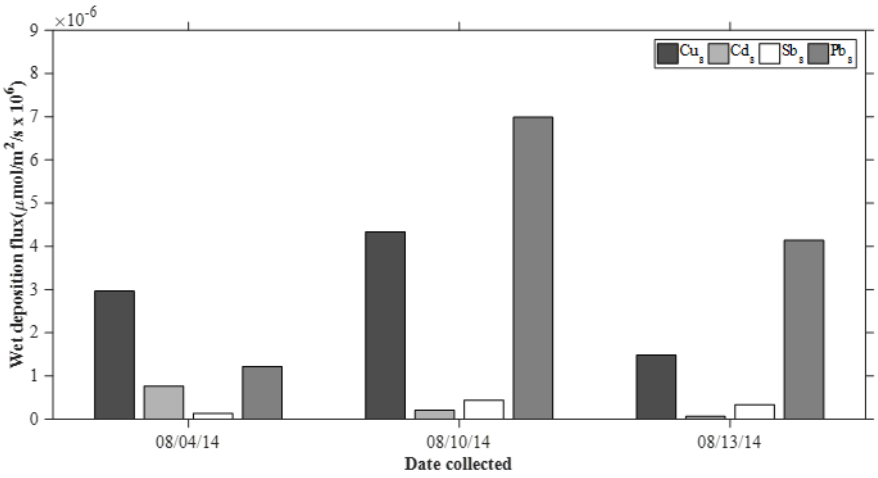

Figure 75. Continued.

3.9 DRY DEPOSITION FLUX AND FRACTIONAL SOLUBILITY OF TRACE METALS IN THE MID-ATLANTIC BIGHT

A five-day AMBT (NOAA HYSPLIT model) showed that the air mass sampled on 5 August 2014 travelled from North America directly to the west of the cruise area and passed over the Eastern Shore of Virginia (Appendix I). Backward trajectories for air masses sampled on 1 August 2014 and 5 August 2014 passed over the Eastern Shore of Virginia, whereas those for 2 August 2014, 3 August 2014, and 4 August 2014 indicated marine origin (Appendix I). The air masses sampled on 7 August 2014, 9 August 2014, 10 August 2014, and 14 August 2014 originated from the southern New York-New Jersey region (Appendix I) and were associated with high fluxes of dry soluble Ti, Mn, Fe, Co, Cu, Zn, and Cd (Figures 77a, 80a, 81a, 82a, 84a, 85a, and 86a). The dry soluble fluxes of crustal elements Al and Fe were also relatively high on 1 August 2014, 2 August 2014, and 5 August 2014 (Figures 76a and 81a). The dry deposition flux of soluble Al and V was greatest for the aerosol sample collected on 5 August 2014 (Figures 76a and 78a). On 1 August 2014 and 5 August 2014, the air masses sampled passed over the Eastern Shore of Virginia, whereas on 2 August 2014 a marine air mass was sampled (Appendix I). The concentrations of dry soluble Cr and Ni were below detection in offshore dry deposition samples (Figures 79a and 83a).

The total fluxes of most trace metals (Mn, Fe, Co, Zn, Cd, Sb, and Pb) were greatest on 7 August 2014 (Figures 80b, 81b, 82b, 85b, 86b, 87b, and 88b), whereas total Al and Co fluxes were greatest on 9 August 2014 (Figures 76b and 78b). The dates with the highest fractional solubilities for Fe (1 August 2014 and 5 August 2014) correspond to periods during which the air mass sampled passed over the Eastern Shore, while other samples with relatively high aerosol fractional solubilities corresponded to dates 7 August 2014 and 9 August 2014, during which the air mass sampled passed over the New Jersey region (Figure 81b and Appendix I) and was possibly influenced by pollution.

The estimated dry soluble fluxes for all trace metals were lower for offshore samples than for Eastern Shore summer samples (Tables 21 and 22). The dry fluxes of soluble fine Fe and coarse Fe estimated for offshore samples were approximately one third the estimated mean fluxes for Eastern Shore

summer samples (Table 22). The mean fractional solubility of fine Fe in offshore aerosol samples (0.940 ± 0.676 %) was ~5 times lower than that for Eastern Shore summer samples (Table 21). The mean fractional solubility of coarse Fe in offshore aerosol samples (3.31 ± 3.71 %) was slightly greater than that for Eastern Shore summer samples (2.47 ± 0.688 %) (Table 22), but not significantly greater (Table 22).

Enrichment factors were calculated for the total concentrations of trace metals in the fine fraction aerosol samples of 3 August 2014 and 9 August 2014, and the coarse fraction aerosol sample of 5 August 2014. All other offshore aerosol samples had total Al concentrations below the detection limit, therefore EFs could not be calculated for those samples. The fine aerosol sample collected on 3 August 2014 was of marine origin and EFs were obtained only for Co (0.913), Ni (27.9), and Zn (407), suggesting that the air mass sampled was influenced by both crustal and anthropogenic sources. The offshore fine aerosol sample collected on 9 August 2014 passed over the New Jersey region and was enriched in V (EF 40.7), Mn (EF 11.7), Co (EF 11.8), Ni (EF 37.4), Cu (EF 1500), Zn (EF 504), Cd (EF 3010), and Sb (EF 18900) relative to crustal material. The EF for the crustal element Ti (1.8) in the fine fraction of the aerosol sample for 9 August 2014 was <10. The air mass sampled on 5 August 2014 travelled over the Eastern Shore before arriving at the offshore sample location (Appendix I), and EFs for the coarse fraction for total dry Ti (0.112), Mn (5.76), Fe (1.41), and Cd (0.528) were <10, suggesting a predominantly terrigenous source, whereas EFs for V (15.5) and Zn (792) were >10, suggesting enrichment with anthropogenic emissions.

Table 21. Comparison of mean (± standard deviation) dry soluble flux, dry total flux, and aerosol fractional solubility estimated from offshore and summer Eastern Shore fine (<1 µm) aerosol samples. Note that data presented for the Eastern Shore are for the summer season only (for purpose of comparison).

Trace metal	Offshore dry soluble flux (µmol/m^2/d)	Offshore dry total flux (µmol/m^2/d)	Offshore fractional solubility (%)	Eastern Shore dry soluble flux (µmol/m^2/d)	Eastern Shore dry total flux (µmol/m^2/d)	Eastern Shore fractional solubility (%)
Al	$0.558 \times 10^{-3} \pm 1.12 \times 10^{-3}$	$9.93 \times 10^{-3} \pm 23.0 \times 10^{-3}$	–	$7.82 \times 10^{-3} \pm 7.08 \times 10^{-3}$	0.227 ± 0.180	3.41 ± 1.23
Ti	$2.47 \times 10^{-5} \pm 7.41 \times 10^{-5}$	$0.216 \times 10^{-3} \pm 0.383 \times 10^{-3}$	–	$4.16 \times 10^{-5} \pm 1.76 \times 10^{-5}$	$10.2 \times 10^{-3} \pm 7.86 \times 10^{-3}$	0.505 ± 0.324
V	$1.29 \times 10^{-4} \pm 1.17 \times 10^{-4}$	$3.16 \times 10^{-4} \pm 2.31 \times 10^{-4}$	31.0 ± 23.5	$5.25 \times 10^{-4} \pm 1.67 \times 10^{-4}$	$8.50 \times 10^{-4} \pm 2.33 \times 10^{-4}$	63.0 ± 14.1
Cr	–	–	–	$4.24 \times 10^{-5} \pm 1.09 \times 10^{-5}$	$4.7 \times 10^{-5} \pm 8.94 \times 10^{-5}$	1.95 ± 6.17
Mn	$6.74 \times 10^{-4} \pm 1.07 \times 10^{-4}$	$3.24 \times 10^{-4} \pm 4.23 \times 10^{-4}$	9.16 ± 14.8	$4.67 \times 10^{-4} \pm 2.04 \times 10^{-4}$	$14.9 \times 10^{-4} \pm 7.32 \times 10^{-4}$	31.8 ± 6.17
Fe	$1.02 \times 10^{-3} \pm 0.796 \times 10^{-3}$	0.116 ± 0.0747	0.940 ± 0.676	$3.73 \times 10^{-3} \pm 1.07 \times 10^{-3}$	$61.6 \times 10^{-3} \pm 42.3 \times 10^{-3}$	7.31 ± 2.52
Co	$2.05 \times 10^{-6} \pm 5.05 \times 10^{-6}$	$1.5 \times 10^{-5} \pm 1.28 \times 10^{-5}$	17.0 ± 35.8	$9.97 \times 10^{-6} \pm 2.67 \times 10^{-6}$	$3.53 \times 10^{-5} \pm 1.48 \times 10^{-5}$	29.9 ± 5.97
Ni	–	$4.48 \times 10^{-4} \pm 4.21 \times 10^{-4}$	–	$1.39 \times 10^{-4} \pm 0.337 \times 10^{-4}$	$5.24 \times 10^{-4} \pm 1.16 \times 10^{-4}$	26.6 ± 4.46
Cu	$1.53 \times 10^{-4} \pm 2.38 \times 10^{-4}$	$1.66 \times 10^{-3} \pm 1.82 \times 10^{-3}$	6.18 ± 10.0	$3.21x\ 10^{-4} \pm 1.01 \times 10^{-4}$	$7.27 \times 10^{-4} \pm 1.90 \times 10^{-4}$	44.5 ± 8.41
Zn	$1.11 \times 10^{-3} \pm 8.75 \times 10^{-4}$	$7.35 \times 10^{-3} \pm 5.42 \times 10^{-3}$	26.0 ± 30.1	$1.94 \times 10^{-3} \pm 0.709 \times 10^{-3}$	$2.56 \times 10^{-3} \pm 0.591 \times 10^{-3}$	73.7 ± 17.7
Cd	$4.24 \times 10^{-6} \pm 6.50 \times 10^{-6}$	$1.16 \times 10^{-5} \pm 1.09 \times 10^{-5}$	26.5 ± 43.5	$7.84 \times 10^{-6} \pm 2.19 \times 10^{-6}$	$1.36 \times 10^{-5} \pm 0.506 \times 10^{-5}$	59.4 ± 8.72
Sb	$3.02 \times 10^{-5} \pm 4.50 \times 10^{-5}$	$1.24 \times 10^{-4} \pm 1.44 \times 10^{-4}$	12.4 ± 16.2	$4.94 \times 10^{-5} \pm 1.58 \times 10^{-5}$	$1.55 \times 10^{-4} \pm 0.606 \times 10^{-4}$	33.4 ± 8.59
Pb	$3.87 \times 10^{-5} \pm 6.61 \times 10^{-5}$	$1.32 \times 10^{-4} \pm 3.13 \times 10^{-4}$	5.54 ± 11.1	$7.81 \times 10^{-5} \pm 2.68 \times 10^{-5}$	$1.99 \times 10^{-4} \pm 0.652 \times 10^{-4}$	40.1 ± 10.8

Table 22. Comparison of mean (± standard deviation) dry soluble flux, dry total flux, and aerosol fractional solubility estimated from offshore and summer Eastern Shore coarse (>1 μm) aerosol samples. Note that data presented for the Eastern Shore are for the summer season only (for purpose of comparison).

Trace metal	Offshore dry soluble flux (μmol/m^2/d)	Offshore total dry flux (μmol/m^2/d)	Offshore fractional solubility (%)	Eastern Shore dry soluble flux (μmol/m^2/d)	Eastern Shore dry total flux (μmol/m^2/d)	Eastern Shore fractional solubility (%)
Al	0.0260 ± 0.0438	0.0695 ± 0.209	2.21 ± 6.62	0.155 ± 0.0936	6.05 ± 4.15	2.64 ± 0.793
Ti	$5.61 \times 10^{-3} \pm 8.76 \times 10^{-3}$	$1.62 \times 10^{-3} \pm 4.32 \times 10^{-3}$	11.1 ± 33.3	$1.24 \times 10^{-4} \pm 2.62 \times 10^{-4}$	0.269 ± 0.178	$2.85 \times 10^{-2} \pm 6.69 \times 10^{-2}$
V	–	$6.95 \times 10^{-3} \pm 19.5 \times 10^{-3}$	–	$1.4 \times 10^{-3} \pm 4.39 \times 10^{-4}$	$8.15 \times 10^{-3} \pm 3.7 \times 10^{-3}$	19.4 ± 7.01
Cr	–	$20.7 \times 10^{-3} \pm 45.4 \times 10^{-3}$	–	$3.97 \times 10^{-4} \pm 1.22 \times 10^{-4}$	$1.4 \times 10^{-3} \pm 2.07 \times 10^{-3}$	11.5 ± 15.5
Mn	$4.65 \times 10^{-3} \pm 3.8 \times 10^{-3}$	0.0129 ± 0.0176	12.4 ± 15.4	$20.3 \times 10^{-3} \pm 9.55 \times 10^{-3}$	0.0461 ± 0.0201	43.4 ± 4.27
Fe	0.0140 ± 0.0128	0.256 ± 0.237	3.31 ± 3.71	0.0385 ± 0.0119	1.71 ± 0.934	2.47 ± 0.688
Co	$2.86 \times 10^{-4} \pm 5.69 \times 10^{-4}$	$1.02 \times 10^{-4} \pm 2.47 \times 10^{-4}$	11.1 ± 33.3	$1.95 \times 10^{-4} \pm 1.28 \times 10^{-4}$	$7.67 \times 10^{-4} \pm 4.13 \times 10^{-4}$	24.6 ± 2.84
Ni	–	–	–	$2.86 \times 10^{-4} \pm 6.1 \times 10^{-4}$	$4.16 \times 10^{-3} \pm 1.57 \times 10^{-3}$	50.3 ± 11.6
Cu	$3.57 \times 10^{-3} \pm 4.12 \times 10^{-3}$	$6.38 \times 10^{-3} \pm 8.8 \times 10^{-3}$	24.0 ± 38.9	$7.56 \times 10^{-3} \pm 3.33 \times 10^{-3}$	$17.6 \times 10^{-3} \pm 5.62 \times 10^{-3}$	42.1± 8.74
Zn	0.0238 ± 0.0210	0.138 ± 0.122	33.2 ± 38.3	0.0176 ± 0.00660	0.0315 ± 0.0103	56.5 ± 11.9
Cd	$12.0 \times 10^{-5} \pm 18.2 \times 10^{-5}$	$9.43 \times 10^{-5} \pm 8.56 \times 10^{-5}$	44.4 ± 52.7	$5.98 \times 10^{-5} \pm 2.08 \times 10^{-5}$	$12.9 \times 10^{-5} \pm 5.38 \times 10^{-5}$	50.3 ± 18.2
Sb	–	$2.15 \times 10^{-3} \pm 2.69 \times 10^{-3}$	–	$1.27 \times 10^{-4} \pm 0.410 \times 10^{-4}$	$2.17 \times 10^{-3} \pm 0.699 \times 10^{-3}$	6.50 ± 3.12
Pb	$1.25 \times 10^{-4} \pm 2.78 \times 10^{-4}$	–	–	$2.64 \times 10^{-4} \pm 1.05 \times 10^{-4}$	$15.8 \times 10^{-4} \pm 8.25 \times 10^{-4}$	18. 9 ± 7.56

(a) Aerosol aluminum from offshore samples

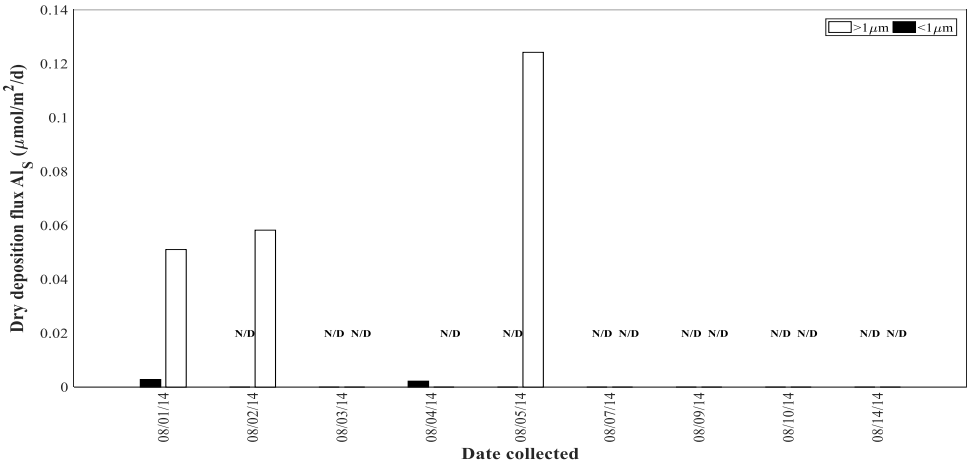

(b) Aerosol total aluminum from offshore samples

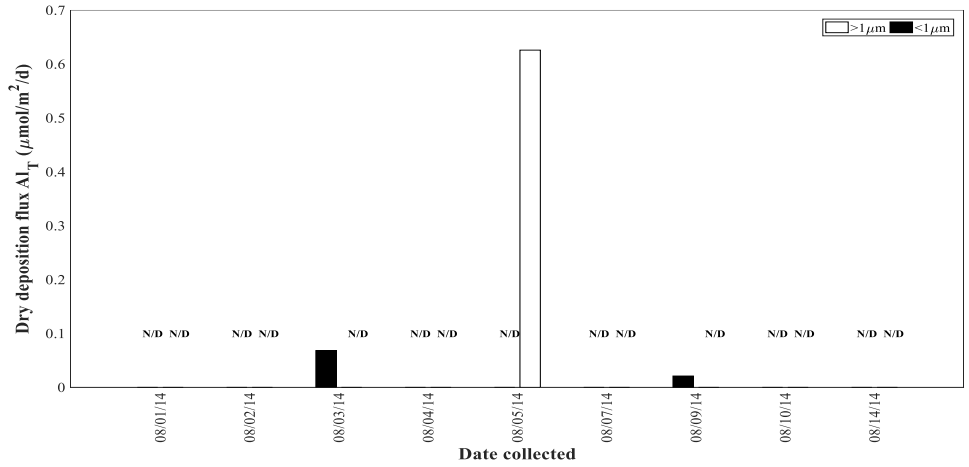

(c) Aerosol aluminum fractional solubility from offshore samples

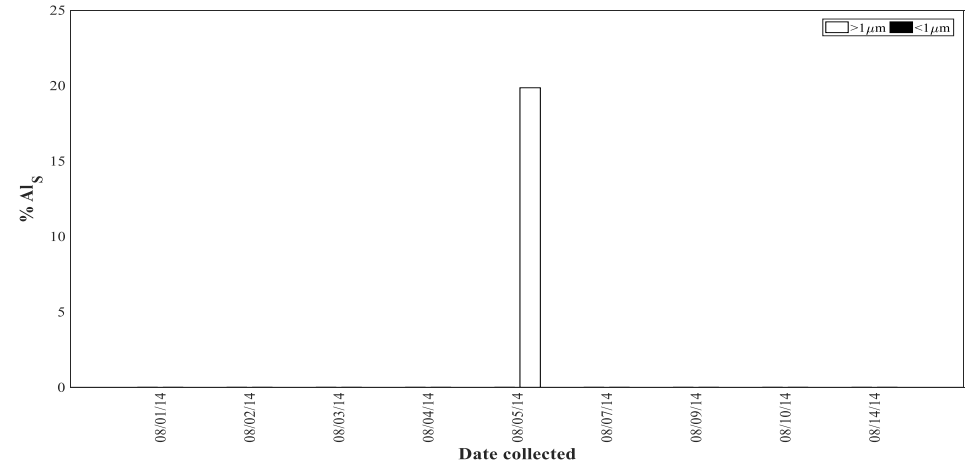

Figure 76. Dry deposition flux of (a) Al_S (μmol/m^2/d) and (b) Al_T (μmol/m^2/d), and (c) %Al_S from offshore aerosol samples. Note "N/D" indicates samples for which aluminum was not detected.

(a) Aerosol soluble titanium from offshore samples

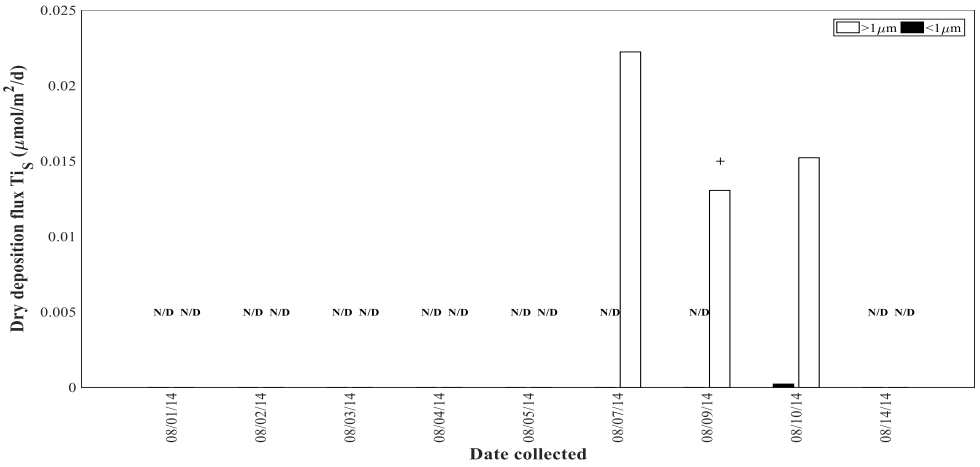

(b) Aerosol total titanium from offshore samples

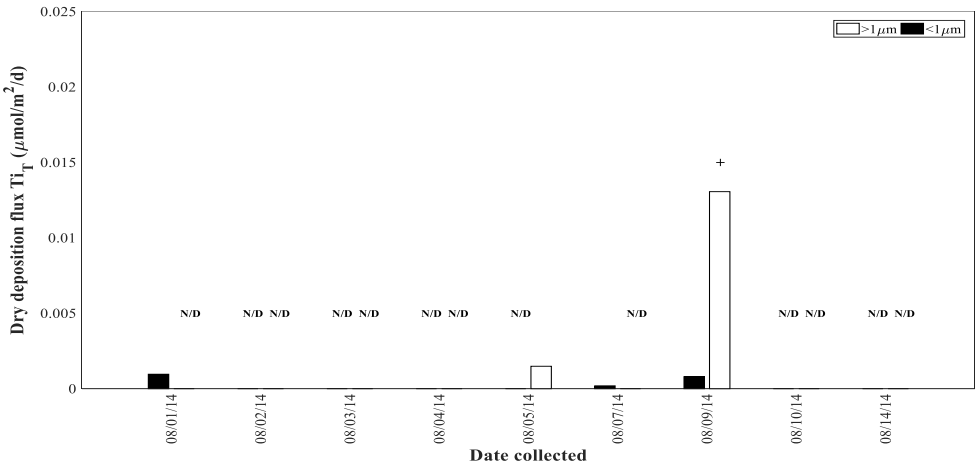

(c) Aerosol titanium fractional solubility from offshore samples

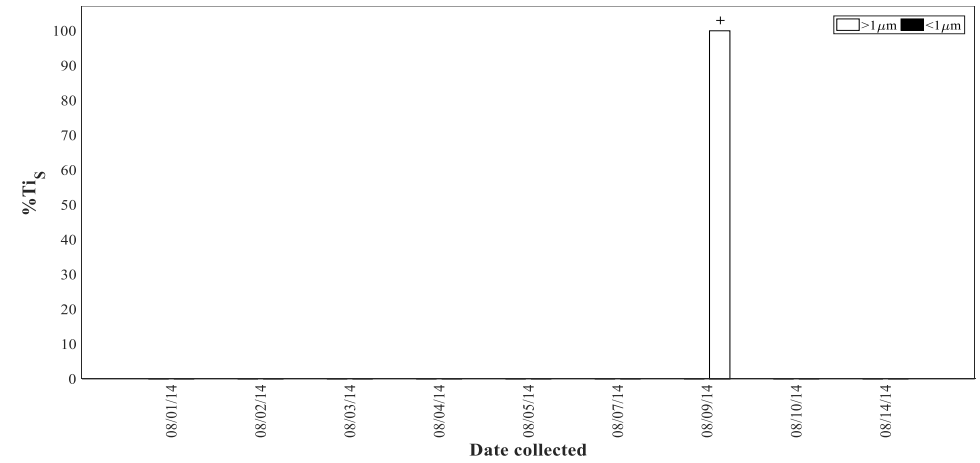

Figure 77. Dry deposition flux of (a) Ti_S (µmol/m^2/d) and (b) Ti_T (µmol/m^2/d), and (c) %Ti_S from offshore aerosol samples. Note "N/D" indicates samples for which titanium was not detected.

(a) Aerosol soluble vanadium from offshore samples

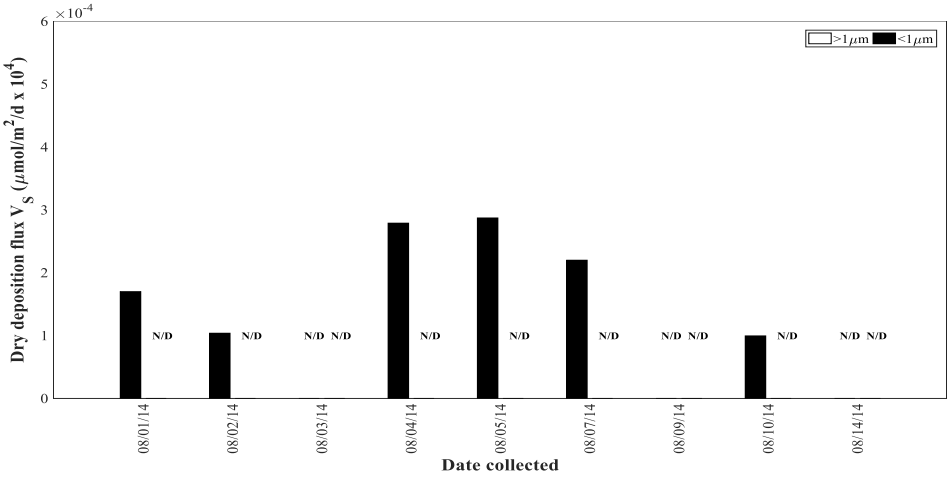

(b) Aerosol total vanadium from offshore samples

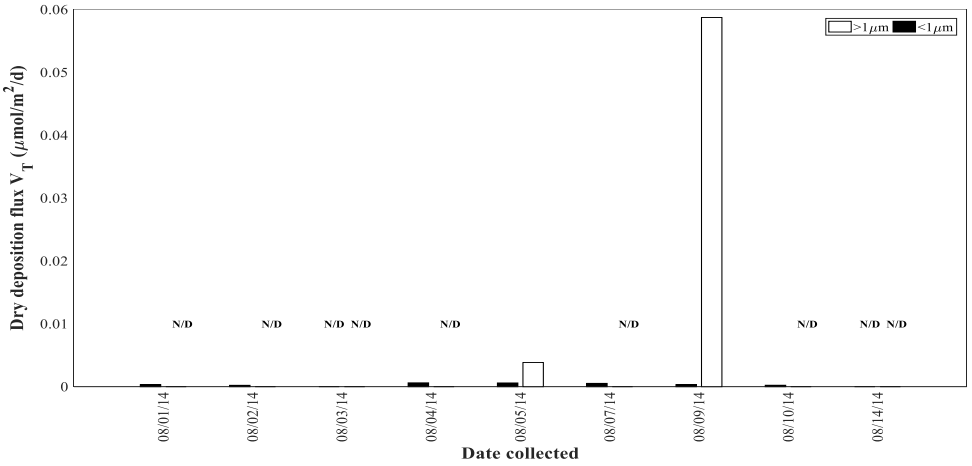

(c) Aerosol vanadium fractional solubility from offshore samples

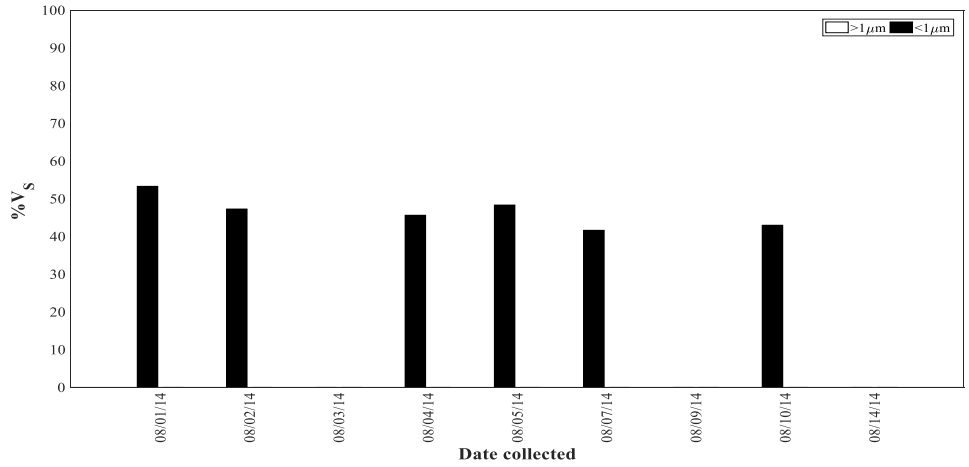

Figure 78. Dry deposition flux of (a) V_S (μmol/m^2/d x 10^4) and (b) V_T (μmol/m^2/d), and (c) %V_S from offshore aerosol samples. Note "N/D" indicates samples for which vanadium was not detected.

(a) Aerosol total chromium from offshore samples

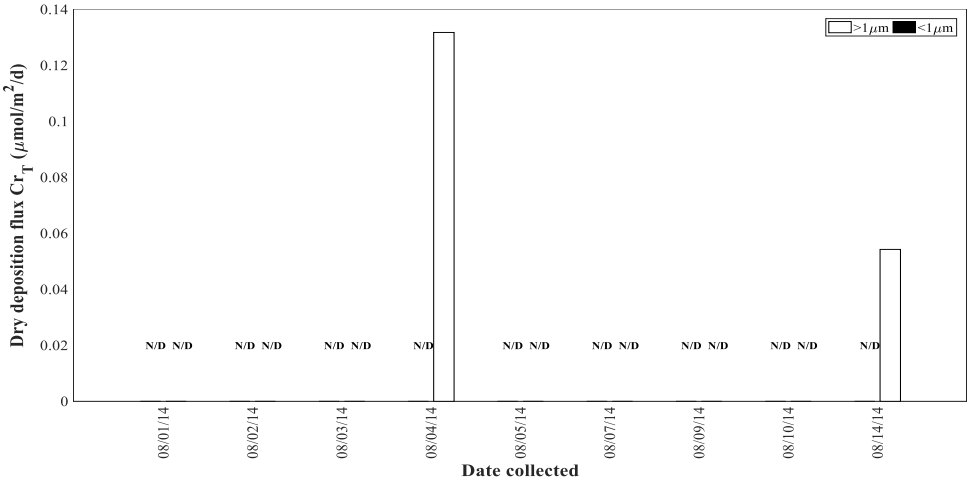

Figure 79. Dry deposition flux of (a) Cr_T (μmol/m^2/d) from offshore aerosol samples. Note "N/D" indicates samples for which chromium was not detected.

(a) Aerosol soluble manganese from offshore samples

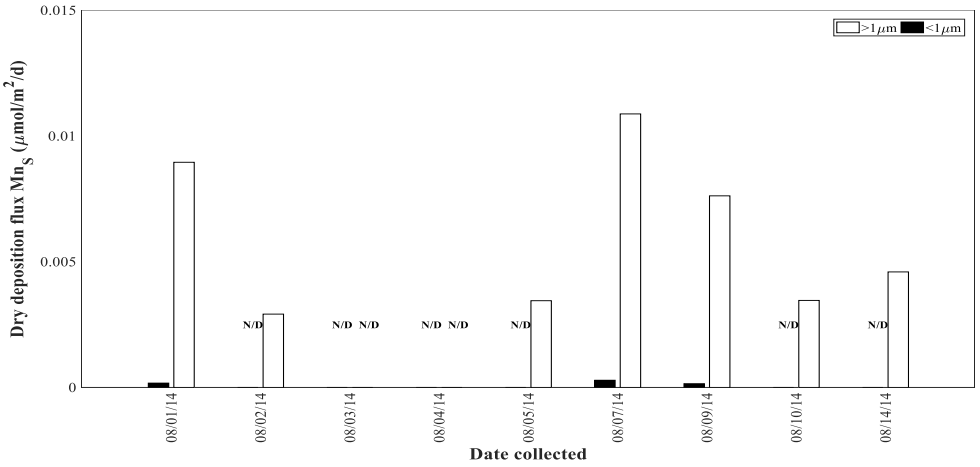

(b) Aerosol total manganese from offshore samples

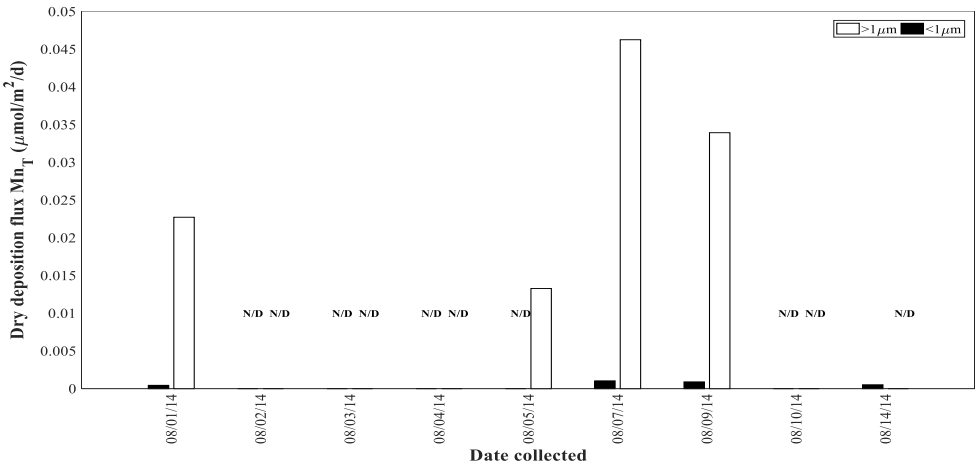

(c) Aerosol manganese fractional solubility from offshore samples

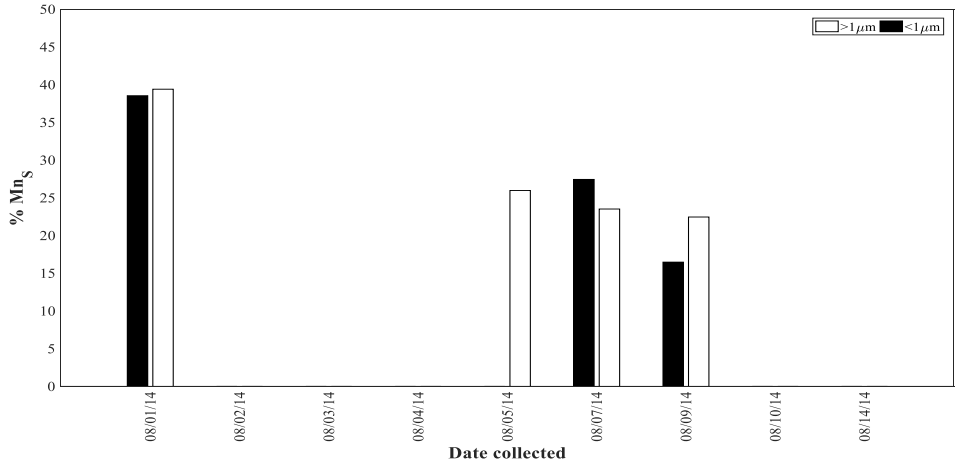

Figure 80. Dry deposition flux of (a) Mn_S (μmol/m^2/d) and (b) Mn_T (μmol/m^2/d), and (c) %Mn_S from offshore aerosol samples. Note "N/D" indicates samples for which manganese was not detected.

(a) Aerosol soluble iron from offshore samples

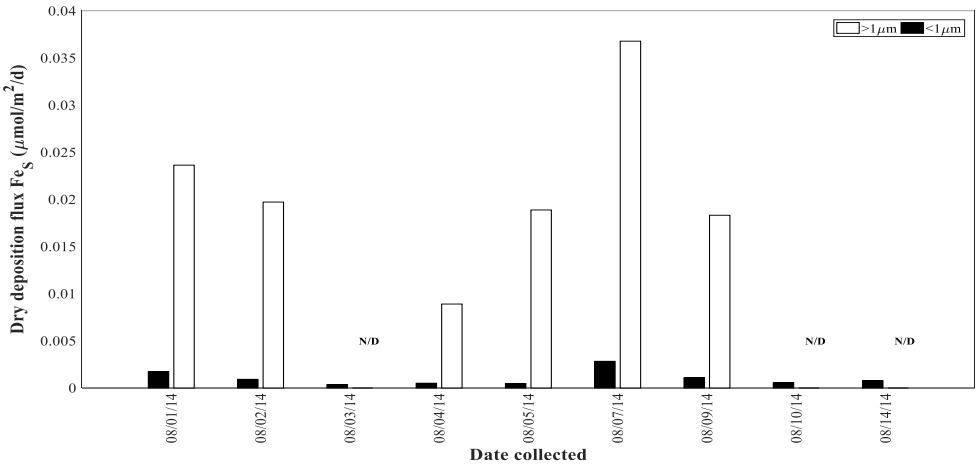

(b) Aerosol total iron from offshore samples

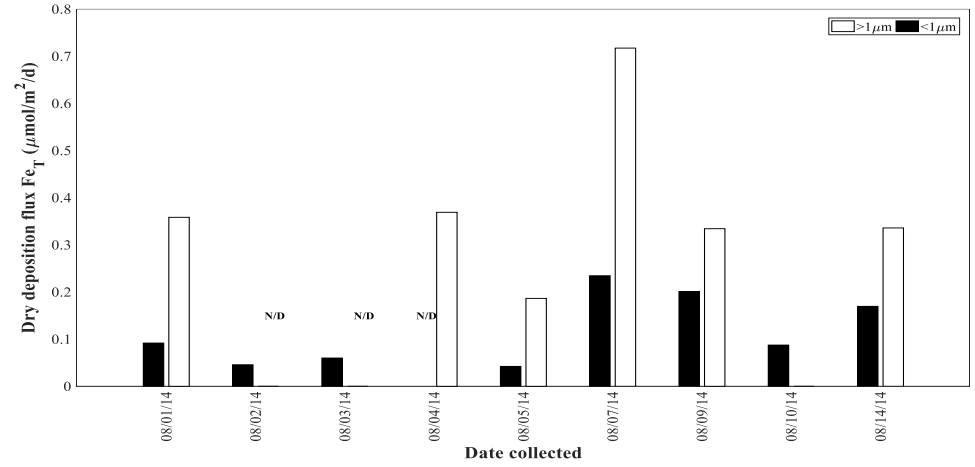

(c) Aerosol iron fractional solubility from offshore samples

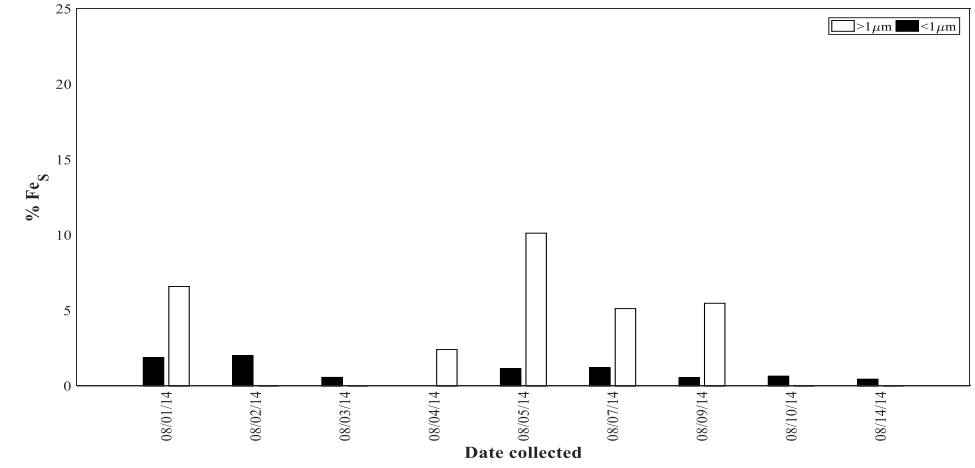

Figure 81. Dry deposition flux of (a) Fe_S (μmol/m^2/d) and (b) Fe_T (μmol/m^2/d), and (c) %Fe_S from offshore aerosol samples. Note "N/D" indicates samples for which iron was not detected.

(a) Aerosol soluble cobalt from offshore samples

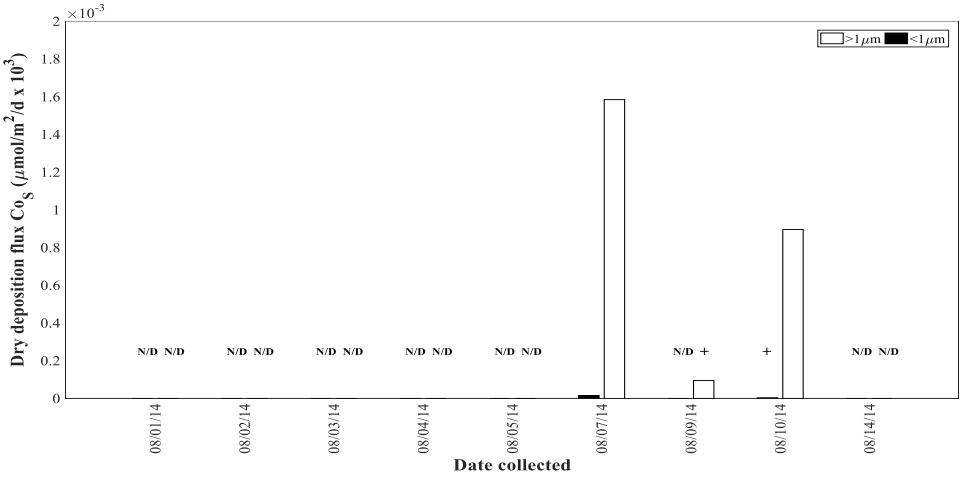

(b) Aerosol total cobalt from offshore samples

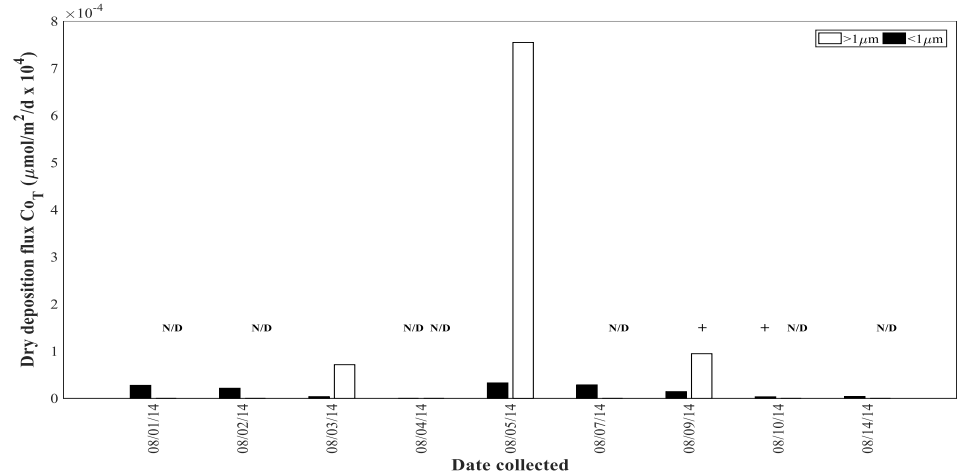

(c) Aerosol cobalt fractional solubility from offshore samples

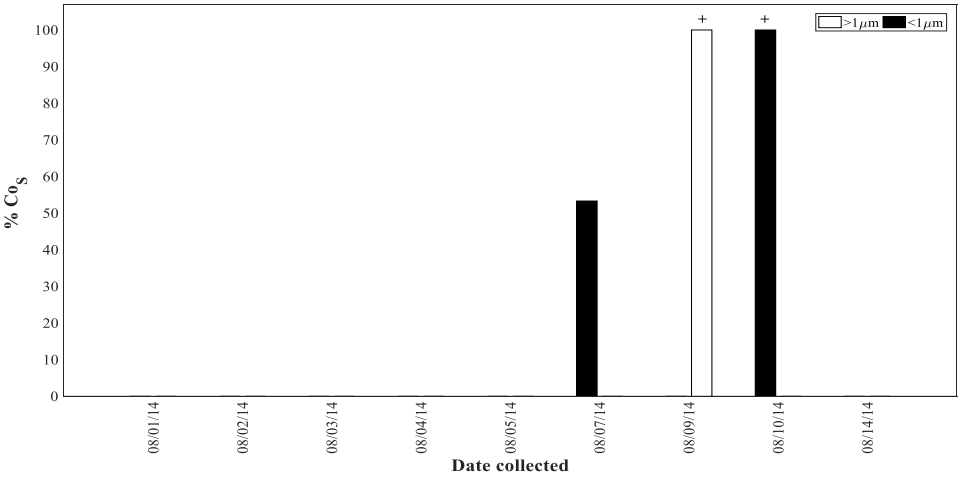

Figure 82. Dry deposition flux of (a) Co_S (μmol/m^2/d x 10^3) and (b) Co_T (μmol/m^2/d x 10^4), and (c) %Co_S from offshore aerosol samples. Note "N/D" indicates samples for which cobalt was not detected.

(a) Aerosol total nickel for offshore samples

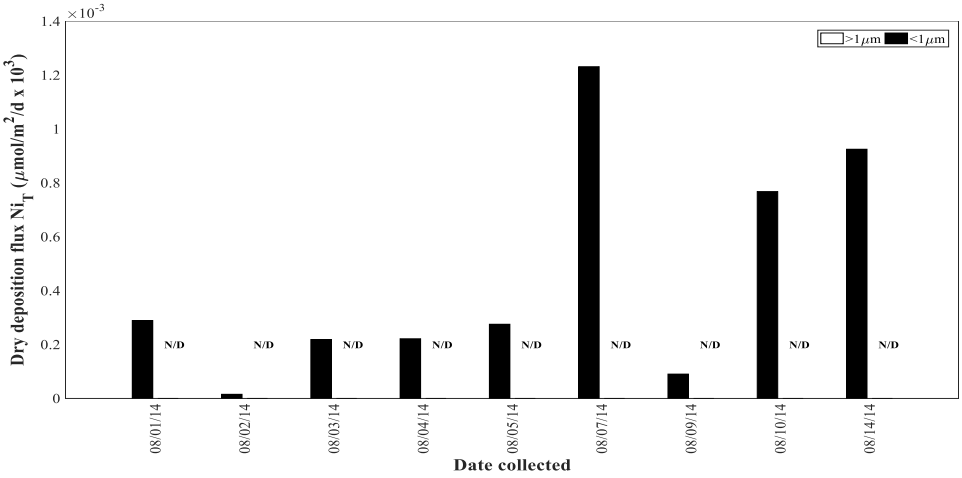

Figure 83. Dry deposition flux of (a) Ni_T (μmol/m^2/d x 10^3). Note "N/D" indicates samples for which nickel was not detected.

(a) Aerosol soluble copper from offshore samples

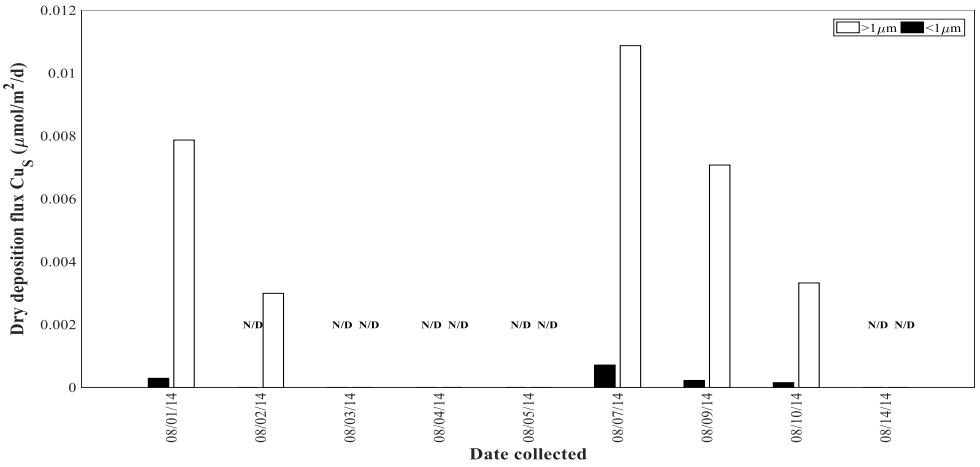

(b) Aerosol total copper from offshore samples

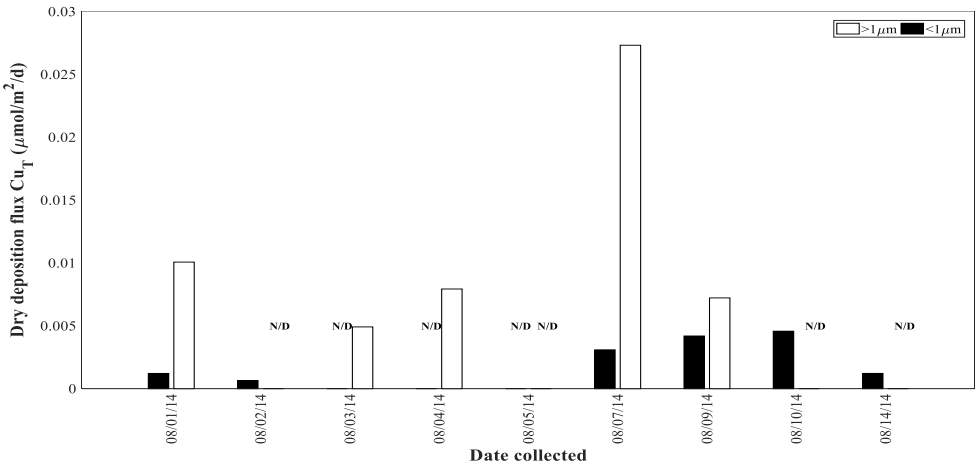

(c) Aerosol copper fractional solubility from offshore samples

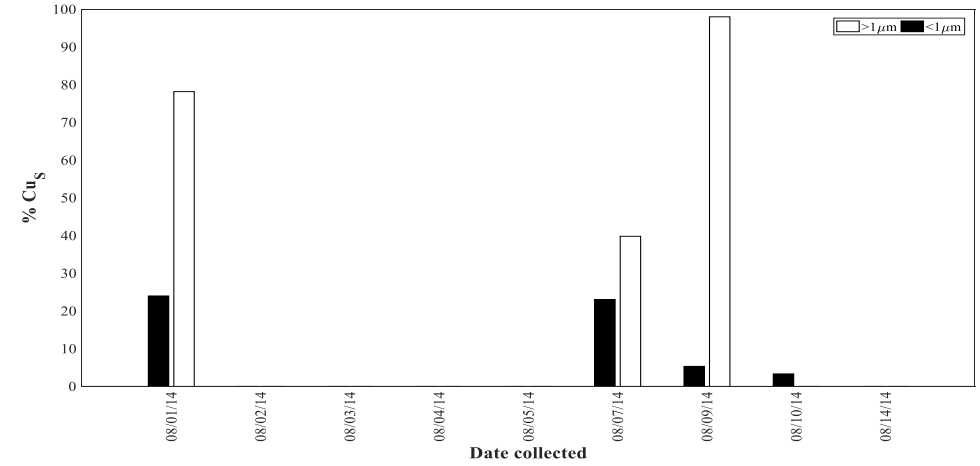

Figure 84. Dry deposition flux of (a) Cu_S (μmol/m^2/d) and (b) Cu_T (μmol/m^2/d), and (c) %Cu_S from offshore aerosol samples. Note "N/D" indicates samples for which copper was not detected.

(a) Aerosol soluble zinc from offshore samples

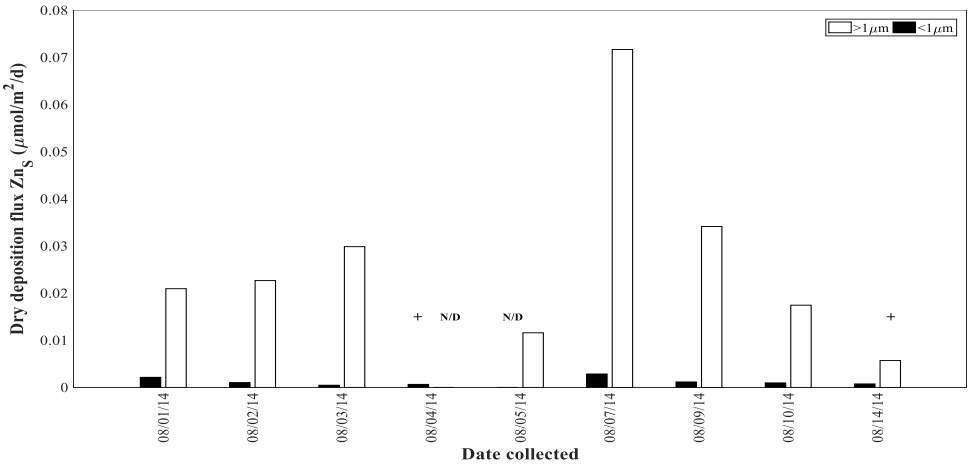

(b) Aerosol total zinc from offshore samples

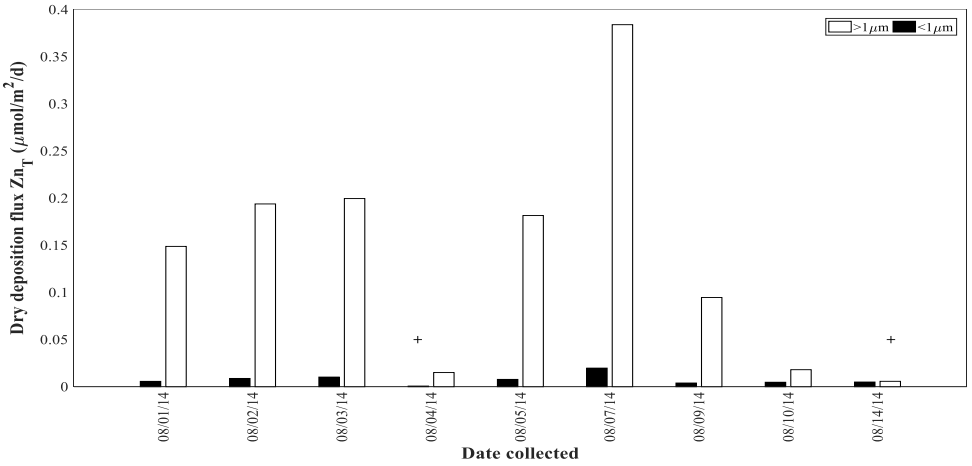

(c) Aerosol zinc fractional solubility from offshore samples

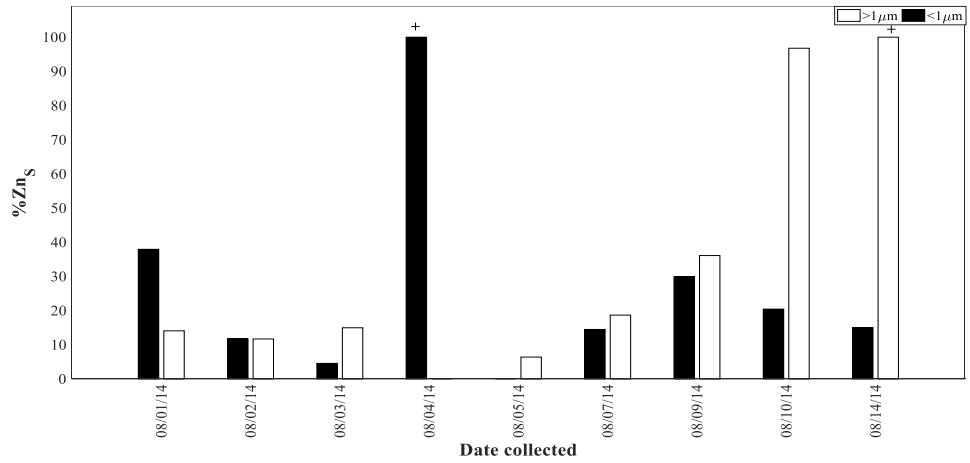

Figure 85. Dry deposition flux of (a) Zn_S (μmol/m^2/d) and (b) Zn_T (μmol/m^2/d), and (c) %Zn_S from offshore aerosol samples. Note "N/D" indicates samples for which zinc was not detected.

(a) Aerosol soluble cadmium from offshore samples

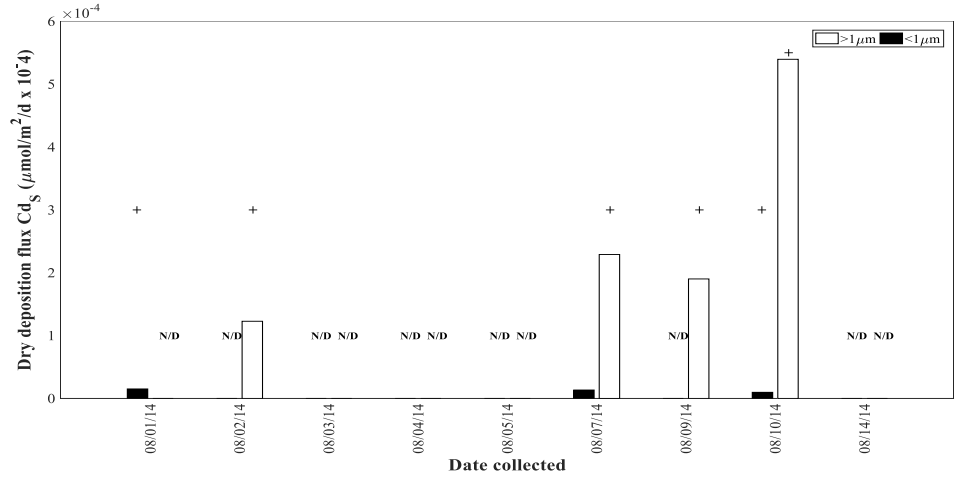

(b) Aerosol total cadmium from offshore samples

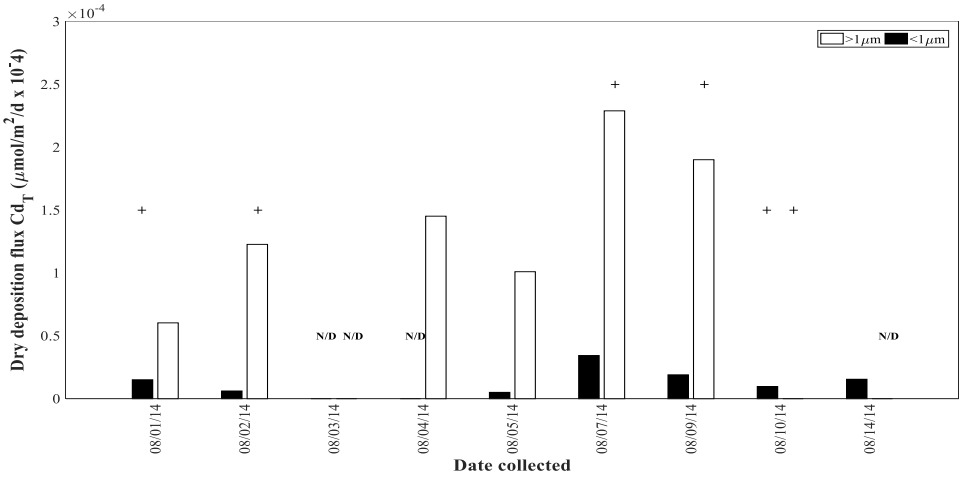

(c) Aerosol cadmium fractional solubility from offshore samples

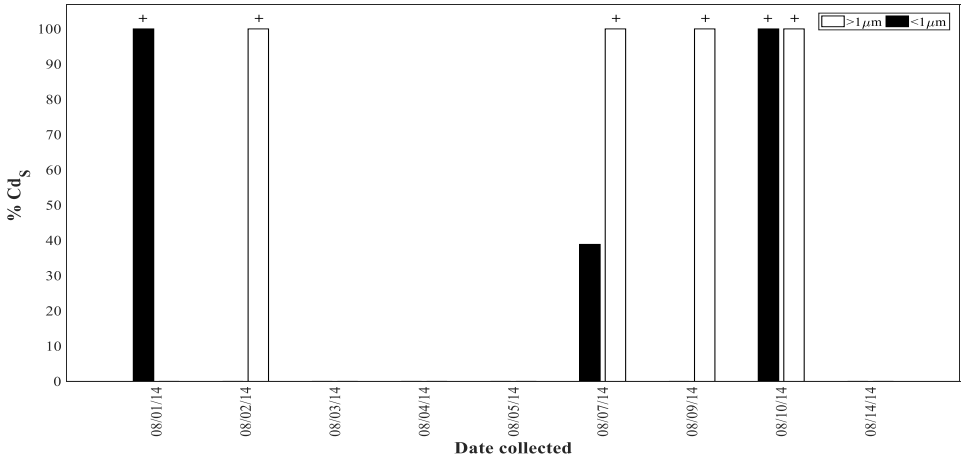

Figure 86. Dry deposition flux of (a) Cd_S (μmol/m^2/d x 10^4) and (b) Cd_T (μmol/m^2/d x 10^4), and (c) %Cd_S from offshore aerosol samples. Note "N/D" indicates samples for which cadmium was not detected.

(a) Aerosol soluble antimony from offshore samples

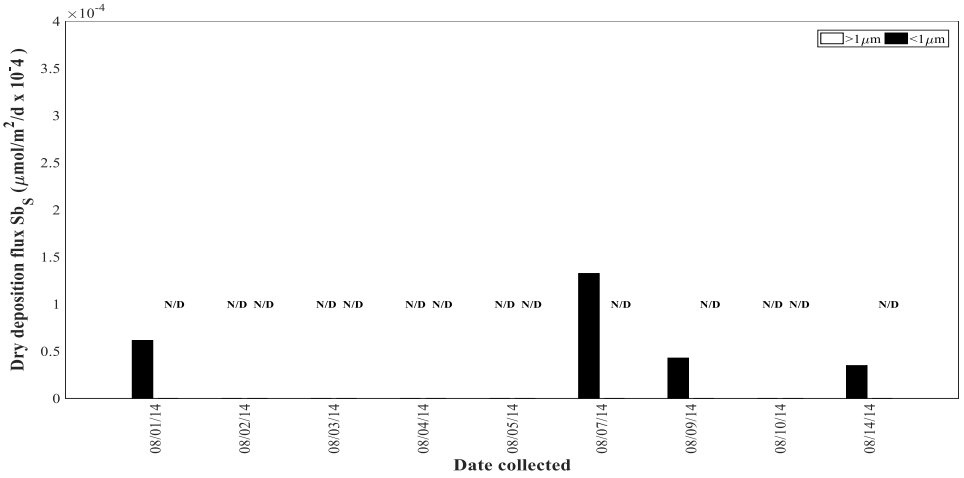

(b) Aerosol total antimony from offshore samples

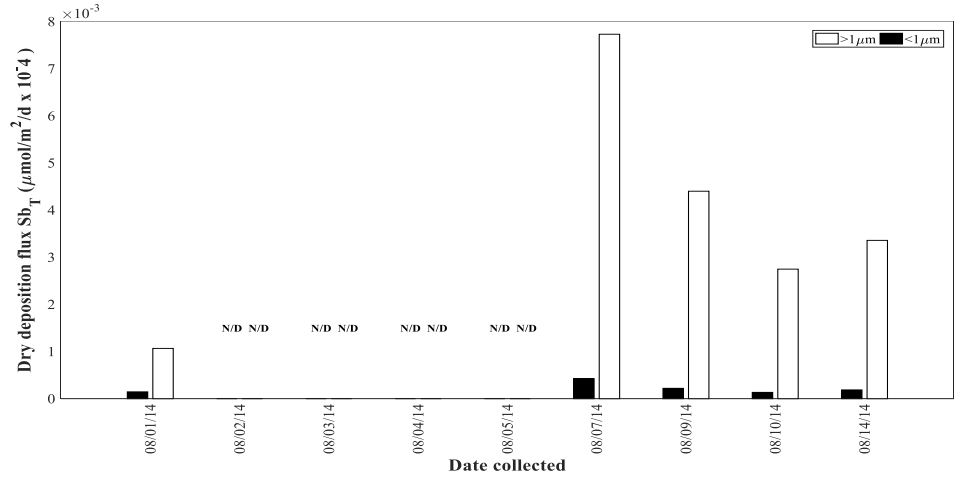

(c) Aerosol antimony fractional solubility from offshore samples

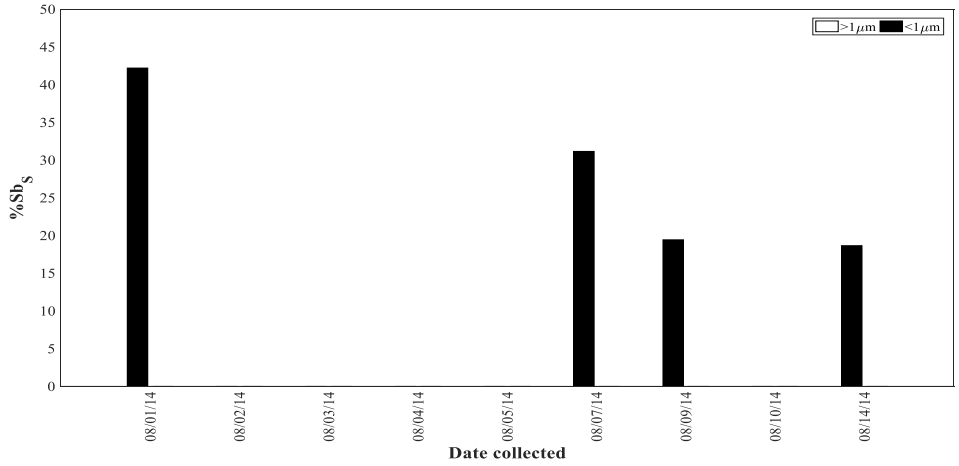

Figure 87. Dry deposition flux of (a) Sb_S (µmol/m^2/d x 10^4) and (b) Sb_T (µmol/m^2/d x 10^3), and (c) $\%Sb_S$ from offshore aerosol samples. Note "N/D" indicates samples for which antimony was not detected.

(a) Aerosol soluble lead from offshore samples

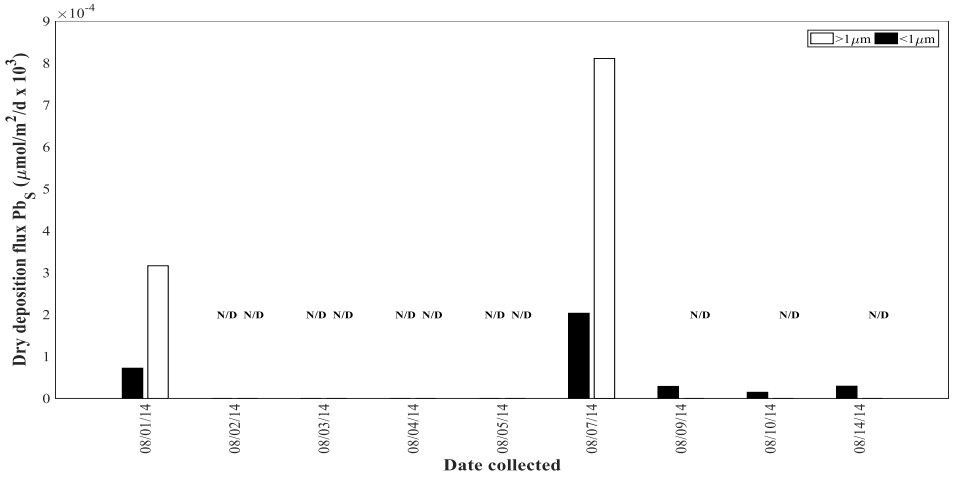

(b) Aerosol total lead from offshore samples

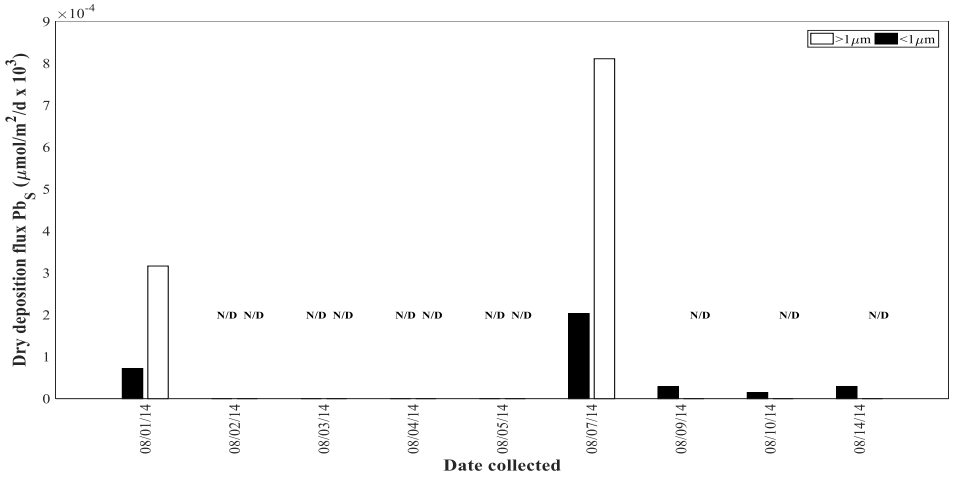

(c) Aerosol lead fractional solubility from offshore samples

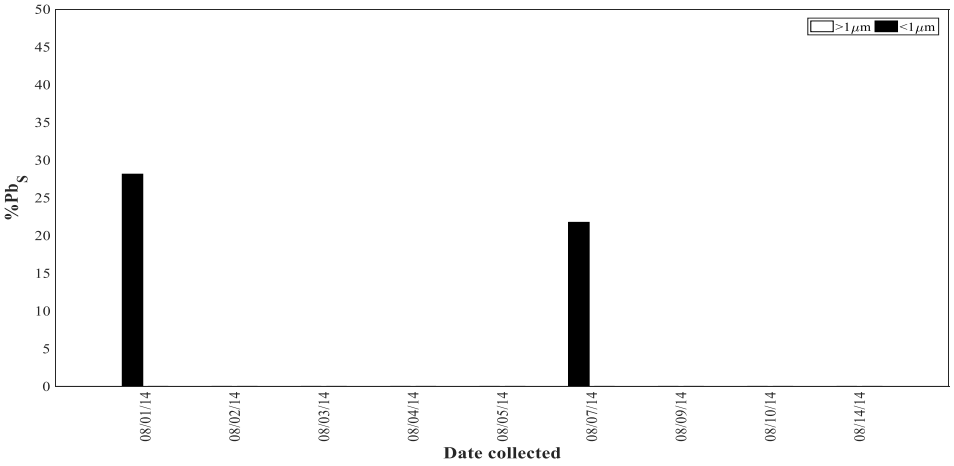

Figure 88. Dry deposition flux of (a) Pb_S (µmol/m^2/d x 10^4) and (b) Pb_T (µmol/m^2/d x 10^4), and (c) $\%Pb_S$ from offshore aerosol samples. Note "N/D" indicates samples for which lead was not detected.

CHAPTER 4

DISCUSSION

4.1 IMPORTANCE OF DEPOSITION MODE AND PARTICLE SIZE FOR THE AEOLIAN FLUX OF NUTRIENTS AT THE EASTERN SHORE SITE

Ammonium was the dominant source of soluble N in wet deposition at the Eastern Shore, with overall mean flux of soluble NH_4^+ (33.4 mmol/m^2/yr), more than twice that of soluble NO_3^- (12.6 mmol/m^2/yr). Regarding question 1, how does the wet and dry atmospheric deposition of nutrients to coastal waters in the MAB vary seasonally, the mean wet deposition flux of soluble NH_4^+ was consistently greater than that for soluble NO_3^- during each season, and the mean wet flux for soluble NH_4^+ was greatest in fall. The higher wet deposition of NH_4^+, compared to NO_3^-, likely reflects the proximity of the land-based field station to regional agricultural activity of the surrounding the southeastern U.S. states [Paerl, 1997; USDA, 1999; Franzluebbers et al., 2005; USDA, 2014]. Agriculture in the southeastern U.S. has shifted towards greater swine (particularly in North Carolina) and broiler production [Franzluebbers et al., 2005], and livestock waste has been recognized as a major contributor of aerosol NH_3 [Paerl, 1997; Gay and Knowlton, 2005], from which NH_4^+ is formed [Baek and Aneja, 2004; Rojas and Venegas, 2009]. The mean wet fluxes of soluble NO_3^- and PO_4^{3-} were highest during summer and lowest during winter.

The soluble NO_3^- in wet deposition is formed from the dissolution of gaseous HNO_3, which mainly originates from NO_x emissions [Russell et al., 1998]. In the U.S., NO_x emissions are regulated due to their link to potential health risks, its association with acid-rain formation, and its role in ground-level ozone formation [Farrell et al., 1999; Galloway et al., 2004; Dentener et al., 2006; Reis et al., 2009; Li et al., 2016]. However, anthropogenic NH_3 emissions are not regulated [Du et al., 2014; Li et al., 2016]. Paerl [1997] found that nearly 20 years (1977-1995) of data from the National Acid Deposition Program showed an increase in the relative concentration of wet deposition NH_4^+, with respect to NO_3^-, in rainwater from eastern North Carolina. The change in regional poultry and swine production was credited

as the cause for this shift in the ammonium/nitrate ratio [Paerl, 1997]. A recent report suggests that at approximately 70% of monitoring sites in the U.S., NH_4^+ is the dominant source of inorganic N in wet deposition [Du et al., 2014]. This agrees well with the results of this study as NH_4^+ was the dominant source of soluble inorganic N in wet deposition samples for the Eastern Shore site during each season.

The overall mean dry deposition fluxes of soluble coarse NH_4^+ (17.1 ± 5.74 μmol/m^2/d) and coarse NO_3^- (17.6 ± 7.52 μmol/m^2/d) at the Eastern Shore site were roughly equal, however, the overall mean flux for fine soluble NH_4^+ flux (3.30 ± 0.905 μmol/m^2/d) was approximately 4-5 times greater than the overall mean fine soluble NO_3^- flux (0.721 ± 0.503 μmol/m^2/d) (Figure 89.). The mean total (fine+coarse) dry deposition flux of soluble NH_4^+ was greater than those for NO_3^- during fall, winter, and spring (Figure 89). The total (fine+coarse) dry deposition fluxes for soluble NO_3^- (18.1 μmol/m^2/d) and NH_4^+ (18.4 μmol/m^2/d) were roughly the same for summer, and greatest during spring (NO_3^- = 23.1 μmol/m^2/d; NH_4^+ = 23.9 μmol/m^2/d) (Figure 89.). Ammonium was also the dominant source of total (fine+coarse) dry soluble inorganic N at the Eastern Shore site during each season.

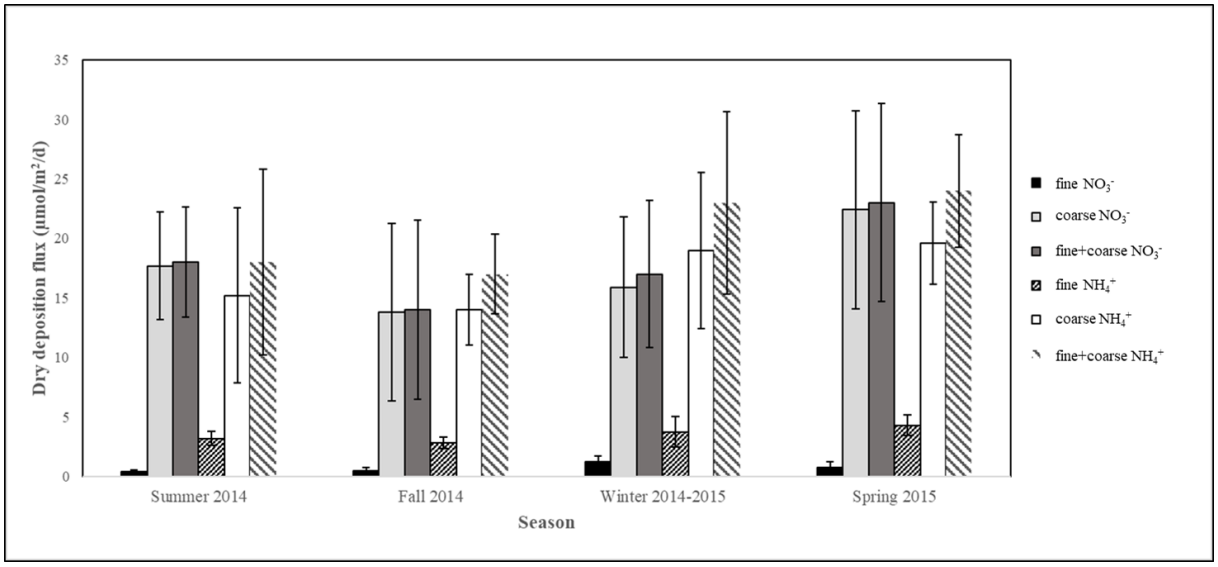

Figure 89. Seasonal mean dry deposition fluxes (µmol/m^2/d) of soluble fine NO_3^-, coarse NO_3^-, fine+coarse NO_3^-, fine NH_4^+, coarse NH_4^+, and fine+coarse NH_4^+ estimated from Eastern Shore aerosol samples. Error bars represent ± 1 standard deviation on the mean.

The overall mean soluble inorganic N (NO_3^-+ NH_4^+) deposition (wet+dry) at the Eastern Shore site was 46 mmol/m^2/yr (126 µmol/m^2/d), of which soluble NO_3^- accounts for only ~27%, therefore NH_4^+ was the dominant aeolian source of soluble inorganic N at this site. This total aeolian flux of total soluble inorganic N (NO_3^-+ NH_4^+) compares reasonably well to that reported for Lewes, Delaware (38 mmol/m^2/yr) and Everglades, Florida (21.8 mmol/m^2/yr) [Prospero et al., 1996]. Jickells et al. [2016] provided estimated inorganic N (wet+dry) deposition flux estimates of 40.1 µmol/m^2/d and 40.9 µmol/m^2/d for the North Atlantic, for the entire ocean basin, using measurements of inorganic N from aerosol and rainwater samples in Baker et al. [2010], and atmospheric chemical transport model results in Dentener et al. [2006], respectively. These estimated fluxes are much lower than the total (wet+dry) soluble inorganic N (NO_3^- + NH_4^+) flux for the Eastern Shore (126.1 µmol/m^2/d), but they provide average deposition rates over a larger region of the North Atlantic, including the remote open ocean, whereas this study provides a regional average for a coastal ocean.

The dry deposition in coarse particles was greater than that in fine particles for all three nutrients. Coarse aerosol particles have greater deposition velocities than fine particles, and are therefore less likely

to be transported great distances from their source [Mahowald et al., 2005]. Both wet and dry atmospheric deposition at the Eastern Shore site were P deficient relative to phytoplankton N and P requirements, where soluble inorganic N includes NO_3^- and NH_4^+, and soluble P includes PO_4^{3-}, with N: P ratios of ~387 and ~700 obtained for wet and dry deposition, respectively. These values far exceed the Redfield ratio (16:1) and agree with the results of previous studies [Baker et al., 2003, 2010; Zamora et al., 2013]. Regarding question 2, what is the dominant deposition mode (wet versus dry) of nutrients to the coastal MAB over the annual cycle, wet deposition was the dominant deposition mode for soluble inorganic nutrients at the Eastern Shore and accounted for 47%, 78%, and 80% of the total (wet+dry) fluxes of NO_3^-, NH_4^+, and PO_4^{3-}, respectively.

Hypothesis 1 posits that atmospheric deposition of inorganic N species will be greatest during the winter months due to increased fossil fuel combustion on the U.S. east coast. The mean total fluxes (wet+dry) for soluble NO_3^- and NH_4^+ were relatively lower, but not significantly different, in winter than during other seasons, therefore the data do not support hypothesis 1. Agricultural farming practices, including soil tillage and fertilizer application, are likely at a minimum during winter, and the agricultural industry of the U.S. southeast is presumed to be a major contributor to the observed inorganic N deposition at the Eastern Shore site. Therefore, lowered agricultural activity during the winter is a probable reason for the observed reductions in the deposition of soluble NH_4^+ at the Eastern Shore site during winter, with greater agricultural activity explaining higher fluxes during the spring and summer.

4.2 IMPORTANCE OF DEPOSITION MODE AND PARTICLE SIZE FOR THE AEOLIAN FLUX OF NUTRIENTS TO OCEAN WATERS IN THE SOUTHERN MID-ATLANTIC BIGHT

Wet and dry deposition fluxes of soluble nutrients for Eastern Shore summer samples were compared to estimated fluxes from shipboard samples to answer question 4, how representative are wet and dry fluxes of nutrients from the coastal field station for deposition in offshore waters (beyond the continental shelf). From wet and dry deposition samples collected at sea, soluble NO_3^- was the dominant source of soluble inorganic N, in contrast to the Eastern Shore site where soluble NH_4^+ was the dominant source of inorganic N. Hypothesis 5 posits that wet and dry fluxes of nutrients and trace metals estimated for the land-based station on the Eastern Shore of Virginia are representative of deposition in offshore MAB waters, beyond the continental shelf. However, wet deposition fluxes of soluble nutrients from both locations did not support hypothesis 5, as the mean wet deposition flux of soluble NO_3^- from Eastern Shore samples was ~twice that for offshore samples, while the mean wet soluble NH_4^+ and PO_4^{3-} fluxes were more than 4 times greater for the Eastern Shore site. These results suggest that a greater proportion of aerosol soluble NO_3^- from the continental U.S. was transported offshore compared to aerosol soluble NH_4^+. Dry deposition fluxes of soluble PO_4^{3-} at both locations were also similar suggesting that this nutrient was not scavenged near the Eastern shore.

The calculated dry deposition flux of soluble NO_3^- was greater for offshore samples collected from, North American air masses, than for samples associated with marine air masses. This agrees with past studies, which suggest that aerosol N concentrations are high in air masses over the temperate North Atlantic that have recently travelled over industrialized and densely populated regions of North America [e.g., Jickells et al., 2016]. The mean dry deposition flux of soluble NO_3^- estimated from offshore samples was slightly greater than that estimated from Eastern Shore summer samples, perhaps due to the sampling of different air masses during the cruise than those typically at the Eastern Shore site. The air masses sampled at sea on 7 August, 9 August, 10 August, and 15 August 2014, during the North Atlantic coastal cruise, travelled from the New York metropolitan area, and were thus different from those typically sampled at the Eastern Shore.

For the Eastern Shore site, the dry fluxes of soluble NO_3^- and NH_4^+ were roughly equal, whereas for offshore samples, the calculated dry soluble NO_3^- flux was ~3 times greater than that for soluble NH_4^+. The lower soluble NH_4^+ dry deposition flux from offshore samples likely reflects the localized input of NH_4^+ by regional agricultural activity around the Eastern Shore site. One probable explanation for the lower mean dry deposition flux of soluble NH_4^+ from offshore samples, compared to that for Eastern Shore site summer samples, is that scavenging of gaseous NH_3 by sea salt aerosol may have removed a great proportion of the aerosol NH_4^+ near the coast [de Leeuw et al., 2001, Spokes and Jickells, 2005]. Therefore, a considerable fraction of NH_3 can be removed from the atmosphere within 10-20 km of the coast [de Leeuw et al., 2001], thus reducing inorganic N inputs in remote ocean waters.

A substantial proportion of the total (fine+coarse) dry soluble NO_3^- and PO_4^{3-} was transported from the U.S. east coast to the offshore waters of the southern MAB, as the deposition fluxes of soluble NO_3^- and PO_4^{3-} estimated from offshore samples were roughly equal to those from Eastern Shore summer samples. Therefore, estimated dry deposition fluxes for soluble NO_3^- and PO_4^{3-} at the Eastern Shore site and offshore locations support hypothesis 5, but the dry fluxes for soluble NH_4^+ from both locations do not support this hypothesis.

The wet and dry soluble inorganic N:P ratios from both Eastern Shore (wet = ~387, dry = ~700) and offshore samples (wet = ~119, dry = ~400) far exceeded the Redfield ratio (16:1). These results agree with those of past studies [e.g., Baker et al., 2003, 2010; Zamora et al., 2013], which found atmospheric deposition to be deficient in P relative to phytoplankton requirements. Atmospheric P is primarily associated with the particle phase [Mahowald et al., 2008; Baker et al., 2010], as this nutrient does not have a stable gaseous phase in the atmosphere [Mahowald et al., 2008], therefore the P cycle has been less anthropogenically perturbed than the N cycle [Mahowald et al., 2008]. Atmospheric inputs of aerosol P are comparatively lower than those for atmospheric N and Fe [Baker et al., 2003, 2007], and atmospheric deposition of N can stimulate primary production in oligotrophic waters provided P is bioavailable, however, an excess of N deposition can lead to P limitation in surface waters [Baker et al., 2003; Krishnamurthy et al., 2009; Zamora et al., 2010].

4.3 IMPORTANCE OF DEPOSITION MODE AND PARTICLE SIZE FOR THE AEOLIAN FLUX OF TRACE METALS AT THE EASTERN SHORE SITE

The mean wet deposition fluxes of total-dissolvable crustal elements Al, Ti, Mn, Fe, and Co were generally greatest during summer, and lower during the fall and winter seasons. Kim et al. [2000] found high Al, Mn, and Fe in wet deposition from two sites on the U.S. east coast to be associated with regional agricultural activity during the spring and summer months. The dry fine and coarse total fluxes of Al, Ti, Mn, Fe, and Co were associated with EOF mode 1, for which air mass back trajectories suggest these trace metals were influenced by both regional agricultural activity and Saharan dust. Seasonal and overall mean crustal enrichment factors for these trace metals were <10, suggesting that these elements were predominantly of lithogenic origin throughout the time series. The peak inputs in wet and dry (total) deposition of Al and Fe at the Eastern Shore during spring and summer appear to be associated with agricultural activity, as these trace metals occur primarily as coarse particles >2.5 μm [Wu et al., 1994; Handler et al., 2008], which are mostly deposited close to their source [Scudlark et al., 1994; Conko et al., 2004].

Regarding question 1, how does the atmospheric deposition (wet and dry) of trace metals to coastal waters in the MAB vary seasonally, the mean wet deposition fluxes of many total-dissolvable trace metals (Al, Ti, V, Cr, Mn, Fe, Co, Cu, and Zn) were greatest during summer, and remained consistently lower through the other seasons. These results do not support hypothesis 2, which posits that the deposition of water-soluble Fe will be greatest for samples collected during the winter months, due to the dominant presence of polluted North American air masses passing over Virginia's Eastern Shore. Similar seasonal wet deposition trends were reported by Pike and Moran [2001] for a coastal site in New Castle, New Hampshire, as the authors found the wet deposition of total-dissolvable Al, Co, Cr, Cu, Fe, V, and Zn to increase from spring through summer. Although the wet deposition fluxes appeared to be greater during summer and fall, only the seasonal means for total-dissolvable V, Mn, and Cd were significantly different. The summer wet deposition of total-dissolvable V was significantly greater than those for winter and spring. The wet deposition total-dissolvable Mn during summer was significantly

greater than that for winter, and the wet deposition of total-dissolvable Cd during fall was significantly greater than that for summer. Wet deposition total-dissolvable Ni data were limited (n = 5), and therefore it could not be determined how the wet deposition of this trace metal changed during the time series. Nickel was only quantified in 5 wet deposition samples from the Eastern Shore site, so the average wet total-dissolvable Ni flux is likely an overestimate.

The estimated annual wet deposition fluxes of total-dissolvable trace metals from this study were generally lower than those reported by previous studies in North Atlantic coastal regions (Table 23). The mean annual wet deposition fluxes of total-dissolvable Al, Mn, Fe, Cu, Zn, Cd, Sb, and Pb at the Eastern Shore site were lower than previous studies (Table 23). Vanadium and Co had wet total-dissolvable fluxes intermediate to values for other field stations along the U.S. east coast (Table 23). The differences from other reported data (in Table 23) may reflect differences in the locations of field sites, and the application of different sample collection and processing methods. Wet deposition data presented by Gao et al. [2016] are from event-based rainwater samples, while estimated fluxes for Conko et al., [2004] are from samples collected bi-weekly (Table 23). Estimated fluxes presented for Kim et al. [2000] and this study are from weekly composite rainwater samples (Table 23). The wet deposition fluxes for Gao et al. [2016], Kim et al. [2000], and this study (Table 23) were estimated using the same rainwater acidification procedure, that is, samples were acidification to 0.4 % v/v with concentrated HCl. However, the wet deposition trace metal flux data for Conko et al. [2004] were estimated from acid digested rainwater and samples were treated with concentrated HNO_3 and HF in a microwave-accelerated reaction system. This likely explains the higher estimated wet fluxes of some metals from this study, compared to those for other U.S. east coast sites in Table 23.

Table 23. Comparison of mean wet deposition fluxes for trace metals (mg/m^2/yr) across East Coast sites. Modified from Gao et al. [2016].

Trace metal	[a]Northern New Jersey	[a]Southern New Jersey	[b]Reston VA	[c]Lewes DE	[c]Still Pond MD	[d]Eastern Shore VA
Al	17.3	12.9	52	15.8	17.8	11
Ti	–	–	–	–	–	0.22
V	0.41	0.57	0.43	–	–	0.048
Cr	0.08	0.22	0.16	0.15	0.14	0.030
Mn	–	–	2	0.96	1.27	0.40
Fe	17.3	17.3	23	12.9	13.1	7.6
Co	0.03	0.05	–	–	–	0.0047
Ni	1.05	4.6	0.24	0.41	0.54	7.5
Cu	2.18	0.33	0.7	0.49	0.43	0.097
Zn	10.9	35.3	4.1	1.9	3	0.49
Cd	0.05	0.06	0.05	0.04	0.05	0.0093
Sb	0.48	1.15	–	–	–	0.022
Pb	0.72	0.85	0.44	0.39	0.51	0.032

[a] Gao et al. [2016], [b] Conko et al. [2004], [c] Kim et al. [2000], and [d] this study.

Aluminum, Ti, Mn, Fe, and Co had generally higher total dry deposition fluxes during the spring and summer, but the fluxes remained consistently lower through the other seasons. In contrast, the total dry deposition fluxes of Cu, Zn, Cd, Sb, and Pb were greatest during the winter. The mean total dry deposition fluxes of Cr, Ni, Cd, and Sb for the Eastern Shore site were less than one tenth of values reported for Northern and Southern New Jersey by Gao et al. [2016] (Table 24). Atmospheric sources of Pb include automobile brake wears, fuel combustion [Pacyna et al., 2007; Song and Gao, 2011], and incinerators [Wu et al., 1994], while Sb is produced from vehicle exhaust [Song and Gao, 2011], brake wear, fossil fuel combustion, non-ferrous metal refining, waste incineration, and incineration of sewage sludge [Filella et al., 2002; Tian et al., 2011; Zhou et al., 2015]. The wet deposition of these two trace metals remained relatively constant during the study period, but the dry deposition was elevated during

the winter possibly due to enhanced anthropogenic activities on the Eastern Shore (e.g., fossil fuel combustion).

Table 24. Comparison of annual dry total deposition fluxes on the U.S east coast ($mg/m^2/yr$).

Trace-metal	[a]Northern New Jersey	[a]Southern New Jersey	[b]Eastern Shore, VA
Al	73.9	28.4	44.3
Ti	–	–	3.48
V	0.27	0.11	0.125
Cr	0.43	1.1	0.0118
Mn	–	–	0.851
Fe	95.9	21.2	28.6
Co	0.05	0.03	0.0137
Ni	0.53	1.11	0.0843
Cu	4.31	0.5	0.489
Zn	3.88	4.21	0.959
Cd	0.01	0.01	0.00522
Sb	0.23	0.5	0.0687
Pb	0.54	0.25	0.142

[a] Gao et al. [2016] and [b]this study

Regarding question 2, what is the dominant deposition mode (wet versus dry) of trace metals to the coastal MAB over the annual cycle, dry deposition was the dominant deposition mode for Al, Ti, V, Mn, Fe, Co, Cu, Zn, Sb, and Pb, while wet deposition was the dominant deposition mode for Cr, Ni, and Cd. More than 80% of the total (wet+dry) mean annual fluxes of crustal trace metals Al, Ti, Mn, Fe, and Co were deposited via dry deposition. These findings are consistent with those of Gao et al. [2016], who found wet deposition to account for only ~20-30% of the total (wet+dry) deposition flux of the crustal elements Al and Fe at New Jersey field sites. Dry deposition (gravitational settling) is thought to be a more important process for mineral particles, whereas wet deposition is more important for anthropogenically produced particles, including Pb and Cu, which are produced by high-temperature combustion processes and occur primarily as fine particles [Scudlark et al., 1994; Pike and Moran, 2001]. Particle size has been identified as factor influencing aerosol solubility [Ridame and Guieu, 2002; Baker

2006d], as fine anthropogenic particles are likely more soluble than coarse lithogenic crustal particles [Baker et al., 2007; Jickells et al., 2016].

The fractional solubility for the fine fraction of aerosol Al, Ti, V, Cr, Fe, Co, Cu, Zn, Cd, Sb, and Pb was greater than that for the coarse fraction of these trace metals in Eastern Shore samples, whereas the fractional solubility of the coarse fraction of Mn was greater than that for the fine fraction at this site. The overall mean and seasonal means for the fractional solubility of Al and Ti were consistently less than 5%, whereas the overall mean and seasonal means for dry fine and coarse Mn varied from 30-44%. Although EFs indicated that Mn at the Eastern Shore is predominantly lithogenic (EF ~3), fine Mn can also be produced from high-temperature combustion processes, including smelting, which produces particles that may be more soluble than mineral dust [Jickells et al., 2016]. The means of the fractional solubilities for the dry fine and coarse fractions of Fe were greatest during the summer. The mean wet flux of total-dissolvable Fe was also greatest during the summer, therefore the data rejects hypothesis 2, which posits that the deposition of soluble Fe will be greatest during the winter. The overall mean fractional solubility for fine and coarse Fe (fine $\%Fe_S = 6.11 \pm 3.15$ %; coarse $\%Fe_S = 1.86 \pm 0.79$ %), as well as the mean seasonal fractional solubilities, were greater than that for mineral dust (~1 %) [Sholkovitz et al., 2012], indicating the influence of anthropogenic emissions on Eastern Shore aerosol samples.

A two-sample t-test indicated that the overall mean fine $\%Fe_S$ (6.11 ± 3.15 %) was significantly greater than the overall mean coarse $\%Fe_S$ (1.86 ± 0.788 %), therefore the data supports hypothesis 3, which posits that aerosol Fe solubility (fractional solubility) will be significantly greater for fine mode particles than that for coarse mode particles. Fine Fe particles are more likely to be associated with anthropogenic processes, which produce aerosol particles with higher solubilities than lithogenic coarse particles where Fe is bound in an aluminosilicate lattice [Mahowald et al., 2005; Sedwick et al., 2007; Sholkovitz et al., 2009, 2012; Wozniak et al., 2015; Jickells et al., 2016]. The fractional solubilities of trace metals often associated with anthropogenic emissions, including V, Cu, Zn, Cd, Pb, and Pb, were also greater for the fine fraction than that for the coarse fraction.

The results from EOF analysis were consistent with AMBTs and calculated EFs, which were used to identify whether the dry total fluxes for groups of trace metals, for the Eastern Shore aerosol samples, showed similar temporal trends. These data were used to answer question 3 (how do the dry fluxes of trace metals from the coastal field station for deposition in offshore waters, beyond the continental shelf ?). Five EOF modes were identified, for which EOF modes 1 and 2 accounted for over 60% of the explained variance in the data. The results of EOF mode 1 showed that the total dry fluxes of fine Ti, coarse Ti, fine V, coarse V, fine Fe, coarse Fe, fine Co, coarse Co, fine Al, coarse Al, fine Mn, and coarse Ni peaked on 9 July 2014, 3 September 2014, 5 November 2014, and 13 May 2015. Air mass back trajectories were then used to identify the source regions of the air masses sampled, and crustal EFs were calculated to confirm whether the aerosols were predominantly lithogenic or anthropogenic. The AMBTs indicated that air masses sampled were likely influenced by Saharan dust and agricultural activities in the southeastern U.S. Crustal EFs near unity were obtained for all EOF mode 1 trace metal variables for those sample periods, confirming a lithogenic source. The data for this study support hypothesis 4, which posits that groups of trace metals will show similar changes in deposition over the annual cycle, indicating a common source. This hypothesis is supported as groups of trace metal variables with likely anthropogenic, lithogenic or mixed sources (anthropogenic and lithogenic) were identified using EOF analysis.

4.4 IMPORTANCE OF DEPOSITION MODE AND PARTICLE SIZE FOR THE AEOLIAN FLUX OF TRACE METALS TO OCEAN WATERS IN THE SOUTHERN MID-ATLANTIC BIGHT

Wet deposition estimates for total-dissolvable trace metals from Eastern Shore and offshore rainwater samples were used to answer question 4 (how representative are wet and dry fluxes of trace metals from the coastal field station for deposition in offshore waters, beyond the continental shelf ?). The wet deposition fluxes of total-dissolvable crustal trace metals Al, Ti, Mn, and Fe, in Eastern Shore summer samples, were around 50 times, 15 times, 15 times, and 20 times greater, respectively, than fluxes from offshore samples. Therefore, the wet deposition fluxes for total-dissolvable Al, Ti, Mn, and Fe from both locations do not support hypothesis 5, which posits that wet and dry fluxes of trace metals estimates for the land-based field station on the Eastern Shore of Virginia are representative of deposition in offshore MAB waters, beyond the continental shelf. However, wet fluxes for all other total-dissolvable trace metals support hypothesis 5. The differences in the wet deposition fluxes of total-dissolvable crustal trace metals for the two sampling locations likely reflects the influence of particle size on the transport of these lithogenic trace metals, which are mainly associated with larger particles (>1 μm) [Jickells et al., 2016], and thus more likely to be deposited closer their source than fine particles [Scudlark et al., 1994]. The atmospheric residence times of particles is influenced by the particle size, as larger particles have shorter residence times and are more likely to be deposited near the source, and smaller particles have longer residence times and can be transported great distances from the source [Baker et 2006d; Mahowald et al., 2005; Luo et al., 2008; Mahowald et al., 2008]. The wet deposition flux of TDNi was over 600 times greater for the Eastern Shore site than that for offshore waters. Nickel is enriched in anthropogenic emissions and is predominantly associated with the fine aerosol fraction [Jickells et al., 2016]. Aerosol processing and rain out events [Song and Gao, 2009] or the sampling of marine air masses during the cruise may explain the lower TDNi fluxes to offshore waters. Eastern Shore wet deposition fluxes of total-dissolvable V, Cr, Co, Cu, and Sb were around 3 to 8 times greater than those estimated from offshore rain samples. Vanadium, Co, Cu, and Sb are enriched in anthropogenic emissions, and occur primarily as fine particles. These fine particles can be transferred at further from their source regions

[Mahowald et al., 2008], therefore the differences in wet deposition fluxes of total-dissolvable V, Co, Cu, and Sb between the Eastern Shore and offshore locations is not as great as those for lithogenic trace metals.

In contrast, the total dry deposition fluxes calculated for offshore samples agreed well with those for Eastern Shore samples, as estimated fluxes for both locations generally fell within the same order of magnitude. These results support hypothesis 5, as dry deposition fluxes of total trace metals for the Eastern Shore site during summer were in close agreement with fluxes estimated from offshore samples. The results suggest that rain out may play an important role in removing larger lithogenic particles (Al, Ti, Mn, and Fe) close to the U.S. east coast as estimated fluxes for the dry deposition of trace metals at the Eastern Shore site and offshore locations were in better agreement than wet deposition fluxes for both sampling sites. In contrast to the Eastern Shore summer samples, the fractional solubilities for the coarse fraction of offshore aerosol metals were greater than those for the fine fraction for Mn, Cu, Zn, and Cd. The fractional solubilities for the coarse aerosol Fe at both locations were roughly equal, with the mean offshore fractional solubility being slightly greater than that for Eastern Shore site summer samples.

CHAPTER 5

CONCLUSIONS

This study has shown that the mean wet deposition flux of soluble NO_3^- at the Eastern Shore site during summer was ~3 times greater than that for rain samples obtained in adjacent offshore waters of the Mid-Atlantic Bight, while mean wet fluxes for soluble NH_4^+ and PO_4^{3-} were ~4 times greater in Eastern Shore samples. In Eastern Shore wet deposition samples, NH_4^+ was the dominant soluble inorganic N species, whereas in offshore rain samples NO_3^- was the main form of soluble inorganic N. The mean total (fine+coarse) dry deposition fluxes of soluble NO_3^- and PO_4^{3-} estimated for Eastern Shore samples were similar to those from offshore samples. However, the mean total (fine+coarse) dry deposition flux of soluble NH_4^+ estimated from Eastern Shore aerosol samples was ~3 times greater than the mean flux from offshore samples. Wet deposition contributed significantly to the soluble aeolian nutrient flux, as it accounted for almost half (~47%) of the soluble NO_3^- flux, and 78-80% of the soluble NH_4^+ and PO_4^{3-} fluxes to the Eastern Shore site. The dry deposition fluxes for the coarse aerosol fraction of the three nutrients studied were higher than those for the fine fraction for both Eastern Shore and offshore aerosol samples.

Atmospheric deposition is a significant source of N_r to the oceans (67 Tg yr^{-1}) and is approximately equal to riverine input, which is estimated to be 50 to 80 Tg yr^{-1} [Duce et al., 2008]. Anthropogenic global production of N_r currently stands at more than 210 Tg yr^{-1} [Fowler et al., 2013; Galloway et al, 2013; Fowler et al., 2015] and exceeds the estimated biological N_2 fixation rate of 177 Tg N yr^{-1} for global oceans [Grosskopf et al., 2012]. The wet and dry deposition soluble inorganic N:P ratios for Eastern Shore and offshore samples far exceeded the Redfield ratio, therefore inorganic P was deficient in atmospheric deposition relative to phytoplankton requirements. Anthropogenic emissions of N_r are projected to continue to increase [Duce et al., 2008] and this may lead to greater P limitation.

The wet deposition fluxes of total-dissolvable trace metals from Eastern Shore summer samples were in good agreement with those for offshore locations, except for trace metals typically associated

with lithogenic particles (Al, Ti, Mn, and Fe). The mean wet deposition fluxes of total-dissolvable Al, Ti, Mn, and Fe were around 50 times, 15 times, 15 times, and 20 times greater, respectively, for Eastern Shore summer samples than for offshore samples. Dry deposition was the dominant depositional mode for Al, Ti, V, Mn, Fe, Co, Cu, Zn, Sb, and Pb at the Eastern Shore site, whereas wet deposition was the dominant deposition mode for Cr, Ni, and Cd. Although the total dry aerosol flux in the coarse fraction (at the Eastern Shore site) was always greater than that in the fine fraction, the aerosol fractional solubility was greater for the fine fraction for all trace metals except Mn. The average seasonal fractional solubility for the fine fraction of aerosol Fe ranged from 5.5-7.3%, while that of the coarse fraction ranged from 1.5-2.5%. For the fine fraction, these values were higher than that reported for mineral dust, reflecting the likely influence of anthropogenic emissions. The mean aerosol Fe fractional solubility for offshore coarse aerosol samples (~3.3 %) was also higher than that of mineral dust [Chuang et al., 2005; Sedwick et al., 2007; Sholkovitz et al., 2012].

Dry deposition of aerosol nutrients and total-dissolvable trace metals for the Eastern Shore site and offshore locations were in better agreement, compared to wet deposition, as dry fluxes for both locations were typically within the same order of magnitude. These results also suggest that rain out likely plays an important role in the removal of larger lithogenic particles close to the continental U.S. The results of this study showed that dry deposition fluxes from the land-based field station are generally representative of deposition in offshore MAB waters, beyond the continental shelf, as dry fluxes of nutrients (NO_3^- and PO_4^{3-}) and trace metals for both locations were in good agreement.

Atmospheric deposition of soluble bioavailable N, P, and Fe to ocean waters in the southern MAB can potentially stimulate new production in these seasonally oligotrophic coastal waters. Sedwick et al. [2018] found primary production in this region to be primarily limited by N and P as shipboard bioassay experiments yielded maxima phytoplankton growth for treatments with iron+nitrate+phosphate additions. In this study, moderate phytoplankton growth was observed in bioassay treatments with additions of rainwater collected in Norfolk, Virginia prior to the research cruise. This confirms that wet

deposition has the potential to stimulate primary production in remote ocean waters of the North Atlantic, far removed from external nutrient input via groundwater and runoff.

Some of the offshore aerosol samples had metal concentrations below detection, therefore future marine aerosol studies in the Mid-Atlantic Bight region should consider collecting aerosol samples over long periods of time, if possible, to improve trace metal detection in samples. The use of multiple atmospheric deposition samplers at land-based field stations or on research cruises would improve the accuracy of flux estimates by providing more replication.

REFERENCES

Adeli, A., et al. (2017). Effects of tillage and broiler litter on crop productions in an eroded soil. *Soil and Tillage Research*, *165*, 198-209.

Anderson, L. D., et al. (2010). Phosphorus associations in aerosols: What can they tell us about P bioavailability?. *Marine Chemistry*, *120*(1-4), 44-56.

Aneja, V. P., et al. (2001). Atmospheric nitrogen compounds II: emissions, transport, transformation, deposition and assessment. *Atmospheric Environment*, *35*(11), 1903-1911.

Aneja, V. P., et al. (2003). Agricultural ammonia emissions and ammonium concentrations associated with aerosols and precipitation in the southeast United States. *Journal of Geophysical Research: Atmospheres*, *108*(D4).

Aneja, V. P., et al. (2008). Ammonia assessment from agriculture: US status and needs. *Journal of Environmental Quality*, *37*(2), 515-520.

Atlas, E., & Pytkowicz, R. M. (1977). Solubility behavior of apatites in seawater. *Limnology and Oceanography*, *22*(2), 290-300.

Ayars, J., & Gao, Y. (2007). Atmospheric nitrogen deposition to the Mullica River-Great Bay estuary. *Marine Environmental Research*, *64*(5), 590-600.

Bacardit, M., & Camarero, L. (2010). Atmospherically deposited major and trace elements in the winter snowpack along a gradient of altitude in the Central Pyrenees: the seasonal record of long-range fluxes over SW Europe. *Atmospheric Environment*, *44*(4), 582-595.

Baek, B. H., & Aneja, V. P. (2004). Measurement and analysis of the relationship between ammonia, acid gases, and fine particles in Eastern North Carolina. *Journal of the Air & Waste Management Association*, *54*(5), 623-633.

Baker, A. R., et al. (2003). Atmospheric deposition of nutrients to the Atlantic Ocean. *Geophysical Research Letters*, *30*(24).

Baker, A. R., et al. (2006a). Trends in the solubility of iron, aluminium, manganese and phosphorus in aerosol collected over the Atlantic Ocean. *Marine Chemistry*, *98*(1), 43-58.

Baker, A. R., et al. (2006b). Nutrients in atmospheric aerosol particles along the Atlantic Meridional Transect. *Deep Sea Research Part II: Topical Studies in Oceanography*, *53*(14), 1706-1719.

Baker, A. R., et al. (2006c). Trends in aerosol nutrient solubility along a west-east transect of the Saharan dust plume. *Geophysical Research Letters*, *33*(7).

Baker, A. R., & Jickells, T. D. (2006d). Mineral particle size as a control on aerosol iron solubility. *Geophysical Research Letters*, *33*(17).

Baker, A. R., et al. (2007). Dry and wet deposition of nutrients from the tropical Atlantic atmosphere: Links to primary productivity and nitrogen fixation. *Deep Sea Research Part I: Oceanographic Research Papers*, *54*(10), 1704-1720.

Baker, A. R., & Croot, P. L. (2010). Atmospheric and marine controls on aerosol iron solubility in seawater. *Marine Chemistry*, *120*(1), 4-13.

Baker, A. R., et al. (2010). Estimation of atmospheric nutrient inputs to the Atlantic Ocean from 50 N to 50 S based on large-scale field sampling: Fixed nitrogen and dry deposition of phosphorus. *Global Biogeochemical Cycles*, *24*(3).

Baker, A. R., et al. (2013). Estimation of atmospheric nutrient inputs to the Atlantic Ocean from 50° N to 50° S based on large-scale field sampling: Iron and other dust-associated elements. *Global Biogeochemical Cycles*, *27*(3), 755-767.

Barrett, P. M., et al. (2012). The trace element composition of suspended particulate matter in the upper 1000 m of the eastern North Atlantic Ocean: A16N. *Marine Chemistry*, *142*, 41-53.

Björkman, K. M., & Karl, D. M. (2003). Bioavailability of dissolved organic phosphorus in the euphotic zone at Station ALOHA, North Pacific Subtropical Gyre. *Limnology and Oceanography*, *48*(3), 1049-1057.

Bouwman, A. F., et al. (1997). A global high-resolution emission inventory for ammonia. *Global Biogeochemical Cycles*, *11*(4), 561-587.

Boyd, P. W., et al. (2000). A mesoscale phytoplankton bloom in the polar Southern Ocean stimulated by iron fertilization. *Nature*, *407*(6805), 695.

Boyd, P. W., et al. (2004). The decline and fate of an iron-induced subarctic phytoplankton bloom. *Nature*, *428*(6982), 549.

Boyd, P. W., et al. (2010). Aerosol iron deposition to the surface ocean-modes of iron supply and biological responses. *Marine Chemistry*, *120*(1-4), 128-143.

Bruland, K. W., et al. (1991). Interactive influences of bioactive trace metals on biological production in oceanic waters. *Limnology and Oceanography*, *36*(8), 1555-1577.

Buck, C. S., et al. (2006). Aerosol iron and aluminum solubility in the northwest Pacific Ocean: Results from the 2002 IOC cruise. *Geochemistry, Geophysics, Geosystems*, *7*(4).

Buck, C. S., et al. (2010). The solubility and deposition of aerosol Fe and other trace elements in the North Atlantic Ocean: observations from the A16N CLIVAR/CO2 repeat hydrography section. *Marine Chemistry*, *120*(1-4), 57-70.

Buck, C. S., et al. (2013). Pacific Ocean aerosols: Deposition and solubility of iron, aluminum, and other trace elements. *Marine Chemistry*, *157*, 117-130.

Calvo, A. I., et al. (2013). Research on aerosol sources and chemical composition: past, current and emerging issues. *Atmospheric Research*, *120*, 1-28.

Capone, D. G., et al. (1997). Trichodesmium, a globally significant marine cyanobacterium. *Science*, *276*(5316), 1221-1229.

Castelao, R., et al. (2010). Temperature, salinity, and density variability in the central Middle Atlantic Bight. *Journal of Geophysical Research: Oceans*, *115*(C10).

Chen, L., & Duce, R. A. (1983). The sources of sulfate, vanadium and mineral matter in aerosol particles over Bermuda. *Atmospheric Environment* (1967), *17*(10), 2055-2064.

Chuang, P. Y., et al. (2005). The origin of water soluble particulate iron in the Asian atmospheric outflow. *Geophysical Research Letters*, *32*(7).

Chester, R., et al. (1993). The atmospheric distributions of trace metals, trace organics and nitrogen species over the North Sea. *Phil. Trans. R. Soc. Lond. A*, *343*(1669), 543-556.

Chester, R., et al. (1999). The trace metal chemistry of atmospheric dry deposition samples collected at Cap Ferrat: a coastal site in the Western Mediterranean. *Marine Chemistry*, *68*(1), 15-30.

Chester, R., et al. (2000). Trace metal chemistry of particulate aerosols from the UK mainland coastal rim of the NE Irish sea. *Atmospheric Environment*, *34*(6), 949-958.

Coale, K. H., et al. (1996). A massive phytoplankton bloom induced by an ecosystem-scale iron fertilization experiment in the equatorial Pacific Ocean. *Nature*, *383*(6600), 495.

Coale, K. H., et al. (2004). Southern Ocean iron enrichment experiment: carbon cycling in high-and low-Si waters. *Science*, *304*(5669), 408-414.

Conko, K. M., et al. (2004). Atmospheric wet deposition of trace elements to a suburban environment, Reston, Virginia, USA. *Atmospheric Environment*, *38*(24), 4025-4033.

Corbett, J. J., et al. (1999). Global nitrogen and sulfur inventories for oceangoing ships. *Journal of Geophysical Research: Atmospheres*, *104*(D3), 3457-3470.

Cornell, S. E., et al. (2003). Organic nitrogen deposition on land and coastal environments: a review of methods and data. *Atmospheric Environment*, *37*(16), 2173-2191.

Cornell, S. E. (2011). Atmospheric nitrogen deposition: Revisiting the question of the importance of the organic component. *Environmental Pollution*, *159*(10), 2214-2222.

Cowling, E. B., & Galloway, J. N. (2002). Challenges and opportunities facing animal agriculture: Optimizing nitrogen management in the atmosphere and biosphere of the Earth 1. *Journal of Animal Science*, *80*(E-Suppl_2), E157-E167.

Croot, P. L., et al. (2004). Influence of the ITCZ on H_2O_2 in near surface waters in the equatorial Atlantic Ocean. *Geophysical Research Letters*, *31*(23).

Dedeurwaerder, H. L., et al. (1983). Estimates of dry and wet deposition and resuspension fluxes of several trace metals in the Southern Bight of the North Sea. *Precipitation scavenging, dry deposition and resuspension*, *2*, 1219-1231.

de Leeuw, G., et al. (2001). Atmospheric input of nitrogen into the North Sea: ANICE project overview. *Continental Shelf Research*, *21*(18-19), 2073-2094.

de Leeuw, G., et al. (2003). Atmospheric nitrogen inputs into the North Sea: effect on productivity. *Continental Shelf Research*, *23*(17-19), 1743-1755.

Dentener, F., et al. (2006). Nitrogen and sulfur deposition on regional and global scales: a multimodel evaluation. *Global Biogeochemical Cycles*, *20*(4).

Doney, S. C., et al. (2007). Impact of anthropogenic atmospheric nitrogen and sulfur deposition on ocean acidification and the inorganic carbon system. *Proceedings of the National Academy of Sciences*, *104*(37), 14580-14585.

Draxler, R., & Rolph, G. (2003). HYSPLIT model. NOAA Air Resources Laboratory, Silver Spring, MD. Available at https://ready.arl.noaa.gov/HYSPLIT.php

Du, E., et al. (2014). Changes in wet nitrogen deposition in the United States between 1985 and 2012. *Environmental Research Letters*, *9*(9), 095004.

Duce, R. A., & Hoffman, G. L. (1976). Atmospheric vanadium transport to the ocean. *Atmospheric Environment (1967)*, *10*(11), 989-996.

Duce, R. A., & Tindale, N. W. (1991). Atmospheric transport of iron and its deposition in the ocean. *Limnology and Oceanography*, *36*(8), 1715-1726.

Duce, R. A., et al. (2008). Impacts of atmospheric anthropogenic nitrogen on the open ocean. *Science*, *320*(5878), 893-897.

Echalar, F., et al. (1995). Aerosol emissions by tropical forest and savanna biomass burning: characteristic trace elements and fluxes. *Geophysical Research Letters*, *22*(22), 3039-3042.

Edwards, D. R., & Daniel, T. C. (1992). Environmental impacts of on-farm poultry waste disposal-A review. *Bioresource Technology*, *41*(1), 9-33.

El Kader, N. A., et al. (2007). Turning, compacting and the addition of water as factors affecting gaseous emissions in farm manure composting. *Bioresource Technology*, *98*(14), 2619-2628.

Eldridge, M. L., et al. (2004). Phytoplankton community response to a manipulation of bioavailable iron in HNLC waters of the subtropical Pacific Ocean. *Aquatic Microbial Ecology*, *35*(1), 79-91.

Eyring, V., et al. (2005). Emissions from international shipping: 1. The last 50 years. *Journal of Geophysical Research: Atmospheres*, *110*(D17).

Eyring, V., et al. (2007). Brief summary of the impact of ship emissions on atmospheric composition, climate, and human health. *Document submitted to the Health and Environment sub-group of the International Maritime Organization*, 6.

Falkowski, P. G., et al. (1998). Biogeochemical controls and feedbacks on ocean primary production. *Science*, *281*(5374), 200-206.

Farrell, A., et al. (1999). The NOx Budget: market-based control of tropospheric ozone in the northeastern United States. *Resource and Energy Economics*, *21*(2), 103-124.

Fennel, K., et al. (2006). Nitrogen cycling in the Middle Atlantic Bight: Results from a three-dimensional model and implications for the North Atlantic nitrogen budget. *Global Biogeochemical Cycles*, *20*(3).

Fernández, A., et al. (2010). Latitudinal distribution of Trichodesmium spp. and N2 fixation in the Atlantic Ocean. *Biogeosciences*, *7*(10), 3167-3176.

Filella, M., et al. (2002). Antimony in the environment: a review focused on natural waters: I. Occurrence. *Earth-Science Reviews*, *57*(1-2), 125-176.

Fowler, D., et al. (2013). The global nitrogen cycle in the twenty-first century. *Phil. Trans. R. Soc. B*, *368*(1621), 20130164.

Fowler, D., et al. (2015). Effects of global change during the 21st century on the nitrogen cycle. *Atmospheric Chemistry and Physics*, *15*(24), 13849-13893.

Franck, V. M., et al. (2003). Iron and zinc effects on silicic acid and nitrate uptake kinetics in three high-nutrient, low-chlorophyll (HNLC) regions. *Marine Ecology Progress Series*, *252*, 15-33.

Franzluebbers, A. J. (2005). Soil organic carbon sequestration and agricultural greenhouse gas emissions in the southeastern USA. *Soil and Tillage Research*, *83*(1), 120-147.

Fung, I. Y., et al. (2000). Iron supply and demand in the upper ocean. *Global Biogeochemical Cycles*, *14*(1), 281-295.

Galloway, J. N., et al. (1995). Nitrogen fixation: Anthropogenic enhancement-environmental response. *Global Biogeochemical Cycles*, *9*(2), 235-252.

Galloway, J. N., et al. (2003). The nitrogen cascade. *AIBS Bulletin*, *53*(4), 341-356.

Galloway, J. N., et al. (2004). Nitrogen cycles: past, present, and future. *Biogeochemistry*, *70*(2), 153-226.

Galloway, J. N., et al. (2008). Transformation of the nitrogen cycle: recent trends, questions, and potential solutions. *Science*, *320*(5878), 889-892.

Galloway, J. N., et al. (2013). A chronology of human understanding of the nitrogen cycle. *Philosophical Transactions of the Royal Society of London B: Biological Sciences*, *368*(1621), 20130120.

Gao, Y., et al. (2001). Seasonal distributions of aeolian iron fluxes to the global ocean. *Geophysical Research Letters*, *28*(1), 29-32.

Gao, Y., et al. (2013). Spatial and particle size distributions of atmospheric dissolvable iron in aerosols and its input to the Southern Ocean and coastal East Antarctica. *Journal of Geophysical Research: Atmospheres*, *118*(22).

Gao, Y., et al. (2016). The air-coastal sea chemical exchange: a case study on the New Jersey coast. *Aquatic Geochemistry*, *22*(4), 275-289.

Gaudichet, A., et al. (1995). Trace elements in tropical African savanna biomass burning aerosols. *Journal of Atmospheric Chemistry*, *22*(1-2), 19-39.

Gay, S. W., & Knowlton, K. F. (2005). Ammonia emissions and animal agriculture.

Gillett, R. W., & Ayers, G. P. (1991). The use of thymol as a biocide in rainwater samples. *Atmospheric Environment. Part A. General Topics*, *25*(12), 2677-2681.

Grosskopf, T., et al. (2012). Doubling of marine dinitrogen-fixation rates based on direct measurements. *Nature*, *488*(7411), 361.

Hagens, M., et al. (2014). Biogeochemical context impacts seawater pH changes resulting from atmospheric sulfur and nitrogen deposition. *Geophysical Research Letters*, *41*(3), 935-941.

Handler, M., et al. (2008). Size and composition of particulate emissions from motor vehicles in the Kaisermühlen-Tunnel, Vienna. *Atmospheric Environment*, *42*(9), 2173-2186.

Ho, T. Y. (2013). Nickel limitation of nitrogen fixation in Trichodesmium. *Limnology and Oceanography*, *58*(1), 112-120.

Hoff, R. V., et al. (2014). Tests of Statistical Hypotheses. *Probability and statistical inference*, 355-414. New York: Macmillan.

Holmes, R. M., et al. (1999). A simple and precise method for measuring ammonium in marine and freshwater ecosystems. *Canadian Journal of Fisheries and Aquatic Sciences*, *56*(10), 1801-1808.

Houghton, R. W., et al. (1982). The Middle Atlantic Bight cold pool: Evolution of the temperature structure during summer 1979. *Journal of Physical Oceanography*, *12*(10), 1019-1029.

Jickells, T. D. (1999). The inputs of dust derived elements to the Sargasso Sea; a synthesis. *Marine Chemistry*, *68*(1-2), 5-14.

Jickells, T. D., et al. (2005). Global iron connections between desert dust, ocean biogeochemistry, and climate. *Science*, *308*(5718), 67-71.

Jickells, T., et al. (2013). The cycling of organic nitrogen through the atmosphere. *Philosophical Transactions of the Royal Society B: Biological Sciences*, *368*(1621), 20130115.

Jickells, T., & Moore, C. M. (2015). The importance of atmospheric deposition for ocean productivity. *Annual Review of Ecology, Evolution, and Systematics*, *46*, 481-501.

Jickells, T. D., et al. (2016). Atmospheric transport of trace elements and nutrients to the oceans. *Philosophical Transactions of the Royal Society A*, *374*(2081), 20150286.

Jickells, T. D., et al. (2017). A reevaluation of the magnitude and impacts of anthropogenic atmospheric nitrogen inputs on the ocean. *Global Biogeochemical Cycles*, *31*(2), 289-305.

Jordi, A., et al. (2012). Copper aerosols inhibit phytoplankton growth in the Mediterranean Sea. *Proceedings of the National Academy of Sciences*, *109*(52), 21246-21249.

Jung, J., et al. (2013). Atmospheric inorganic nitrogen input via dry, wet, and sea fog deposition to the subarctic western North Pacific Ocean. *Atmospheric Chemistry and Physics*, *13*(1), 411-428.

Kanakidou, M., et al. (2016). Past, present, and future atmospheric nitrogen deposition. *Journal of the Atmospheric Sciences*, *73*(5), 2039-2047.

Kane, M. M., et al. (1994). Atmospheric scavenging processes over the North Sea. *Atmospheric Environment*, *28*(15), 2523-2530.

Karl, D. M., & Björkman, K. M. (2014). Dynamics of dissolved organic phosphorus. In *Biogeochemistry of Marine Dissolved Organic Matter (Second Edition)* (pp. 233-334).

Kaufman, Y. J., et al. (2005). Dust transport and deposition observed from the Terra-Moderate Resolution Imaging Spectroradiometer (MODIS) spacecraft over the Atlantic Ocean. *Journal of Geophysical Research: Atmospheres*, *110*(D10).

Keene, W. C., et al. (2002). Organic nitrogen in precipitation over Eastern North America. *Atmospheric Environment*, *36*(28), 4529-4540.

Keene, W. C., et al. (2004). Closure evaluation of size-resolved aerosol pH in the New England coastal atmosphere during summer. *Journal of Geophysical Research: Atmospheres*, *109*(D23).

Kim, G., et al. (2000). Atmospheric wet deposition of trace elements to Chesapeake and Delaware Bays. *Atmospheric Environment*, *34*(20), 3437-3444.

Kim, T. W., et al. (2014). Influence of precipitation events on phytoplankton biomass in coastal waters of the eastern United States. *Global Biogeochemical Cycles*, *28*(1), 1-13.

Kolowith, L. C., et al. (2001). Composition and cycling of marine organic phosphorus. *Limnology and Oceanography*, *46*(2), 309-320.

Krishnamurthy, A., et al. (2007). Effects of atmospheric inorganic nitrogen deposition on ocean biogeochemistry. *Journal of Geophysical Research: Biogeosciences*, *112*(G2).

Krishnamurthy, A., et al. (2009). Impacts of increasing anthropogenic soluble iron and nitrogen deposition on ocean biogeochemistry. *Global Biogeochemical Cycles*, *23*(3).

Krishnamurthy, A., et al. (2010). Impacts of atmospheric nutrient inputs on marine biogeochemistry. *Journal of Geophysical Research: Biogeosciences*, *115*(G1).

Lantzy, R. J., & Mackenzie, F. T. (1979). Atmospheric trace metals: global cycles and assessment of man's impact. *Geochimica et Cosmochimica Acta*, *43*(4), 511-525.

Lentz, S., et al. (2003). Evolution of stratification over the New England shelf during the Coastal Mixing and Optics study, August 1996–June 1997. *Journal of Geophysical Research: Oceans*, *108*(C1).

Li, F., et al. (2008). Distribution, transport, and deposition of mineral dust in the Southern Ocean and Antarctica: Contribution of major sources. *Journal of Geophysical Research: Atmospheres*, *113*(D10).

Li, Y. H. (2000). A compendium of geochemistry: from solar nebula to the human brain. Princeton University Press.

Li, Y., et al. (2014). Observations of ammonia, nitric acid, and fine particles in a rural gas production region. *Atmospheric Environment*, *83*, 80-89.

Li, Y., et al. (2016). Increasing importance of deposition of reduced nitrogen in the United States. *Proceedings of the National Academy of Sciences*, *113*(21), 5874-5879.

Luo, C., et al. (2008). Combustion iron distribution and deposition. *Global Biogeochemical Cycles*, *22*(1).

Mackey, K. R., et al. (2015). Rapid and gradual modes of aerosol trace metal dissolution in seawater. *Frontiers in Microbiology*, *5*, 794.

Mahaffey, C., et al. (2014). Alkaline phosphatase activity in the subtropical ocean: insights from nutrient, dust and trace metal addition experiments. *Frontiers in Marine Science*, *1*, 73.

Mahowald, N. M., et al. (2005). Atmospheric global dust cycle and iron inputs to the ocean. *Global Biogeochemical Cycles*, *19*(4).

Mahowald, N. M., et al. (2008). Atmospheric iron deposition: global distribution, variability, and human perturbations.

Martin, J., & Fitzwater, S. (1988). Iron Deficiency Limits Phytoplankton Growth in the North-East Pacific Subarctic. *Nature*, *331*(6154), 341.

Martin, J. H. (1990). Glacial-interglacial CO2 change: The iron hypothesis. *Paleoceanography*, *5*(1), 1-13.

Martin, J. H., et al. (1994). Testing the iron hypothesis in ecosystems of the equatorial Pacific Ocean. *Nature*, *371*(6493), 123.

Martino, M., et al. (2014). Western Pacific atmospheric nutrient deposition fluxes, their impact on surface ocean productivity. *Global Biogeochemical Cycles*, *28*(7), 712-728.

Mather, R. L., et al. (2008). Phosphorus cycling in the North and South Atlantic Ocean subtropical gyres. *Nature Geoscience*, 1(7), 439.

Mendez, J., et al. (2010). Atmospheric input of manganese and iron to the ocean: Seawater dissolution experiments with Saharan and North American dusts. *Marine Chemistry*, *120*(1-4), 34-43.

Mills, M. M., et al. (2004), Iron and phosphorus co-limit nitrogen fixation in the eastern tropical North Atlantic. *Nature*, *429*(6989), 292.

Moore, C. M., et al. (2013). Processes and patterns of oceanic nutrient limitation. *Nature Geoscience*, *6*(9), 701.

Morel, F. M. M., & Price, N. M. (2003). The biogeochemical cycles of trace metals in the oceans. *Science*, *300*(5621), 944-947.

Morton, P. L., et al. (2013). Methods for the sampling and analysis of marine aerosols: results from the 2008 GEOTRACES aerosol intercalibration experiment. *Limnology and Oceanography: Methods*, *11*(2), 62-78.

Moulin, C., et al. (1997). Control of atmospheric export of dust from North Africa by the North Atlantic Oscillation. *Nature*, *387*(6634), 691.

Nenes, A., et al. (2011). Atmospheric acidification of mineral aerosols: a source of bioavailable phosphorus for the oceans. *Atmospheric Chemistry and Physics*, *11*(13), 6265-6272.

NOAA National Centers for Environmental Information, State of the Climate: National Climate Report for Annual 2014, published online January 2015, retrieved on November 16, 2017 from https://www.ncdc.noaa.gov/sotc/national/201413.

NOAA National Centers for Environmental Information, State of the Climate: National Climate Report for Annual 2015, published online January 2016, retrieved on November 16, 2017 from https://www.ncdc.noaa.gov/sotc/national/201513.

Okin, G. S., et al. (2011). Impacts of atmospheric nutrient deposition on marine productivity: Roles of nitrogen, phosphorus, and iron. *Global Biogeochemical Cycles*, *25*(2).

Pacyna, J. M., & Pacyna, E. G. (2001). An assessment of global and regional emissions of trace metals to the atmosphere from anthropogenic sources worldwide. *Environmental Reviews*, *9*(4), 269-298.

Pacyna, E. G., et al. (2007). Current and future emissions of selected heavy metals to the atmosphere from anthropogenic sources in Europe. *Atmospheric Environment*, *41*(38), 8557-8566.

Paerl, H. W. (1997). Coastal eutrophication and harmful algal blooms: Importance of atmospheric deposition and groundwater as "new" nitrogen and other nutrient sources. *Limnology and Oceanography*, *42*(5part2), 1154-1165.

Paerl, H. W., et al. (1998). Ecosystem responses to internal and watershed organic matter loading: consequences for hypoxia in the eutrophying Neuse River Estuary, North Carolina, USA. *Marine Ecology Progress Series*, *166*, 17-25.

Paerl, H. W., et al. (1999). Rainfall stimulation of primary production in western Atlantic Ocean waters: roles of different nitrogen sources and co-limiting nutrients. *Marine Ecology Progress Series*, *176*, 205-214.

Paerl, H. W., et al. (2001). Atmospheric deposition of nitrogen in coastal waters: biogeochemical and ecological implications. *Nitrogen loading in coastal water bodies: an atmospheric perspective*, 11-52.

Paerl, H. W., et al. (2002). Atmospheric deposition of nitrogen: implications for nutrient over-enrichment of coastal waters. *Estuaries*, *25*(4), 677-693.

Parsons, T. R., et al. (1984). A Manual of Chemical and Biological Methods for Seawater Analysis. 1. *Pergamon Press Inc.*

Paudel, K. P., & McIntosh, C. S. (2005). Country report: Broiler industry and broiler litter-related problems in the southeastern United States. *Waste Management*, *25*(10), 1083-1088.

Paytan, A., et al. (2009). Toxicity of atmospheric aerosols on marine phytoplankton. *Proceedings of the National Academy of Sciences*, *106*(12), 4601-4605.

Peierls, B. L., & Paerl, H. W. (1997). Bioavailability of atmospheric organic nitrogen deposition to coastal phytoplankton. *Limnology and Oceanography*, *42*(8), 1819-1823.

Pike, S. M., & Moran, S. B. (2001). Trace elements in aerosol and precipitation at New Castle, NH, USA. *Atmospheric Environment*, *35*(19), 3361-3366.

Preisendorfer, R. Ä. N. Ü. (1988). Principal component analysis in meteorology and oceanography. *Elsevier Sci. Publ.*, *17*, 425.

Prospero, J. M., et al. (1996). Atmospheric deposition of nutrients to the North Atlantic Basin. In *Nitrogen Cycling in the North Atlantic Ocean and its Watersheds* (pp. 27-73). Springer, Dordrecht.

Quinn, T. L., & Ondov, J. M. (1998). Influence of temporal changes in relative humidity on dry deposition velocities and fluxes of aerosol particles bearing trace elements. *Atmospheric Environment*, *32*(20), 3467-3479.

Raes, F., et al. (2000). Formation and cycling of aerosols in the global troposphere. *Atmospheric Environment*, *34*(25), 4215-4240.

Ratten, J. M., et al. (2015). Sources of iron and phosphate affect the distribution of diazotrophs in the North Atlantic. *Deep Sea Research Part II: Topical Studies in Oceanography*, *116*, 332-341.

Reis, S., et al. (2009). Reactive nitrogen in atmospheric emission inventories. *Atmospheric Chemistry and Physics*, *9*(19), 7657-7677.

Ridame, C., & Guieu, C. (2002). Saharan input of phosphate to the oligotrophic water of the open western Mediterranean Sea. *Limnology and Oceanography*, *47*(3), 856-869.

Roberts-Semple, D., et al. (2012). Seasonal characteristics of ambient nitrogen oxides and ground-level ozone in metropolitan northeastern New Jersey. *Atmospheric Pollution Research*, *3*(2), 247-257.

Rojas, A. L. P., & Venegas, L. E. (2009). Atmospheric deposition of nitrogen emitted in the Metropolitan Area of Buenos Aires to coastal waters of de la Plata River. *Atmospheric Environment*, *43*(6), 1339-1348.

Rojas, A. L. P., & Venegas, L. E. (2010). Interannual variability of estimated monthly nitrogen deposition to coastal waters due to variations of atmospheric variables model input. *Atmospheric Research*, *96*(1), 88-102.

Rolph, G., et al. (2017). Real-time environmental applications and display system: Ready. *Environmental Modelling & Software*, *95*, 210-228.

Russell, K. M., et al. (1998). Sources of nitrogen in wet deposition to the Chesapeake Bay region. *Atmospheric Environment*, *32*(14-15), 2453-2465.

Sanchez-Rodas, D., et al. (2017). Antimony speciation as geochemical tracer for anthropogenic emissions of atmospheric particulate matter. *Journal of hazardous materials*, *324*, 213-220.

Sarthou, G., et al. (2003). Atmospheric iron deposition and sea-surface dissolved iron concentrations in the eastern Atlantic Ocean. *Deep Sea Research Part I: Oceanographic Research Papers*, *50*(10-11), 1339-1352.

Schlosser, C., et al. M. (2014). Seasonal ITCZ migration dynamically controls the location of the (sub) tropical Atlantic biogeochemical divide. *Proceedings of the National Academy of Sciences*, *111*(4), 1438-1442.

Scudlark, J. R., et al. (1994). Atmospheric wet deposition of trace elements to Chesapeake Bay: CBAD study year 1 results. *Atmospheric Environment*, *28*(8), 1487-1498.

Sedwick, P. N., et al. (2007). Impact of anthropogenic combustion emissions on the fractional solubility of aerosol iron: Evidence from the Sargasso Sea. *Geochemistry, Geophysics, Geosystems*, *8*(10).

Sedwick, P. N., et al. (2018). Assessing phytoplankton nutritional status and potential impact of wet deposition in seasonally oligotrophic waters of the Mid-Atlantic Bight. *Geophysical Research Letters*, *45*(7), 3203-3211.

Seitzinger, S. P., & Sanders, R. W. (1999). Atmospheric inputs of dissolved organic nitrogen stimulate estuarine bacteria and phytoplankton. *Limnology and Oceanography*, *44*(3), 721-730.

Shelley, R. U., et al. (2015). Elemental ratios and enrichment factors in aerosols from the US-GEOTRACES North Atlantic transects. *Deep Sea Research Part II: Topical Studies in Oceanography*, *116*, 262-272.

Shelley, R. U., et al. (2017). Quantification of trace element atmospheric deposition fluxes to the Atlantic Ocean (> 40 N; GEOVIDE, GEOTRACES GA01) during spring 2014. *Deep Sea Research Part I: Oceanographic Research Papers*, *119*, 34-49.

Shi, J. H., et al. (2013). Concentration, solubility and deposition flux of atmospheric particulate nutrients over the Yellow Sea. *Deep Sea Research Part II: Topical Studies in Oceanography*, *97*, 43-50.

Sholkovitz, E. R., et al. (2009). Influence of anthropogenic combustion emissions on the deposition of soluble aerosol iron to the ocean: Empirical estimates for island sites in the North Atlantic. *Geochimica et Cosmochimica Acta*, *73*(14), 3981-4003.

Sholkovitz, E. R., et al. (2010). On the fractional solubility of copper in marine aerosols: Toxicity of aeolian copper revisited. *Geophysical Research Letters*, *37*(20).

Sholkovitz, E. R., et al. (2012). Fractional solubility of aerosol iron: Synthesis of a global-scale data set. *Geochimica et cosmochimica acta*, *89*, 173-189.

Slinn, S. A., & Slinn, W. G. N. (1980). Predictions for particle deposition on natural waters. *Atmospheric Environment (1967)*, *14*(9), 1013-1016.

Song, F., & Gao, Y. (2009). Chemical characteristics of precipitation at metropolitan Newark in the US East Coast. *Atmospheric Environment*, *43*(32), 4903-4913.

Song, F., & Gao, Y. (2011). Size distributions of trace elements associated with ambient particular matter in the affinity of a major highway in the New Jersey-New York metropolitan area. *Atmospheric Environment*, *45*(37), 6714-6723.

Spokes, L. J., et al. (2000). Nitrogen deposition to the eastern Atlantic Ocean. The importance of south-easterly flow. *Tellus B: Chemical and Physical Meteorology*, *52*(1), 37-49.

Spokes, L., et al. (2001). Atmospheric inputs of trace metals to the northeast Atlantic Ocean: the importance of southeasterly flow. *Marine Chemistry*, *76*(4), 319-330.

Spokes, L. J., & Jickells, T. D. (2005). Is the atmosphere really an important source of reactive nitrogen to coastal waters?. *Continental Shelf Research*, *25*(16), 2022-2035.

Stein, A. F., et al. (2015). NOAA's HYSPLIT atmospheric transport and dispersion modeling system. *Bulletin of the American Meteorological Society*, *96*(12), 2059-2077.

Stephen, K., & Aneja, V. P. (2008). Trends in agricultural ammonia emissions and ammonium concentrations in precipitation over the Southeast and Midwest United States. *Atmospheric Environment*, *42*(14), 3238-3252.

Taylor, B. W., et al. (2007). Improving the fluorometric ammonium method: matrix effects, background fluorescence, and standard additions. *Journal of the North American Benthological Society*, *26*(2), 167-177.

Taylor, S. R., & McLennan, S. M. (1985). The continental crust: Its evolution and composition. *Lon on: Blackwell*.

Tian, Z., et al. (2008). Atmospheric Fe deposition modes at Bermuda and the adjacent Sargasso Sea. *Geochemistry, Geophysics, Geosystems*, *9*(8).

Tian, H. Z., et al. (2011). Temporal and spatial distribution of atmospheric antimony emission inventories from coal combustion in China. *Environmental Pollution*, *159*(6), 1613-1619.

Tramontano, J. M., et al. (1987). A method for the collection, handling, and analysis of trace metals in precipitation. *Environmental Science & Technology*, *21*(8), 749-753.

U.S. Department of Agriculture (1999). 1997 Census of Agriculture Volume 1:Part 1, Chapter 2, Nat. Agric, Stat, Serv., Washington, D.C.

U.S. Department of Agriculture (2014). 2012 Census of Agriculture Volume 1:Part 1, Chapter 2, Nat. Agric, Stat, Serv., Washington, D.C.

U.S. Energy Information Administration. (2012), 2009 Residential Energy Consumption Survey. Table CE3.1. Household Site End-Use Consumption in the U.S., Totals and Averages, 2009.

Ussher, S. J., et al. (2013). Impact of atmospheric deposition on the contrasting iron biogeochemistry of the North and South Atlantic Ocean. *Global Biogeochemical Cycles*, *27*(4), 1096-1107.

Wang, R., et al. (2015). Sources, transport and deposition of iron in the global atmosphere. *Atmospheric Chemistry and Physics*, *15*(11), 6247-6270.

Wang, R., et al. (2015). Significant contribution of combustion-related emissions to the atmospheric phosphorus budget. *Nature Geoscience*, *8*(1), 48.

Walker, J. T., et al. (2000). Atmospheric transport and wet deposition of ammonium in North Carolina. *Atmospheric Environment*, *34*(20), 3407-3418.

Whitall, D., et al. (2003). Importance of atmospherically deposited nitrogen to the annual nitrogen budget of the Neuse River estuary, North Carolina. *Environment International*, *29*(2-3), 393-399.

Williams, R. M. (1982). A model for the dry deposition of particles to natural water surfaces. *Atmospheric Environment (1967)*, *16*(8), 1933-1938.

Winton, V. H. L., et al. (2015). Fractional iron solubility of atmospheric iron inputs to the Southern Ocean. *Marine Chemistry*, *177*, 20-32.

Wisconsin Department of Natural Resources, Laboratory Certificate Program (1996). Analytical Detection Limit Guidance & Laboratory Guide for Determining Method Detection Limits.

Wozniak, A. S., et al. (2013). Relationships among aerosol water soluble organic matter, iron and aluminum in European, North African, and Marine air masses from the 2010 US GEOTRACES cruise. *Marine Chemistry*, *154*, 24-33.

Wozniak, A. S., et al. (2015). Aerosol water soluble organic matter characteristics over the North Atlantic Ocean: Implications for iron-binding ligands and iron solubility. *Marine Chemistry*, *173*, 162-172.

Wu, Z. Y., et al. (1994). Chesapeake Bay atmospheric deposition study, year 1: sources and dry deposition of selected elements in aerosol particles. *Atmospheric Environment*, *28*(8), 1471-1486.

Wu, J., et al. (2000). Phosphate depletion in the western North Atlantic Ocean. *Science*, *289*(5480), 759-762.

van Vuuren, D. P., et al. (2011). Global projections for anthropogenic reactive nitrogen emissions to the atmosphere: an assessment of scenarios in the scientific literature. *Current Opinion in Environmental Sustainability*, *3*(5), 359-369.

Vasconcellos, P. C., et al. (2007). Water-soluble ions and trace metals in airborne particles over urban areas of the state of São Paulo, Brazil: influences of local sources and long range transport. *Water, Air, and Soil pollution*, *186*(1-4), 63-73.

Violaki, K., et al. (2017). Organic phosphorus in atmospheric deposition over the Mediterranean Sea: An important missing piece of the phosphorus cycle. *Progress in Oceanography*.

Zamora, L., et al. (2010), Atmospheric deposition of nutrients and excess N formation in the North Atlantic. *Biogeosciences (BG)*, *7*, 777-793.

Zamora, L. M., et al. (2013). Atmospheric P deposition to the subtropical North Atlantic: sources, properties, and relationship to N deposition. *Journal of Geophysical Research: Atmospheres*, *118*(3), 1546-1562.

Zhou, J., et al. (2015). Future trends of global atmospheric antimony emissions from anthropogenic activities until 2050. *Atmospheric Environment*, *120*, 385-392.

APPENDIX A

STATISTICAL ANALYSIS OF EASTERN SHORE WET DEPOSITION: SOLUBLE NUTRIENTS

Summary of one-way ANOVA and Kruskal-Wallis statistical tests for Eastern Shore wet deposition flux of soluble nutrients.

Nutrient	ANOVA			Kruskal-Wallis			Notes
	p	df	F	p	df	chi-sq	
NO_3^-	0.2148	46	1.55				The means for the four seasons were not significantly different.
NH_4^+				0.0532	45	7.67	The medians for the four seasons were not significantly different.
PO_4^{3-}	0.0908	34	2.36				The means for the four seasons were not significantly different.

APPENDIX B

STATISTICAL ANALYSIS OF EASTERN SHORE DRY DEPOSITION: SOLUBLE NUTRIENTS

Summary of one-way ANOVA and Kruskal-Wallis statistical tests for Eastern Shore wet deposition flux of soluble nutrients.

Nutrient	Size fraction	ANOVA			Kruskal-Wallis			Notes
		p	df	F	p	df	chi-sq	
NO_3^-	>1µm	0.0026	46	5.57				The mean of spring was significantly different that of both fall and winter.
	<1µm	< 0.0001	48	11.06				The mean of winter was significantly different from that of summer, fall and spring.
NH_4^+	>1µm	0.0248	48	3.43				The means of fall and spring were significantly different.
	<1µm	0.1148	49	2.09				The means of the four seasons were not significantly different.
PO_4^{3-}	>1µm				0.0002	45	19.37	The median of summer was significantly different from that of both winter and spring. The median of fall was significantly different from that of both winter and spring.
	<1µm	0.0041	48	5.08				The mean of winter was significantly different from that of summer, fall and spring.

APPENDIX C

STATISTICAL ANALYSIS OF EASTERN SHORE WET DEPOSITION: TOTAL-DISSOLVABLE TRACE METALS

Summary of the one-way ANOVA and Kruskal Wallis test results for the wet deposition flux of total-dissolvable trace metals for Eastern Shore samples.

Trace metal	One-way ANOVA			Kruskal-Wallis			Notes
	p	df	F	p	df	chi-sq	
Al	0.109	45	2.14				The means of the four seasons were not significantly different.
Ti	0.3039	44	1.25				The means of the four seasons were not significantly different.
V	0.0115	45	4.15				The mean of summer was significantly different from winter and spring.
Cr	0.7991	44	0.34				The means of the four seasons were not significantly different.
Mn	0.0446	45	2.93				The means of summer and winter were significantly different.
Fe	0.1706	45	0.175				The means of the four seasons were not significantly different.
Co	0.0917	38	2.33				The means of the four seasons were not significantly different.
Ni	0.3975	4	1.52				The means of the four seasons were not significantly different.
Cu				0.3577	45	3.23	The medians of the four seasons were not significantly different.
Zn	0.2621	45	1.38				The means of the four seasons were not significantly different.
Cd	0.0233	44	3.52				The means of summer and fall were significantly different.
Sb	0.2903	45	1.29				The means of the four seasons are not significantly different.
Pb				0.8287	44	0.89	The medians of the four seasons are not significantly different.

APPENDIX D

STATISTICAL ANALYSIS OF EASTERN SHORE DRY DEPOSITION: SOLUBLE TRACE METALS

Summary of one-way ANOVA and Kruskal-Wallis analysis of dry soluble trace metal fluxes for Eastern Shore samples.

Trace metal	Size fraction	ANOVA			Kruskal-Wallis			Notes
		p	df	F	p	df	chi-sq	
Al	<1 µm	0.0033	49	5.28				The mean of summer was significantly different from that of fall and winter.
	>1 µm	0.0005	49	7.22				The mean of summer was significantly different from that of fall and winter.
Ti	<1 µm	0.0996	34	2.27				The means of the four seasons were not significantly different.
	>1 µm	0.3605	3	0.3605				The means of the four seasons were not significantly different.
V	<1 µm	0.0021	49	5.71				The mean of summer was significantly different from that of winter and spring.
	>1 µm				0.0609	49	7.37	The medians of the four seasons were not significantly different.
Cr	<1 µm				0.435	49	2.73	The medians of the four seasons were not significantly different.
	>1 µm	0.0633	47	2.61				The means of the four seasons were not significantly different.
Mn	<1 µm	0.4703	49	0.86				The means of the four seasons were not significantly different.
	>1 µm	0.0132	49	3.99				The mean of winter was significantly different from that of summer and fall.
Fe	<1 µm	0.0011	49	6.36				The means of summer and winter were significantly different.
	>1 µm	< 0.0001	49	9.75				The mean of summer was significantly different from that of fall and winter. The mean of winter was significantly different from that of summer and spring.
Co	<1 µm	0.0046	48	4.98				The mean of summer was significantly different from that of winter and spring.
	>1 µm	0.003	46	5.42				The means of summer and winter were significantly different.
Ni	<1 µm	0.0544	47	2.74				The means of summer and spring were significantly different.
	>1 µm	0.0274	19	3.96				The means of winter and spring were significantly different.
Cu	<1 µm	0.8092	49	0.32				The means of the four seasons were not significantly different.
	>1 µm	0.5238	49	0.76				The means of the four seasons were not significantly different.
Zn	<1 µm				< 0.0001	49	34.16	The median of spring was significantly different from those for summer, fall, and winter.
	>1 µm	0.0619	49	2.62				The means of the four seasons were not significantly different.
Cd	<1 µm	0.0048	49	4.91				The means of summer and fall were significantly different.
	>1 µm				0.5732	48	2	The medians of the four seasons were not significantly different.
Sb	<1 µm	0.0269	49	3.35				The means of the four seasons were not significantly different.
	>1 µm	0.344	49	1.14				The means of the four seasons were not significantly different.
Pb	<1 µm	1.77	49	0.1664				The means of the four seasons were not significantly different.
	>1 µm	0.2146	49	1.55				The means of the four seasons were not significantly different.

APPENDIX E

STATISTICAL ANALYSIS OF EASTERN SHORE DRY DEPOSITION: TOTAL TRACE METALS

Summary of one-way ANOVA and Kruskal-Wallis analysis of dry total trace metal fluxes for Eastern Shore samples.

Trace metal	Size fraction	ANOVA			Kruskal-Wallis			Notes
		p	df	F	p	df	chi-sq	
Al	<1 µm	0.182	49	0.1822				
	>1 µm				0.0002	48	49.42	The median of winter was significantly different from that of summer, fall, and spring.
Ti	<1 µm	0.2292	49	1.49				The means of the four seasons were not significantly different.
	>1 µm				0.0009	48	16.49	The median of winter were significantly different from those for summer, fall, and spring.
V	<1 µm	0.0266	49	3.36				The means of summer and spring were significantly different.
	>1 µm				0.0227	48	9.56	The medians of summer and winter were significantly different.
Cr	<1 µm	0.0004	9	32				The mean of winter was significantly different from that of summer, fall, and spring.
	>1 µm	0.1512	7	2.82				The means of the four seasons were not significantly different.
Mn	<1 µm	0.4952	49	0.81				The means of the four seasons were not significantly different.
	>1 µm	0.2122	48	1.56				The means of the four seasons were not significantly different.
Fe	<1 µm	0.2713	49	1.35				The means of the four seasons were not significantly different.
	>1 µm				0.0004	48	18.03	The median of winter was significantly different from summer and spring.
Co	<1 µm	0.3452	49	1.13				The means of the four seasons were not significantly different.
	>1 µm				0.0038	48	13.44	The median of winter was significantly different from summer and spring.
Ni	<1 µm				0.0008	48	6.62	The median of spring was significantly different from that of summer and fall.
	>1 µm	0.5868	48	0.65				The means of the four seasons were not significantly different.
Cu	<1 µm	0.1524	49	1.84				The means of the four seasons were not significantly different.
	>1 µm				0.576	48	1.98	The medians of the four seasons were not significantly different.
Zn	<1 µm	0.0003	49	7.53				The mean of winter was significantly different from that of summer, fall and spring.
	>1 µm	0.4246	48	0.95				The means of the four seasons were not significantly different.
Cd	<1 µm	0.0026	49	5.5				The mean of winter was significantly different from the means of summer and spring.
	>1 µm	0.2315	48	1.48				The means of the four seasons were not significantly different.
Sb	<1 µm	0.02	49	3.61				The means of fall and winter were significantly different.
	>1 µm				< 0.0001	48	22.99	The medians of summer and fall were significantly different.
Pb	<1 µm	0.0166	49	3.78				The means of summer and winter were significantly different.
	>1 µm				0.9314	48	0.44	The medians of the four seasons were not significantly different.

APPENDIX F

STATISTICAL ANALYSIS OF EASTERN SHORE FRACTIONAL SOLUBILITY OF AEROSOL TRACE METALS

Summary of one-way ANOVA and Kruskal-Wallis analysis of aerosol trace metal fractional solubility for Eastern Shore samples.

Trace metal	Size fraction	ANOVA			Kruskal-Wallis			Notes
		p	df	F	p	df	chi-sq	
Al	<1 µm	0.0033	49	5.28				The mean of summer was significantly different from that of fall and winter.
	>1 µm	0.0005	49	7.22				The mean of summer was significantly different from that of fall and winter.
Ti	<1 µm	0.0996	34	2.27				The means of the four seasons were not significantly different.
	>1 µm	0.3605	3	0.3605				The means of the four seasons were not significantly different.
V	<1 µm	0.0021	49	5.71				The mean of summer was significantly different from that of winter and spring.
	>1 µm				0.0609	49	7.37	The medians of the four seasons were not significantly different.
Cr	<1 µm				0.435	49	2.73	The medians of the four seasons were not significantly different.
	>1 µm	0.0633	47	2.61				The means of the four seasons were not significantly different.
Mn	<1 µm	0.4703	49	0.86				The means of the four seasons were not significantly different.
	>1 µm	0.0132	49	3.99				The mean of winter was significantly different from that of summer and fall.
Fe	<1 µm	0.0011	49	6.36				The means of summer and winter were significantly different.
	>1 µm	<0.0001	49	9.75				The mean of summer was significantly different from that of fall and winter. The mean of winter was significantly different from that of summer and spring.
Co	<1 µm	0.0046	48	4.98				The mean of summer was significantly different from that of winter and spring.
	>1 µm	0.003	46	5.42				The means of summer and winter were significantly different.
Ni	<1 µm	0.0544	47	2.74				The means of summer and spring were significantly different.
	>1 µm	0.0274	19	3.96				The means of winter and spring were significantly different.
Cu	<1 µm	0.8092	49	0.32				The means of the four seasons were not significantly different.
	>1 µm	0.5238	49	0.76				The means of the four seasons were not significantly different.
Zn	<1 µm				< 0.0001	49	34.16	The median of spring was significantly different from those for summer, fall, and winter.
	>1 µm	0.0619	49	2.62				The means of the four seasons were not significantly different.
Cd	<1 µm	0.0048	49	4.91				The means of summer and fall were significantly different.
	>1 µm				0.5732	48	2	The medians of the four seasons were not significantly different.
Sb	<1 µm	0.0269	49	3.35				The means of the four seasons were not significantly different.
	>1 µm	0.344	49	1.14				The means of the four seasons were not significantly different.
Pb	<1 µm	1.77	49	0.1664				The means of the four seasons were not significantly different.
	>1 µm	0.2146	49	1.55				The means of the four seasons were not significantly different.

APPENDIX G

EMPIRICAL ORTHOGONAL ANALYSIS: EIGENVALUES FOR MODES 1-5

The eigenfunction values for trace metal variables associated with EOF modes 1 through 5 are provided. The larger the eigenfunction value, the greater the variance of the trace metal variable is represented by that EOF mode. Positive eigenfunction values indicated that the total flux of that trace metal variable changed in the same direction as indicated on the flux time mode plot, while negative eigenfunction values indicated that the total flux of the trace metal variables changed in the opposite direction as that shown on the flux time mode plot.

Trace metal variable	Description	Eigenfunction values				
		Mode 1	Mode 2	Mode 3	Mode 4	Mode 5
1	Coarse Cd	N/A	N/A	-0.27	N/A	N/A
2	Fine Cd	N/A	-0.31	0.29	N/A	N/A
3	Coarse Sb	N/A	N/A	-0.33	N/A	N/A
4	Fine Sb	N/A	-0.33	N/A	N/A	N/A
5	Coarse Pb	N/A	-0.24	N/A	N/A	N/A
6	Fine Pb	N/A	-0.34	N/A	N/A	N/A
7	Coarse Al	0.25	0.21	N/A	N/A	N/A
8	Fine Al	0.25	N/A	0.22	N/A	N/A
9	Coarse Ti	0.26	N/A	N/A	N/A	N/A
10	Fine Ti	0.25	N/A	0.24	N/A	N/A
11	Coarse V	0.26	N/A	N/A	N/A	N/A
12	Fine V	0.21	N/A	N/A	-0.34	-0.37
13	Coarse Cr	N/A	N/A	N/A	-0.24	0.34
14	Fine Cr	N/A	N/A	N/A	-0.44	0.55
15	Coarse Mn	0.24	N/A	N/A	0.26	-0.20
16	Fine Mn	0.22	N/A	0.37	N/A	N/A
17	Coarse Fe	0.25	N/A	N/A	N/A	N/A
18	Fine Fe	0.26	N/A	0.25	N/A	N/A
19	Coarse Co	0.26	N/A	N/A	N/A	N/A
20	Fine Co	N/A	N/A	N/A	N/A	N/A
21	Coarse Ni	0.23	N/A	-0.26	N/A	N/A
22	Fine Ni	N/A	N/A	N/A	-0.42	-0.28
23	Coarse Cu	N/A	-0.26	N/A	0.42	N/A
24	Fine Cu	N/A	-0.29	0.28	N/A	N/A
25	Coarse Zn	N/A	N/A	N/A	0.2	0.30
26	Fine Zn	N/A	-0.33	0.3	N/A	N/A

APPENDIX H

ENRICHMENT FACTORS FOR EASTERN SHORE AEROSOL TOTAL TRACE METALS

(a) Enrichment factors for Eastern Shore aerosol total titanium

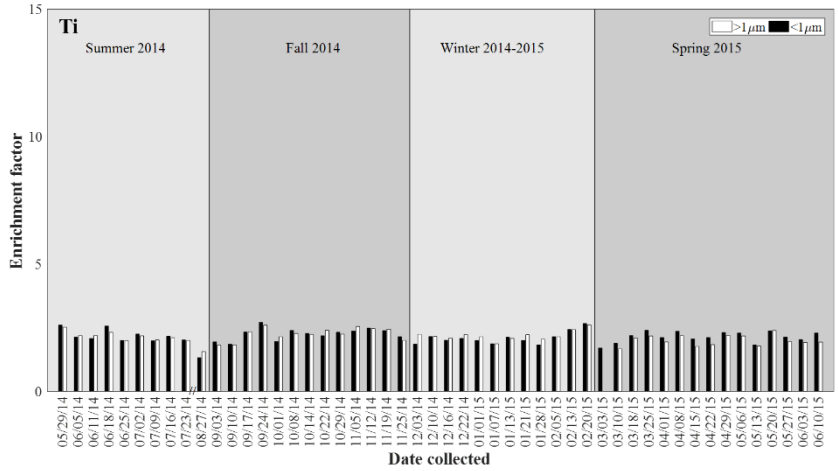

(b) Enrichment factors for Eastern Shore aerosol total vanadium

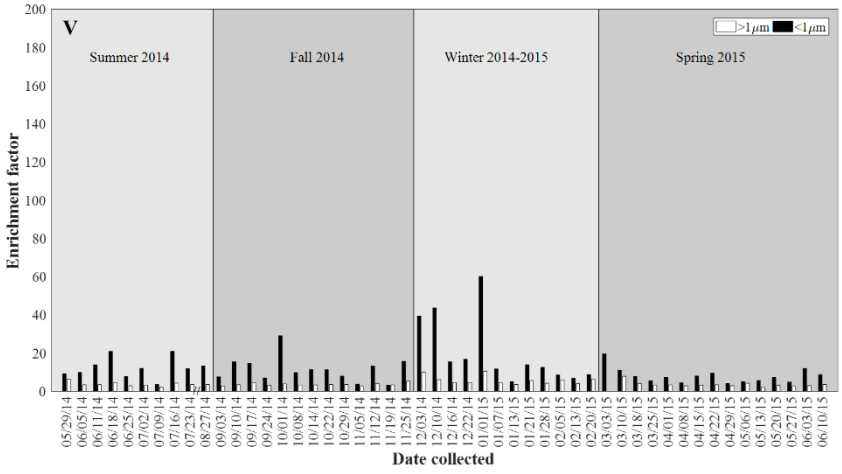

Figure 1. Enrichment factors calculated for total concentrations of (a) Ti, (b) V, (c) Cr, (d) Mn, (e) Fe, (f) Co, (g) Ni, (h) Cu, (i) Zn, (j) Cd, (k) Sb, and (l) Pb from Eastern Shore aerosol samples.

APPENDIX H. Continued.

(c) Enrichment factors for Eastern Shore aerosol total chromium

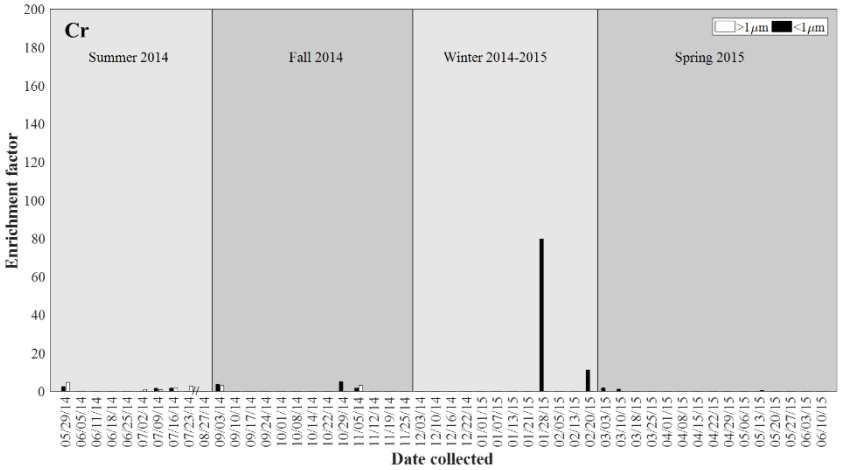

(d) Enrichment factors for Eastern Shore aerosol total manganese

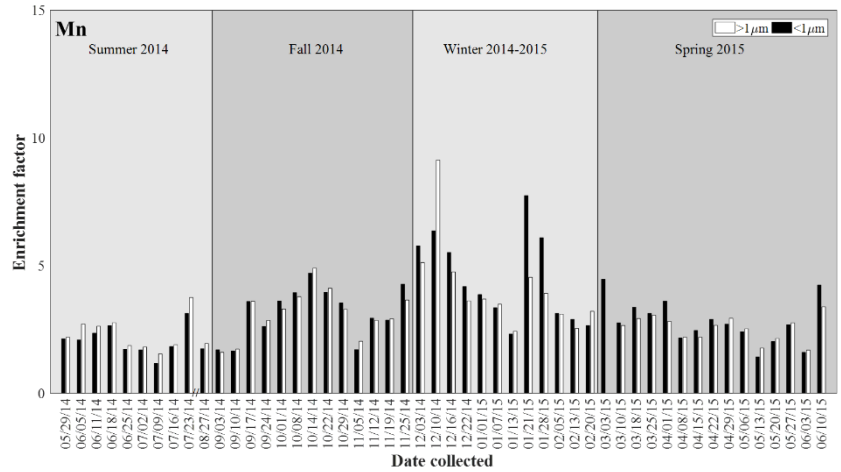

(e) Enrichment factors for Eastern Shore aerosol total iron

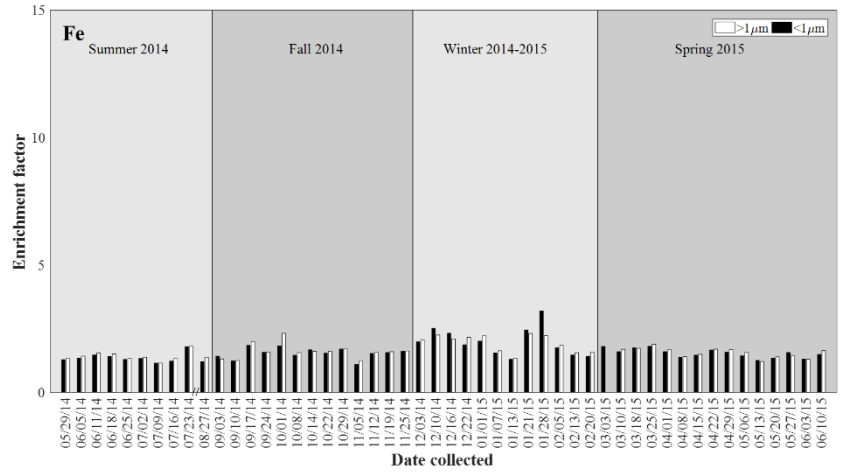

APPENDIX H. Continued.

(f) Enrichment factors for Eastern Shore aerosol total cobalt

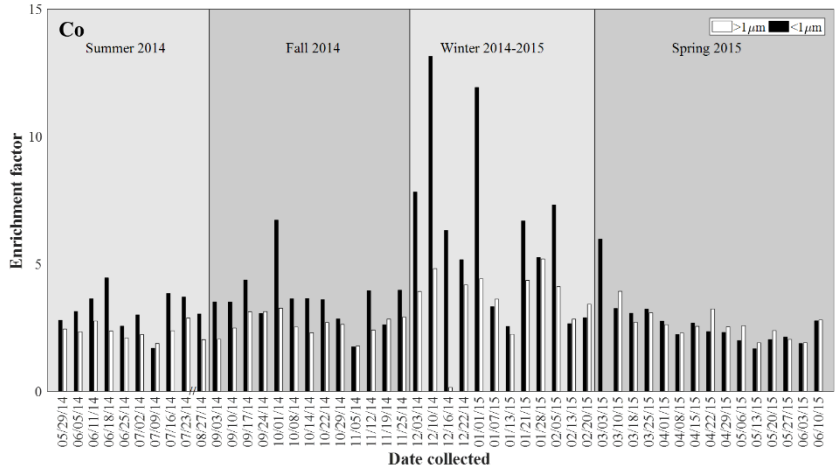

(g) Enrichment factors for Eastern Shore aerosol total nickel

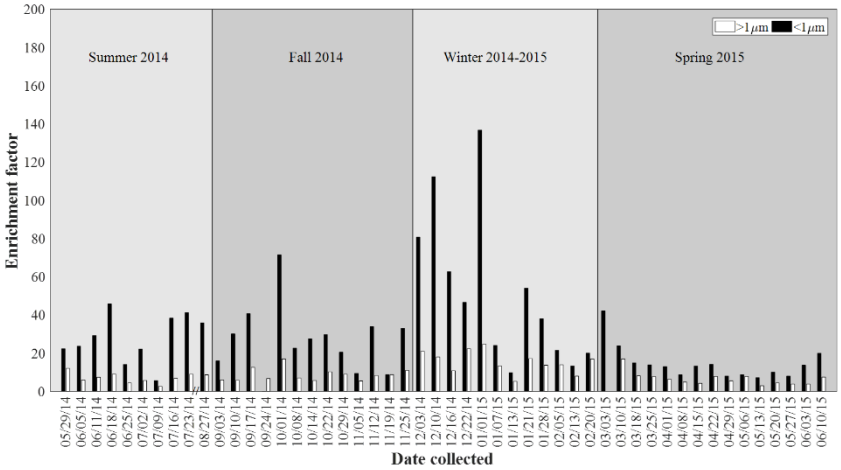

(h) Enrichment factors for Eastern Shore aerosol total copper

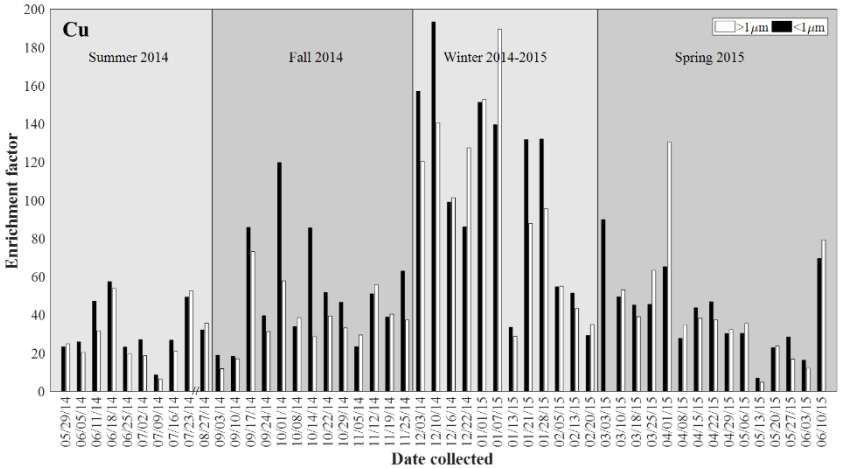

APPENDIX H. Continued.

(i) Enrichment factors for Eastern Shore aerosol total zinc

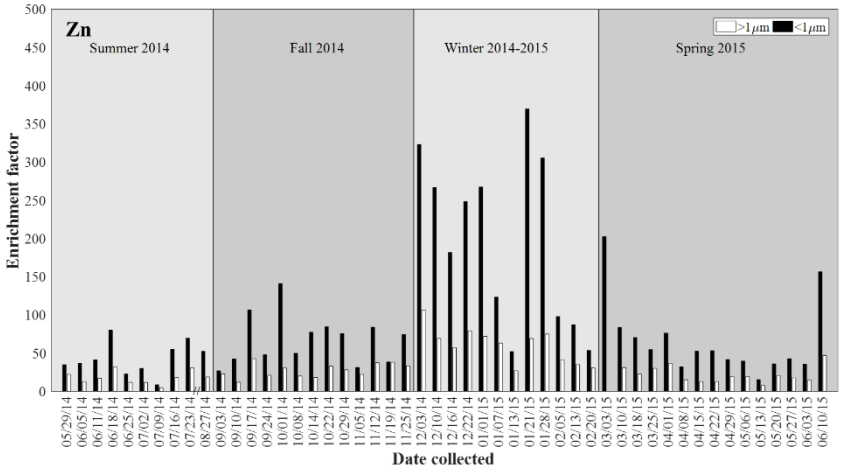

(j) Enrichment factors for Eastern Shore aerosol total cadmium

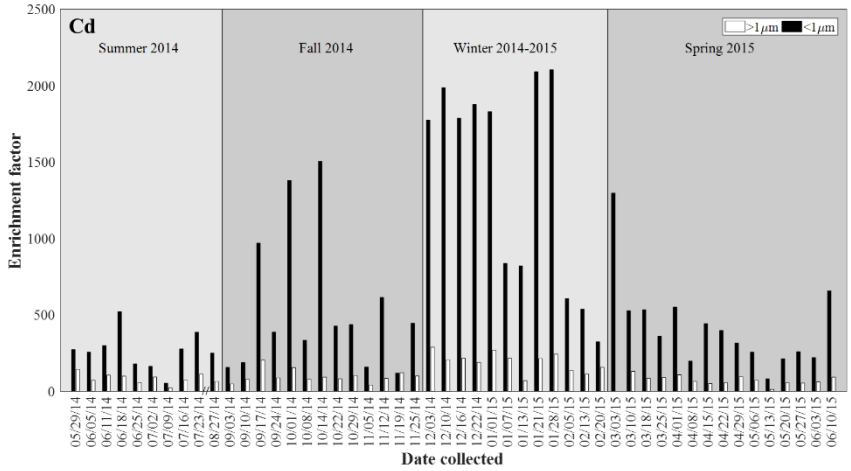

(k) Enrichment factors for Eastern Shore aerosol total antimony

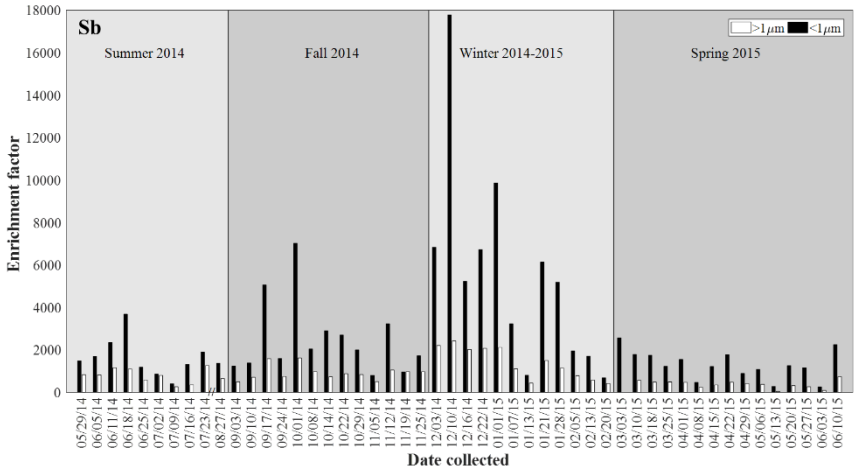

APPENDIX H. Continued.

(l) Enrichment factors for Eastern Shore aerosol total lead

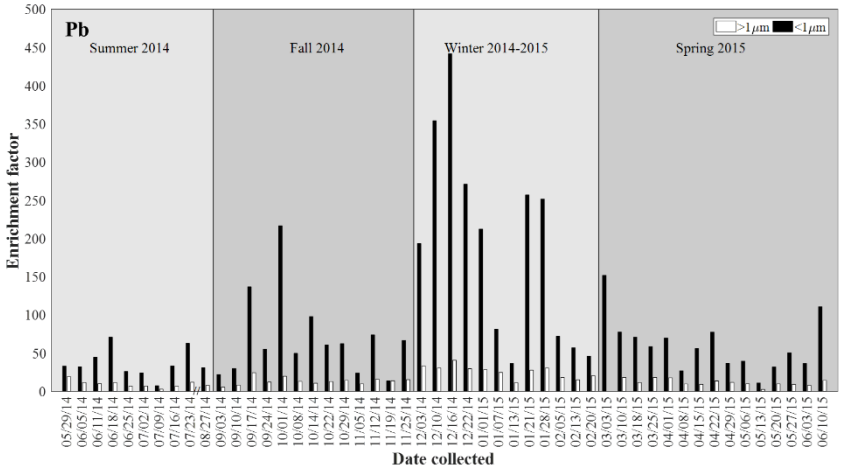

APPENDIX I

NOAA HYSPLIT BACKWARD TRAJECTORIES FOR AEROSOL SAMPLES COLLECTED IN COASTAL WATERS OF THE MID-ATLANTIC BIGHT

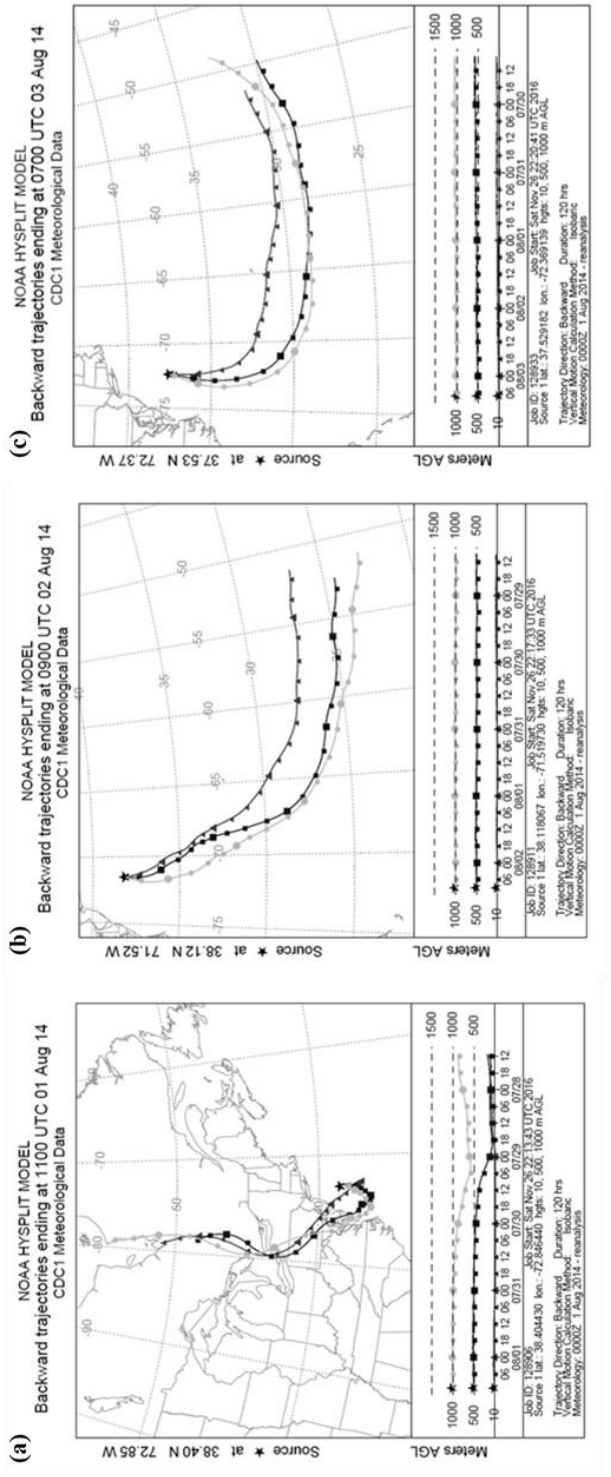

Figure I1. Five-day air mass backward trajectories (NOAA HYSPLIT) with arrival heights of 10 m, 500 m and 1000 m for offshore aerosol samples collected in coastal waters of the Mid-Atlantic Bight on (a) 1 August 2014, (b) 2 August 2014, (c) 3 August 2014, (d) 4 August 2014, (e) 5 August 2014, (f) 5 August 2014, (g) 7 August 2014, (h) 9 August 2014, (i) 10 August 2014, and (j) 15 August 2014.

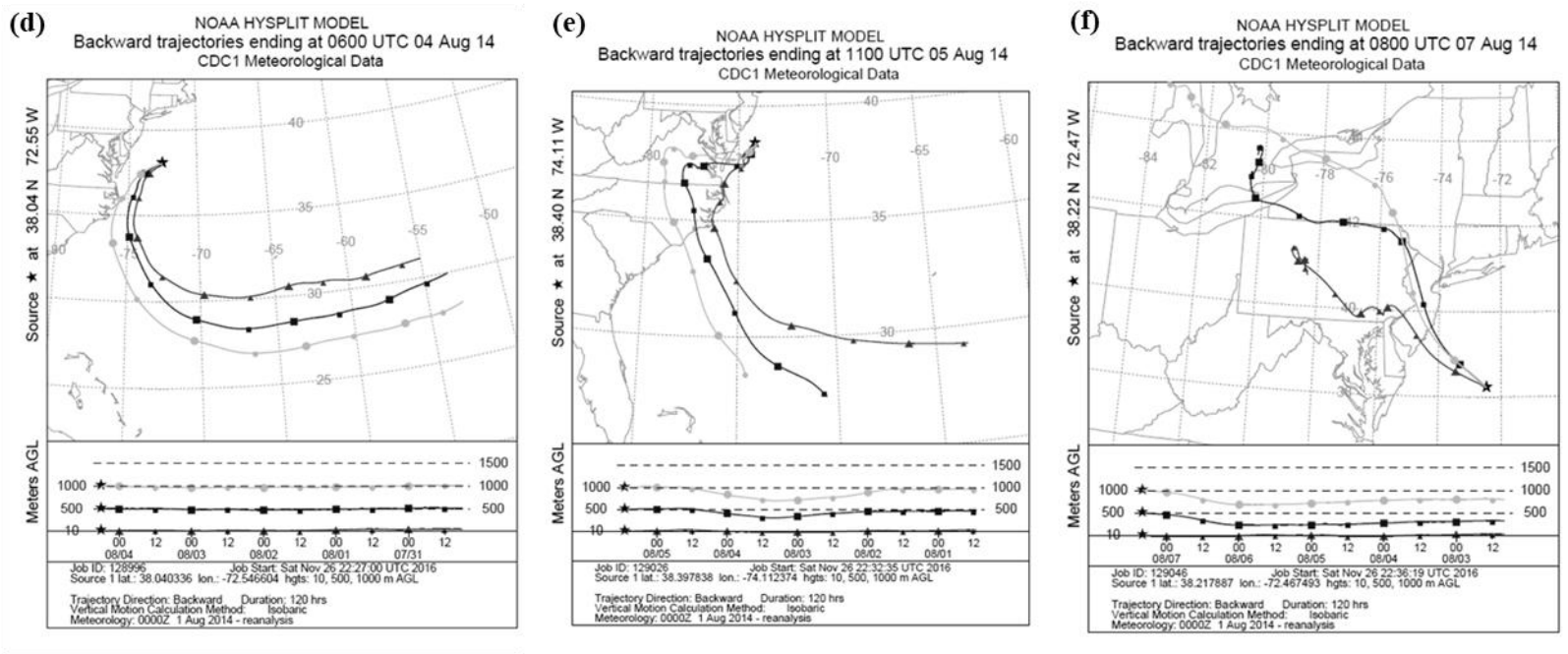

Figure I1. Continued.

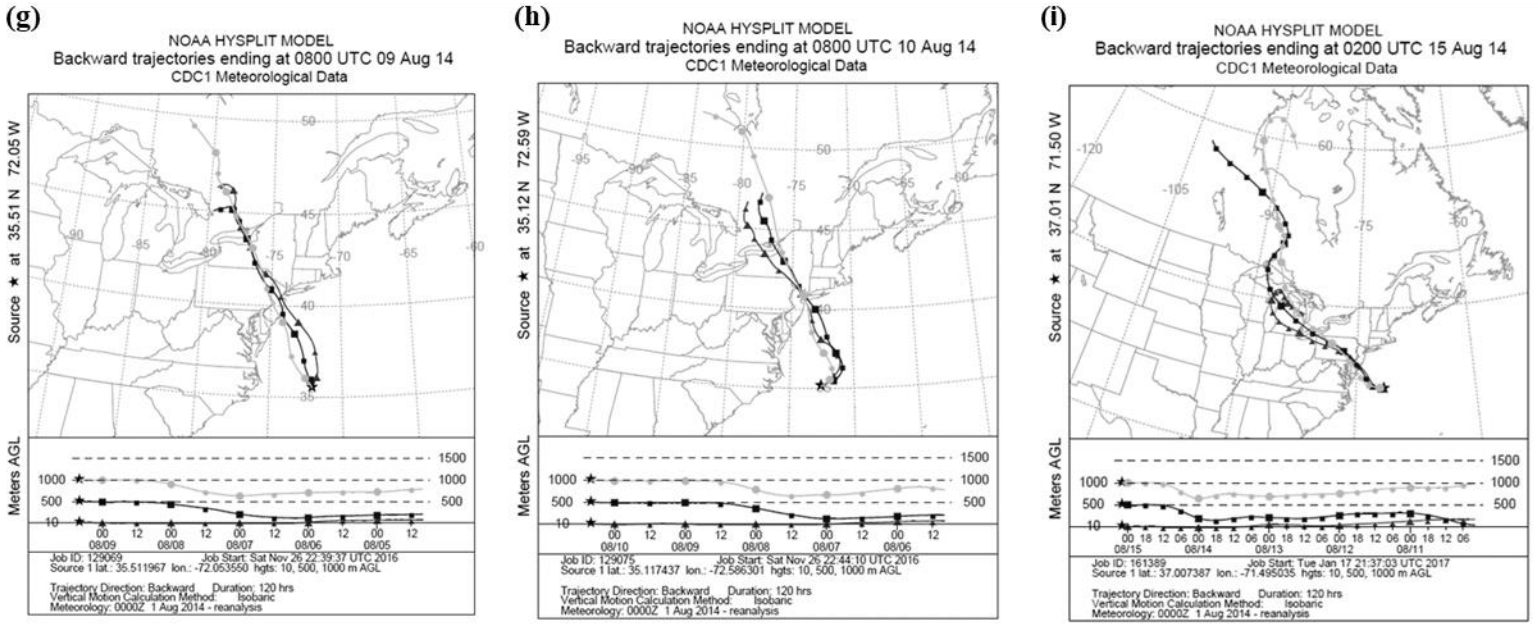

Figure I1. Continued.

VITA

Christine Sookhdeo

Department of Ocean, Earth, and Atmospheric Sciences, Old Dominion University, Norfolk, VA 23529
csook002@odu.edu

EDUCATION
Master of Science, Ocean and Earth Sciences, December 2018
Old Dominion University, Norfolk, VA

Bachelor of Science, Environmental Sciences, May 2012
Rider University, Lawrenceville, NJ

PROFESSIONAL EXPERIENCE
January 2016-May 2017, Old Dominion University, Graduate Teaching Assistant
August 2013-May 2014

May 2014-December 2015, Old Dominion University, Graduate Research Assistant

June 2010-August 2010, University of Arizona, Biosphere 2, Intern

PRESENTATIONS AND PUBLICATIONS
Sedwick, P. N., Bernhardt, P. W., Mulholland, M. R., Najjar, R. G., Blumen, L. M., Sohst, B. M., ... & Widner, B. (2018). Assessing phytoplankton nutritional status and potential impact of wet deposition in seasonally oligotrophic waters of the Mid-Atlantic Bight. Geophysical Research Letters, 45(7), 3203-3211.

Pavao-Zuckerman, M.A. and Sookhdeo, C. (2017). Nematode community response to green infrastructure design in a semi-arid city. Journal of Environmental Quality. doi:10.2134/jeq2016.11.0461

Sookhdeo, C., Bernhardt, P.W., Mendonca, I.R., Mulholland, M.R., Najjar, R.G., Sohst, B.M., Schwarzschild, A., Widner, B., Sedwick, P.N. (2015). Estimating Wet Deposition of Nutrients to Seasonally Oligotrophic waters off the U.S. East Coast using a Coastal Sampling Station. (poster, 2015 Aquatic Sciences Meeting).

Sookhdeo, C. and Druckenbrod, D. (2012). Effect of forest age and past land use on organic carbon content of Mount Vernon, VA soils. New Jersey Academy of Science. (paper & poster, 2011 Mid-Atlantic Ecological Society of America Meeting).

Sookhdeo, C. and Druckenbrod, D. (2011). Analysis of properties of Post Agricultural Soils, Lawrenceville, NJ (poster, 2012 Association of American Geographers Meeting).

Sookhdeo, C., Pavao-Zuckerman, M.A., and Tepler, S. (2011). Short and long term environmental effects on N-mineralization rates in arid ecosystems of Biosphere 2. (poster, 2011 Ecological Society of America Meeting).